OPTIMISATION OF RADIATION DOSE, IMAGE QUALITY AND CONTRAST MEDIUM ADMINISTRATION IN CORONARY COMPUTED TOMOGRAPHY ANGIOGRAPHY

TAN SOCK KEOW

FACULTY OF MEDICINE
UNIVERSITY OF MALAYA
KUALA LUMPUR

2018

OPTIMISATION OF RADIATION DOSE, IMAGE QUALITY AND CONTRAST MEDIUM ADMINISTRATION IN CORONARY COMPUTED TOMOGRAPHY ANGIOGRAPHY

TAN SOCK KEOW

THESIS SUBMITTED IN FULFILMENT OF THE REQUIREMENTS FOR THE DEGREE OF DOCTOR OF PHILOSOPHY

FACULTY OF MEDICINE
UNIVERSITY OF MALAYA
KUALA LUMPUR

2018

UNIVERSITY OF MALAYA

ORIGINAL LITERARY WORK DECLARATION

Name of Candidate: Tan Sock Keow

Matric No: MHA 150056

Name of Degree: Doctor of Philosophy

Title of Project Paper/Research Report/Dissertation/Thesis ("this Work"):

Optimisation of radiation dose, image quality and contrast medium administration in coronary computed tomography angiography.

Field of Study: Bio-medical imaging

I do solemnly and sincerely declare that:

(1) I am the sole author/writer of this Work;
(2) This Work is original;
(3) Any use of any work in which copyright exists was done by way of fair dealing and for permitted purposes and any excerpt or extract from, or reference to or reproduction of any copyright work has been disclosed expressly and sufficiently and the title of the Work and its authorship have been acknowledged in this Work;
(4) I do not have any actual knowledge nor do I ought reasonably to know that the making of this work constitutes an infringement of any copyright work;
(5) I hereby assign all and every rights in the copyright to this Work to the University of Malaya ("UM"), who henceforth shall be owner of the copyright in this Work and that any reproduction or use in any form or by any means whatsoever is prohibited without the written consent of UM having been first had and obtained;
(6) I am fully aware that if in the course of making this Work I have infringed any copyright whether intentionally or otherwise, I may be subject to legal action or any other action as may be determined by UM.

Candidate's Signature Date:

Subscribed and solemnly declared before,

Witness's Signature Date:

Name:

Designation:

OPTIMISATION OF RADIATION DOSE, IMAGE QUALITY AND CONTRAST MEDIUM ADMINISTRATION IN CORONARY COMPUTED TOMOGRAPHY ANGIOGRAPHY

ABSTRACT

Radiation dose and contrast medium administration are two major concerns in coronary computed tomography angiography (CCTA). This study aimed to assess the radiation dose and risk of radiation-induced cancer associated with different prospectively ECG-triggered CCTA protocols, and to optimise the radiation dose, image quality and contrast medium administration with an improved retrospectively ECG-triggered CCTA protocol. The study is divided into four phases whereby the phases that involved patients recruitment were approved by the Institutional Ethics Committee (Medical Ethics No: 989.35). Firstly, radiation dose received from prospectively ECG-triggered CCTA using different generations of CT scanners was assessed through organ doses measurement in a standard female adult anthropomorphic phantom. The measured organ doses were used for the estimation of lifetime attributable risk (LAR) of cancer incidence in different sex and age. Secondly, a low tube voltage (100 kVp) protocol was developed for retrospectively ECG-triggered CCTA and tested in 30 patients. The radiation dose and image quality were compared to the routine 120 kVp protocol. Then, a personalised contrast volume calculation model based on patient characteristics and test bolus parameters was developed and validated in 30 recruited patients. Finally, an improved retrospectively ECG-triggered CCTA protocol was developed using the combination of 100 kVp and personalised contrast protocol and validated in 30 recruited patients. Among the prospectively ECG-triggered CCTA protocols, the highest effective dose (H_E) was received from 2 × 32-detector-row dual-source CT (DSCT) scanner (6.06 ± 0.72 mSv). Although the heart is the organ of interest in CCTA imaging, the highest

radiation dose was received by breasts and lungs (4 to 8 times higher than heart). The estimated LARs were generally low for all cancers (less than 0.02 to 113 cases per 100,000 population). For patient's body mass index (BMI) less than 30 kgm^{-2}, using automatic tube current modulation, statistical significant ($p < 0.05$) radiation dose reduction (37.8 %) and higher vessel contrast enhancement (VCE) were achieved at 100 kVp. A strong linear relationship was found between VCE and contrast volume ($r = 0.97$, $p < 0.05$). Age, sex, body surface area (BSA) and peak contrast enhancement (PCE) at test bolus were found to be significant predictors for VCE ($p < 0.05$). A personalised contrast volume calculation model was then developed by applying these factors. The model successfully reduced the total iodine dose (TID) while achieving optimal VCE and image quality at 120 kVp compared to the routine contrast protocol (9.8 %, $p < 0.05$). When combining both the low tube voltage (100 kVp) and personalised contrast protocol, optimal VCE and image quality were achieved with statistical significant ($p < 0.05$) radiation dose (33.8 %) and TID reduction (43.9 %) compared to 120 kVp. The radiation doses and LAR for cancer incidence from a prospectively ECG-triggered CCTA are relatively low and depend on the scanner model and imaging protocol. This study successfully developed a scanning protocol using low tube voltage (100 kVp) and personalised volume calculation that optimise radiation dose, image quality and contrast medium administration for retrospectively ECG-triggered CCTA.

Keywords: Coronary computed tomography angiography, tube voltage, radiation dose, image quality and contrast medium.

PENGOPTIMUMAN DOS RADIASI, KUALITI IMEJ DAN PENGGUNAAN MEDIUM KONTRAS DALAM ANGIOGRAFI TOMOGRAFI BERKOMPUTER KORONARI

ABSTRAK

Dedahan radiasi dan pengunaan medium kontras telah menjadi bimbangan dalam angiografi tomografi berkomputer koronari (CCTA). Tujuan kajian ini adalah untuk menilai dos radiasi dan risiko kanser aruhan-radiasi daripada protokol-protokol "prospectively ECG-triggered CCTA" yang berbeza dan mengoptimumkan dos radiasi, kualiti imej serta penggunaan medium kontras melalui sebuah protokol penambahbaikan dalam "retrospectively ECG-triggered CCTA". Kajian ini dibahagikan kepada empat fasa di mana fasa yang melibatkan pesakit telah menerima kelulusan daripada Jawatankuasa Etika Institusi (No. Etika Perubatan: 989.35). Pertama, penilaian dos radiasi bagi prosedur "prospectively ECG-triggered CCTA" telah dilakukan melalui pengukuran dos-dos organ dalam sebuah fantom antropomorfik wanita dewasa piawaian dan generasi mesin CT yang berbeza. Berdasarkan dos-dos organ yang telah diukur, anggaran risiko atribut hayat (LAR) insidens kanser bagi jantina dan umur yang berbeza telah dilakukan. Kedua, sebuah protokol "retrospectively ECG-triggered CCTA" dengan voltan tiub rendah (100 kVp) telah dibina dan diuji dengan 30 pesakit. Perbandingan dos radiasi dan kualiti imej telah dilakukan di antara protokol ini dan protokol 120 kVp rutin. Seterusnya, sebuah model pengiraan isipadu kontras peribadi berdasarkan ciri-ciri pesakit dan parameter-parameter bolus ujian telah dibina dan disahkan dengan 30 pesakit. Akhirnya, sebuah protokol penambahbaikan dalam "retrospectively ECG-triggered CCTA" telah dibina melalui kombinasi 100 kVp dan protokol kontras peribadi serta disahkan dengan 30 pesakit. Di kalangan protokol-protokol "prospectively ECG-triggered CCTA", mesin CT dual-source (DSCT) dengan barisan pengesan 2 × 32 memberi dos berkesan (H_E) yang tertinggi (6.06 ± 0.72 mSv). Walaupun jantung merupakan organ terpenting dalam

pengimejan CCTA, tetapi payudara dan peparu menerima dos radiasi yang paling tinggi (4 hingga 8 kali ganda lebih tinggi berbanding dengan jantung). Secara keseluruhannya, LAR anggaran didapati adalah rendah bagi semua kanser (kurang daripada 0.02 ke 113 kes dalam 100,000 populasi). Dengan menggunakan modulasi arus tiub otomatik, pengurangan dos radiasi (37.8 %) dan peningkatan dalam peneguhan kontras salur darah (VCE) yang signifikan dari segi statistikal ($p < 0.05$) telah dicapai dengan menggunakan 100 kVp bagi pesakit yang mempunyai indeks jisim tubuh (BMI) kurang daripada 30 kgm^{-2}. VCE didapati berhubung secara linear dan kuat dengan isipadu kontras ($r = 0.97$, $p < 0.05$). Umur, jantina, luas permukaan tubuh (BSA) dan peneguhan kontras puncak (PCE) bolus ujian didapati merupakan peramal-peramal signifikan untuk VCE ($p < 0.05$). Kemudian, sebuah model pengiraan isipadu kontras peribadi telah dibina berdasarkan faktor-faktor tersebut. Model in telah berjaya mengurangkan dos iodin total (TID) untuk 120 kVp berbanding dengan protokol kontras rutin (9.8 %, $p < 0.05$) dan mencapai VCE serta kualiti imej yang optimal. Apabila kombinasi voltan tiub rendah (100 kVp) dan protokol kontras peribadi digunakan, VCE dan kualiti imej yang optimal telah dicapai dengan pengurangan dos radiasi (33.8 %) dan TID (43.9 %) yang signifikan dari segi statistical ($p < 0.05$) berbanding dengan 120 kVp . Secara relatif, dos radiasi dan LAR insidens kanser yang berpunca daripada sebuah prosedur “prospectively ECG-triggered CCTA” adalah rendah dan bergantung kepada model mesin CT serta protokol pengimejan. Kajian ini telah berjaya membina satu protokol pengimbasan untuk mengoptimumkan dos radiasi, kualiti imej dan penggunaan medium kontras dalam “retrospectively ECG-triggered CCTA” melalui penggunaan voltan tiub rendah (100 kVp) dan pengiraan kontras peribadi.

Kata kunci: Angiografi tomografi berkomputer koronari, voltan tiub, dos radiasi, kualiti imej dan medium kontras.

ACKNOWLEDGEMENTS

First and foremost, I would like to express my deepest appreciation to my supervisor, Professor Dr. Ng Kwan Hoong, for his patience, scholarly inputs and consistent encouragement in my PhD study and research. His valuable guidance helped me in all the time of research and writing of this thesis.

My sincere gratitude goes to my co-supervisor, Associate Professor Dr. Yeong Chai Hong, School of Medicine, Taylor's University Malaysia, for her continuous guidance and support. She has been very helpful in reviewing my written works, providing me with comments and encouragement. I really appreciate her effort and time in all the useful discussions and brainstorming sessions.

I would like to thank my co-supervisor, Dr. Raja Rizal Azman bin Raja Aman for his constant guidance and support. His helpful comments and professional advices in CCTA incented me to widen my research from various perspectives.

Very special thanks to Professor Dr. Zhonghua Sun, Department of Medical Radiation Sciences, Curtin University, Perth, Australia, for his professional advice in my research study and effort in reviewing my manuscripts for publication.

I would like to sincerely thank, Professor Yang Faridah bin Abdul Aziz and Dr. Fadhli bin Mohamed Sani for their professional advice and support in this research, particularly in the image quality assessment.

I would like to thank the personnel from University of Malaya and University of Malaya Medical Centre: Associate Professor Dr. Chee Kok Han, Dr. Jeannie Wong Hsiu Ding, Dr. Mohammad Nazri bin Md Shah, Dr. Susie Lau, Dr. Jong Wei Loong, Dr. Mohammad Javad Safari, Mr. Chia Chi Kuan, Mdm. Sogol Givehchi, Mdm. Shalina Sri Karan, Mdm. Lilian Yap Poh Poh, Mr. Mohd Kamil bin Mohamad Fabell, Mdm. Priya

Kudheravelu, Ms. Kirthiga Veeramohan, Mdm. Tun Suraiya binti Tun Abd Majid, Mdm. Intan Shuhada binti Mohd Fuat, Ms. Foo Sue Anne, Mdm. Rozelyn Tey Mei Ai, Mdm. Suraya binti Khalid, Mdm. Nur Fadlina Adila binti Mohamad, Mdm. Harpreet Kaur Rajput A/P Balgit Singh, Ms. Nurdiyanah binti Affindi, and Ms. Farah Nadia binti Musa.

I would also like to thank the personnel from the following institution: Mr. Chin Hoe Kit and Mr. Li Chee Chong, iHeal Medical Centre; Dr. Soo Chee Siong and Mr. Hanafes bin Aziz, HSC Medical Center; Dr. Ong Kee Liang and Dr. Chin Loi Chung, Life Care Diagnostic Medical Centre; Mr. Chung King Keong, Ms. Bong Yoke Siew and Mr. Fairus Afiz bin Mohd Den, Tung Shin Hospital.

Last but not least, I am very indebted to my family for their love, support and encouragement. To my parent and siblings who never failed to motivate me, thanks for filling my life with warmth. To my husband, Mr. Ong Chien Ooi, thanks for being there for me all the times through the hardships. This thesis is dedicated to you.

TABLE OF CONTENTS

LIST OF FIGURES

LIST OF TABLES

LIST OF SYMBOLS AND ABBREVIATIONS

a	:	Attained age
AA	:	Ascending aorta
AHA	:	American Heart Association
ATVS	:	Automatic tube voltage selection
BEIR	:	Biological Effects of lonizing Radiation
BMI	:	Body mass index
bpm	:	Beats per minute
BSA	:	Body surface area
CACS	:	Coronary artery calcium scoring
CAD	:	Coronary artery disease
CTDI	:	CT dose index
$CTDI_{vol}$	:	CTDI volume
$CTDI_W$	:	Weighted CTDI
CCTA	:	Coronary computed tomography angiography
CMR	:	Cardiac magnetic resonance imaging
CNR	:	Contrast-to-noise ratio
DSCT	:	Dual-source CT
DLP	:	Dose length product
$D_{T,R}$	:	Average absorbed dose to tissue T
D(z)	:	Radiation dose profile along the z-axis
e	:	Exposed age of the patient
EAR	:	Excess absolute risk
EC	:	European Commission
ECG	:	Electrocardiography

E_{KL}	:	P_{KL}-to-H_E conversion factor
ERR	:	Excess relative risk
FDA	:	Food and Drug Administration
FOM	:	Figure of merit
FOV	:	Field of view
HDL	:	High-density lipoprotein
H_E	:	Effective dose
HU	:	Hounsfield units
I	:	Table increment per gantry rotation
IDR	:	Iodine delivery rate
ICRP	:	International Commission on Radiological Protection
IVUS	:	Intravascular ultrasound
l	:	Irradiated length in z-axis
L	:	Risk-free latent period
LAD	:	Left anterior descending
LAR	:	Lifetime attributable risk
LAR_{joint}	:	Joint lifetime attributable risk
LCA	:	Left coronary artery
LCx	:	Left circumflex
LDL	:	Low-density lipoprotein
LET	:	Linear energy transfer
LM	:	Left main
LR	:	Lifetime risk
LR_{joint}	:	Joint lifetime risk
mAs	:	Tube current-time product
MDCT	:	Multi-detector row CT

M(*D, e, a*)	:	Excess absolute risk
MIP	:	Maximum-intensity projections
MIRD	:	Medical Internal Radiation Dosimetry
MPR	:	Multiplanar reformations
MPS	:	Myocardial perfusion scintigraphy
n	:	Number of sections per scan
N	:	Number of acquired sections per scan
NRPB	:	National Radiological Protection Board
NSTEMI	:	Non-ST-segment elevation myocardial infarction
OCT	:	Optical coherence tomography
OSLD	:	Optically stimulated luminescence dosimeter
P_a	:	LAR or LR for organ "a" divided by 100,000
P_b	:	LAR or LR for organ "b" divided by 100,000
PCE	:	Peak contrast enhancement
$PCE_{(100)}$	:	Peak contrast enhancement of test bolus at 100 kVp
$PCE_{(120)}$	:	Peak contrast enhancement of test bolus at 120 kVp
PDA	:	Posterior descending artery
PHE	:	Public Health England
P_{joint}	:	Joint probability
P_{KL}	:	Air kerma-length product
PROTECTION	:	Prospective Multicenter Study on Radiation Dose Estimates of Cardiac CT Angiography
RCA	:	Right coronary artery
ROI	:	Region of interest
RR	:	Relative risk
RR_{joint}	:	Joint relative risk

S(a)	:	Probability of survival until age "*a*"
S(e)	:	Probability of survival until age "*e*"
SCCT	:	Society of Cardiovascular Computed Tomography
SCORE	:	Systematic Coronary Risk Evaluation
SNR	:	Signal-to-noise ratio
SPR	:	Scan projection radiograph
SSCT	:	Single source CT
STEMI	:	ST-segment elevation myocardial infarction
t	:	Section thickness
T	:	Nominal width of each acquired section
TCFA	:	Thin-cap fibroatheroma
TID	:	Total iodine dose
TTP	:	Time-to-peak
UA	:	Unstable angina
VCE	:	Vessel contrast enhancement
$VCE_{(60/120)}$	:	Vessel contrast enhancement achieved with 60 mL contrast medium at 120 kVp
$VCE_{(t100)}$	:	Targeted vessel contrast enhancement for 100 kVp
$VCE_{(t120)}$	:	Targeted vessel contrast enhancement for 120 kVp
VRT	:	Volume-rendering techniques
w_R	:	Radiation-weighting factor
w_T	:	Tissue-weighting factor
WHO	:	World Health Organization

LIST OF APPENDICES

CHAPTER 1: GENERAL INTRODUCTION

1.1 Research background

Coronary artery disease (CAD) is the most common form of cardiovascular disease. It is characterized by the presence of atherosclerotic plaque(s) in the coronary arteries. The plaques progressively narrow and occlude the arterial lumen, impair blood flow and reduce oxygen supply to the myocardium. CAD may subsequently leads to myocardial ischaemia, myocardial infarction or heart failure and at times to sudden death (Mahmood, 2009).

CAD is a serious health problem worldwide, leading to cardiovascular disability and death. According to the World Health Organization (WHO), cardiovascular diseases are number one causes of death globally. In 2015, 17.7 million (31.0 %) of worldwide deaths were reported due to cardiovascular diseases. Of these deaths, an estimated 7.4 million were due to CAD (WHO, 2017).

In Malaysia, cardiovascular diseases have been the leading causes of morbidity and mortality for more than a decade (MOH, 2017, 2016; IHME, 2015; WHO, 2014b, 2014a). In 2012, 20.1 % (29.4 thousand) of deaths in Malaysia were reported due to CAD (WHO, 2014a). Data from 2011 to 2013 in National Cardiovascular Disease-Acute Coronary Syndrome Registry indicated that Malaysians developed acute coronary syndrome at a younger age than that seen in neighbouring countries. The mean age was 58.5 years and the peak incidence was in the 51 to 60 year age group (MOH, 2017).

The current gold standard for diagnosis of CAD is invasive coronary angiography (ICA). As the invasive nature of ICA carries a nonnegligible risk and adds significant costs, coronary computed tomography angiography (CCTA) has been used with increasing frequency as a non-invasive modality for the assessment of CAD, particularly for the investigation of symptomatic patients with low-to-intermediate cardiovascular risk

(Dewey, 2011a; Jolly et al., 2009). During the CCTA scanning, an iodinated contrast medium is administrated to fill up the arterial lumen, which allows direct assessment of coronary stenosis (Voros et al., 2011). Using post-processing software, it is possible to identify the location and distribution of plaques, characterize the type of plaques into calcified, non-calcified and mixed plaques, as well as to assess the composition of plaque (Sun & Xu, 2014; Sun, 2012a). Nevertheless, patient safety issues due to radiation and contrast medium doses are still the reasons for concern in CCTA.

In response to the concern of radiation exposure to patients, tremendous progress has been made and various dose-reducing techniques have been proposed. These include electrocardiography (ECG)-dependent tube current modulation (Abada et al., 2006), low tube voltage protocol (Oda et al., 2011), prospectively ECG-triggered protocol (Hausleiter et al., 2012), high-pitch helical scanning on dual-source CT (DSCT) (Lell et al., 2009), application of noise reduction filters (Alkadhi, 2009), and scan length optimisation (Leschka et al., 2010).

Currently, prospectively ECG-triggered protocol has been recommended as the first line default technique for CCTA examination, which should be used whenever possible and practical (Raff et al., 2014). Although significant reduction (more than 60 %) of air kerma-length product (P_{KL}) and effective dose (H_E) in prospectively ECG-triggered compared to retrospectively ECG-triggered CCTA protocol has been reported in the literature, each CT manufacturer has developed their own protocol and the scanning parameters used in these protocols are very much dependent on the hardware (CT scanner) specifications (Sun & Ng, 2012b). So far, there has been no study reported the radiation dose among these protocols to the best of our knowledge.

Furthermore, in majority of the studies, assessment of radiation dose in prospectively ECG-triggered CCTA protocol was dependent on the P_{KL} reported at the CT console. The

H_E was calculated by multiplying the P_{KL} with a P_{KL}-to-H_E conversion factor (E_{KL}) for chest region. This calculated H_E has been reported to underestimate the amount of patient exposure that actually incurred (Hurwitz et al., 2007; Groves et al., 2004). In fact, the radiation dose to individual organs is not represented by these numbers and the patient-specific organ or tissue absorbed dose, not the H_E, is needed for assessing the probability of cancer induction in exposed individuals (ICRP, 2007).

Despite the substantial reduction of radiation dose, prospectively ECG-triggered CCTA protocol has a few limitations: firstly, it requires a regular and low heart rate (less than 70 beats per minute (bpm)), which may not be achievable in all patients; secondly, it is usually restricted to non-overlapping scanning or slice increments with a small overlap, thus there is a high demand in the z-axis coverage of CT scanner for implementing this protocol; thirdly, as ECG-triggered acquisition targets only a specific phase of the cardiac cycle, the data are acquired during a small portion of the R-R interval. Hence, it cannot provide any functional information about cardiac valve or ventricular wall (Sun, 2012b; Husmann et al., 2008; Stolzmann et al., 2008).

To overcome these limitations, another dose-reducing strategy that could be considered is the retrospectively ECG-triggered protocol with low tube voltage. Instead of using a standard 120 kVp for scanning, low tube voltage protocol utilises a lower tube voltage, such as 80 and 100 kVp. This technique has drastically reduced the radiation dose and effectively increased vessel contrast enhancement (VCE) (Andreini et al., 2016; Di Cesare et al., 2016; Wu et al., 2016; Cao et al., 2014; Blankstein et al., 2011). Less X-ray photons are being generated at low tube voltage and as the mean photon energy of low tube voltage approaches the iodine K-edge energy of 33.2 keV, it produces better image contrast, meaning an equivalent VCE can be achieved at a lower amount of

administered iodine (Nakaura et al., 2011; Bae, 2010). These have addressed the concerns of both radiation and contrast medium doses in performing CCTA.

Due to lower X-ray output, increased image noise is one of the main disadvantages of low tube voltage protocol. One solution to improve image quality is by applying a compensatory increase in tube current to balance image noise, at the cost of increasing patient dose. Furthermore, it is challenging to quantify the optimum increase in tube current for individual patient (Aschoff et al., 2017). To overcome this problem, a dedicated software (Care kV, Siemens Healthcare, Forchheim, Germany) has been introduced that allows automatic selection of tube voltage based on the patients' size and attenuation characteristics (Lee et al., 2012). However, this software is costly and may not be readily available in the existing CT scanner. Thus, a combination of manual patient selection and automatic tube current modulation is an alternative to reduce image noise in low tube voltage CCTA protocol.

As the relative attenuation of iodinated contrast medium increases at lower tube voltage, several studies have tried to reduce total iodine dose (TID) used in low tube voltage CCTA protocol, mainly by two different methods: (1) lowering the iodine concentration; and (2) reducing the contrast volume administrated. Generally, these studies have focused on reducing TID while maintaining VCE above 250 HU. Limited studies have considered the upper limit of VCE. High VCE of 500 HU has been reported to decrease the detectability of stenosis in smaller vessels (Fei et al., 2008). Taking into consideration of the detection of coronary stenosis, quantitative analysis of atherosclerotic plaque and diagnostic performance of CCTA, the optimal range of VCE could fall between more than 250 and less than 450 HU (Abbara et al., 2016; Komatsu et al., 2013; Abbara et al., 2009; Cademartiri et al., 2008; Fei et al., 2008; Horiguchi et al., 2007).

In CCTA, a parameter obtained from time-attenuation curve of test bolus scan, the time-to-peak (TTP) is commonly used to calculate the scan delay (Weininger et al., 2011). Test bolus parameters such as TTP and peak contrast enhancement (PCE) are closely associated with the patient's cardiovascular and contrast pharmacokinetic response during CCTA scanning. PCE and TTP at test bolus scan has been reported as a predictable parameter for VCE in previous studies (Zhu et al., 2015; Yang et al., 2013; Mahnken et al., 2007; van Hoe et al., 1995). These have created the interest of using test bolus parameters for contrast volume calculation. As of to date only one study has combined patient characteristics (body surface area (BSA)) and test bolus parameters (PCE and TTP) for personalised contrast volume calculation (Komatsu et al., 2013) at iodine delivery rate (IDR) of 1.40 gI/s. H igh IDR has been reported to be able to achieve PCE at a lower TID in CCTA. A personalised contrast volume calculation model using a high IDR is expected to allow better contrast volume estimation for achieving VCE within the optimal range and further reduce the TID, especially at low tube voltage CCTA protocol.

1.2 Problem statements

Corresponding to the various points and arguments mentioned above, the statement of research problems are listed as follows:

1. Despite the fact that many studies have reported substantial radiation dose reduction in prospectively ECG-triggered compared to retrospectively ECG-triggered CCTA protocol, there has been no study conducted to compare the radiation dose among the different prospectively ECG-triggered CCTA protocols to the best of our knowledge.
2. The H_E reported based on P_{KL} and an E_{KL} for chest region may underestimate the amount of patient exposure that actually incurred during prospectively ECG-triggered CCTA protocols.

3. There is limited study focused on the assessment of individualised absorbed doses to the major irradiated organs during prospectively ECG-triggered CCTA protocols, as well as the risk of radiation-induced cancer associated with CCTA.
4. Development of low tube voltage CCTA protocol which involves a combination of patient selection and automatic tube current modulation is necessary to achieve radiation dose reduction without affecting the image quality.
5. A personalised contrast volume calculation model using a high IDR is expected to allow better contrast volume estimation for achieving VCE within the optimal range and further reduce the TID, especially at low tube voltage CCTA protocol.

1.3 Research objectives

The main objectives of this research were to assess the radiation dose and the risk of radiation-induced cancer associated with different prospectively ECG-triggered CCTA protocols, and to optimise the radiation dose, image quality and contrast medium administration with an improved retrospectively ECG-triggered CCTA protocol.

The specific objectives are listed as follows:

I. To assess the radiation dose received from prospectively ECG-triggered CCTA using different generations of CT scanners through direct measurement of organ doses in a standard female adult anthropomorphic phantom.

II. To estimate the risk of radiation-induced cancer associated with prospectively ECG-triggered CCTA based on different sex and age.

III. To develop a low tube voltage (100 kVp) retrospectively ECG-triggered CCTA protocol and assess the radiation dose and image quality.

IV. To develop and clinically validate a personalised contrast volume calculation model using high IDR of 2.22 gI/s for 100 and 120 kVp retrospectively ECG-triggered CCTA protocols.

V. To assess the achievable radiation dose and TID reduction and image quality in an improved retrospectively ECG-triggered CCTA protocol, developed using the combination of low tube voltage (100 kVp) and a personalised contrast protocol.

1.4 Research hypotheses

The research hypotheses are listed as follows:

1. H_0 : There is no difference in radiation dose between 100 and 120 kVp retrospectively ECG-triggered CCTA protocols.

   H_a : 100 kVp retrospectively ECG-triggered CCTA protocol gives lower radiation dose compared to 120 kVp retrospectively ECG-triggered CCTA protocol.

2. H_0 : There is no difference in VCE between 100 and 120 kVp retrospectively ECG-triggered CCTA protocols.

   H_a : 100 kVp retrospectively ECG-triggered CCTA protocol produces higher VCE compared to 120 kVp retrospectively ECG-triggered CCTA protocol.

3. H_0 : There is no difference in image quality between 100 and 120 kVp retrospectively ECG-triggered CCTA protocols.

   H_a : There is a difference in image quality between 100 and 120 kVp retrospectively ECG-triggered CCTA protocols.

4. H_0 : There is no difference in VCE between personalised contrast and routine contrast protocol.

H_a : There is a difference in VCE between personalised contrast and routine contrast protocol.

5. H_0 : There is no difference in TID between personalised contrast and routine contrast protocol.

   H_a : Personalised contrast protocol gives lower TID compared to routine contrast protocol.

6. H_0 : There is no difference in image quality between personalised contrast and routine contrast protocol.

   H_a : There is a difference in image quality between personalised contrast and routine contrast protocol.

7. H_0 : There is no difference in VCE between improved and routine protocol.

   H_a : There is a difference in VCE between improved and routine protocol.

8. H_0 : There is no difference in radiation dose between improved and routine protocol.

   H_a : The improved protocol gives lower radiation dose compared to the routine protocol.

9. H_0 : There is no difference in TID between improved and routine protocol.

   H_a : The improved protocol gives lower TID compared to the routine protocol.

10. H_0 : There is no difference in image quality between improved and routine protocol.

    H_a : There is a difference in image quality between improved and routine protocol.

1.5 Organisation of the thesis

In this chapter (Chapter 1), background on CAD, strategies for radiation dose and contrast medium reduction in CCTA are discussed. This is then followed by the statement of research problems and the objectives of this research project. Organisation of the thesis which describing the contents and works in different chapters is also provided.

Chapter 2 provides a description on anatomy and physiology of the heart, which is then followed by the explanation on CAD. The development of different scanning techniques and contrast medium administration protocols, radiation dose and image quality in CCTA are discussed in further detail.

In Chapter 3, assessment of radiation dose received from prospectively ECG-triggered CCTA using five different state-of-the-art CT scanners through direct measurement of organ doses in a standard female adult anthropomorphic phantom is reported. It is then followed by the estimation of LAR of cancer incidence based on the measured organ doses. In this chapter, research problems (1), (2) and (3) are addressed, and objectives (I) and (II) are achieved.

In Chapter 4, development of a low tube voltage (100 kVp) retrospectively ECG-triggered CCTA protocol with a combination of patient selection based on body mass index (BMI) and automatic tube current modulation is described. It is then followed by the assessment of achievable radiation dose reduction and image quality in the protocol developed, compared to the routine 120 kVp protocol. Research problem (4) is addressed, objective (III) is achieved, and research hypotheses (1), (2) and (3) are tested.

In Chapter 5, a process of developing and validating a personalised contrast volume calculation model using high IDR of 2.22 gI/s for 120 kVp retrospectively ECG-triggered

CCTA protocol is described. Research problems (5) is addressed, objective (IV) is achieved, and research hypotheses (4), (5) and (6) are tested.

In Chapter 6, a process of developing and validating a personalised contrast volume calculation model for low tube voltage (100 kVp) retrospectively ECG-triggered CCTA protocol is described. It is then followed by the assessment of achievable radiation dose and TID reduction and image quality in an improved retrospectively ECG-triggered CCTA protocol, developed using the combination of low tube voltage (100 kVp) and a personalised contrast protocol. Research problem (5) is addressed, objective (IV) and (V) are achieved, and research hypotheses (7), (8), (9) and (10) are tested.

Finally, in Chapter 7, an overall conclusion summarizing the findings and limitations of this research are provided. Future research with suggestions to improve the work in this research are also proposed and discussed in more details.

CHAPTER 2: LITERATURE REVIEW

This chapter begins with description on anatomy and physiology of the heart, which is then followed by the explanation on CAD. The development of different scanning techniques and contrast medium administration protocols, the assessment of radiation dose and image quality in CCTA are discussed in further detail.

2.1 Anatomy and physiology of the heart

The cardiovascular system consists of the heart and circulatory system. The heart is a muscular pump that serves two functions: (1) to collect blood from the tissues of the body and pump it to the lungs; (2) to collect blood from the lungs and pump it to all tissues of the body. Blood delivers oxygen and essential nutrients to every cell and removes the metabolic end products from those cells. Blood is carried from the heart to the rest of the body through a complex network of arteries, arterioles, and capillaries and subsequently returned to the heart through venules and veins (Weinhaus & Roberts, 2005).

The heart is a hollow, muscular organ enclosed in the middle mediastinum. It weighs approximately 250 to 300 g and divided into four distinct chambers with muscular walls of different thickness: the left and right atrium, left and right ventricle. The ventricles are larger thick-walled chambers that pump blood out of the heart (Applegate, 2010; Shah et al., 2009). Figure 2.1 shows the heart chambers and pathway of blood flow through the heart and lungs.

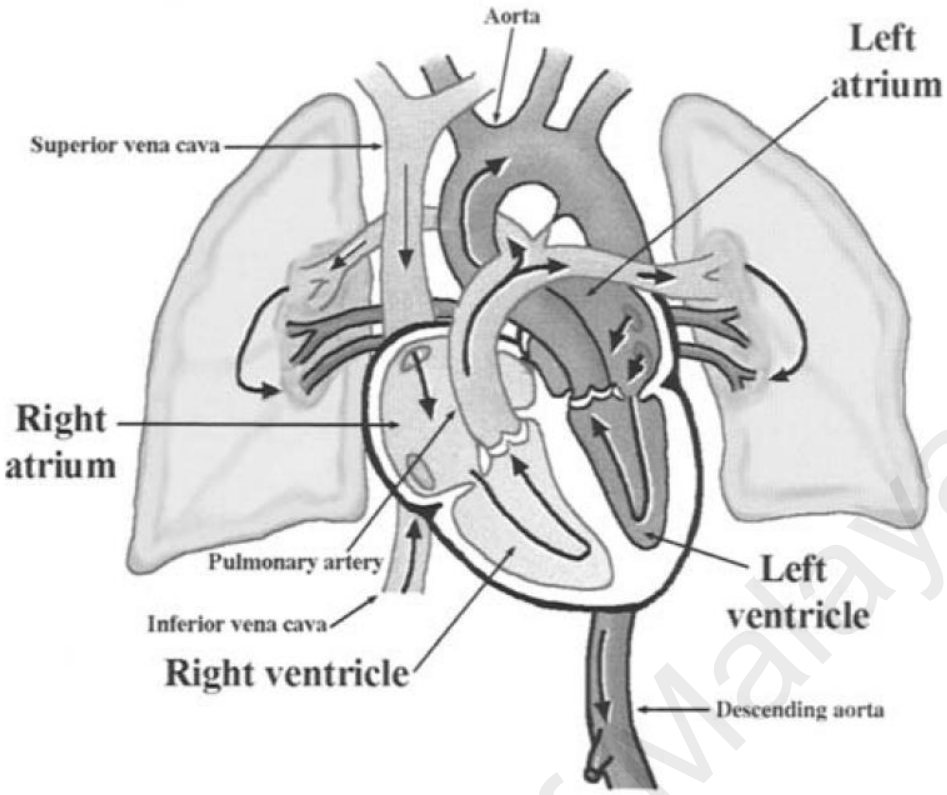

Figure 2.1: Heart chambers and pathway of blood flow through the heart and lungs (reproduced from Weinhaus & Roberts, 2005; Tortora & Grabowski, 2003).

2.1.1 Coronary arteries

The heart receives blood from coronary arteries (Figure 2.2). In the normal situation, the left and right coronary arteries arise from the left and right sinus of Valsalva (located at the proximal aorta), respectively. Left coronary artery (LCA) arises from the left aortic sinus as a single short main artery, the left main (LM) coronary artery (length of 0 to15 mm) which usually bifurcates to form the left anterior descending (interventricular) (LAD) artery and left circumflex (LCx) artery. In one third of the population, the LM ends as a trifurcation with an intermediate branch (also called ramus medianus), arising between the LAD and the LCx (Dewey, 2011a; Shah et al., 2009).

The LAD artery descends towards the apex in the anterior interventricular groove then anastomoses with the posterior descending (interventricular) artery (PDA), a branch of the right coronary artery (RCA). The major branches of the LAD artery are the septal and the diagonal branches. The LAD artery supplies the interventricular septum (anterior two-

thirds), the apex, and the anterior aspects of the left and right ventricles (Dewey, 2011a; Shah et al., 2009).

The LCx artery has a major branch, the left marginal artery (usually one to three are present), in around 10 to 15 % of the population. The LCx anastomoses with the RCA to give rise to the PDA. In general, the LCx artery supplies the posterior aspect of the left atrium and superior portion of the left ventricle (Dewey, 2011a; Shah et al., 2009).

The RCA arises from the right aortic sinus and has major branches such as the PDA (supplying the posterior one third of the interventricular septum and atrioventricular node), the nodal artery (supplying the right atrium and the sinoatrial node), and the right marginal artery (supplying a portion of the right ventricle, the inferior left ventricular wall, and the PDA). Finally, the coronary arteries branch into small arteries and arterioles. These vessels terminate in end arteries that supply the myocardial tissue with blood (Dewey, 2011a; Shah et al., 2009).

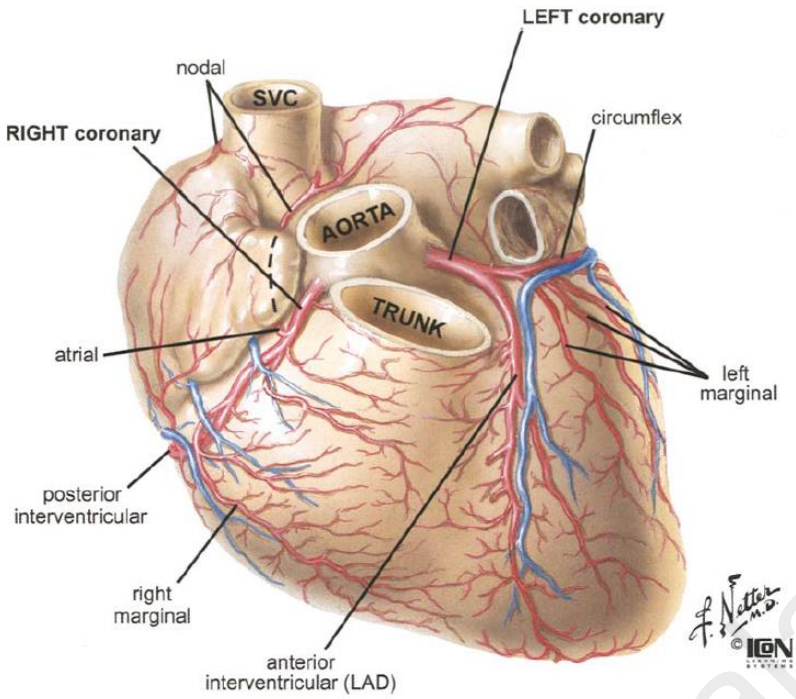

Figure 2.2: Vascular supply to the heart (reproduced from Weinhaus & Roberts, 2005).

The main coronary arteries (RCA, LAD and LCx) can be schematically seen as a "circle and half-loop" (Figure 2.3). The circle is formed by the RCA and the LCx artery which descend on the right and left atrioventricular groove, whereas the half loop is formed by the LAD artery and the PDA which descend on anterior and posterior interventricular groove (Kim et al., 2006).

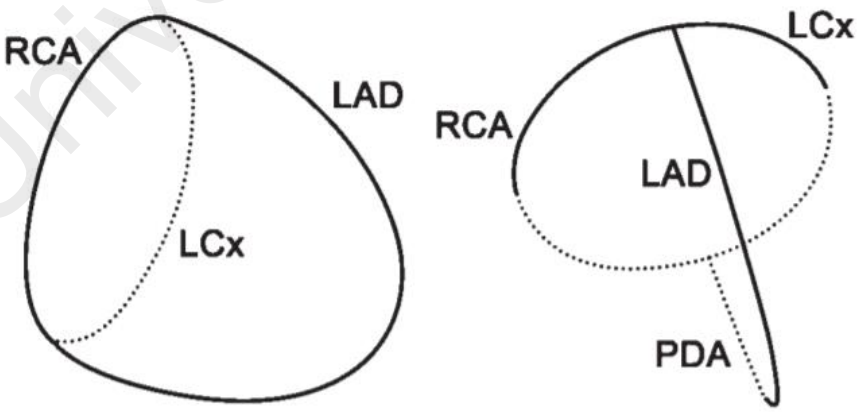

Figure 2.3: Diagrams illustrate the coronary artery anatomy (circle and half-loop model) (reproduced from Kim et al., 2006).

2.1.2 Cardiac cycle

A single cardiac cycle includes all the events within one heartbeat. In each cardiac cycle, the atria and ventricles alternately contract (systole) and relax (diastole), pushing blood from the areas of higher pressure to the areas of lower pressure. The myocardial contraction is regulated by an electrical conduction system. Electrical impulses begin in the sinoatrial node, located at the top of the right atrium, travel through the muscle fibres of the atria and ventricles, and cause them to contract in a coordinated fashion (Tortora & Grabowski, 2003).

Figure 2.4 shows ECG wave of a cardiac cycle. The cardiac cycle begins with the depolarisation of sinoatrial node (marked as the P wave in the ECG), then continues with the atrial depolarisation. Atrial depolarisation causes atria systole, which last for about 0.1 s. As the atria contract, it causes a higher pressure in the atria, and forces the blood to flow through the opened atrioventricular valves, into the ventricles (Tortora & Grabowski, 2003).

The QRS complex in the ECG marks the onset of ventricular depolarisation that causes ventricular systole, which lasts for about 0.3 s. While the ventricles are contracting, the atria are relaxed in atrial diastole. The pressures rises inside the ventricles, and pushes the blood up against the atrioventricular valves, forcing them to close, and prevent back flow of blood. Oppositely, the pulmonary and aortic valves open, allows ejection of blood from left ventricle into aorta, and from right ventricle into pulmonary trunk (Tortora & Grabowski, 2003).

The T wave in the ECG marks the onset of ventricular repolarization that causes ventricular diastole. As the ventricles relax, pressure within the chambers drops. Blood in the aorta and pulmonary trunk begins to flow backward, causing the pulmonary and aortic valves to close. During the relaxation period, the atria and ventricles are both

relaxed. This period lasts for about 0.4 second until the next cardiac cycle begins (Tortora & Grabowski, 2003).

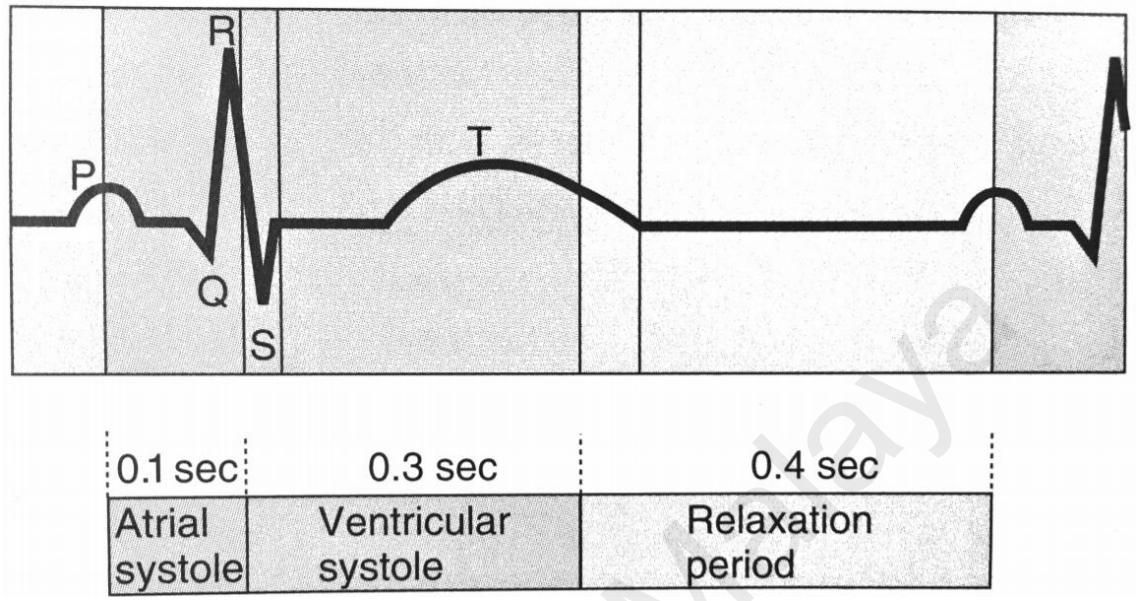

Figure 2.4: ECG wave of a cardiac cycle (reproduced from Tortora & Grabowski, 2003).

2.2 Coronary artery disease (CAD)

Clinical CAD is due to atherosclerosis, a process in which arteries become narrowed and hardened, due to gradual atherosclerotic plaque build-up in the inner lining of an artery. The word of "atherosclerosis" comes from the Greek words, "athere" (gruel) means focal accumulation and "sclerosis" (hardening) means thickening of intima (Mahmood, 2009). Clinically, atherosclerotic plaques defined as asymmetric focal thickenings of the intima. It is due to the accumulation of foamy macrophages, blood products, smooth muscle cells, lipids, collagen, necrotic debris, and calcium in varying quantities (Saremi & Achenbach, 2015).

Atherosclerosis is initiated in a coronary artery when the arterial wall is damaged, or the normal function of endothelium is interfered (Kinlay et al., 2001). It is usually due to the present of coronary risk factors, including high blood cholesterol, particularly increase in low-density lipoprotein (LDL) and decreased in high-density lipoprotein (HDL) cholesterol levels, hypertension, diabetes, smoking or genetics. These risk factors can be

further classified into two groups: the modifiable (high blood cholesterol, hypertension, smoking, obesity, sedentary life style, and stress) and unmodifiable risk factors (sex, family history, race, and genetics) (Galobardes et al., 2003; Manolio, 2003; Lee et al., 2001; Raitakari et al., 1999; Ridker et al., 1998; Levine et al., 1995; Kannel & McGee, 1979). Figure 2.5 shows the sequence of events in CAD.

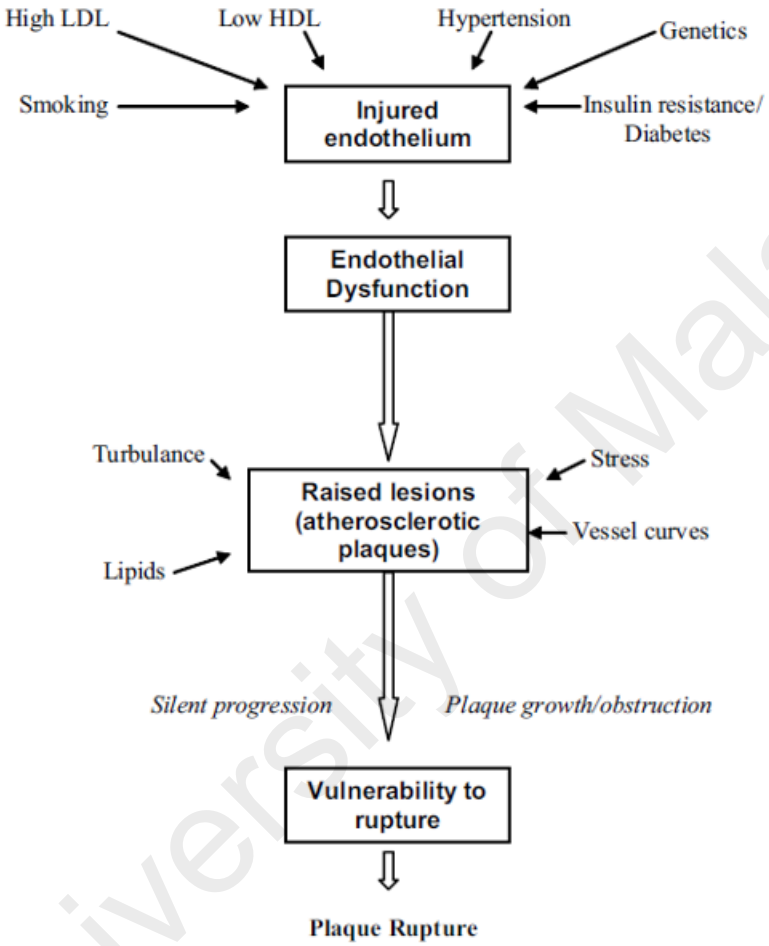

Figure 2.5: The sequence of events in CAD (reproduced from Mahmood, 2009).

Due to endothelium dysfunction, blood monocytes move to the subendothelium and differentiate into macrophages. These macrophages then digest the LDL and transform into foam cells, which form the early "fatty streak" in the intimal layer of vessel wall (Hansson, 2005). In these early stages, the lesions formed are classified as type I or type II, based on the American Heart Association (AHA) classification (Stary et al., 1995).

The next progression of atherosclerosis involves the pathologic intimal thickening (AHA type III), due to progressive lipid accumulation and proliferation of the smooth muscle cells. At this stage, the lesion is primarily consists of collagen matrix, smooth muscle cells, underlying lipid pool, foamy macrophages and microcalcifications. It may later progress to form an atheroma (AHA type IV), fibrolipid plaque, or fibroatheroma (AHA type V) (Mintz et al., 2001; Stary et al., 1995). One of the common characteristic of these lesions is the lipid or necrotic core which usually associated with some microcalcifications (Kolodgie et al., 2001). The lipid core is made of free cholesterol. It has a thick fibrous cap (more than 0.25 mm), consists of collagen matrix and smooth muscle cells (Virmani et al., 2006; Virmani et al., 2002). For AHA type V lesion, it is covered by a thinner fibrous cap, therefore it is also known as thin-cap fibroatheroma (TCFA). This TCFA is referred as "vulnerable" or high risk plaque, due to it's potential to rupture (Saremi & Achenbach, 2015; Virmani et al., 2002; Kolodgie et al., 2001).

In a case of endothelial erosion or plaque rupture, the lipid core material is exposed to the circulating blood, which lead to the activation and acceleration of blood coagulation process. Subsequently, partial or complete occlusion of vessel lumen (stenosis) may occurs, as a result of luminal thrombus formation (Saremi & Achenbach, 2015; Mahmood, 2009). As the occlusion of vessel lumen may impair blood supply to myocardium (acute myocardial ischemia), a plaque rupture may therefore results in acute coronary syndrome, which includes a spectrum of clinical conditions caused by acute myocardium ischemia, ranging from unstable angina (UA) to non-ST-segment elevation myocardial infarction (NSTEMI) and to ST-segment elevation myocardial infarction (STEMI). The later complications can be congestive heart failure, cardiac arrhythmias, or sudden death (Kumar & Cannon, 2009).

However, in most of the cases, the ruptured plaque follows a healing process without triggering any clinical conditions, and subsequently become more stable. This healing process involves extended plaque calcification (AHA type VI) and fibrosis (AHA type VII), which may associated with moderate to severe stenosis (Saremi & Achenbach, 2015; Virmani et al., 2006; Virmani et al., 2002; Kolodgie et al., 2001; Virmani et al., 2000; Stary et al., 1995).

2.2.1 Diagnosis of CAD

CAD has been reported to have a long asymptomatic latent period, hence the diagnosis of CAD can be either begins with the assessment of CAD risk in an asymptomatic patient, or pretest probability of significant CAD in a symptomatic patient (Taylor et al., 2010).

2.2.1.1 Assessment of CAD risk and pretest probability of CAD

The risk assessment of CAD in an asymptomatic patient involves the use of patient's risk-factor profile, which is a combined evaluation based on physiological, genetic, social and environmental factors. It is aimed to determine the appropriate lifestyle changes and pharmacological interventions to reduce a patient's risk of cardiac death. Several global risk scores, such as Framingham, Systematic Coronary Risk Evaluation (SCORE), Reynolds, or Prospective Cardiovascular Munster were developed to categorise patient risk as low, intermediate, or high. The calculated patient risk is an absolute risk, which is the probability of developing CAD, including myocardial infarction or cardiac death over a given time period, example over the next 10 years. One main limitation in this risk assessment is the use of strong population-based markers as risk factors for calculation. These risk factors provide poor individual discriminators for CAD. As a result, a cardiac event may not occur in an individual who has 1 or more risk factors (Earls et al., 2014).

One common symptom for CAD is chronic stable angina, an initial manifestation of CAD which occurs in approximately 50 % of CAD patient (Kannel & Feinleib, 1972).

Angina is due to the mismatch between oxygen demand and supply in myocardium, resulted by myocardial ischemia (Cassar et al., 2009). In these symptomatic patients, the pretest probability of CAD is calculated. Unlike risk assessment in asymptomatic patient, pretest probability presents the probability of a patient having CAD before any further diagnostic test is performed. It helps to determine the appropriateness of a particular diagnostic test for further CAD assessment (Taylor et al., 2010). A number of risk algorithms are available for the calculation of pretest probability, and categorise it as low, intermediate, or high (Morise et al., 1997; Pryor et al., 1993).

2.2.1.2 Imaging of CAD

It is generally believed that therapeutic intervention for atherosclerosis is most effective when started at an early stage of the progressive disease process (Stone et al., 2014). Recent advances in imaging technology have made it possible to detect subclinical coronary atherosclerosis (AHA type III onwards). Imaging examinations for evaluating CAD can be divided into two groups: noninvasive examination including chest radiography, coronary artery calcium scoring (CACS), CCTA, cardiac magnetic resonance imaging (CMR), myocardial perfusion scintigraphy (MPS), and echocardiography; invasive examination including ICA, intravascular ultrasound (IVUS) and optical coherence tomography (OCT). The appropriateness of an imaging examination for assessment of CAD is determined based on the calculated CAD risk in asymptomatic patient, or pretest probability of significant CAD in symptomatic patient (Earls et al., 2014) (Table 2.1). Figure 2.6 shows imaging assessment of CAD correspond to the progression of disease.

Table 2.1 The appropriateness and imaging details for CAD assessment using different noninvasive and invasive imaging examination (Earls et al., 2014) .

Imaging examination	Appropriateness for CAD assessment	Imaging details
Noninvasive		
Chest radiography	It is used in asymptomatic individuals as part of a routine or pre-surgical examination.	It allows detection of abnormalities of the lungs and thorax, cardiomegaly, coronary calcium, or serve as a baseline for future follow-up.
Coronary artery calcium scoring (CACS)	It is recommended for asymptomatic, intermediate-risk patients, and in low-risk patients who had a family history of premature CAD.	It allows visualization of coronary calcification.
Coronary computed tomography angiography (CCTA)	It is indicated for evaluation of coronary arteries in patients with new onset heart failure to assess etiology, symptomatic patients at intermediate pretest probability of CAD and patients with angina regardless of acute or chronic with interpretable stress test. Currently, it is not recommended in asymptomatic patients.	It allows assessment of coronary lumen patency, the arterial wall, calcified, mixed and non-calcified plaques, and ventricular function.
Cardiac magnetic resonance imaging (CMR)	It is indicated for symptomatic patients. Currently, there is no consensus guideline recommended on the use of MRI in asymptomatic patients.	It allows evaluation of cardiac anatomy and ventricular function. It has been reported as an excellent imaging technique for the detection of myocardial ischemia and myocardial infarction.
Myocardial perfusion scintigraphy (MPS)	It is indicated for risk assessment in asymptomatic patients who have diabetes or a strong family history of congenital heart disease and patients with previous risk assessment suggested a high risk of CAD, such as a CACS more than 400.	It is a useful method for detection of silent myocardial ischemia.

'Table 2.1, continued'

Imaging examination	Appropriateness for CAD assessment	Imaging details
Echocardiography	It is indicated for the screening of high risk asymptomatic patients, but not for cardiovascular risk assessment in low- or intermediate-risk asymptomatic patients.	It allows detection of myocardial ischemia.
Invasive		
Invasive coronary angiography (ICA)	It is recommended for risk stratification in symptomatic patients at high pretest probability of CAD, in patients with typical angina and a reduced left ventricular ejection fraction.	It is currently gold standard for the assessment of coronary stenosis.
Intravascular ultrasound (IVUS)	It is used as additional step during ICA.	It is currently gold standard for plaque quantification.
Optical coherence tomography (OCT)	It is used as additional step during ICA.	It allows plaque quantification.

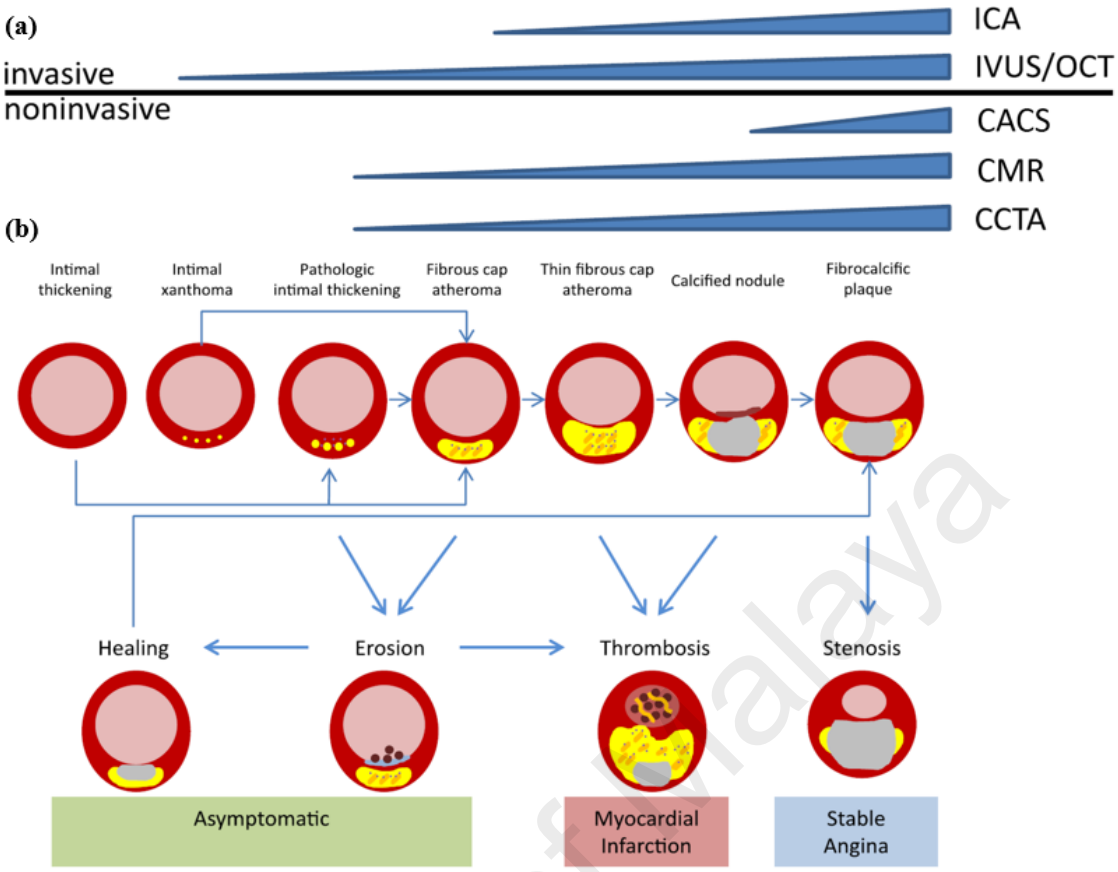

CACS, coronary artery calcium scoring; CCTA, coronary computed tomography angiography; CMR, cardiac magnetic resonance imaging; ICA, invasive coronary angiography; IVUS, intravascular ultrasound; OCT; optical coherent tomography

Figure 2.6: (a) Imaging assessment for CAD, (b) progression of disease (reproduced from Sandfort et al., 2015).

CACS is a noninvasive screening technique for coronary calcification, scanned using a multi-detector row CT (MDCT) scanner. The calculated calcium score is a proven marker for coronary atherosclerosis. It is useful for the stratification and reclassification of CAD risk as it provides incremental prognostic information and more accurate risk assessment, compared to traditional risk factor evaluation (Polonsky et al., 2010; Arad et al., 2005). The most common method to quantify calcium in CACS is the Agatston calcium score, which focuses on the calcified plaque component. However, CACS unable to quantify vascular stenosis. Several guidelines have recommended the usage of CACS in asymptomatic, intermediate-risk patients, and in low-risk patients who had a family history of premature CAD (Earls et al., 2014; Ferket et al., 2011; Taylor et al., 2010).

Unlike CACS, the contrast-enhanced examination, CCTA is currently not recommended in asymptomatic patients, primarily due to higher radiation dose, the use of nephrotoxic contrast medium and added cost. Studies have reported the incremental prognostic value of CCTA, compared with a baseline clinical risk model plus CACS. CCTA allows noninvasively assessment of the coronary lumen patency, arterial wall, calcified, mixed and non-calcified plaques, and ventricular function. In symptomatic patients, CCTA can be used to independently predict future events, and improve risk stratification beyond traditional scoring methods (Earls et al., 2014). Currently, CCTA is indicated for evaluation of coronary arteries in patients with new onset heart failure to assess aetiology, symptomatic patients at intermediate pretest probability of CAD and patients with angina regardless of acute or chronic with interpretable stress test (Taylor et al., 2006).

2.3 Coronary computed tomography angiography (CCTA)

Although the use of CCTA in asymptomatic patients remains controversial, but it has the potential to provide useful data beyond what is derived from CACS (Earls et al., 2014). In symptomatic patients, numerous studies have confirmed CCTA as a reliable tool to rule out CAD. The high sensitivity of CCTA reduces unnecessary ICA in symptomatic patients who do not have CAD (Zeb et al., 2014; Dewey, 2011a).

As a contrast-enhanced examination, CCTA involves several steps, including patient preparation, image acquisition, contrast medium administration and image reconstruction (Dewey, 2011c; Weigold, 2006). Figure 2.7 shows the steps in performing CCTA examination.

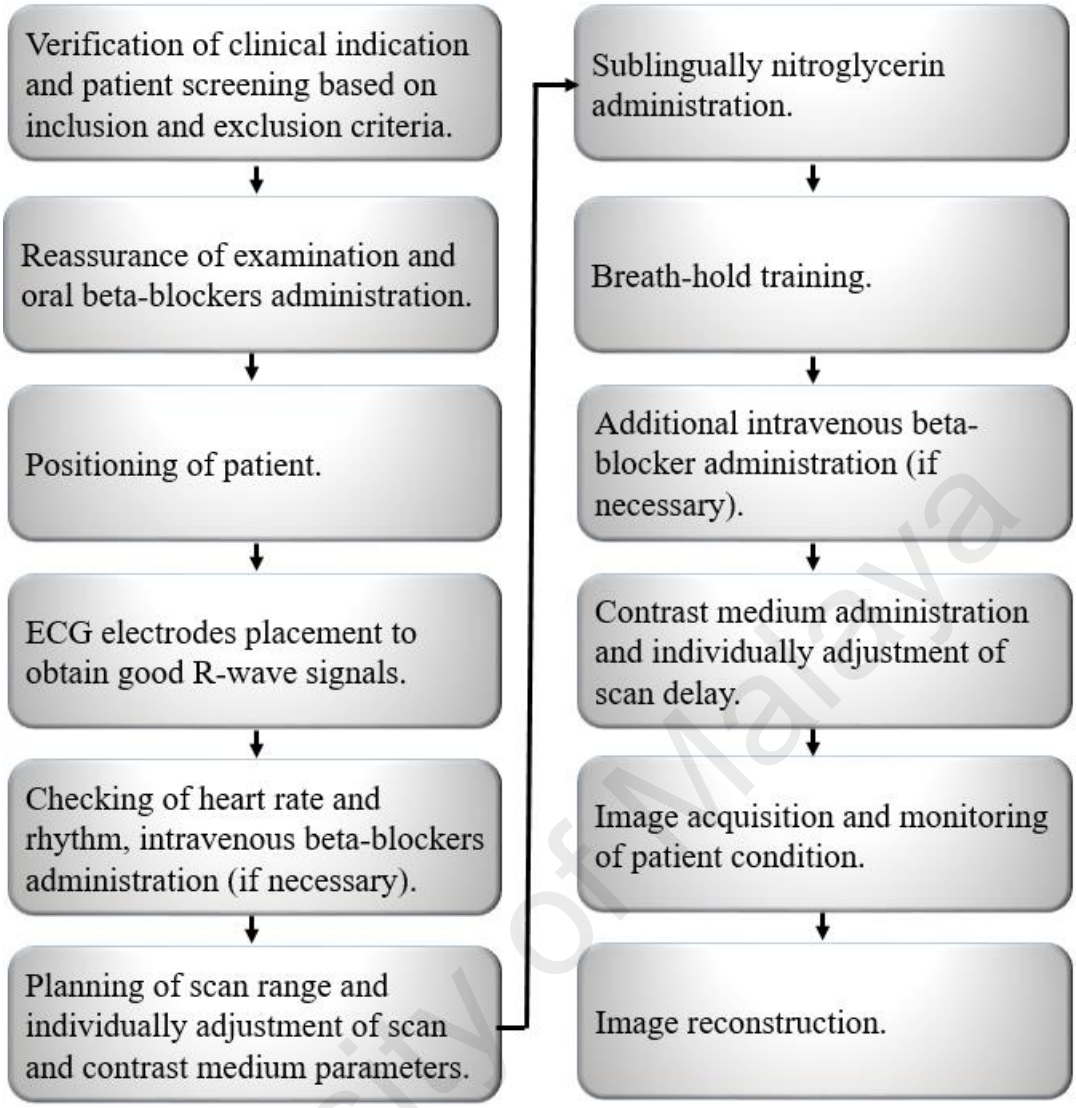

Figure 2.7: Steps in performing coronary computed tomography angiography (CCTA) (adapted from Dewey, 2011c; Weigold, 2006)

2.3.1 Patient preparation

Patient preparation plays an important role in performing an effective CCTA. Inadequate patient preparation can influence all the subsequent steps, and in the end, affect the diagnostic result of the study. An optimal patient preparation for CCTA examination includes patient selection, pharmacological management, the delivery of explicit patient instructions and patient positioning for scanning (Maffei, Martini, et al., 2012).

The process of patient selection begins with the verification of clinical indication by operator, to make sure that the examination is performed based on correct indications. It continues with the patient screening based on inclusion and exclusion criteria. The inclusion criteria are low heart rate (preferably equal or lesser than 70 bpm), spontaneous or induced by beta-blockers and ability to maintain breath-hold for a period compatible with the scan time. These criteria aim to avoid motion artefacts caused by the cardiac and respiratory motion. Beta-blockers is widely used in CCTA studies to reduce the heart rate and to make the cardiac rhythm more regular (Pannu et al., 2006). It is usually given orally about 1 hour before the scanning, or intravenously administrated for a rapid onset and shorter duration of action (Dewey, 2011b). Patients with known allergies to iodinated contrast medium, renal insufficiency (serum creatinine more than 120 $mmolL^{-1}$), pregnancy, respiratory failure, unstable clinical conditions and severe heart failure are excluded from CCTA examination (Unal et al., 2015; Maffei, Martini, et al., 2012).

A well-trained nurse, physician assistant, technician, or a physician will discuss the entire procedure with the patient, obtain written informed consent and provide explicit instructions to the patient before scanning. A patient who scheduled for CCTA examination need to nil by mouth for at least 4 hours before the scan but they are encouraged to drink water to avoid dehydration. Sildenafil or similar medications should

be stopped for at least 48 hours before the examination, as it may interact with the nitroglycerin, and result in serious hypotension. In patients with abnormal renal function, metformin-containing medications need to be discontinued for at least 48 hours to avoid lactic acidosis due to acute renal failure (Dewey, 2011c; Weigold, 2006).

During the patient positioning, patient is in supine position with the arms above head on CT table (Figure 2.8 (a)). In order to make sure the heart is positioned as close to the centre of the gantry, it is necessary to slightly shift the patient to the right side of the table. ECG electrodes are placed to identify R-wave signals for ECG triggering during scanning. Figure 2.8 (b) shows the location of ECG lead attachments for CCTA examination. The number and preferred location of ECG leads depend on scanner type and design. ECG leads should be attached outside scan range to avoid artefacts from the ECG electrodes and cables. After placement of ECG leads, breath-hold training on the table is performed to determine whether a patient is able to hold his or her breath for the scan duration (Dewey, 2011b).

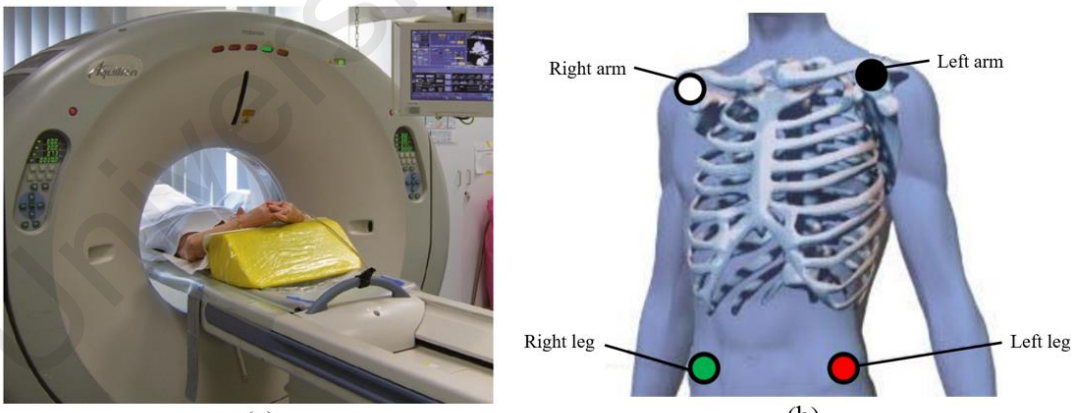

Figure 2.8: (a) Patient positioning, (b) location of ECG lead attachments for CCTA (modified from Dewey, 2011b).

Furthermore, sublingual nitroglycerin is given to patient before scanning, to dilate the coronary arteries. It facilitates image interpretation and to produce comparable results with cardiac catheter examination. The onset of action of sublingual nitroglycerin is about

10 to 20 s after administration, and its effect lasts for about 10 minutes (Kang, 2015; Dewey, 2011b).

2.3.2 Image acquisition

The image acquisition of CCTA consists of three main steps: (1) scan projection radiograph (SPR) or topogram; (2) test scan that used to determine the adequate initiation of image acquisition; and (3) CCTA scan. A low-radiation-dose SPR is acquired as the first step. It is used for planning of the scan range in the later scan (Hoffmann et al., 2006). In most cases, after SPR, prior to CCTA scan, a CACS is performed with prospective triggering and without contrast medium administration, typically using 3 mm slice collimation. The acquired images can helps in reducing radiation exposures by allowing exact determination of the scan range required for subsequent CCTA (Dewey, 2011b).

In the second step, two techniques are available for performing test scan to determine the adequate initiation of image acquisition: the test bolus and bolus tracking. For test bolus technique, a small bolus (10 to 20 mL) of contrast medium is injected at the same injection rate as the full bolus in CCTA scan. Immediately after the injection, a series of low-radiation-dose sequential images are acquired at the level of ascending aorta (AA). Then, by placing a region of interest (ROI) in the AA, the CT attenuation value (measured in HU) is measured in each sequential image and a time-attenuation curve is produced. From this time-attenuation curve, the TTP, which is the time needed to reach the PCE for the test bolus is determined (Saade et al., 2011; Weininger et al., 2011; Bae, 2010). Although TTP is commonly used as scan delay in CCTA with single-detector CT scanner, additional delay should be added when CCTA is performed with a fast MDCT scanner. It is to prevent the condition of scanning too early before maximum enhancement is reached. This additional delay should be added by considering the scan time and the injection duration of contrast medium (Bae, 2010, 2005; Cademartiri et al., 2004).

Unlike test bolus, no test injection of contrast medium is required in the bolus tracking technique. It is based on real-time monitoring of the full bolus during injection with acquisition of a series of dynamic low-radiation-dose monitoring scans, at the level of AA. A trigger threshold and a post trigger delay are set prior to the scan. Once the contrast medium arrives or after the trigger threshold is exceeded, scanning will be started manually or automatically after the post trigger delay (Saade et al., 2011; Weininger et al., 2011; Bae, 2010; Birnbaum et al., 1999).

In the third step, which is the CCTA scan, image acquisition is performed to cover the entire heart from the proximal AA (10 to 20 mm below the carina) to the diaphragmatic surface of the heart, typically 120 to 150 mm in scan length. In a single breath-hold during comfortable inspiration, the scan is acquired with injection of a high iodine concentration contrast medium (300 to 400 $mgmL^{-1}$) at an injection rate of 4 to 6 mLs^{-1} (Mahesh & Cody, 2007; Hoffmann et al., 2006).

2.3.3 Image reconstruction

The source images of CCTA are usually reconstructed in axial plane with a medium smooth reconstruction kernel at slice thickness of 0.75 mm and pixel matrix of 512 × 512. For evaluation of coronary stents, a sharper reconstruction kernel is used (Hoffmann et al., 2006).

For interpretation and reporting purposes, five additional image reconstructions are performed: (1) multiplanar reformations (MPR) in coronal and sagittal (orthogonal) planes; (2) curved MPR; (3) maximum-intensity projections (MIP); (4) angiographic emulations; and (5) three-dimensional volume-rendering techniques (VRT). The MPR images have a spatial resolution similar to that of the axial images. Hence, the axial and MPR images are considered as the primary source of information, any conclusions and final diagnoses should be based on these images (Kroft & Dewey, 2011).

The other reconstructions such as curved MPR, MIP, angiographic emulations and VRT tend to reduce the information content and may even obscure relevant information. Based on the centreline along the coronary vessel path, the curved MPR shows large parts of the coronary lumen in a single image. By demonstrating the coronary lumen around its longitudinal axis, estimation of the severity of stenosis can be easily performed with these images. It also facilitates the quantification of the percentage of stenosis (based on reference and stenosis diameters) (Kroft & Dewey, 2011). MIP gives an overview of vessel continuity and course in a single image, but it tends to obscure stenosis and cause overestimation of calcified lesions. Angiographic emulations and VRT are more elegant ways to display and present the findings, but these three-dimensional reconstructions are not recommended to be used alone for diagnosis due to the abovementioned limitations (Kroft & Dewey, 2011).

In addition to quantification of the severity of stenosis, measurement of coronary bifurcation angle formed by two main coronary branches, the LAD and LCx arteries can be performed using MPR and VRT images. This bifurcation angle was reported to be strongly related to the development of CAD and can be used for the prediction of significant coronary stenosis (Cui et al., 2017; Xu & Sun, 2015; Sun, 2013; Van Mieghem et al., 2007). In a study conducted by Givehchi et al. (2018), the authors compared the accuracy of bifurcation angle measurement using MPR and VRT images. MPR technique was found to be more accurate and less sensitive to operator subjectivity.

2.4 Retrospectively ECG-triggered and prospectively ECG-triggered CCTA

Currently, two image acquisition techniques are commonly used in CCTA; retrospectively ECG-triggered and prospectively ECG-triggered. Both retrospectively ECG-triggered and prospectively ECG-triggered techniques are characterised based on

its scanning mode, helical and sequential, respectively (Sun, 2012b; Mahesh & Cody, 2007).

In retrospectively ECG-triggered technique, the helical scanning mode allows the CT table to move continuously through the gantry in the z-direction while the X-ray tube and detectors rotate 360° around the patient. ECG signals are monitored continuously and the scan is acquired continuously (simultaneously) (Figure 2.9) (Mahesh & Cody, 2007). This technique allows scanning of patient with high heart rate of more than 85 bpm (Meyer et al., 2017). As the data are acquired throughout the cardiac cycle, it is possible to reconstruct the optimal images by selecting the data with lesser motion during the cardiac cycle (Mahesh & Cody, 2007).

The main limitation of retrospectively ECG-triggered technique is the increase of radiation dose as the data are acquired throughout the cardiac cycle, but partial data are actually used in the final image reconstruction. In helical scanning mode, the overlapping of X-ray beam is determined by a pitch factor. This pitch factor is defined as the ratio of table increment per gantry rotation to the total X-ray beam width. A pitch factor of less than 1 imply overlapping of the X-ray beam and higher patient dose; pitch factor of greater than 1 imply a gapped X-ray beam and reduced patient dose. Since CCTA requires a low pitch factor for achieving a minimal data gaps in the scan projection data, radiation dose to the patients is increased (Mahesh & Cody, 2007).

Prospectively ECG-triggered technique is similar to the conventional CT “step and shoot” method, where CT table is being stationary while the X-ray tube and detectors rotate 360° around the patient, to acquire data from different angular positions or projections. The scan is triggered by ECG signal which is called a partial-scan technique (Figure 2.9). This technique allows acquisition of data in a certain phase of cardiac cycle when cardiac motion is minimal, preferably in the mid-diastolic phase. Thus, projection

data are acquired for only part of the complete gantry rotation (Sun, 2012b; Mahesh & Cody, 2007).

As temporal resolution is referred to the time taken to collect the complete data set required to construct a complete CT image in axial plane, the minimum amount of data is 180° of gantry rotation plus the fan angle of the CT detector. The best temporal resolution that can be achieved in the partial-scan technique is slightly greater than half of the gantry rotation time. Once the desired data are acquired, the CT table is translated to the next position and the scanner acquires more projections. This cycle repeats until the entire scan length is covered (Sun, 2012b; Mahesh & Cody, 2007).

One of the advantages of prospectively ECG-triggered technique is reduction of radiation exposure as the projection data are acquired for short periods and not throughout the cardiac cycle (Sun, 2012b; Mahesh & Cody, 2007). However, it also comes with several limitations. Firstly, it is strictly limited to patient with regular and low heart rate (equal or lesser than 70 bpm). Heart rate changes such as arrhythmia can cause incorrect estimation of the R-R interval. A better temporal resolution is required when patient has higher heart rate. Secondly, it is usually restricted to non-overlapping scanning or slice increments with a small overlap. As the scan time to cover the heart volume is directly proportional to the slice increment, a longer scan time is required. There is a high risk of misalignment when acquiring images of the entire heart with 4 to 5 heart beats. Furthermore, cardiac images are acquired during only a small portion of the R-R interval, any patient movement during the acquisition will causes inconsistency of data obtained among different projections, resulting in stair-step artefact, which causes image degradation with limited diagnostic value. A greater z-axis coverage of CT scanners is required to solve this problem. Lastly, it is impossible to have functional information

about cardiac valve or ventricular wall with the limited data acquired (Sun, 2012b; Mahesh & Cody, 2007).

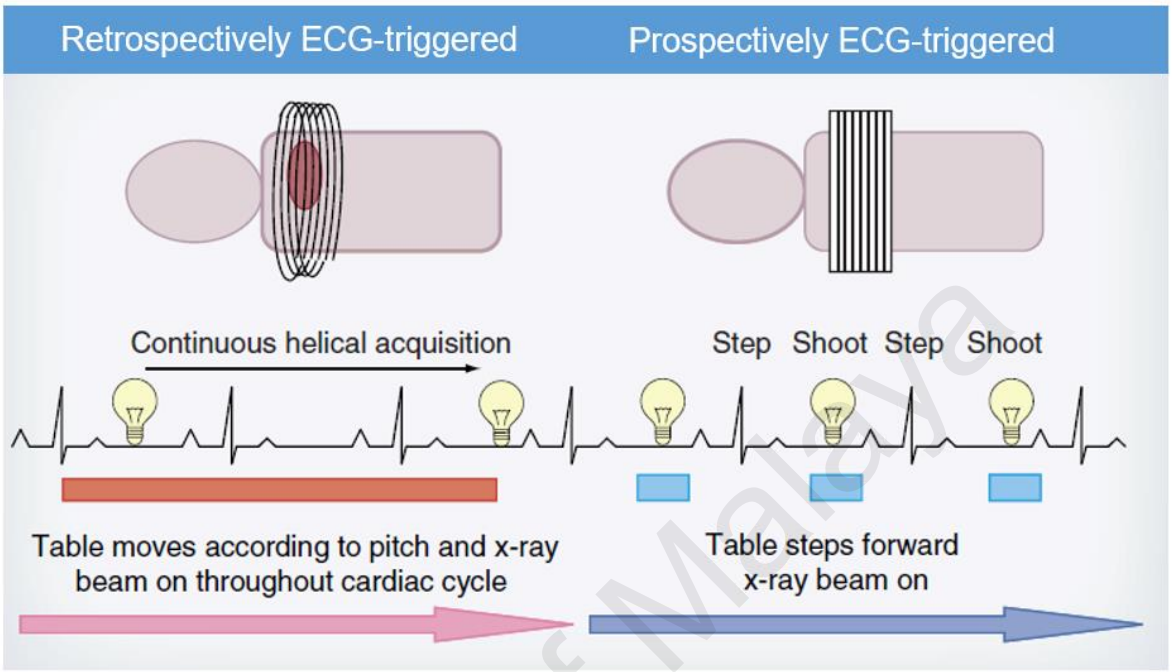

Figure 2.9: Retrospectively ECG-triggered image acquisition technique with helical mode and prospectively ECG-triggered image acquisition technique with "step and shoot" or sequential mode (reproduced from Small et al., 2012).

A few strategies have been suggested to overcome the limitations of both retrospectively and prospectively ECG-triggered image acquisition techniques. These includes ECG-controlled tube current modulation in retrospectively ECG-triggered CCTA and padding in prospectively ECG-triggered CCTA (Figure 2.10). For ECG-controlled tube current modulation in retrospectively ECG-triggered CCTA, the tube current is raised to the nominal level during a limited interval in the diastolic phase, where data are most likely to be reconstructed. Then, for the remaining part of the cardiac cycle, a low tube current (20 % of normal tube current) is applied for patient dose reduction (Figure 2.10 (d)) (Sabarudin & Sun, 2013a; Jakobs et al., 2002). For padding in prospectively ECG-triggered CCTA, it involves adding of surrounding X-ray beam time to the mid-diastolic window that allow assessment of the heart in several phases of cardiac

cycle, with the cost of substantial increase in patient dose (Figure 2.10 (b)) (Labounty et al., 2010).

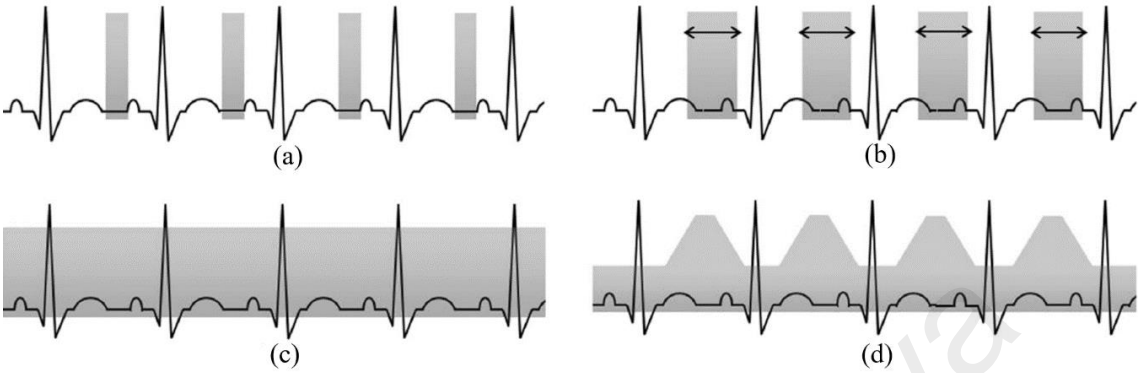

Figure 2.10: ECG-triggered techniques; (a) prospectively ECG-triggered, (b) prospectively ECG-triggered with padding, (c) retrospectively ECG-triggered and, (d) retrospectively ECG-triggered with tube current modulation; The tall grey bar represents diagnostic levels of radiation (reproduced from Harden et al., 2016).

2.5 Contrast medium administration in CCTA

During CCTA scan, the iodinated contrast medium usually administrated intravenously via median cubital vein, located at median position of the arm (Figure 2.11). Contrast medium flows through the injection vein into the superior vena cava, enters the right atrium, passes through the pulmonary circulation and finally arrives in the aorta. The mixing of contrast medium and blood starts at right atrium and completes in the right ventricle. Once the contrast-enhanced blood arrives at the proximal aorta, it enhances the coronary arteries during an arterial phase and enters into the coronary veins during portal venous phase. The veins then join into coronary sinus which drains into the right atrium, then the contrast-enhanced blood flows back to right heart and the recirculation effects occur. The contrast medium is excreted from the body via the kidneys and the excretion rate is controlled by the glomerular filtration rate (Prokop & Van der Mollen, 2011; Bae, 2010).

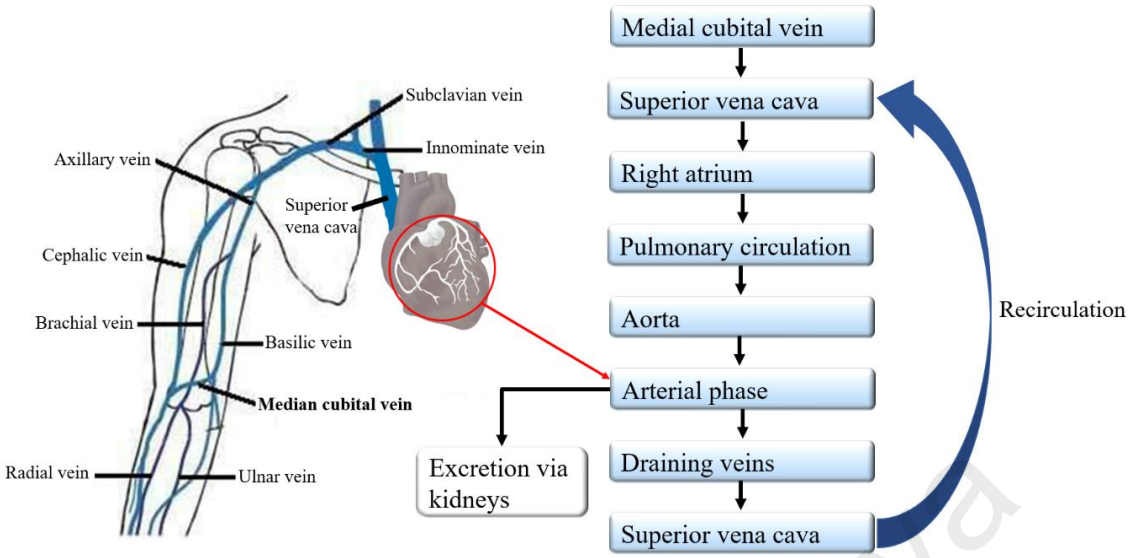

Figure 2.11: The flow of contrast medium for coronaries enhancement during CCTA (Prokop & Van der Mollen, 2011; Bae, 2010).

Four main contrast medium administration protocols have been used in CCTA: uniphase, biphase, triphase and exponentially-decay. Before the introduction of dual-syringe power injector, administration of an undiluted contrast medium at a constant injection rate (uniphasic protocol) was a common practice. The streak and beam-hardening artefacts caused by the remaining contrast medium in brachiocephalic veins during image acquisition is one of the main limitation of uniphasic protocol (Numburi et al., 2007; Bae, 2003; Cademartiri et al., 2002).

With the availability of dual-syringe power injector, biphasic protocol was introduced. It consists of two boluses: an initial undiluted contrast medium, followed by a saline flush that usually injected at the same injection rate as the contrast medium. Studies have reported the possibility of achieving equivalent VCE at a reduced contrast volume with a saline flush (Haage et al., 2000; Hopper et al., 1997). The saline flush reduces the residual contrast medium in the tubing from power injector and the venous system, resulted in a higher PCE (Saade et al., 2011; Bae, 2010). It also allows reduction of streak and beam-hardening artefacts caused by the undiluted contrast medium in peripheral veins, the right atrium and ventricle of the heart (Bae, 2010).

A modified biphasic protocol, which is known as biphasic-concentration protocol was introduced later. It utilizes two boluses, each consisting of a different contrast concentration: an initial undiluted contrast bolus, followed by a diluted contrast bolus. This protocol has been reported to be useful in reducing the artefacts caused by undiluted contrast medium in the superior vena cava. However, with this protocol, there is a risk of low or completely no enhancement in the right ventricle. The right ventricle enhancement is crucial for visualization of the ventricular septum or pathologic abnormalities, such as thromboembolisms or tumours (Weininger et al., 2011).

Currently, the most commonly used contrast medium administration protocol is triphasic protocol. This protocol utilizes three distinct boluses: an initial undiluted contrast bolus, followed by a contrast medium-saline mixture injected at the same injection rate as the first bolus, and completed by a saline flush. A power injector capable of simultaneous contrast medium and saline injection is required to produce a mixture of contrast medium and saline during the middle phase. Study has reported a 32 % higher enhancement of right ventricle in triphasic protocol compared to biphasic protocol (Kerl et al., 2008).

Bae et al. (2004) investigated a multiphasic protocol with an exponentially decelerating injection. The author reported that uniform and prolonged VCE can be achieved in exponentially-decay protocol. As this protocol required longer scan time, it is less preferable in the clinical practice (Weininger et al., 2011; Bae et al., 2004).

2.6 CT technology in CCTA

Due to rapid motion of the heart and the imaging of small structures, CCTA is considered as the most challenging clinical applications in CT. Recent developments in CT scanner have focused in addressing these challenges, particularly in improving the

spatial resolution, temporal resolution and z-axis (longitudinal) coverage (Lewis et al., 2016).

2.6.1 Spatial resolution

The evaluation of coronary stenosis requires accurate imaging of small structures. There is a large difference in the luminal diameter of coronary arteries, for instance, 4.5 mm in LM artery to 1.9 mm in the distal LAD in normal male adult (Dodge et al., 1992). Thus, a submillimetre and isotropic spatial resolution in three dimensions (x,y and z) is key requirement in CCTA (Figure 2.12).

CT spatial resolution refers to the ability to separate two structures. It is scientifically determined by measuring the ability of a CT system to separate the line pairs (Judy, 1976). The voxel size has become the main parameter for spatial resolution as the smaller the voxel size, the better the spatial resolution. Voxel size is depended on the size of pixel (field of view (FOV) divided by the image matrix) and detector (detector z-axis dimension) (Sprawls, 1992). Pixel size determines the xy-axis resolution, whereas the detector size is a major determinant of the resolution in z-axis, together with the interpolation algorithm, sampling frequency and detector design (Lewis et al., 2016).

The thinnest detector size in the current top-end CT systems ranged from 0.5 to 0.625 mm (Mahesh & Cody, 2007). With double z-sampling or z-flying focal technique, the z-axis resolution is further improved to less than 0.3 mm. In this technique, a flying focal spot of the X-ray tube is used with two focal spot positions for the same projection angle, shifted by half the detector size. This doubles the number of data points within the plane without a dose increase as only half the dose is applied for each projection (Flohr et al., 2005).

With isotropic spatial resolution of less than 0.3 mm, it is possible to produces a uniform image quality in all dimensions which improve the multiplanar and three-dimensional imaging. Furthermore, the reduction of partial volume effect in axial (x-y) plane further improves the contrast resolution. These allow differentiation of a 10 to 20 % coronary stenosis (Lewis et al., 2016). However, this resolution is still generally considered insufficient for quantitative assessments of coronary stenosis with high confidence, especially at the distal segment of the coronary arteries, compared to ICA which has a spatial resolution of approximately 0.16 mm (Otero et al., 2009).

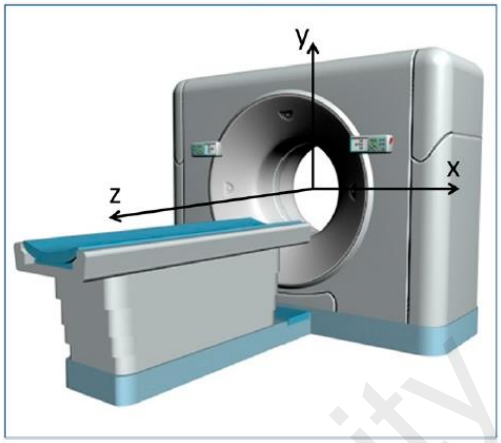

Figure 2.12: The co-ordinate system used in CT scanning (reproduced from Lewis et al., 2016).

2.6.2 Temporal resolution

Temporal resolution refers to the time needed to acquire the minimum amount of data (180° of gantry rotation plus the fan angle) for image reconstruction. It is corresponds to approximately half of the gantry rotation time (Mahesh & Cody, 2007).

Due to the rapid and complex movement of the coronary arteries throughout the cardiac cycle, a good temporal resolution is another crucial requirement for CCTA. Superior temporal resolution improves the ability to freeze cardiac motion. For majority of the current single source CT (SSCT) scanners with gantry rotation time of 250 to 350 ms, the temporal resolution is ranged from 125 to 175 ms. These temporal resolution are generally adequate for patients with regular and low heart rate (less or equal to 70 bpm).

However, for patient with higher heart rate and contraindicated for beta-blocker, a better temporal resolution is needed (Lewis et al., 2016).

One of the methods to improve temporal resolution is by applying multi-segment reconstruction in retrospectively ECG-triggered CCTA. Instead of acquired the scan projection data from a single cardiac cycle, the multiple-segment reconstruction acquires the data from several cardiac cycles and directly improve the temporal resolution. For example, consider a SSCT with 350 ms gantry rotation time. In single-segment reconstruction, the images are reconstructed with 175 (350/2) ms temporal resolution from one R-R interval. In two-segment reconstruction, the same slice of images is reconstructed from projections data over two R-R intervals. Thus, only half the data is required per R-R interval, and the temporal resolution is further improved to 87.5 (175/2) ms. This method successfully reduce motion artefacts but associated with increase of patient dose and a longer exposure time as the number of segments increases (Lewis et al., 2016; Otero et al., 2009).

In an attempt to improve temporal resolution and reduce radiation exposure to patient, DSCT scanner (Somatom Definition DS, Siemens Healthcare, Forchheim, Germany) was introduced. With the two X-ray tubes and two detectors mounted at orthogonal orientations in the gantry, the transmission data required for the reconstruction of one slice image can be acquired in half of the time needed by a SSCT (Johnson et al., 2006). The temporal resolution is further improved (approximately 75 to 83 ms) as only one quarter of a gantry rotation (90°) is needed for image reconstruction in DSCT (Figure 2.13) (Lewis et al., 2016; Cademartiri et al., 2013).

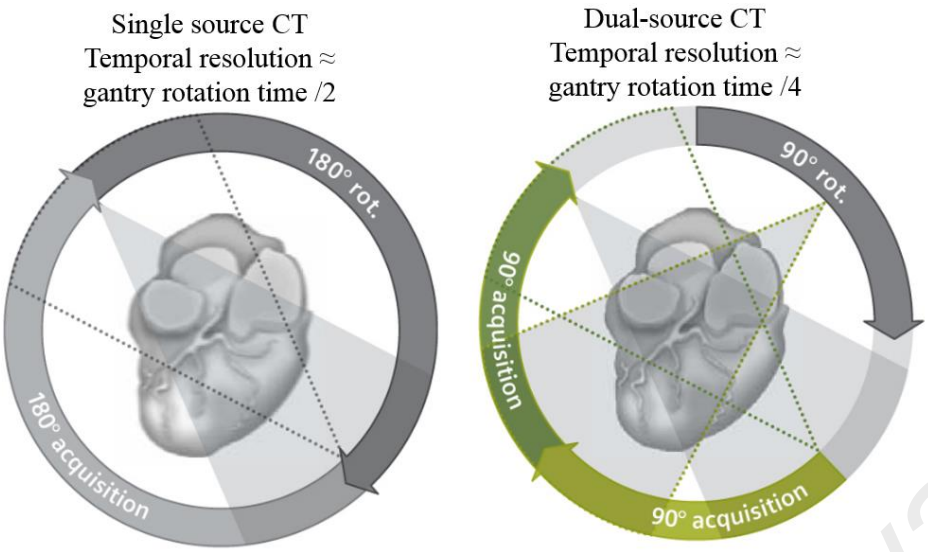

Figure 2.13: Temporal resolution in SSCT and DSCT (reproduced from SIEMENS Healthineers, 2016).

2.6.3 z-axis coverage

Typically, a scan length of 120 to 150 mm is required to cover the entire heart in CCTA (Hoffmann et al., 2006). Majority of current, top-end CT scanners come with z-axis detector length that is shorter than this. It is impossible to cover the whole cardiac volume within a single gantry rotation using these CT scanners. Thus, the coverage of cardiac anatomy is acquired with a series of slabs over several cardiac cycles. The risk of motion and stair-step artefacts due to misregistration between acquired slabs increase as the scan time increase, particularly in CT scanners with limited z-axis coverage (Lewis et al., 2016). Figure 2.14 shows detector array design and z-axis coverage for MDCT scanners from different CT manufacturers.

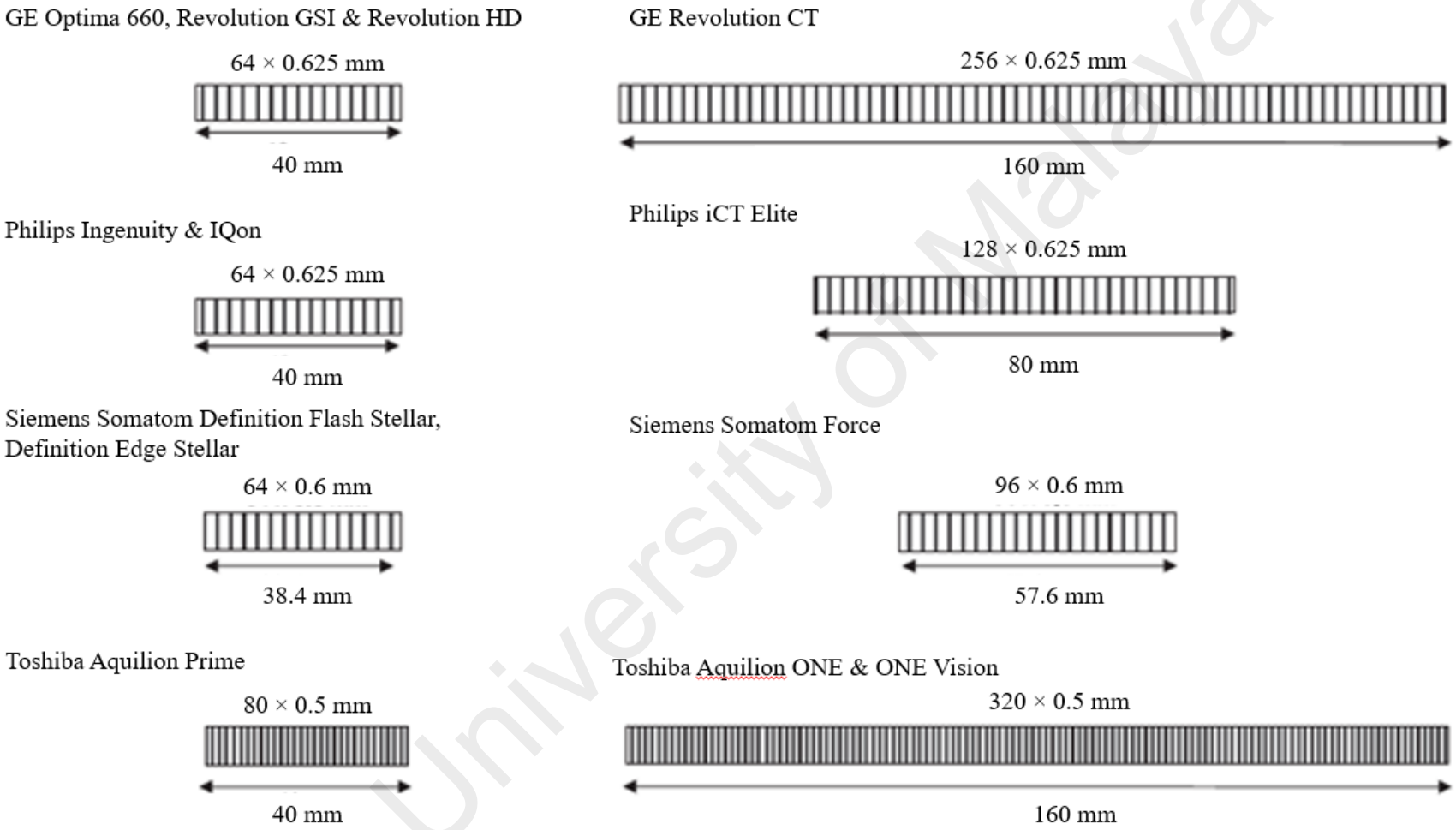

Figure 2.14: Detector array design and z-axis coverage for MDCT scanners from different CT manufacturers (reproduced from Lewis et al., 2016).

In order to improve z-axis coverage, two different methods were introduced by CT manufacturers: invention of CT scanners with a greater z-axis detector length and DSCT that enables a helical scan to be performed with a very high pitch factor (more than 3.0). CT scanners with a greater z-axis detector length enables coverage of entire heart in a single R-R interval or cardiac cycle and a single gantry rotation, without any table movement (Figure 2.15). The largest z-axis coverage to date is 160 mm with a 256 × 0.625 mm (Revolution CT, GE Healthcare, Milwaukee, WI) or 320 × 0.5 mm (Aquilion One and Acquilion One Vision, Toshiba Medical Systems Corporation, Otawara, Japan) detector configuration (Figure 2.14).

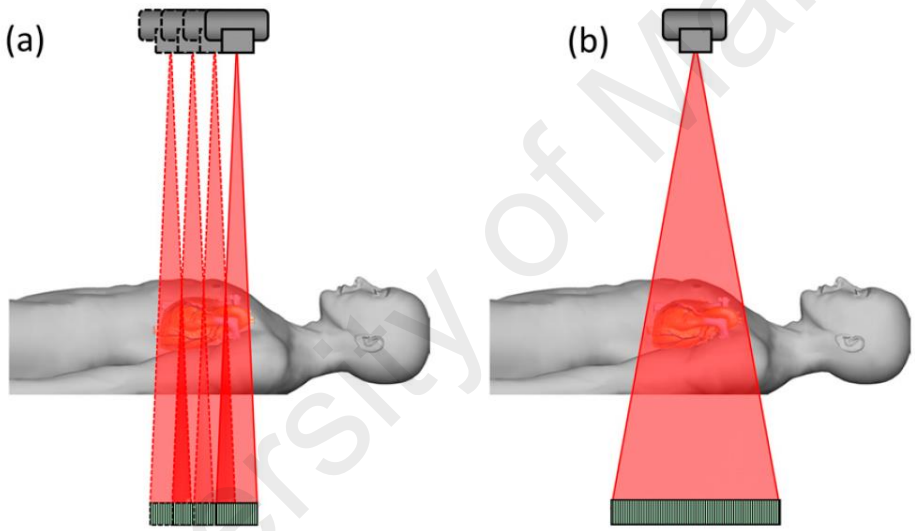

Figure 2.15: a) In CT scanners with limited z-axis coverage, several gantry rotations are required to cover the entire cardiac anatomy; (b) CT scanners with a wider z-axis coverage can acquire the full cardiac anatomy in a single cardiac cycle and gantry rotation (reproduced from Lewis et al., 2016).

Acquisition of complete data in a single cardiac cycle can also be achieved with high-pitch helical scan with DSCT (Somatom Definition Flash and Definition Force, Siemens Healthcare, Forchheim, Germany). Due to dual-source geometry, this scanning allows substantially increase in the pitch factor (Lewis et al., 2016; Sun, 2012b; Otero et al., 2009). The patient dose is reduced as the overlapping radiation dose is avoided. Studies have reported a high pitch factor of 3.4 enables the coverage of entire heart in approximately 260 ms with complete data acquisition in a single cardiac cycle, excellent

image quality and consistent radiation dose lower than 1.0 mSv (Achenbach et al., 2010; Alkadhi et al., 2010).

2.7 Radiation dose in CCTA

Various dose parameters have been used for measurement of radiation dose associated with CCTA. Dose quantity and dose measurement parameters that are commonly used in CCTA can be described by two categories: general radiation dose measures and CT specific radiation dose measures. The general radiation dose measures consists of absorbed dose, organ dose and H_E, while the CT specific radiation dose measures consists of CT dose index (CTDI), $CTDI_{100}$, weighted CTDI ($CTDI_W$), CTDI volume ($CTDI_{vol}$) and P_{KL} or dose length product (DLP) and H_E (Mayo-Smith et al., 2014; Rehani, 2011; Huda et al., 2010; McNitt-Gray, 2002).

2.7.1 General radiation dose measures

Various dose quantities have been used to describe radiation dose delivered by CCTA, but the most relevant being organ dose and H_E. Absorbed dose describes the amount of energy absorbed per unit mass at a specific point. It is measured in grays (1 Gy = 1 J/kg) (Mayo-Smith et al., 2014; Rehani, 2011; ICRP, 2007; McNitt-Gray, 2002).

Organ dose is the absorbed dose or distribution of dose in the organ that largely determine the level of risk to that organ from the radiation (Rehani, 2011). It can be calculated using a computer simulated dosimetry techniques (Monte Carlo simulation) or measured with dosimeters embedded in an anthropomorphic phantom (Groves et al., 2004). Studies have reported the underestimation of organ doses using computer simulated dosimetry techniques compared to phantom measurements (Groves et al., 2004; Geleijns et al., 1994). This is mainly due to the differences between mathematical and anthropomorphic phantoms used in both techniques. The computer simulated technique employs the geometric Medical Internal Radiation Dosimetry (MIRD) or Eva

phantom, which approximates the organs by simplified geometric shapes, contrary to the situation in practical circumstances (Groves et al., 2004).

It is important to note that the potential biological effects from radiation depend not only on the radiation dose to a tissue or organ, but also the radiosensitivity of the irradiated tissues or organs. H_E is a dose descriptor which take into account the radiosensitivity in tissues or organs. It is a weighted sum of organ doses, as described in Eq. 2.1:

$$H_E = \sum_T (w_T \times w_R \times D_{T,R}) \qquad \text{Eq. 2.1}$$

Where w_T is the tissue-weighting factor (Table 2.2), w_R is the radiation-weighting factor (1 for X-ray) (Table 2.3), $D_{T,R}$ is the average absorbed dose to tissue T, T is the subscript for each radiosensitive tissue, and R is the subscript for each type of radiation . H_E is expressed in sieverts (Sv) (Rehani, 2011; ICRP, 2007; McNitt-Gray, 2002).

Table 2.2: Tissue-weighting factors (w_T) (reproduced from ICRP, 2007).

Tissue	w_T	Σw_T
Bone-marrow (red), colon, lung, stomach, breast, remainder tissues (Norminal w_T applied to the average dose to 14 tissues). Remainder tissues (14 in total): Adrenals, extrathoracic region, gall bladder, heart, kidneys, lymphatic nodes, muscle, oral mucosa, pancreas, prostate, small intestine, spleen, thymus, uterus/cervix.	0.12	0.72
Gonads	0.08	0.08
Bladder, esophagus, liver, thyroid	0.04	0.16
Bone surface, brain, salivary glands, skin	0.01	0.04

Σw_T, summation of tissue-weighting factors.

Table 2.3: Radiation-weighting factors (w_R) (reproduced from ICRP, 2007).

Type and energy range	w_R
Photons, all energies	1
Electrons and muons, all energies	1
Neutrons, energy < 10 keV	5
10 keV to 100 keV	10
> 100 keV to 2 MeV	20
> 2 MeV to 20 MeV	10
> 20 MeV	5
Protons, other than recoil protons, energy > 2 MeV	5
Apha particles, fission fragments, heavy nuclei	20

2.7.2 CT specific radiation dose measures

The CTDI is the primary dose measurement concept in CT:

$$\mathrm{CTDI} = \left(\frac{1}{nt}\right)\int_{-7t}^{7t} D(z)dz \qquad \text{Eq. 2.2}$$

In Eq. 2.2, n is the number of sections per scan, t is the section thickness and D(z) is the radiation dose profile along the z-axis. CTDI is defined as the radiation dose, normalized to X-ray beam width, measured from 14 contiguous sections. Measurements of exposure usually obtain with a pencil ionisation chamber with fixed length of 100 mm, means that only 14 sections of 7 mm thickness could be measured with that chamber alone. For a thinner nominal sections (thickness < 7mm), it is necessary to cover the part of chamber that exceeded 14 sections width with lead sleeves (Rehani, 2011; McNitt-Gray, 2002).

To overcome the limitation of CTDI, $CTDI_{100}$ was introduced. $CTDI_{100}$ allows calculation of CTDI for 100 mm, regardless of the nominal section width:

$$CTDI_{100} = \left(\frac{1}{NT}\right)\int_{-50mm}^{50\ mm} D(z)dz$$

Eq. 2.3

In Eq. 2.3, N is the number of acquired sections per scan and T is the nominal width of each acquired section. The $CTDI_{100}$ was later found to have dependency on position within the scan plane, then the $CTDI_W$ was developed. $CTDI_W$ provides a weighted average of the centre and peripheral contributions to dose within the scan plane:

$$CTDI_W = \left(\frac{1}{3}\right)(CTDI_{100})_{centre} + \left(\frac{2}{3}\right)(CTDI_{100})_{periphery}$$

Eq. 2.4

In Eq. 2.4, the values of 1/3 and 2/3 are approximates of the relative areas represented by the centre and periphery values. $CTDI_W$ is a useful indicator for scanner radiation output for a specific tube voltage and current. Subsequently, $CTDI_{vol}$, another CTDI descriptor which take into accounts helical pitch factor was introduced:

$$CTDI_{vol} = CTDI_W \times \left(\frac{NT}{I}\right)$$

Eq. 2.5

$$\frac{NT}{I} = \frac{1}{Pitch}$$

Eq. 2.6

$$CTDI_{vol} = \frac{CTDI_W}{Pitch}$$

Eq. 2.7

In Eq. 2.5, N and T are as defined earlier and represent the total collimated width of the X-ray beam and I is the table increment per gantry rotation (360º) for a helical scan. Since pitch factor is defined as the ratio of table increment per gantry rotation to the total X-ray beam width (Eq. 2.6) , therefore $CTDI_{vol}$ can be calculated as a ratio of $CTDI_w$ to pitch factor (Eq. 2.7) (Rehani, 2011; AAPM Task Group 23, 2008; McNitt-Gray, 2002).

$CTDI_{vol}$ represents the average absorbed dose over the x, y, and z dimensions and is given with a units of miliGrays (mGy). It provides information regarding the radiation

dose to two cylindrical poly-methyl methacrylate cylindrical phantom representing the attenuation of respectively the adult head (160 mm diameter) or the body (320 mm diameter). $CTDI_{vol}$ measurements can be performed using a 100 mm ionisation chamber placed along the 150 mm phantom length in the centre and periphery, for specific CT scanner techniques (tube voltage, tube current, rotation time, beam collimation, pitch, FOV, and tube filtration) with correction for chamber calibration, partial volume irradiation, and conversion constants (Rehani, 2011; AAPM Task Group 23, 2008).

Although the measurements in a phantom should somehow reflect the attenuation in a human body, $CTDI_{vol}$ should not be used as an indication of patient dose as it does not take into account the patient's size, and therefore does not reflect patient absorbed dose. It is only useful as a measure of scanner output when comparing different protocols and different CT scanners (Seibert et al., 2014; McCollough et al., 2011; Otero et al., 2009).

Another dose descriptor that is related to CTDI, P_{KL}, is defined as the product of the $CTDI_{vol}$ and the irradiated length in z-axis (l) (Eq. 2.8).

$$P_{KL} = \frac{CTDI_{vol}}{l} \qquad \text{Eq. 2.8}$$

P_{KL} is expressed in units of mGy × centimetres (mGy-cm). It reflects the total energy absorbed (and thus the potential biological effect) attributable to the complete scan acquisition (Rehani, 2011; AAPM Task Group 23, 2008). Even though P_{KL} reflects most closely the radiation dose for a specific CT examination, but it is not an appropriate risk indicator as it takes no account of the radiosensitivity of the irradiated tissues. For that purpose, the concept of H_E was introduced (Rothenberg & Pentlow, 2000).

As discussed earlier, H_E is a weighted sum of organ doses. In practical circumstances, for instance in patient, direct measurement of the absorbed dose in the organs is not

possible. Therefore, a generic estimation method was proposed by the European Working Group for Guidelines on Quality Criteria in Computed Tomography. The H_E values calculated from the Public Health England (PHE) (formerly National Radiological Protection Board (NRPB)) Monte Carlo organ coefficients were compared to P_{KL} values for the corresponding clinical examinations to determine a set of E_{KL}. The values of E_{KL} are dependent only on the region of the body being scanned (head, neck, thorax, abdomen, or pelvis) (Jones & Shrimpton, 1991). Using this method, H_E can be estimated from P_{KL}, which can be retrieved from a dose report displayed at CT console after a scanning is performed.

$$H_E = E_{KL} \times P_{KL} \qquad \text{Eq. 2.9}$$

In Eq. 2.9, E_{KL} is region-specific, P_{KL} normalized H_E ($mSv.mGy^{-1}cm^{-1}$) conversion factor (Mayo-Smith et al., 2014; AAPM Task Group 23, 2008). Over the years, different values of E_{KL} were proposed and updated in different publications and reports (Table 2.4) (Christner et al., 2010). For CCTA examination, most of the studies have applied E_{KL} of chest region for calculation of H_E, which is 0.014 $mSv.mGy^{-1}cm^{-1}$. An E_{KL} of 0.028 $mSv.mGy^{-1}cm^{-1}$ has been suggested for cardiac-specific imaging, to give a better estimation of H_E (Sabarudin et al., 2013; Gosling et al., 2010). However, there were no guideline on the appropriate E_{KL} for CCTA to date.

Table 2.4: Published P_{KL}-to-H_E conversion factor (E_{KL}) (reproduced from Christner et al., 2010).

Anatomic Region	P_{KL}-to-H_E Conversion Factor (E_{KL}) (mSv.mGy^{-1}cm^{-1})				Phantom (mm)
	Jessen et al. (1999)	EC (2000)	EC Appendix B (2004)	EC Appendix C (2004) and PHE- or NRPB-W67 (2005)	
Head	0.0021	0.0023	0.0023	0.0021	160
Head and neck	-	-	-	0.0031	160
Neck	0.0048	0.0054	-	0.0059	320
Chest	0.014	0.017	0.018	0.014	320
Abdomen	0.012	0.015	0.017	0.015	320
Pelvis	0.019	0.019	0.017	0.015	320
Chest, abdomen, and pelvis	-	-	-	0.015	320

EC, European Commission; H_E, effective dose; PHE, Public Health England (formerly National Radiological Protection Board (NRPB)); P_{KL}, air-kerma length product.

2.7.3 Cancer risk estimation

Nonetheless, increasingly widespread use of CCTA has raised concerns about potential risks of radiation-induced cancer, as CT leads to 5 to 20 times higher H_E compared to conventional radiology (Mettler et al., 2008; Shrimpton et al., 1991).

The concept of H_E was designed for radiation protection of occupationally exposed personnel. According to International Commission on Radiological Protection (ICRP) Publication 103, H_E should be used for prospective dose assessment for: (1) planning and optimisation in radiological protection (compared to dose limits); (2) establishing a radiation worker's dose of record; (3) demonstrating compliance with dose limits for regulatory purposes; (4) and comparing typical doses from different diagnostic procedures and similar technologies in medical examinations (ICRP, 2007). H_E assumes the validity of the linear no-threshold dose-response model which is still controversial and it is applies generally to an age-averaged, sex-averaged (male plus female) and region-averaged reference model. Furthermore, H_E is not a physical measured quantity which applicable to individual medical patient. It cannot predict any short-term, normal-organ radiation damage (Fisher & Fahey, 2017).

For risk estimation in CT, the patient-specific organ or tissue absorbed dose is the preferred quantity for assessing the probability of cancer induction in exposed individuals. The organ or tissue absorbed dose correlates with biological effects of radiation, including both short-term deterministic and long-term stochastic effects (Fisher & Fahey, 2017).

Several models for estimating the cancer risk from exposure to low levels of low-linear energy transfer (LET) ionising radiation have been developed by the national and international organizations. These include the work of the Biological Effects of lonizing Radiation (BEIR) V committee (NRC, 1990), the ICRP (ICRP, 1991), the National

Council on Radiation Protection and Measurements (NCRP, 1993), the Environmental Protection Agency (EPA, 1999, 1994), the United Nations Scientific Committee on the Effects of Atomic Radiation (UNSCEAR, 2000), the National Institutes of Health (NIH, 2003) and BEIR VII phase 2 (NRC, 2006).

Most of the quantitative information used for risk estimation of radiation-induced cancer comes from Life Span Study of the Japanese Atomic Bomb survivor cohort studies (Ozasa et al., 2012). Data from these survivors are generally used as the basis for predicting radiation-related risks in a population for several reasons: (1) the large size of the studied population (approximately 100,000 survivors) with substantial subcohort (approximately 25,000 survivors) received radiation doses in the range relevant to diagnostic medical radiation (< 1m Gy to ~ 50 m Gy) ; (2) the long length of follow-up over a period of many decades; (3) the breadth of the population exposed (including males and females of all age groups); (4) the fact that population selection was not in any way based on cancer status; and (5) the fact that individuals received a whole body exposure rather than targeted exposures to individual organs, so that risks for most solid cancers / leukaemia can be estimated (Shah et al., 2012). Furthermore, there are other supporting studies on both medically exposed persons and nuclear workers exposed at relatively low doses. The findings from these studies were quantitatively consistent with those reported for the atomic bomb survivors (NRC, 2006).

The latest risk estimation model was proposed in BEIR VII report and it has been widely used in publications (Khan et al., 2014; Hurwitz et al., 2007). In this report, the lifetime attributable risk (LAR) has been described and expressed as:

$$\text{LAR}\ (D,e)=\frac{\text{M}(D,\ e,\ a)\ \text{S(a)}}{\text{S}(e)}$$

Eq. 2.10

In Eq. 2.10, *D* is the absorbed dose (in the BEIR VII report, it is normalized to 0.1 Gy), "*e*" is the exposed age of the patient, "*a*" is the attained age, which is from e + L to 100 (L is the risk-free latent period, which L = 5 for solid cancers) accounting for remaining lifetime, *S(a)* being the probability of survival until age "*a*", *S(e)* being the probability of survival until age "*e*" and M(*D, e, a*) is the excess absolute risk (EAR). EAR is the rate of disease in an exposed population minus the rate of disease in an unexposed population.

LAR is a measures which estimates the probability that an individual will die from or develop cancer associated with the exposure. It does not take account of persons dying of other radiation-induced disease. To ease the calculation of LAR for radiation-induced cancer, the lifetime risk (LR) estimates for cancer incidence resulting from a single dose of 0.1 Gy at several specific ages was tabulated (TABLE 12D-1, BEIR VII report) (Table 2.5). The estimates were shown for all cancer, leukaemia, all solid cancer, and cancer of several specific sites for both sex. Based on the tabulated values, the LAR for cancer incidence can be calculated from organ doses (NRC, 2006).

From the LAR, it is possible to estimate the lifetime relative risk (RR) of radiation-induced cancer on the basis of baseline values of LR in the absence of exposure (Hurwitz et al., 2007; NRC, 2006) (Eq. 2.11).

$$\text{RR} = \frac{(\text{LAR} + \text{LR})}{\text{LR}}$$

Eq. 2.11

The baseline values of LR used in Eq. 2.11 can be obtained from the report (TABLE 12-4, BEIR VII report) (Table 2.6) (NRC, 2006) .

Table 2.5: LAR of cancer incidence (reproduced from NRC, 2006).

	Age at Exposure										
Cancer Site	**0**	**5**	**10**	**15**	**20**	**30**	**40**	**50**	**60**	**70**	**80**
Males											
Stomach	76	65	55	46	40	28	27	25	20	14	7
Colon	336	285	241	204	173	125	122	113	94	65	30
Liver	61	50	43	36	30	22	21	19	14	8	3
Lung	314	261	216	180	149	105	104	101	89	65	34
Prostate	93	80	67	57	48	35	35	33	26	14	5
Bladder	209	177	150	127	108	79	79	76	66	47	23
Other	1123	672	503	394	312	198	172	140	98	57	23
Thyroid	115	76	50	33	21	9	3	1	0.3	0.1	0.0
All solid	2326	1667	1325	1076	881	602	564	507	407	270	126
Leukaemia	237	149	120	105	96	84	84	84	82	73	48
All cancers	2563	1816	1445	1182	977	686	648	591	489	343	174
Females											
Stomach	101	85	72	61	52	36	35	32	27	19	11
Colon	220	187	158	134	114	82	79	73	62	45	23
Liver	28	23	20	16	14	10	10	9	7	5	2
Lung	733	608	504	417	346	242	240	230	201	147	77

‘Table 2.5, continued’

Cancer Site	Age at Exposure										
	0	**5**	**10**	**15**	**20**	**30**	**40**	**50**	**60**	**70**	**80**
Breast	1171	914	712	553	429	253	141	70	31	12	4
Uterus	50	42	36	30	26	18	16	13	9	5	2
Bladder	104	87	73	60	50	34	31	25	18	11	5
Other	212	180	152	129	109	79	78	74	64	47	24
Thyroid	1339	719	523	409	323	207	181	148	109	68	30
All solid	634	419	275	178	113	41	14	4	1	0.3	0.0
Leukaemia	4592	3265	2525	1988	1575	1002	824	678	529	358	177
All cancers	185	112	86	76	71	63	62	62	57	51	37

Number of cases per 100,000 persons exposed to a single dose of 0.1 Gy.

Table 2.6: Baseline lifetime risk (LR) estimates of cancer incidence and mortality (reproduced from NRC, 2006)

	Incidence		Mortality	
Cancer site	**Males**	**Females**	**Males**	**Females**
Solid cancer	45,500	36,900	22,100 (11)	17,500 (11)
Stomach	1,200	720	670 (11)	430 (12)
Colon	4,200	4,200	2,200 (11)	2,100 (11)
Liver	640	280	490 (13)	269 (12)
Lung	7,700	5,400	7,700 (120	4,600 (14)
Breast	-	12,000	-	3,000 (15)
Prostate	15,900	-	3,500 (8)	-
Uterus	-	3,000	-	750 (150
Ovary	-	1,500	-	980 (14)
Bladder	3,400	1,100	770 (9)	330 (10)
Other solid cancer	12,500	8,800	6,800 (13)	5,100 (13)
Thyroid	230	550	40 (12)	60 9912)
Leukaemia	830	590	710 (12)	530 (13)

Number of estimated cancer cases or deaths in population of 100,000 (No. of years of life lost per death).

The calculation of joint lifetime attributable risk (LAR_{joint}) for more than one radiation-induced cancer can also be performed (Eq. 2.12).

$$LAR_{joint} = P_{joint} \times 100{,}000 \quad \text{Eq. 2.12}$$

$$P_{joint} = (P_a + P_b) - (P_a \times P_b) \quad \text{Eq. 2.13}$$

The joint probability (P_{joint}) used in Eq. 2.12 can be calculated from Eq. 2.13, where P_a is the LAR for organ "a" divided by 100,000 and P_b is the LAR for organ "b" divided by 100,000. Subsequently, joint relative risk (RR_{joint}) can be calculated as follow (Hurwitz et al., 2007; NRC, 2006):

$$RR_{joint} = \frac{(LAR_{joint} + LR_{joint})}{LR_{joint}} \quad \text{Eq. 2.14}$$

$$LR_{joint} = P_{joint} \times 100{,}000 \quad \text{Eq. 2.15}$$

The joint lifetime risk (LR_{joint}) used in Eq. 2.14 can be calculated from Eq. 2.13 and Eq. 2.15, where P_a is the LR for organ "a" divided by 100,000 and P_b is the LR for organ "b" divided by 100,000. To estimate the amount of additional relative risk above baseline,

excess relative risk (ERR) is described as a percentage over baseline in Eq. 2.16 (NRC, 2006).

$$ERR = (RR\text{-}1.0) \times 100 \quad \text{Eq. 2.16}$$

2.8 Image quality assessment in CCTA

The final image quality of CCTA is affected by technical and patient-related factors, as well as the radiation exposure. Therefore, image quality is a complex entity for which there is no single objective scale. In clinical practice, the final endpoint of all factors that affecting CCTA image quality is their impact on image interpretation, which assumes that all of quantitative measurement or qualitative scaling of the following variables should be within an "acceptable" range: VCE, image noise and artefacts (Ghekiere et al., 2017).

2.8.1 Vessel contrast enhancement (VCE)

The main purpose of intravenous contrast medium administration is to achieve VCE for direct assessment of coronary stenosis. Consistent and homogenous arterial enhancement are crucial for a diagnostically accurate and high quality CCTA scan. The VCE is affected by several interacting factors, which can be described in three categories: patient-, contrast-, and CT-related factors (Figure 2.16) (Weininger et al., 2011).

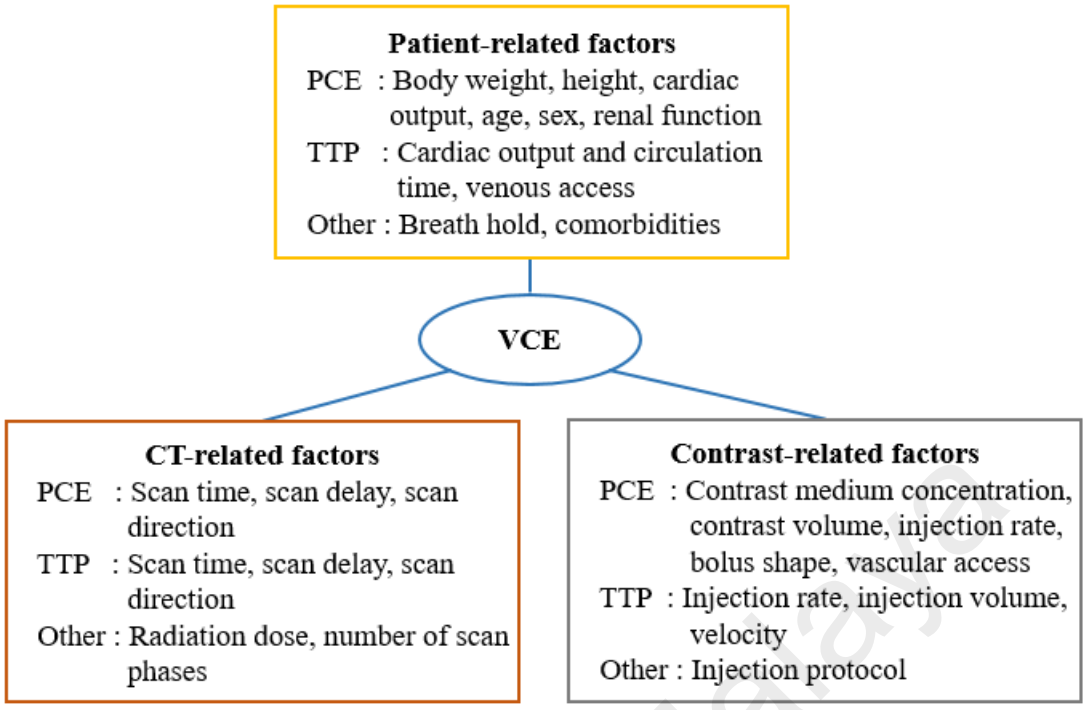

PCE, peak contrast enhancement; TTP, time-to-peak; VCE, vessel contrast enhancement.

Figure 2.16: Factors affecting VCE (reproduced from Weininger et al., 2011).

2.8.1.1 Patient-related factors

Body weight and cardiac output are the main patient-related factors which affecting the VCE. Numerous studies have reported the inverse relationship between body weight and PCE (Yanaga et al., 2009; Bae et al., 2008; Schoellnast et al., 2006; Awai & Hori, 2003; Platt et al., 1999). The influence of cardiac output is mainly on TTP and cardiovascular circulation. The other less influential factors include age, sex, height, venous access, renal function as well as various other pathologic conditions. The effect of these factors on PCE and TTP can be best described by their relationship with blood volume and cardiac output (Bae, 2010).

2.8.1.2 Contrast-related factors

The PCE is proportionally increase with the IDR and TID. The IDR is calculated as a product of contrast concentration and injection rate; whereas the TID is calculated as a product of contrast volume and contrast concentration. Four main contrast-related factors that affecting IDR and TID are contrast concentration, contrast volume, injection rate and

duration. Injection duration is defined as the time from the starting to the completion of contrast medium injection. It can be calculated by dividing the contrast volume to the injection rate (Weininger et al., 2011; Bae, 2010). The relationship between contrast concentration, injection rate, contrast volume, injection duration, IDR, TID, PCE and TTP are described in Figure 2.17.

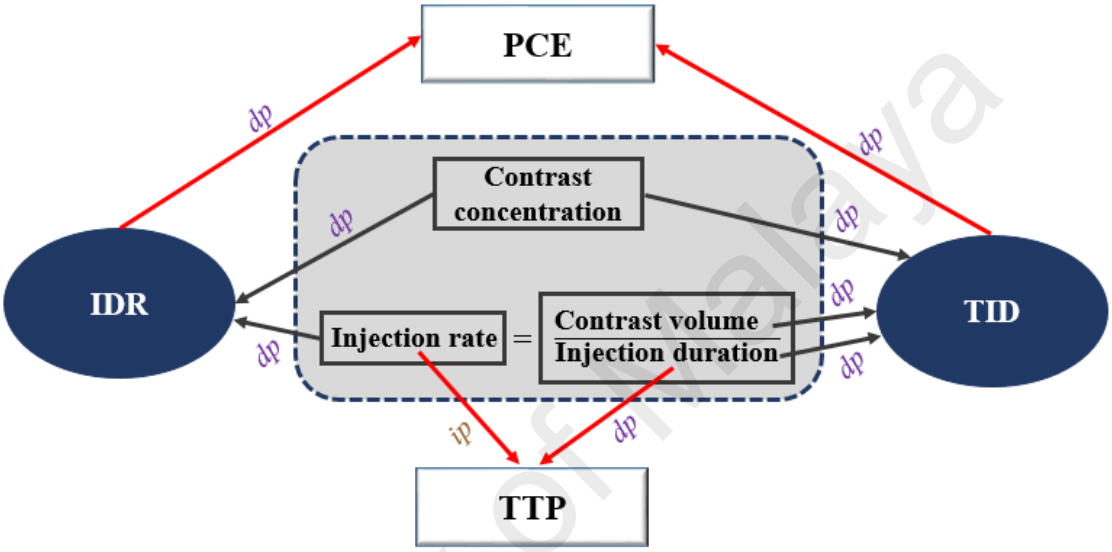

IDR, iodine delivery rate; PCE, peak contrast enhancement; TID, total iodine dose; TTP, time-to-peak; *dp*, directly proportional; *ip*, inversely proportional

Figure 2.17: Relationship between contrast concentration, injection rate, contrast volume, injection duration, IDR, TID, PCE and TTP (Weininger et al., 2011; Bae, 2010).

Three different scenarios are included below to discuss the relationship of the main injection parameters. Firstly, when the contrast volume and injection rate are fixed or alternatively the same injection duration, any increase in contrast concentration will proportionally increases the IDR and TID, then increases the PCE. Secondly, when the contrast concentration and contrast volume are fixed or alternatively the same TID, a faster injection rate will cause shorter injection duration and a higher IDR. This results in a shorter TTP and higher PCE. Thirdly, when the contrast concentration and injection rate are fixed or alternatively the same IDR, any increase in contrast volume will cause longer injection duration and increases the TID given. This results in a longer TTP and a higher PCE. This protocol is preferable for delivering a higher TID in large patient (Bae,

2010). In a randomized study conducted by Yamashita et al. (2000), the authors increased the contrast volume from 1.5 to 2.5 $mLkg^{-1}$ in 0.5 $mLkg^{-1}$ intervals. The results showed increase in the PCE from 238 to 270 HU, respectively.

Alternatively, higher TID in large patient can also be achieved by applying a fixed contrast concentration and injection duration, but with a higher injection rate. A fixed injection duration has its advantages over the fixed injection rate, particularly more easy for the standardisation of scan timing (Bae, 2010).

Another important contrast-related factor which affecting the contrast medium delivery and enhancement is the viscosity of contrast medium. The viscosity of contrast medium is affected by temperature, and it is lower at higher temperature (Brunette et al., 2008; Halsell, 1987). In a study conducted by Hazirolan et al. (2009), the authors compared the PCE and TTP between a group of patients given with contrast medium-saline mixture at constant room temperature (24 °C) and another group of patients given with warmed contrast medium-saline mixture at constant temperature of 37 °C. The results showed higher PCE and shorter TTP in the warmed contrast medium-saline mixture group.

2.8.1.3 CT-related factors

In addition to patient- and contrast-related factors, CT scanning factors play a critical role for the acquisition of contrast-enhanced CT images. Scan time, scan direction, timing of multiphasic acquisitions, and scan delay in relation to the beginning or completion of contrast medium injection are the critically important CT-related factors that affecting both PCE and TTP. To achieve diagnostically adequate PCE, it is essential to know the estimated scan time for CCTA scan. The main influence of scan time is on injection duration and rate or contrast volume used in CCTA (Weininger et al., 2011; Bae, K. T., 2010(Weininger et al., 2011; Bae, 2010).

CCTA is usually performed corresponding to the direction of contrast medium propagation. Since the VCE reduces as the contrast medium propagates from the central blood circulation to the distal arteries, a scanning performed by following the directional flow of contrast medium will improve PCE and makes efficient use of contrast medium (Weininger et al., 2011; Bae, 2010).

In addition to scan time and direction, exact determination of the TTP is crucial for consistent PCE. The TTP is strongly dependent on patient's cardiovascular circulation and commonly used to decide the scan delay in CCTA (Weininger et al., 2011; Bae, 2010). As discussed earlier, the TTP can be determined by a test scan, either with test bolus or bolus tracking technique.

2.8.2 Image noise and artefacts

Image noise is one of the major factor that affecting the image quality. It is mainly depends on the number of X-ray photons reaching the detector. A low number of X-ray photons that reaching the detectors lead to a larger Poisson error, which subsequently increase the image noise (quantum mottle) (Kalisz et al., 2016; Boas & Fleischmann, 2012). Image noise is influenced by technical and patient-related factors (body weight and anatomy structures), as well as the filters used during the image reconstruction process (Ghekiere et al., 2017).

CCTA is vulnerable to a wide variety of artefacts, such as motion artefacts, partial volume averaging, beam hardening and metal artefacts. Motion caused by patient, cardiac, or respiratory movement is the primary source of artefacts in CCTA. Cardiac motion artefacts can occurs in cross-sectional (xy-axis) and longitudinal (z-axis) plane. In the cross-sectional plane, artefacts occurs within a single heart beat and typically manifest as areas of blurring, ghosting, winging, or streaking (Kalisz et al., 2016). The extent of motion depends on the region of the heart considered. For instance, the RCA

has been reported to have the most motion over the cardiac cycle, followed by the LCx, LM, and LAD arteries. This is due to the high-velocity movement and positional change of RCA in the cross-sectional plane (Choi et al., 2004; Achenbach et al., 2000). Furthermore, stair-step artefacts along the z-axis is mainly due to irregular rhythms or premature beats that causes misregistration between acquired slabs for image reconstruction. It is generally shown as areas of discontinuity of anatomic structures and it can be misdiagnosed as a finding of stenosis, particularly on axial views (Kalisz et al., 2016).

Cardiac motion can be reduced by several methods: (1) decrease the heart rate and variability; (2) reduce the duration of data acquisition; (3) adjust the placement of the data acquisition window within a cardiac cycle; (4) perform scanning in single heart beat; and (5) apply multi-segment reconstruction and motion-correction algorithms. A proper breath-holding and shortened scan time are also beneficial in reducing cardiac and respiratory motion (Kalisz et al., 2016).

Partial volume averaging is caused by the averaging of attenuation values from all tissue contained within a voxel. It can be reduced by improving the spatial resolution, using a higher X-ray energy, or displaying images with a wider window width. Beam-hardening artefacts are caused by the polyenergetic nature of the X-ray beam. It can be reduced by using X-ray filtration, applying higher-energy X-rays, altering patient position, modifying contrast medium protocols, and applying certain reconstruction algorithms. Finally, metal artefacts are complex and have multiple causes, including X-ray scatter, underpenetration, motion, and attenuation values that exceed the typical dynamic range of Hounsfield units (HU) (Kalisz et al., 2016).

2.8.3 Quantitative and qualitative assessment

VCE can be measured quantitatively by placing a ROI in lumen of contrast-enhanced arteries. According to the literature, the reported locations of the ROI have included the mean of the LCA and RCA origins and the AA (Cademartiri et al., 2008; Cademartiri, Runza, et al., 2005); the origin or the proximal LCA and RCA (Di Cesare et al., 2016; Sun et al., 2015; Johnson et al., 2007; Cademartiri, Mollet, et al., 2006); the origin or proximal four coronary arteries (Delhaye et al., 2007; Dewey et al., 2007; Frydrychowicz et al., 2007; Cademartiri, de Monye, et al., 2006; Cademartiri, Luccichenti, et al., 2005); the proximal, middle, or distal arterial segments (Kerl et al., 2008; Nakaura et al., 2008; Yamamuro et al., 2007; Utsunomiya et al., 2006); and the proximal and middle coronary artery segments combined (Kim et al., 2008).

VCE decreases from the AA to the coronary arteries (Kim et al., 2008; Frydrychowicz et al., 2007; Funabashi et al., 2007; Johnson et al., 2007; Yamamuro et al., 2007) and along the length of the coronary arteries (Yamamuro et al., 2007; Utsunomiya et al., 2006). In addition, VCE that incorporating CT attenuation in AA are higher than those derived only from the coronary arteries (Johnson et al., 2009).

Optimal VCE is crucial in CCTA for the detection of coronary stenosis and quantitative analysis of atherosclerotic plaque. Based on the guidelines established by Society of Cardiovascular Computed Tomography (SCCT) in 2009, an optimal CCTA image requires VCE of more than 250 HU, however, no upper limit of VCE was recommended (Abbara et al., 2016; Abbara et al., 2009). In a phantom study conducted by Fei et al. (2008), high VCE of 500 HU was reported to be associated with the underestimation of coronary stenosis. The authors further suggested an optimal VCE target of 350 HU for CCTA. Furthermore, VCE was reported to have significant impact on the density of non-calcified plaque (Dalager et al., 2011; Horiguchi et al., 2007). In a

phantom study conducted by Horiguchi et al. (2007), VCE of 350 and 450 HU were reported to cause overestimation of non-calcified plaque with a density of 40 HU. VCE of 250 HU with a low heart rate was found to give the most precise measurements. Nevertheless, there were studies that reported the association of higher number of false-positives and negatives with low VCE. In a study conducted by Cademartiri et al. (2008), higher VCE of 326 to 540 HU was found to give a significantly higher sensitivity (96 %) and positive predictive value (92 %) compared to low VCE of 182 to 325 HU. Taking into consideration of the detection of coronary stenosis, quantitative analysis of atherosclerotic plaque and diagnostic performance of CCTA, the optimal range of VCE could fall between more than 250 and less than 450 HU.

Image noise can be measured quantitatively by placing a ROI in contrast-enhanced structures, usually at lumen of AA, coronary arteries or left ventricle. Then, the obtained standard deviation of the CT attenuation values (measured in HU) within the ROI is a measure of image noise (Ghekiere et al., 2017). Background noise can also be measured as the standard deviation of a ROI within chest wall muscle (Pan et al., 2016). In several studies, a value of equal or less than 30 HU was suggested for improved CCTA image quality (Tatsugami et al., 2015; Tatsugami et al., 2012; Leschka et al., 2008). However, as of to date, no standard cut-off value of image noise has been reported.

Another two commonly used quantitative measurements for image quality assessment are the signal-to-noise ratio (SNR) and contrast-to-noise ratio (CNR). SNR indicates the amount of signal versus the amount of noise in a particular image. CNR is defined as the differences in CT attenuation values between different materials versus the noise. Different methods have been used to calculate SNR and CNR in CCTA. For SNR, it is usually calculated by a ratio of VCE to image noise or background noise. Whereas for CNR, it is calculated as the difference between VCE and the attenuation of perivascular

fat or chest wall muscles divided by the image noise or background noise (Di Cesare et al., 2016; Mangold et al., 2016; Pan et al., 2016; Lu et al., 2015; Shen et al., 2015; Sun et al., 2015; Yin et al., 2015; Zhang, C. et al., 2015; Zheng et al., 2014; Gagarina et al., 2011; Zhang et al., 2011).

In recent years, to standardise the effects of different doses of radiation on image quality, the concept figure of merit (FOM) was proposed. FOM is defined as a ratio of squared CNR to H_E. The higher the value of FOM, the higher is the quality of the CT images (Schindera et al., 2008)

The assessment of VCE, image noise and artefacts can also be performed using qualitative scaling with Likert scale of 2- to 5-points and scored by 2 to 3 observers. The observers assess the image quality as a whole, or perform separate assessments for different segments of coronary arteries (Durmus et al., 2016; Lu et al., 2015; Shen et al., 2015; Khan et al., 2014; Zheng et al., 2014). Several guidelines are available for coronary artery segmentation, including the AHA guidelines with 15-segment, modified 16-segment and the latest modified 17-segment model (Habets et al., 2012; Hamdan et al., 2011; Zhang et al., 1975), and the SCCT guidelines with 18-segment model (Leipsic et al., 2014).

2.9 Optimisation of radiation dose and image quality in CCTA

Several strategies have been proposed to optimise the radiation dose and image quality in CCTA. These strategies can be divided into three categories: patient-related factors, CT-related factors and CCTA-related factors (Figure 2.18) (Mayo-Smith et al., 2014; Sabarudin & Sun, 2013b; Torres et al., 2010; Budoff, 2009).

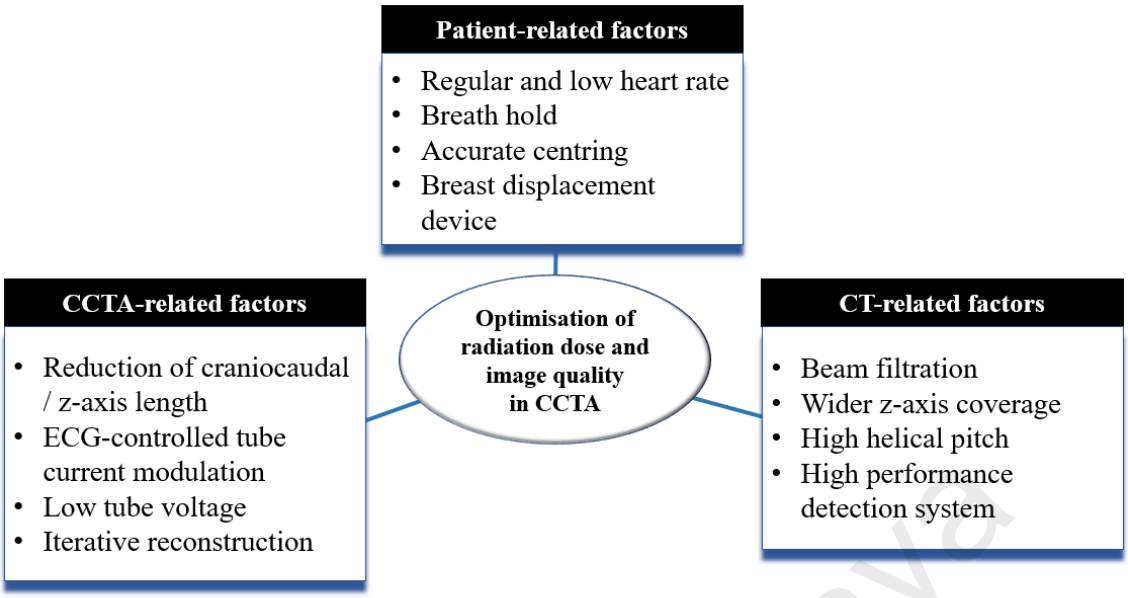

CCTA, coronary computed tomography angiography

Figure 2.18: Strategies for optimisation of radiation dose and image quality in CCTA (Mayo-Smith et al., 2014; Sabarudin & Sun, 2013b; Torres et al., 2010; Budoff, 2009).

2.9.1 Patient-related factors

Patient's heart rate is one of the most important determinants of radiation dose and image quality in CCTA. A regular and low heart rate allows the application of prospectively ECG-triggered protocol and reduce the risk of motion artefacts (Kalisz et al., 2016; Torres et al., 2010). The most common method used to control the patient's heart rate during CCTA is by administrating the beta-blockers, preferably a short acting agent such as metoprolol (Pannu et al., 2006). Breath-hold is generally performed during CCTA to avoid motion artefacts caused by respiratory movement. Furthermore, it is also possible to achieve a mean heart rate reduction of 5 bpm with a proper breath-hold (Husmann et al., 2011).

Another important step that helps in reducing the radiation dose and optimising image quality is the proper positioning of patient. It is important to position the patient in the centre of the gantry to avoid variations in image noise and an unnecessary increase in surface radiation dose due to off-centring effects (Li et al., 2007). Ideally, the heart should

be placed at the isocentre as the spatial resolution is highest in the centre of the scan field (Dewey, 2011b; Torres et al., 2010).

In an attempt to reduce direct irradiation of the breast during CCTA, the use of a displacement device has been tested with and without the use of lead strip in a study conducted by Foley et. al. (2011). A 36 % reduction in breast surface dose was reported in this study using the combination of displacement device and lead strip.

2.9.2 CT-related factors

Bowtie filters are used in CT scanners to shape the X-ray beam and eliminate lower energy photons before the beam reaches the patient. It helps in reducing the beam hardening effects, results in a better image quality and lower radiation dose to the patients. By simply applying an appropriate sized bowtie filter, it is possible to achieve a 40 % radiation dose reduction. As the size of the filter is depended on the scan FOV, choosing an optimal FOV according to the anatomical size and acquisition region of the patient is important. Generally, all hearts can be fit in a small bowtie filter, larger patients may require a medium filter but a large filter would never be necessary in CCTA (Budoff, 2009).

CT scanner with greater z-axis coverage provides a few advantages in term of radiation dose and image quality. Firstly, it allows a faster overall image acquisition (less than 1 s). This decreases the probability of an irregular cardiac rhythm, thus, helps in eliminating the motion and stair-step artefacts. Secondly, it potentially reduces radiation exposure by avoiding the oversampling related to helical scanning. Thirdly, it has ability to capture the state of iodinated contrast medium at a single point in time and produces a better VCE along the blood vessels (Lewis et al., 2016; Otero et al., 2009). Currently, the largest z-axis coverage from the top-end CT scanners is 160 mm, with a 256 × 0.625 mm (Revolution CT, GE Healthcare, Milwaukee, WI) or 320 × 0.5 mm (Aquilion One and

Acquilion One Vision, Toshiba Medical Systems Corporation, Otawara, Japan) detector configuration.

Another low-dose technique, high helical pitch scanning mode was introduced in the second generation DSCT scanner. The dual-source geometry and high table feed of 46 cms^{-1} allow data to be acquired at a high helical pitch of 3.4. In a single diastolic phase, the data are acquired in a quarter of gantry rotation time or 75 ms. Compared to scanners that acquire images in several cardiac cycles, images acquisition in a single phase eliminates additional radiation dose from overlapping slices (Achenbach et al., 2010; Alkadhi et al., 2010). In addition, high diagnostic accuracy was also reported in this technique with per-patient sensitivity of 100 %, specificity of 90.5 %, positive predictive value of 81.5% and negative predictive value of 100 % for CAD (Leschka et al., 2009).

Several CT manufacturers have introduced high performance detection system, basically by increasing the efficiency of X-ray detection or reducing the electronic noise level. One of the manufacturer introduced a new gemstone material (Gemstone Detector, GE Healthcare, WI, USA) as scintillator in the detection system. This scintillator provides high X-ray detection efficiency which significantly reduce radiation dose (Geyer et al., 2016). Similarly, the second manufacturer introduced a praseodymium-activator scintillator (^{PURE}ViSION Detector, Toshiba Medical Systems Corporation, Otawara, Japan) which provides high X-ray detection efficiency. Unlike the first two manufacturers, the third manufacturer introduced an integrated CT detectors (Stellar and Stellar^{INFINITY} Detectors, Siemens Healthcare, Forchheim, Germany) which reduce the electronic noise by directly couples the photodiode to the analog-to-digital converter (Seeram, 2015).

2.9.3 CCTA-related factors

Craniocaudal or z-axis length is a major factor that influences the total radiation dose in CCTA examination as it directly related to the P_{KL}. The effort of reducing radiation dose can be made by limiting the z-axis length. Currently, the average z-axis length of a CCTA ranges from 120 to 150 mm, based on the rigidly selected z-axis length from carina to diaphragm, as is frequently recommended by CT scanner manufacturers. CACS images acquired prior to the CCTA scan can be used to further refine the z-axis length for CCTA to 1 cm above the origin of the coronaries and end by 1 cm below the PDA. This method has been reported to be associated with radiation dose reduction of 16 to 22 % (Leschka et al., 2010; Gopal & Budoff, 2009). Furthermore, for optimal z-axis length planning, it is crucial to ensure the patient breath hold during inspiration is at similar depth during acquisition of the SPR, CACS and the actual CCTA examination to minimize differences in the position of the diaphragm and heart between scans (Halliburton et al., 2011).

Current generation of CT scanners are capable of varying tube current output (mA) in synchronization with the patient's ECG, known as ECG-controlled tube current modulation technique. The basic principle of this technique is by applying a standard tube current over the phases in cardiac cycle with less motion, for instance, the mid-diastolic phase (70 to 80 % in R-R interval) and the end-systolic phase (40 % in R-R interval), while reducing the radiation during the phases when the heart is moving dynamically. Dose reduction of 37 to 48 % have been reported with the use of this technique in retrospectively ECG-triggered CCTA compared to conventional CCTA (Jakobs et al., 2002; Poll et al., 2002). In prospectively ECG-triggered CCTA protocol, further dose reduction was achieved by completely turned off the X-rays outside the pulsing window. Radiation dose reduction of 44 to 83 % was reported in this technique compared to retrospectively ECG-triggered CCTA (Lehmkuhl et al., 2010; Gopal et al., 2009; Klass et al., 2009; Shuman et al., 2008).

As radiation dose is directly proportional to the square of tube voltage, applying lower tube voltage during CCTA is another approach for reducing the radiation dose. A study conducted by Zhang et al. (2015) showed reduction of patient dose by 47 and 69 % when lowering the tube voltage from 120 kVp to 100 and 80 kVp, respectively. Although image noise increases at lower tube voltage due to fewer number of X-ray photons produced, a lower tube voltage also associated with increase of signals or image contrast (Siegel et al., 2004; Huda, 2002; Huda et al., 2000). Since the SNR and CNR are the key factors for image quality in CCTA, image noise is negligible when the amount of signals or level of contrast are high in lower tube voltage (Huda, 2002).

Currently, iterative reconstruction has been implemented clinically as an effective technique for reducing radiation dose, image noise and artefacts in CCTA (Padole et al., 2015; Nelson et al., 2011). The concept of iterative reconstruction has been around for decades. However, due to its high computational demand and long reconstruction time, a faster and robust method, filtered back projection has been widely used in CT scanners. Despite its acceptable performance, CT studies using filtered back projection were heavily affected by image noise, especially when radiation dose was reduced (Lee et al., 2012). With recent improvements in computer processing, using iterative reconstruction as a noise-suppressing technique became more feasible in clinical setting. For the past ten years, iterative reconstruction technologies had evolved from image-based denoising procedures to statistical or hybrid iterative reconstruction, before becoming model based iterative reconstruction and to the latest knowledge-based model iterative reconstruction (Armstrong et al., 2016; Den Harder et al., 2016; Den Harder et al., 2015; Shammakhi & Sun, 2015). In CCTA, iterative reconstruction has been reported to be able to reduce radiation dose by 48 % with preserved image quality, compared to filtered back projection reconstruction (Den Harder et al., 2016).

2.10 Low tube voltage protocol in CCTA

Low tube voltage is an emerging technique for dose optimisation in CT examinations. The most substantial benefits of low tube voltage at CT examinations include: (1) a reduction in the radiation dose delivered to the patient and (2) an increase in the image contrast for structures with high effective atomic number, such as calcium and iodine (Guimaraes et al., 2010). For CCTA, a low tube voltage protocol is beneficial as the higher X-ray absorption of iodine and the increased CNR allow better visualisation of the contrast-enhanced vessels (Aschoff et al., 2017).

2.10.1 Fundamental of low tube voltage

Radiation output or the number of X-ray photons is generally accepted to be proportional to the square of the X- ray tube voltage. As the number of X-ray photons is directly proportional to the radiation dose, a small decrease in the tube voltage can results in a substantial radiation dose reduction. This can be explained by the fact that when the tube current and the exposure time are kept constant, a lower tube potential results in both lower number of X-ray photons and mean energy of the X-ray beam and, thus, lower radiation dose delivered. For instance, a reduction from 120 to 100 kVp will result in 31 % less X-ray photons being produced, meaning 31 % reduction in radiation dose, and this figure will increase to 56 % with further reduction of tube voltage to 80 kVp.

Unlike the tube voltage, the tube current has a linear relationship with the radiation dose. Hence, reducing the tube voltage allows a greater dose reduction when compared with a similar percentage of reduction in the tube current (Aschoff et al., 2017; Seyal et al., 2015).

Image noise is proportional to the square root of the number of X-ray photons. The lower the number of photons delivered, the greater the image noise. Low tube voltage protocols with unchanged tube current-time product (mAs) will deliver a reduced

radiation dose but will also suffer from increased image noise. To balance this increased image noise, a compensatory increase of mAs is required (Aschoff et al., 2017).

Another effect of low tube voltage settings in CCTA is the increase of X-ray absorption of iodine. The X-ray absorption of iodine increases with decreasing tube voltage, as long as the mean energy of X-ray beam remains above the K-edge of iodine (33.2 keV). From the iodine K-edge absorption and CT X-ray spectrum shown in Figure 2.19, the lower energy spectrum of 80 kVp or 100 kVp are much more affected by the K-edge absorption of iodine.

When more low energy X-ray photons are being absorbed by the iodine atoms, it increases the photoelectric effect, then causes a higher CT number of iodine in the CT image that was taken by a lower kVp. Higher signals are produced in low tube voltage settings with the same amount of contrast medium applied. Owing to this higher signal, constant SNR can be maintained even with a higher noise. When the SNR is kept constant, only a moderate compensatory increase in mAs is needed. Furthermore, increase in iodine CNR also benefits the evaluation iodine-enhanced vessels in CCTA (Aschoff et al., 2017; Seyal et al., 2015; Lee & Park, 2014).

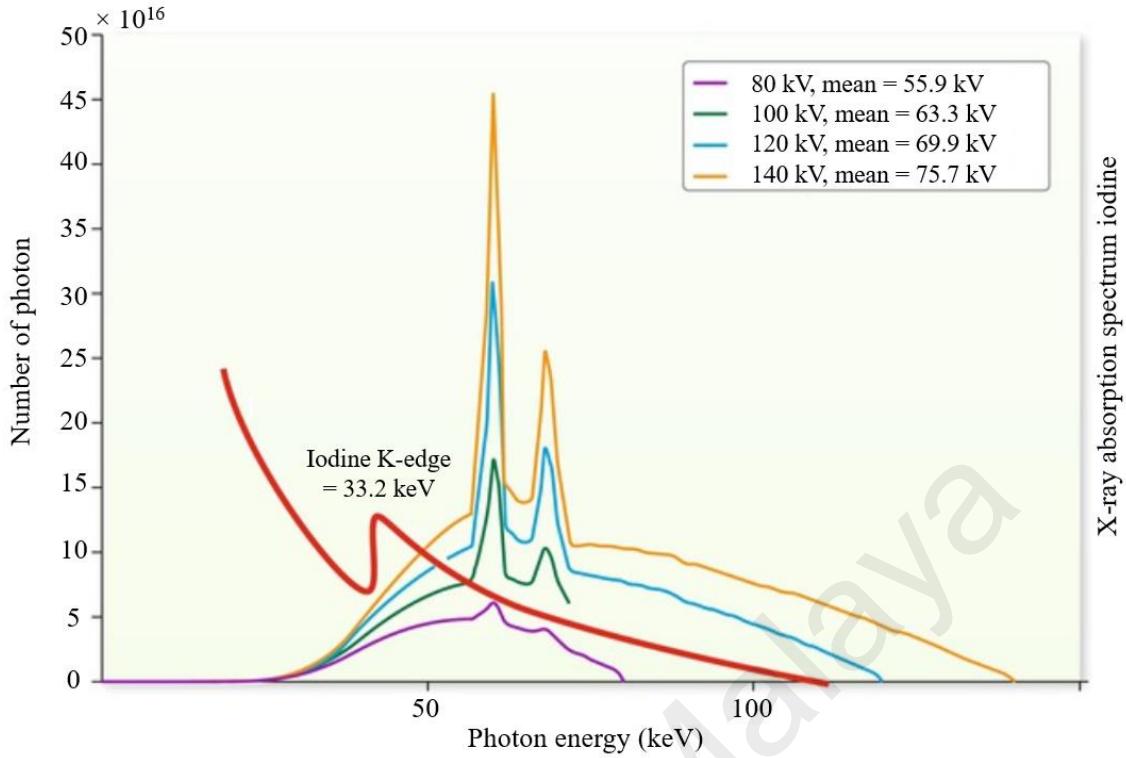

Figure 2.19: Iodine K-edge absorption and CT X-ray spectrum (reproduced from Lee & Park, 2014).

2.10.2 Radiation dose, image quality and contrast medium reduction

In an attempt to reduce the radiation exposure to patients while maintaining the image quality, CT scanner manufacturers have introduced different protocols based on lower tube voltage and/or tube current combined with iterative reconstruction and other radiation dose-reducing techniques, together with contrast medium reduction methods. From the literature, the mean H_E reported for low tube voltage CCTA protocols were ranged from 0.31 to 2.75 mSv at 80 kVp and 0.69 to 6.29 mSv at 100 kVp. The radiation doses were reduced by 38 to 83 % at 80 kVp and 3 to 80 % at 100 kVp when compared to 120 kVp (1.53 to 10.7 mSv). Dose reduction without loss of quantitative and qualitative image quality was also reported in these studies (Di Cesare et al., 2016; Iyama et al., 2016; Pan et al., 2016; Wu et al., 2016; Lu et al., 2015; Oda et al., 2015; Shen et al., 2015; Sun et al., 2015; Yin et al., 2015; Zhang, C. et al., 2015; Zhang, J. et al., 2015; Khan et al., 2014; Zheng et al., 2014; Nakaura, Kidoh, Sakaino, Nakamura, et al., 2013; Nakaura,

Kidoh, Sakaino, Utsunomiya, et al., 2013; Gagarina et al., 2011; Zhang et al., 2011; Alkadhi et al., 2008). Nevertheless, the increased VCE due to greater photoelectric effect at lower tube voltage has compensated the SNR and CNR at a higher image noise levels (Nakaura, Kidoh, Sakaino, Nakamura, et al., 2013).

As the relative attenuation of iodine increases at lower tube voltage, there is possibility to reduce TID applied in CCTA. Several studies have tried to reduce the TID by adjusting the routine contrast medium administration protocol for 120 kVp. These studies successfully achieved similar VCE as 120 kVp and TID reduction at lower tube voltage. Two common contrast medium reduction methods were used in these studies: (1) lowering the iodine concentration of contrast medium; and (2) reducing the contrast volume. In the first method, reduction of contrast concentration from 370 $mgmL^{-1}$ at 120 kVp to 270 $mgmL^{-1}$ at lower tube voltage (80 and 100 kVp) was commonly used (Pan et al., 2016; Wu et al., 2016; Shen et al., 2015; Yin et al., 2015; Zheng et al., 2014). In the second method, reduction of contrast volume was achieved with two main techniques: (1) adjust the body weight-adapted protocol, from 1.0 $mLkg^{-1}$ for 120 kVp to 0.5 $mLkg^{-1}$ for 80 kVp (Nakaura, Kidoh, Sakaino, Utsunomiya, et al., 2013); and (2) adjust the fixed contrast volume protocol, from 55 to 60 mL for 120 kVp to 45 to 50 mL for 100 kVp (Zhang et al., 2011). In these studies, injection rate ranged from 4.0 to 5.0 mLs^{-1} and injection duration ranged from 12.0 to 14.0 s were used. These resulted in IDR of 1.35 to 1.45 gs^{-1} with TID of 10.9 to 16.2 g at 80 kVp and IDR of 1.08 to 1.70 gs^{-1} with TID of 18.9 to 20.9 g at 100 kVp (Tan et al., 2018).

CHAPTER 3: ASSESSMENT OF RADIATION DOSE AND ESTIMATION OF LIFETIME ATTRIBUTABLE RISK (LAR) OF CANCER INCIDENCE ASSOCIATED WITH PROSPECTIVELY ECG-TRIGGERED CCTA PROTOCOLS

3.1 Introduction

According to the WHO, cardiovascular diseases are the number one causes of death globally. In 2015, 17.7 million (31.0 %) of worldwide deaths were reported due to cardiovascular diseases. Of these deaths, an estimated 7.4 million were due to CAD (WHO, 2017).

While ICA remains as the gold standard for the diagnosis of CAD, its associated costs and morbidity including a 1.7 % rate of major complications have led to the development of non-invasive imaging modalities. CCTA is a well-established imaging technique that has high per-patient sensitivity (99 %), positive predictive value (92 %) and negative predictive value (95 %) for obstructive CAD (Chow et al., 2009). The increasing utilisation of CCTA has raised considerable concern over the risks associated with exposure to ionising radiation, particularly with regard to the risk of radiation-induced cancer.

In an attempt to reduce radiation exposure to patients, prospectively ECG-triggered protocol is currently recommended as the first line default technique for CCTA examination which should be used whenever possible and practical (Raff et al., 2014). Several clinical studies have been conducted to assess radiation dose during prospective ECG-triggered CCTA, the data mainly rely on the P_{KL} reported in the CT console (Sabarudin et al., 2013, 2012). It is important to assess the radiation dose imparted to the specific organs that are being exposed, such as breasts, lungs, heart, liver, stomach, etc. The organ dose is the quantity that correlates with biological effects of radiation,

including both short-term deterministic and long-term stochastic effects (Fisher & Fahey, 2017). However, research in this area is scare, and this is the main reason to conduct this study to fill this gap in the current literature.

Due to the widespread use of CCTA, in particular, different generations of CT scanners are being used in clinical centres, it is necessary to determine the risk of radiation-induced malignancy based of measured organ doses, corresponding to each type of CT scanner. However, this issue has not been well addressed in the literature.

This study aimed to assess the radiation dose received from prospectively ECG-triggered CCTA using different generations of CT scanners through direct measurement of organ doses in a standard female adult anthropomorphic phantom. The estimated LARs of breast and lung cancer incidence for sex and age were also compared.

3.2 Literature review

CCTA was first approved by the U.S. Food and Drug Administration (FDA) in 2004 using 64-slice CT. The 64-slice per gantry rotation can be achieved using either 64-detector-row, or 32-detector-row with a strategy to double the slice number by alternating the focal spot of the X-ray source (Otero et al., 2009). The technology has then rapidly evolved from 64-slice to 128-, 256-, 320- and the recent 640-slice CT to achieve better spatial resolution, temporal resolution, larger z-axis coverage and lower radiation dose to the patients.

As motion artefact is one of the most significant challenges in CCTA, temporal resolution of less than 100 ms is usually desirable. Temporal resolution of a single X-ray tube corresponds to approximately half of the gantry rotation time (typically 330 ms). Further improvement of temporal resolution has been achieved in 128- and 256-detector-row CT scanners, with gantry rotation time ranged between 270 and 280 ms. With the

introduction of DSCT, temporal resolution was further improved from 165 to 83 and 75 ms. High diagnostic accuracy (93 %), sensitivity (94 %) and negative predictive value (97 %) have been reported in CCTA using 2 × 64-detector-row DSCT scanner (Alkadhi et al., 2010).

Being another latest scanner version for CCTA, the 320-detector-row SSCT provides the largest z-axis coverage per gantry rotation (160 mm), sufficiently covering the whole heart at one gantry rotation. This configuration allows 3-dimensional volumetric heart imaging to be carried out within diastole of one R-R interval (Diagnostic and Interventional Cardiology, 2013). In addition, 4-dimensional CT or volumetric cine imaging is possible if the X-ray beam is turned on for a longer period to capture the heart over one or more cardiac cycles (Hsiao et al., 2010). Other proposed methods to overcome motion-induced image degradation include an opening of the padding (adding surrounding X-ray beam time to the mid-diastolic window), multi-segmental reconstruction and motion correction algorithm (Fuchs et al., 2014; Yang et al., 2011; Labounty et al., 2010). Padding with prospectively ECG-triggered and multi-segmental reconstruction in retrospectively ECG-triggered are associated with substantial increase of patient dose. Fuchs et al. (2014) have reported image quality improvement and interpretability of prospectively ECG-triggered CCTA with motion correction algorithm at average heart rate of 69 ± 9 bpm.

While ICA may expose the patient with radiation dose in the range of 3 to 9 mSv, H_E as high as 12 to 26 mSv have been reported in CCTA using 64-detector-row CT scanners (Sun & Ng, 2010; Hermann et al., 2008; Peebles, 2006). Hurwitz et al. (2007) performed organ dose measurements for retrospectively ECG-triggered CCTA protocols in 64-detector-row CT scanner, using a female adult anthropomorphic phantom. From their study, skin, breast, oesophagus and heart received the highest radiation dose and H_E was

ranged from 17.9 to 31.8 mSv. Underestimation of H_E by 20 to 30 % was reported with the use of E_{KL} for chest region of 0.017 $mSv.mGy^{-1}cm^{-1}$.

Different prospectively ECG-triggered CCTA protocols have been introduced by CT manufacturers. These protocols are strongly dependent on the hardware specifications. According to the literature, significantly lower H_E (2.7 to 4.5 mSv) was reported in prospectively ECG-triggered CCTA for patients with a low and regular heart rate (less or equal to 70 bpm), compared to retrospectively ECG-triggered CCTA (Sun & Ng, 2012b, 2012a; von Ballmoos et al., 2011). With the later generation of CT scanners (higher than 64-detector-row) that allow volumetric imaging or high helical pitch scanning, H_E as low as 0.4 to 1.2 mSv can be achieved for an average sized patient (Benz et al., 2016; Chen et al., 2013; Achenbach et al., 2010).

Einstein et al. (2007) estimated the LAR of cancer incidence associated with radiation exposure from 64-detector-row CCTA. From their study, the estimated LAR were found to vary markedly and is considerably greater for women and younger patients due to the higher radiosensitivity of the breasts and lungs in women. Similar results were also reported in two later studies that assess the radiation exposure in CCTA using 128- and 320-detector-row CT scanners (Khan et al., 2014; Perisinakis et al., 2010).

3.3 Materials and methods

3.3.1 Study design

This study was designed to measure organ doses received from a prospectively ECG-triggered CCTA examination using a standard female adult anthropomorphic phantom and optically stimulated luminescence dosimeters (OSLDs). Dose measurement was carried out using five CT scanners of different generations, located at five different centres; HSC Medical Center, iHeal Medical Centre, Life Care Diagnostic Medical

Centre, Tung Shin Hospital and University Malaya Medical Centre. The recommended CCTA imaging protocols were used according to the manufacturers' guidelines.

3.3.2 Anthropomorphic phantom and optically stimulated luminescence dosimeters (OSLD)

A female adult anthropomorphic phantom (702-G, CIRS Inc., Norfolk, Virginia, USA) assembled with multiple holes for the placement of the OSLDs (NanoDot, Landauer Inc., Glenwood, IL) was used. The phantom represented a female adult of 160 cm height and 55 kg weight. The phantom is made of tissue-equivalent materials that simulate average soft tissues, average bone tissues, cartilage, spinal cord and disks, lung, brain and sinus, where the linear attenuation coefficient of the materials are within 3 % of the actual tissues for photon energies ranged 40 to 150 keV (Zhang et al., 2013). The phantom is sectioned into 38 contiguous slabs of 25 mm thickness. Each section contains several 14 mm-diameter holes and plugs for OSLDs placement across 19 organs (Figure 3.1 (a)). The phantom has a pair of detachable breasts with base diameter 10.8 cm and height 4.3 cm. The ratio of glandular: adipose tissues is 50: 50. Specific holes and plugs are located in the breasts, at 1 cm below the skin surface for OSLD placement (Appendix F).

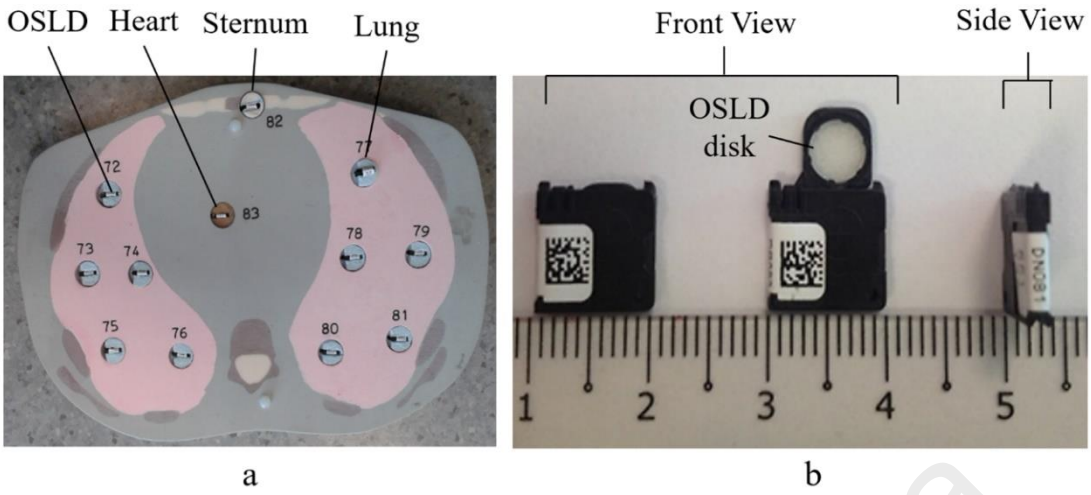

Figure 3.1: (a) Axial view of the phantom's sectional slab showing the lungs, spine, heart and sternum. The OSLDs are loaded into the tissue-equivalent plugs within the organs. (b) Front and side views of OSLD's holder.

The OSLD is made of aluminum oxide doped with carbon ($Al_2O_3:C$). It is in disk-shaped of 5 mm diameter and 0.2 mm thickness, wrapped in a light-tight 10 × 10 × 2 mm^3 black plastic carrier with a density of 1.03 $g.cm^{-3}$ (Figure 3.1 (b)). The OSLDs used in this study were calibrated for X-ray energy of 120 kVp. A calibrated OSLD reader system (MicroStar InLight reader, Landauer, Glenwood, Illinois, USA) was used to acquire the energy released by each OSLD and subsequently converted it to absorbed dose (mGy) based on the calibration curve.

3.3.3 CT scanners and imaging protocols

The five different generations CT scanners used in this study include 64-detector-row SSCT system (Optima CT 660, GE Healthcare, USA), 64-detector-row SSCT system (Ingenuity 128, Philips Healthcare, USA), 2 × 32-detector-row DSCT system (Somatom Definition Dual Source, Siemens Healthcare, Germany), 2 × 64-detector-row DSCT system (Somatom Definition Flash, Siemens Healthcare, Germany) and 320-detector-row SSCT system (Aquilion ONE, Toshiba Medical System, Japan) (Figure 3.2 to Figure 3.6). Specifications of CT scanners are included in Appendix A to E. The prospectively ECG-triggered CCTA protocols recommended by the respective CT manufacturers were used. These protocols include Snapshot Pulse Acquisition (Optima CT 660, GE Healthcare,

USA) – thereafter referred as “protocol A”, Step and Shoot Cardiac Acquisition (Ingenuity 128, Philips Healthcare, USA) – thereafter referred as “protocol B”, Adaptive Cardio Sequence Acquisition (Somatom Definition Dual Source, Siemens Healthcare, Germany) – thereafter referred as “protocol C”, Flash Spiral Acquisition (Somatom Definition Flash, Siemens Healthcare, Germany) – thereafter referred as “protocol D”, and Volumetric Cardiac Acquisition (Aquilion ONE, Toshiba Medical Centre, Japan) – therefore referred as “protocol E”.

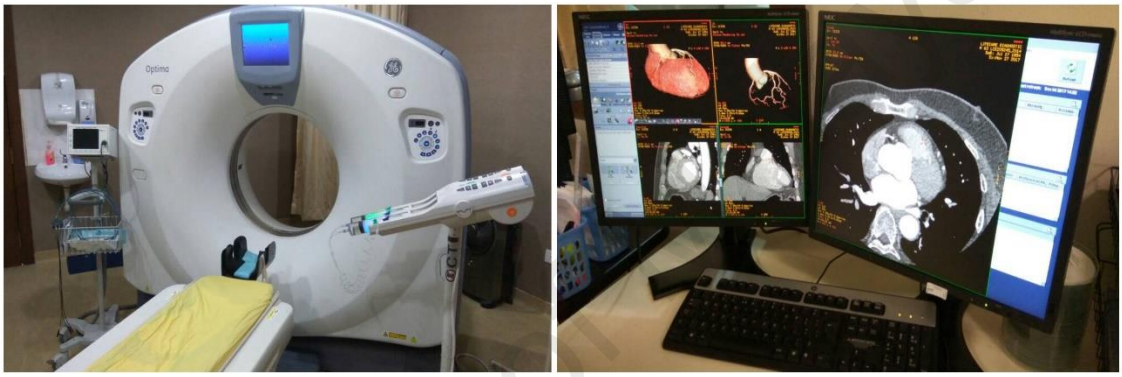

Figure 3.2: 64-detector-row SSCT system (Optima CT 660, GE Healthcare, USA) at Life Care Diagnostic Medical Centre.

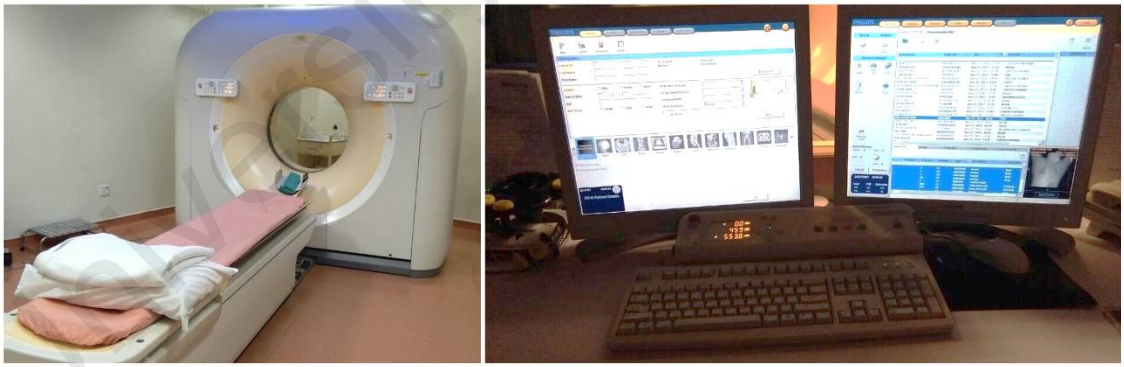

Figure 3.3: 64-detector-row SSCT system (Ingenuity 128, Philips Healthcare, USA) at Tung Shin Hospital.

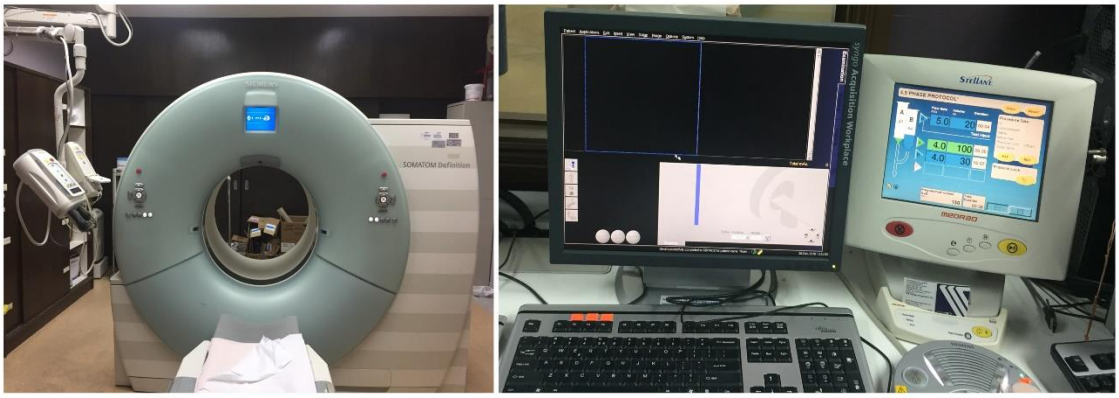

Figure 3.4 : 2 × 32-detector-row DSCT system (Somatom Definition Dual Source, Siemens Healthcare, Germany) at University of Malaya Medical Centre.

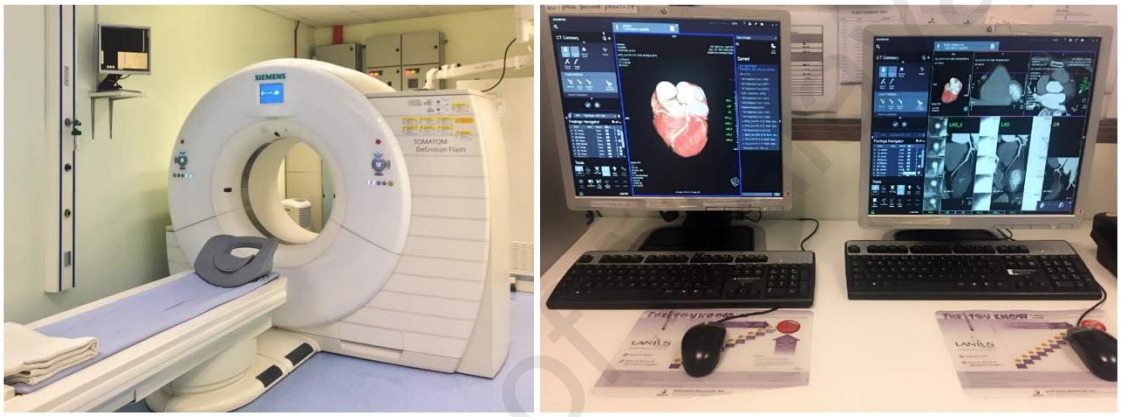

Figure 3.5: 2 × 64-detector-row DSCT system (Somatom Definition Flash, Siemens Healthcare, Germany) at HSC Medical Center.

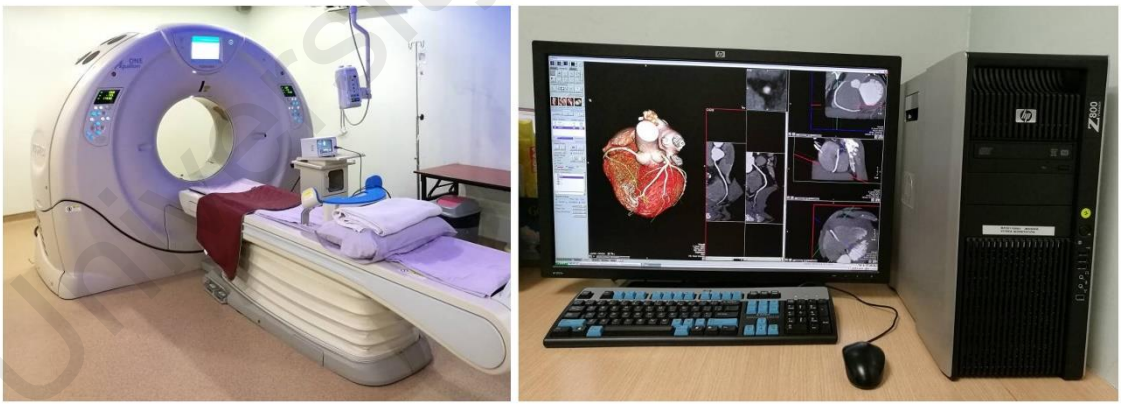

Figure 3.6: 320-detector-row SSCT system (Aquilion ONE, Toshiba Medical System, Japan) at iHeal Medical Centre.

The anthropomorphic phantom pre-loaded with 244 OSLDs from brain to femora was positioned on the CT scanner table (Figure 3.7 (a)). The scan range was fixed at 140 mm covering from the carina of trachea to the apex of the heart (Figure 3.7 (b)). The CT scanner was connected to an ECG monitor and a constant heart rate of 60 bpm was applied

using ECG demo mode. Table 3.1 summarizes the scanning parameters for a complete CCTA examination including the SPR, bolus tracking or test bolus and prospectively ECG-triggered CCTA using the respected CT scanners. For bolus tracking technique, threshold of 150 HU was set at the ROI to initiate the scan. For the test bolus technique, six exposures were performed at the ROI to identify the triggering threshold and continued with the prospectively ECG-triggered CCTA. All image acquisition were performed at the mid-diastolic phase (70 to 80 % in R-R interval) without padding.

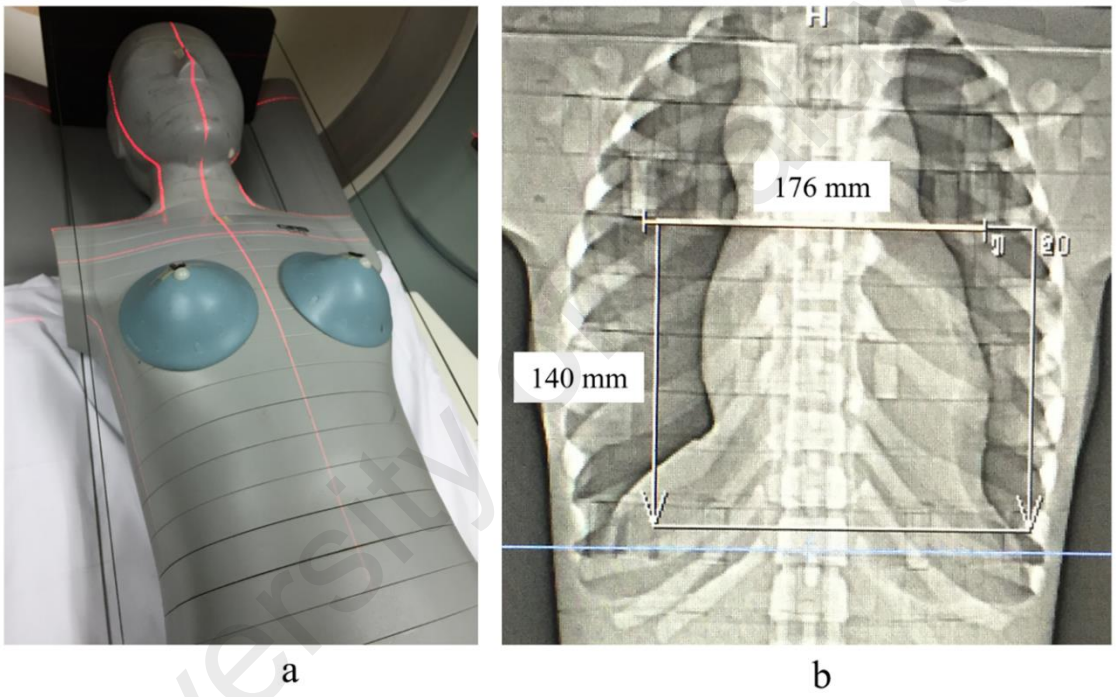

Figure 3.7: (a) Positioning of phantom according to the clinical CCTA settings; (b) scan projection radiograph (SPR) image of phantom with the scan range planned for CCTA (white box).

Table 3.1: Scanning parameters for prospectively ECG-triggered CCTA using five different CT scanners.

Imaging Protocol	**Protocol A**	**Protocol B**	**Protocol C**	**Protocol D**	**Protocol E**
Scanner model	Optima CT 660	Ingenuity 128	Somatom Definition Dual Source	Somatom Definition Flash	Aquilion ONE
Manufacturer	GE Healthcare	Philips Healthcare	Siemens Healthcare	Siemens Healthcare	Toshiba Medical System Corporation

'Table 3.1 continued'

Imaging Protocol	Protocol A	Protocol B	Protocol C	Protocol D	Protocol E
Number of slices	128	128	128	256	640
Detector type	HiLight V-Res VolaraDAS	NanoPanel	Ultrafast ceramic	Ultrafast ceramic	Solid-stateGd2O2S
Detector-row	64	64	2 × 32	2 × 64	320
Detector thickness (mm)	0.625	0.625	0.6	0.6	0.5
z-axis coverage per gantry rotation (mm)	40.0	40.0	19.2	38.4	160.0
Gantry rotation time (ms)	350	300	330	280	350
Scan Projection Radiograph (SPR)					
Tube voltage (kVp)	120	120	120	120	120
Tube current (mA)	40	30	35	50	50
Bolus tracking/Test bolus					
Tube voltage (kVp)	120	120	120	120	120
Tube current-time product (mAs)	40	30	45	60	25
Contrast timing method	Bolus tracking	Bolus tracking	Test bolus	Test bolus	Test bolus
Number of scan	6	6	6	6	6
Threshold (HU)	150	150	-	-	-
Scanning time (s)	8.76	10.0	10.5	10.3	10.0
Prospectively ECG-triggered CCTA					
Acquisition technique	Snapshot Pulse	Step and Shoot Cardiac	Adaptive Cardio Sequence	Flash Spiral	Volumetric Cardiac
Tube voltage (kVp)	120	120	120	120	120

'Table 3.1 continued'

Imaging Protocol	Protocol A	Protocol B	Protocol C	Protocol D	Protocol E
Tube current-time (mAs)	197	180	218	169	15
Heart rate (bpm)	60	60	60	60	60
Total exposure time (s)	1.76	1.96	3.04	0.45	1.22
Acquisition slice thickness (mm)	0.625	0.625	0.6	0.6	0.5
Reconstruction slice thickness (mm)	0.625	0.9	3.0	0.75	0.5

3.3.4 Organ dose measurement

A total of three measurements were done for each imaging protocol. Each measurement was obtained by averaging the results from five exposures. The OSLD signals were analysed and converted to absorbed dose using the calibration curve. Organ doses were obtained by multiplying the absorbed dose with individual w_T recommended by the ICRP-103 publication (ICRP, 2007).

3.3.5 Effective dose (H_E) estimation

The H_E was estimated using two different approaches in this study and the results were compared. Firstly, the H_E was computed by summing up all the organ doses measured from the anthropomorphic phantom. Secondly, the H_E was calculated by multiplying the P_{KL} (previously known as DLP) recorded from the CT console with the E_{KL}, as in Eq. 2.9 (IAEA, 2007; ICRP, 2007).

E_{KL} is region-specific, P_{KL} normalized H_E ($mSv.mGy^{-1}cm^{-1}$) conversion factor. The E_{KL} for chest region, 0.014 $mSv.mGy^{-1}cm^{-1}$ as recommended by the EC and PHE (formerly NRPB) was used in this study (Shrimpton et al., 2005; Shrimpton, 2004).

3.3.6 Cancer risk estimation

The LAR for the incidence of radiation-induced cancer of lung for male and female and breast for female aged 20, 30, 40, 50, 60, 70 and 80 years were estimated, respectively. The breast and lung absorbed doses used in these calculations were the average of right and left sides of the organ doses measured in this study. The LAR has been described in the BEIR VII report (NCRP, 1993) and is expressed by Eq. 2.10. A simplified method can be used for calculation of LAR, based LR estimates for cancer incidence resulting from a single dose of 0.1 Gy at several specific ages tabulated in TABLE 12D-1, BEIR VII report. For instance, the average dose for CCTA to the lungs was 0.013 Gy. From the BEIR VII report, the lung incidence for 20-year-old women is 346 cases per 100,000. Thus, the LAR from a 0.013 Gy dose is $\frac{0.013}{0.1} \times 346 = 45$ per 100,000 population.

Lifetime RR of radiation-induced cancer was estimated on the basis of baseline values of LR in the absence of exposure, as in Eq. 2.11 (Hurwitz et al., 2007; NCRP, 1993). Whereas the estimation of the P_{joint} of inducing either breast cancer or lung cancer in radiation-exposed female patients were calculated as in Eq. 2.13 (NCRP, 1993). LAR_{joint} and RR_{joint} were calculated as in Eq. 2.12 and Eq. 2.14 (Hurwitz et al., 2007; NRC, 2006).

ERR, the amount of additional RR above baseline, was calculated as a percentage over baseline, as in Eq. 2.16 (Committee to assess health risks from exposure to low levels of ionizing radiation, 2006).

3.4 Statistical analysis

Statistical analyses were performed (SPSS software version 23.0, IBM Corporation, Armonk, New York, USA). Continuous variables were presented as mean ± standard deviation. The organ doses measured from all the protocols were compared using one-way ANOVA, followed by post-hoc Fisher's LSD test to identify the significance of the

differences between each data pair. 95 % confidence interval was used in all the statistical tests.

3.5 Results

3.5.1 Organ doses

The organ doses measured from the anthropomorphic phantom are tabulated in Table 3.2. There were 34 organs involved from brain to femora excluding skin. Comparison of organ doses across different scanners is better presented in a graph format, as shown in Figure 3.8. Ten organs were directly exposed to the primary beam in the FOV during CCTA, i.e. breasts, lungs, oesophagus, liver, stomach, sternum, heart, thoracic spine, ribs and scapula. Among these organs, breasts received the highest radiation dose followed by lungs, oesophagus, liver, stomach, etc. Using 320-detector-row SSCT scanner and Protocol E, the organ doses were significantly reduced compared to all other scanners and protocols. The second lowest radiation dose was achieved by using 2 × 64-detector-row DSCT scanner and protocol D, followed by 64-detector-row SSCT scanner with Protocol B and Protocol A. The 2 × 32-detector-row DSCT scanner contributed higher dose compared to the 64-detector-row SSCT. One-way ANOVA test shows significant difference ($p < 0.05$) for organ doses measured in different protocols. On post-hoc Fisher's LSD test, organ doses measured in protocol E was statistically different ($p < 0.05$) to organ doses measured in protocols A, B and C; organ doses measured in protocol D was statistically significant different ($p < 0.05$) to organ doses measured in protocol A and C, while no other comparison was statistically significant different (Table 3.3). Figure 3.9 illustrates the distribution of dose at different organs at a glance. The colour coding indicates the level of radiation dose received by the respective organs, and the red box shows the FOV. Protocol E contributed the least dose to all organs among all the protocols.

Table 3.2: Mean organ doses measured from the female anthropomorphic phantom during prospectively ECG-triggered CCTA.

Organ	Mean absorbed dose (mGy)				
	Protocol A	**Protocol B**	**Protocol C**	**Protocol D**	**Protocol E**
Adrenals	3.96 ± 0.05	3.46 ± 0.16	3.72 ± 0.04	3.20 ± 0.02	0.83 ± 0.13
Bladder	0.05 ± 0.06	0.01 ± 0.02	0.11 ± 0.17	0.22 ± 0.01	0.30 ± 0.33
Brain	0.36 ± 0.30	0.01 ± 0.02	0.26 ± 0.20	0.04 ± 0.02	0.04 ± 0.07
Breast, Left	16.20 ± 0.32	14.58 ± 0.24	15.76 ± 0.28	3.50 ± 0.02	4.60 ± 0.45
Breast, Right	14.23 ± 0.32	13.77 ± 0.31	15.23 ± 0.53	3.83 ± 0.06	4.24 ± 0.14
Cervical Spine	0.77 ± 0.35	0.29 ± 0.41	0.62 ± 0.01	0.29 ± 0.20	0.29 ± 0.19
Clavicle	1.43 ± 0.14	0.37 ± 0.13	1.95 ± 0.54	0.86 ± 0.06	0.25 ± 0.32
Colon	0.43 ± 0.27	0.20 ± 0.07	0.22 ± 0.11	0.20 ± 0.01	0.06 ± 0.08
Cranium	0.29 ± 0.30	0.01 ± 0.01	0.27 ± 0.30	0.03 ± 0.01	0.20 ± 0.38
Femora	0.12 ± 0.17	0.01 ± 0.02	0.17 ± 0.19	0.01 ± 0.00	0.27 ± 0.39
Gallbladder	1.16 ± 0.69	0.82 ± 0.30	1.11 ± 0.54	0.55 ± 0.32	0.64 ± 0.56
Heart	15.28 ± 0.18	11.51 ± 0.78	18.91 ± 0.66	5.14 ± 0.41	4.17 ± 0.23
Kidney, Left	0.95 ± 0.51	0.87 ± 0.51	0.95 ± 0.35	0.41 ± 0.11	0.29 ± 0.20
Kidney, Right	0.60 ± 0.29	0.62 ± 0.25	0.90 ± 0.80	0.57 ± 0.27	0.37 ± 0.44
Liver	11.83 ± 1.22	9.47 ± 0.92	14.06 ± 1.45	3.98 ± 0.17	2.91 ± 1.15
Lumbar Spine	0.31 ± 0.38	0.15 ± 0.14	0.40 ± 0.30	0.20 ± 0.27	0.07 ± 0.06

'Table 3.2, continued'

Organ	Mean absorbed dose (mGy)				
	Protocol A	**Protocol B**	**Protocol C**	**Protocol D**	**Protocol E**
Lung, Left	12.06 ± 1.61	12.04 ± 1.72	12.36 ± 1.88	4.07 ± 0.47	2.25 ± 1.22
Lung, Right	13.57 ± 2.04	12.57 ± 1.94	14.54 ± 2.30	4.54 ± 0.54	2.48 ± 1.17
Mandible	0.57 ± 0.38	0.06 ± 0.11	0.43 ± 0.09	0.19 ± 0.03	0.05 ± 0.09
Oesophagus	13.21 ± 1.26	11.58 ± 4.69	16.63 ± 0.69	6.89 ± 3.25	2.08 ± 1.05
Ovary, Left	0.02 ± 0.01	0.05 ± 0.00	0.04 ± 0.01	0.02 ± 0.00	0.03 ± 0.01
Ovary, Right	0.01 ± 0.01	0.01 ± 0.01	0.05 ± 0/01	0.02 ± 0.00	0.01 ± 0.02
Pancreas	1.15 ± 0.37	0.66 ± 0.47	0.96 ± 0.31	0.55 ± 0.06	0.41 ± 0.21
Pelvis	0.22 ± 0.21	0.07 ± 0.08	0.11 ± 0.10	0.05 ± 0.02	0.14 ± 0.31
Ribs	9.90 ± 1.37	8.92 ± 1.17	11.00 ± 2.47	3.62 ± 0.42	2.13 ± 1.43
Scapula	8.60 ± 1.00	9.62 ± 0.79	10.94 ± 0.12	4.64 ± 0.65	0.62 ± 0.40

Protocol A, Snapshot Pulse Acquisition (Optima CT 660, GE Healthcare, USA);
Protocol B, Step and Shoot Cardiac Acquisition (Ingenuity 128, Philips Healthcare, USA);
Protocol C, Adaptive Cardio Sequence Acquisition (Somatom Definition Dual Source, Siemens Healthcare, Germany);
Protocol D, Flash Spiral Acquisition (Somatom Definition Flash, Siemens Healthcare, Germany);
Protocol E, Volumetric Cardiac Acquisition (Aquilion ONE, Toshiba Medical Centre, Japan).

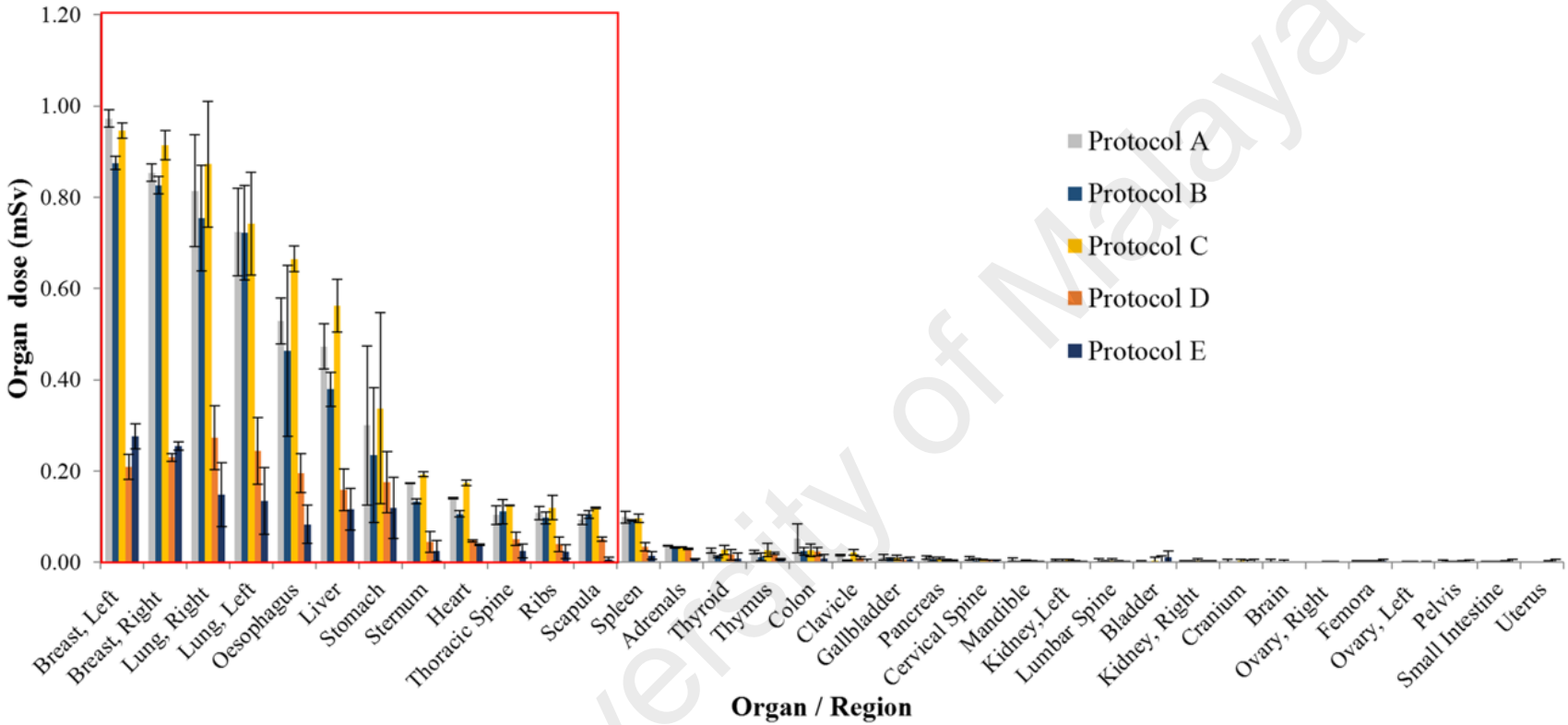

Protocol A, Snapshot Pulse Acquisition (Optima CT 660, GE Healthcare, USA);
Protocol B, Step and Shoot Cardiac Acquisition (Ingenuity 128, Philips Healthcare, USA);
Protocol C, Adaptive Cardio Sequence Acquisition (Somatom Definition Dual Source, Siemens Healthcare, Germany);
Protocol D, Flash Spiral Acquisition (Somatom Definition Flash, Siemens Healthcare, Germany);
Protocol E, Volumetric Cardiac Acquisition (Aquilion ONE, Toshiba Medical Centre, Japan).

Figure 3.8: Graph shows the organ dose of 34 organs obtained using prospectively ECG-triggered CCTA in five different generations CT scanners. The red box indicates organs included in the scanning field of view (FOV).

Table 3.3: Results of post-hoc Fisher's LSD test to evaluate significance level of each protocol pair.

Data-Pair	*p*-value
Protocol A – Protocol B	0.750
Protocol A – Protocol C	0.799
Protocol A – Protocol D	0.047*
Protocol A – Protocol E	0.023*
Protocol B – Protocol C	0.567
Protocol B – Protocol D	0.094
Protocol B – Protocol E	0.050
Protocol C – Protocol D	0.025*
Protocol C – Protocol E	0.012*
Protocol D – Protocol E	0.774

* $p < 0.05$ is considered statistically significant different.
Protocol A, Snapshot Pulse Acquisition (Optima CT 660, GE Healthcare, USA);
Protocol B, Step and Shoot Cardiac Acquisition (Ingenuity 128, Philips Healthcare, USA);
Protocol C, Adaptive Cardio Sequence Acquisition (Somatom Definition Dual Source, Siemens Healthcare, Germany);
Protocol D, Flash Spiral Acquisition (Somatom Definition Flash, Siemens Healthcare, Germany);
Protocol E, Volumetric Cardiac Acquisition (Aquilion ONE, Toshiba Medical Centre, Japan).

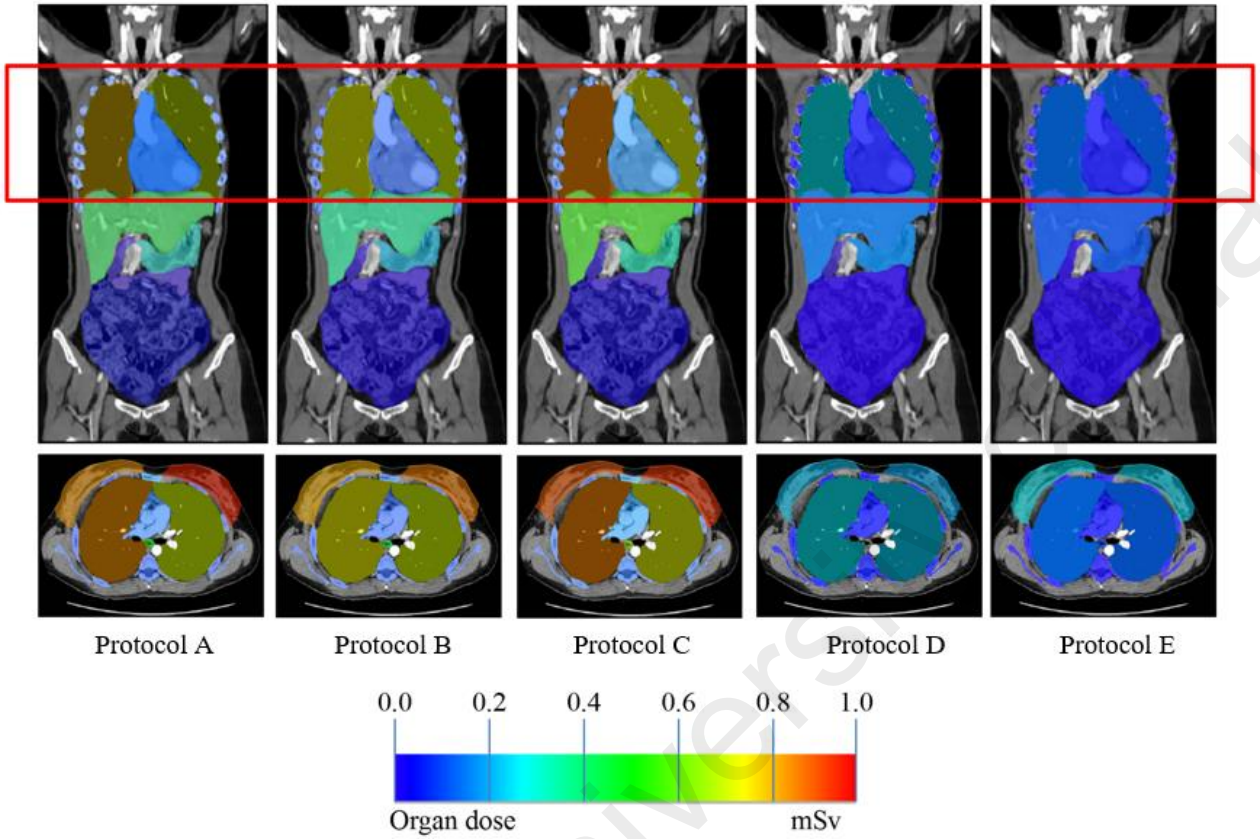

Protocol A, Snapshot Pulse Acquisition (Optima CT 660, GE Healthcare, USA);
Protocol B, Step and Shoot Cardiac Acquisition (Ingenuity 128, Philips Healthcare, USA);
Protocol C, Adaptive Cardio Sequence Acquisition (Somatom Definition Dual Source, Siemens Healthcare, Germany);
Protocol D, Flash Spiral Acquisition (Somatom Definition Flash, Siemens Healthcare, Germany);
Protocol E, Volumetric Cardiac Acquisition (Aquilion ONE, Toshiba Medical Centre, Japan).

Figure 3.9: Organ dose obtained in different prospectively ECG-triggered CCTA protocols.

3.5.2 H_E estimation

The comparison of H_E obtained by summing up all the organ doses from the phantom measurement (measured H_E) and by computing using the E_{KL} (computed H_E) is shown in Table 3.4. In general, the measured H_E was higher than the computed H_E by 38.3 to 53.2 %. Protocol C contributed the highest H_E, followed by protocol A, B, D and E.

3.5.3 Cancer risk estimation

The estimated LAR of cancer incidence for breast and lung are summarized in Table 3.5 and Table 3.6. The estimated LAR decreased as a function of age (Figure 3.10). For lung cancer, LAR ranged from 1 case per 100,000 in 80-year-old male using protocol D and E to 20 cases per 100,000 in 20-year-old using protocol C; LAR ranged from 2 cases per 100,000 in 80-year-old female using protocol E to 47 cases per 100,000 in 20-year-old using protocol C. The LAR of lung cancer in female is higher than male at all age (Figure 3.10). For breast cancer, the LAR ranged from less than 0.02 cases per 100,000 in 80-year-old female using protocol E to 66 cases per 100,000 in 20-year-old using protocol C.

The LAR_{joint} for either breast or lung cancer ranged from 2 cases per 100,000 in 80-year-old female using protocol E to 113 cases per 100,000 in 20-year-old using protocol C. The highest estimated RR_{joint} (1.006) and ERR_{joint} (0.65 %) were recorded in 20-year-old female patient using protocol C (Table 3.7). Finally, Table 3.8 shows the estimated LAR, RR and ERR for other cancers incidence in a female patient. For other cancers in female, the estimated risks were considerably lower compared to breast and lung cancer. Generally, the LAR were quite similar between protocol A, B and C; protocol D and E showed very low LAR for all cancers at all age of exposure (below 30 cases per 100,000 population).

Table 3.4: Estimated effective doses (H_E) obtained from prospectively ECG-triggered CCTA using different generations CT scanners and protocols.

Parameter	Protocol A	Protocol B	Protocol C	Protocol D	Protocol E
P_{KL} (mGy.cm)	193.40 ± 2.52	168.10 ± 3.44	204.00 ± 3.30	83.00 ± 3.01	57.90 ± 1.21
Measured H_E (mSv)	5.60 ± 0.68	5.02 ± 0.73	6.06 ± 0.72	1.88 ± 0.25	1.34 ± 0.48
Computed H_E (mSv)	2.71 ± 0.04	2.35 ± 0.05	2.86 ± 0.05	1.16± 0.04	0.81 ± 0.02
% difference (Measured H_E – Computed H_E)	51.6 %	53.2 %	52.8 %	38.3 %	39.6 %

H_E, effective dose; P_{KL}, air-kerma length product.
Protocol A, Snapshot Pulse Acquisition (Optima CT 660, GE Healthcare, USA);
Protocol B, Step and Shoot Cardiac Acquisition (Ingenuity 128, Philips Healthcare, USA);
Protocol C, Adaptive Cardio Sequence Acquisition (Somatom Definition Dual Source, Siemens Healthcare, Germany);
Protocol D, Flash Spiral Acquisition (Somatom Definition Flash, Siemens Healthcare, Germany);
Protocol E, Volumetric Cardiac Acquisition (Aquilion ONE, Toshiba Medical Centre, Japan).

Table 3.5: Estimated LAR, RR and ERR for lung cancer incidence from prospectively ECG-triggered CCTA using different CT scanners and protocols.

Age at Exposure (y)	Sex	Protocol A			Protocol B			Protocol C			Protocol D			Protocol E		
		LAR (cases per 100,000)	RR	ERR (%)	LAR (cases per 100,000)	RR	ERR (%)	LAR (cases per 100,000)	RR	ERR (%)	LAR (cases per 100,000)	RR	ERR (%)	LAR (cases per 100,000)	RR	ERR (%)
20	male	19	1.004	0.37	18	1.003	0.34	20	1.004	0.35	6	1.001	0.12	4	1.001	0.07
30	male	13	1.003	0.26	13	1.002	0.24	14	1.002	0.25	5	1.001	0.08	2	1.000	0.05
40	male	13	1.003	0.26	13	1.002	0.24	14	1.002	0.25	4	1.001	0.08	2	1.000	0.05
50	male	13	1.003	0.25	12	1.002	0.23	14	1.002	0.24	4	1.001	0.08	2	1.000	0.04
60	male	11	1.002	0.22	11	1.002	0.20	12	1.002	0.21	4	1.001	0.07	2	1.000	0.04
70	male	8	1.002	0.16	8	1.001	0.15	9	1.002	0.15	3	1.001	0.05	2	1.000	0.03
80	male	4	1.001	0.07	4	1.001	0.07	4	1.001	0.07	1	1.000	0.02	1	1.000	0.01
20	Female	44	1.008	0.82	43	1.008	0.79	47	1.009	0.86	15	1.003	0.28	8	1.002	0.15
30	Female	31	1.006	0.57	30	1.006	0.55	33	1.006	0.60	10	1.002	0.19	6	1.001	0.11
40	Female	31	1.006	0.57	30	1.005	0.55	32	1.006	0.60	10	1.002	0.19	6	1.001	0.11
50	Female	30	1.005	0.55	28	1.005	0.52	31	1.006	0.57	10	1.002	0.18	5	1.001	0.10
60	Female	26	1.005	0.48	25	1.005	0.46	27	1.005	0.50	9	1.002	0.16	5	1.001	0.09
70	Female	19	1.003	0.35	18	1.003	0.33	20	1.004	0.37	6	1.001	0.12	3	1.001	0.06
80	Female	10	1.002	0.18	9	1.002	0.18	10	1.002	0.19	3	1.001	0.06	2	1.000	0.03

ERR, excess relative risk; LAR, lifetime attributable risk; RR, Relative risk;
Protocol A, Snapshot Pulse Acquisition (Optima CT 660, GE Healthcare, USA);
Protocol B, Step and Shoot Cardiac Acquisition (Ingenuity 128, Philips Healthcare, USA);
Protocol C, Adaptive Cardio Sequence Acquisition (Somatom Definition Dual Source, Siemens Healthcare, Germany);
Protocol D, Flash Spiral Acquisition (Somatom Definition Flash, Siemens Healthcare, Germany);
Protocol E, Volumetric Cardiac Acquisition (Aquilion ONE, Toshiba Medical Centre, Japan).

Table 3.6: Estimated LAR, RR and ERR for breast cancer incidence from prospectively ECG-triggered CCTA using different CT scanners and protocols.

Age at Exposure (y)	Protocol A			Protocol B			Protocol C			Protocol D			Protocol E		
	LAR (cases per 100,000)	RR	ERR (%)	LAR (cases per 100,000)	RR	ERR (%)	LAR (cases per 100,000)	RR	ERR (%)	LAR (cases per 100,000)	RR	ERR (%)	LAR (cases per 100,000)	RR	ERR (%)
20	65	1.005	0.54	61	1.005	0.51	66	1.006	0.55	2	1.000	0.00	2	1.000	0.00
30	38	1.003	0.32	36	1.003	0.30	39	1.003	0.33	1	1.000	0.00	1	1.000	0.00
40	21	1.002	0.18	20	1.002	0.17	22	1.002	0.18	1	1.000	0.00	1	1.000	0.00
50	11	1.001	0.09	10	1.001	0.08	11	1.001	0.09	<0.3	1.000	0.00	<0.4	1.000	0.00
60	5	1.000	0.04	4	1.000	0.04	5	1.000	0.04	<0.2	1.000	0.00	<0.2	1.000	0.00
70	2	1.000	0.02	2	1.000	0.01	2	1.000	0.02	<0.05	1.000	0.00	<0.06	1.000	0.00
80	1	1.000	0.01	1	1.000	0.00	1	1.000	0.01	<0.02	1.000	0.00	<0.02	1.000	0.00

ERR, excess relative risk; LAR, lifetime attributable risk; RR, Relative risk;
Protocol A, Snapshot Pulse Acquisition (Optima CT 660, GE Healthcare, USA);
Protocol B, Step and Shoot Cardiac Acquisition (Ingenuity 128, Philips Healthcare, USA);
Protocol C, Adaptive Cardio Sequence Acquisition (Somatom Definition Dual Source, Siemens Healthcare, Germany);
Protocol D, Flash Spiral Acquisition (Somatom Definition Flash, Siemens Healthcare, Germany);
Protocol E, Volumetric Cardiac Acquisition (Aquilion ONE, Toshiba Medical Centre, Japan).

Table 3.7: Estimated LAR for either breast or lung cancer incidence in female from prospectively ECG-triggered CCTA using different CT scanners and protocols.

Age at Exposure (y)	Protocol A			Protocol B			Protocol C			Protocol D			Protocol E		
	LAR_{joint} (cases per 100,000)	RR_{joint}	ERR_{joint} (%)	LAR_{joint} (cases per 100,000)	RR_{joint}	ERR_{joint} (%)	LAR_{joint} (cases per 100,000)	RR_{joint}	ERR_{joint} (%)	LAR_{joint} (cases per 100,000)	RR_{joint}	ERR_{joint} (%)	LAR_{joint} (cases per 100,000)	RR_{joint}	ERR_{joint} (%)
20	110	1.006	0.63	103	1.006	0.59	113	1.006	0.65	16	1.001	0.09	10	1.001	0.06
30	70	1.004	0.40	66	1.004	0.38	72	1.004	0.41	11	1.001	0.07	7	1.000	0.04
40	52	1.003	0.30	50	1.003	0.28	54	1.003	0.31	11	1.001	0.06	6	1.000	0.04
50	40	1.002	0.23	38	1.002	0.22	42	1.002	0.24	10	1.001	0.06	6	1.000	0.03
60	30	1.002	0.18	29	1.002	0.17	32	1.002	0.18	9	1.001	0.05	5	1.000	0.03
70	21	1.001	0.12	20	1.001	0.11	22	1.001	0.12	6	1.000	0.04	4	1.000	0.02
80	10	1.001	0.06	10	1.001	0.06	11	1.001	0.06	3	1.000	0.02	2	1.000	0.01

ERR_{joint}, joint excess relative risk; LAR_{joint}, joint lifetime attributable risk; RR_{joint}, joint relative risk.
Protocol A, Snapshot Pulse Acquisition (Optima CT 660, GE Healthcare, USA);
Protocol B, Step and Shoot Cardiac Acquisition (Ingenuity 128, Philips Healthcare, USA);
Protocol C, Adaptive Cardio Sequence Acquisition (Somatom Definition Dual Source, Siemens Healthcare, Germany);
Protocol D, Flash Spiral Acquisition (Somatom Definition Flash, Siemens Healthcare, Germany);
Protocol E, Volumetric Cardiac Acquisition (Aquilion ONE, Toshiba Medical Centre, Japan).

Table 3.8: Estimated LAR, RR and ERR for other cancers incidence in female from prospectively ECG-triggered CCTA using different CT scanners and protocols.

Age at Exposure (y)	Protocol A			Protocol B			Protocol C			Protocol D			Protocol E		
	LAR (cases per 100,000)	RR	ERR (%)	LAR (cases per 100,000)	RR	ERR (%)	LAR (cases per 100,000)	RR	ERR (%)	LAR (cases per 100,000)	RR	ERR (%)	LAR (cases per 100,000)	RR	ERR (%)
20	24	1.002	0.20	21	1.002	0.17	28	1.002	0.23	10	1.000	0.00	5	1.000	0.00
30	16	1.001	0.13	13	1.001	0.11	18	1.001	0.15	6	1.000	0.00	3	1.000	0.00
40	14	1.001	0.11	12	1.001	0.10	16	1.001	0.13	6	1.000	0.00	3	1.000	0.00
50	11	1.001	0.09	9	1.001	0.08	13	1.001	0.11	5	1.000	0.00	2	1.000	0.00
60	8	1.001	0.07	7	1.001	0.06	9	1.001	0.08	3	1.000	0.00	2	1.000	0.00
70	5	1.000	0.04	4	1.000	0.04	6	1.000	0.05	2	1.000	0.00	1	1.000	0.00
80	2	1.000	0.02	2	1.000	0.02	3	1.000	0.02	1	1.000	0.00	< 0.5	1.000	0.00

ERR, excess relative risk; LAR, lifetime attributable risk; RR, relative risk;
Protocol A, Snapshot Pulse Acquisition (Optima CT 660, GE Healthcare, USA);
Protocol B, Step and Shoot Cardiac Acquisition (Ingenuity 128, Philips Healthcare, USA);
Protocol C, Adaptive Cardio Sequence Acquisition (Somatom Definition Dual Source, Siemens Healthcare, Germany);
Protocol D, Flash Spiral Acquisition (Somatom Definition Flash, Siemens Healthcare, Germany);
Protocol E, Volumetric Cardiac Acquisition (Aquilion ONE, Toshiba Medical Centre, Japan).

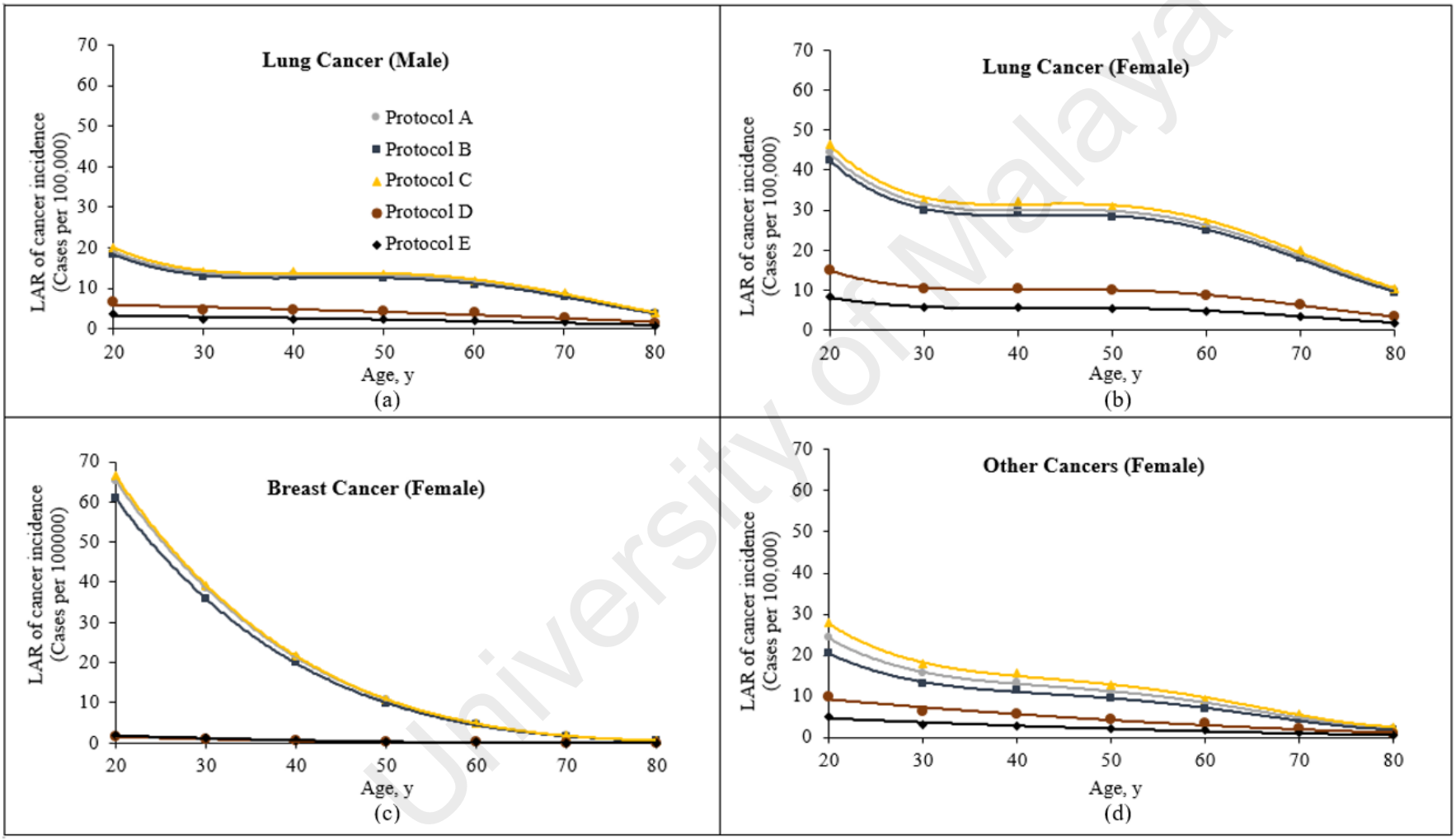

Figure 3.10: Estimated lifetime attributable risk (LAR) of (a) lung cancer incidence for male; (b) lung, (c) breast and (d) other cancers incidence for female from a prospectively ECG-triggered CCTA using different CT scanners and protocols.

3.6 Discussion

In this study, the dose measurement setup in a standard female adult anthropomorphic followed exactly the procedures of a typical CCTA examination of a female patient that include the positioning, SPR, bolus tracking or test bolus and prospectively ECG-triggered CCTA imaging. The imaging parameters recommended by different CT scanner manufacturers are used according to the CT scanner model. Low heart rate of 60 bpm was used during ECG-triggered CCTA considering that this is the average heart rate in most of the clinical cases after beta-blocker is applied. Low heart rate is desirable to guarantee a better image quality and lower radiation dose to the patient during prospectively ECG-triggered CCTA (Hsiao et al., 2010).

The data from this study show that, if excluding skin, breasts received the highest radiation dose, followed by lungs, oesophagus, liver, stomach, sternum and heart. It is therefore important to note that, although heart is the organ of interest in CCTA imaging, other organs such as breasts, lungs, oesophagus, liver and stomach receive relatively higher radiation dose due to their higher sensitivity towards ionising radiation. According to ICRP-103 publication, heart is one of the most radioresistant organs which are categorised as "remainder tissues" when considering its w_T (ICRP, 2007). Although spleen was not included in the FOV, it still received comparable dose as the scapula, ribs and thoracic spine due to scattered radiation from the nearest organ such as liver. The scattered radiation doses received by other organs were negligible.

Among all the CT scanners, 320-detector-row SSCT system gave lowest radiation dose to most of the organs. The measured H_E was 1.34 ± 0.48 mSv while computed H_E was 0.81 ± 0.02 mSv. It is the current latest CT system that has wide z-axis coverage of 160 mm, enabling the whole heart to be imaged in a single gantry rotation. This configuration allows volumetric whole heart imaging during the diastole of one R-R

interval and the entire heart is imaged without temporal delay (Hsiao et al., 2010). However, the scanner has a standard temporal resolution of approximately 175 ms which is inferior to the 83 ms from DSCT, therefore, this type of scanner is only suitable to image patients with low and regular heart rate. The recently developed Revolution CT by GE Healthcare shows promise in imaging patients with high heart rate as it has 160 mm detector array and improved temporal resolution of 140 ms (Latif et al., 2016).

In the comparison of measured versus computed H_E, the mean difference observed from this study ranged between 38.3 and 53.2 %. These findings were consistent with the findings from Hurwitz et al where the measured H_E were higher than the computed H_E (Hurwitz et al., 2007). In this study, the latest E_{KL} as recommended by the EC and PHE was applied (Shrimpton et al., 2005; Shrimpton, 2004). The measured H_E were considered more reliable than computed H_E because the radiation doses were directly measured from all the organs, including those located outside of the primary beam during the CCTA imaging. The use of E_{KL} of 0.014 $mSv.mGy^{-1}cm^{-1}$ may underestimate the overall radiation exposure from CCTA imaging, hence this method may need to be reviewed and improved. In fact, Gosling et al. (2010) and Sabarudin et al. (2013) have both suggested that a E_{KL} of 0.028 $mSv.mGy^{-1}cm^{-1}$ would give a better estimation of the H_E in cardiac-specific imaging.

In this study, the 2 × 32-detector-row DSCT scanner contributed highest H_E in prospectively ECG-triggered CCTA, followed by 64-detector-row SSCT scanners, 2 × 64-detector-row DSCT scanner and 320-detector-row SSCT scanner. Although the H_E varied from 1.34 ± 0.48 to 6.06 ± 0.72 mSv among different generations of CT scanners and imaging protocols, the radiation doses were relatively low compared to many other CT examinations, such as CT for chest (11.0 mSv), abdomen (17.0 mSv) and chest and abdomen (17.0 mSv) (Smith-Bindman et al., 2015). A study carried out by Sabarudin et

al. (2013) found no significant difference in the H_E between sex, however BMI is identified as the main factor that significantly affects the radiation dose. This is also confirmed by a recent study using latest CT model (Latif et al., 2016).

Although the two models of 64-detector-row SSCT scanners and one model of 2 × 32-detector-row DSCT scanner used in this study have the same total number of detector row, the radiation doses contributed by the SSCT scanners were generally lower than the DSCT scanner by 7 and 17 %, respectively. This may be due to the wider z-axis coverage per gantry rotation (40 mm) in 64-detector-row SSCT scanners, compared to only 19.2 mm z-axis coverage per gantry rotation in 2 × 32-detector-row DSCT scanner. Consequently, the 2 × 32-detector-row DSCT scanner requires more than 2 times acquisition time in order to achieve the same volume coverage. Since there is slight overlap in each acquisition slice, this may result in higher dose. Fortunately, this first generation DSCT scanner has now been replaced by the second generation DSCT scanner. Several improvements have been introduced in the second generation DSCT system. Firstly, the detector row was increased from 2 × 32-detector-row to 2 × 64-detector-row with z-axis coverage of 38.4 mm. Secondly, the gantry rotation speed was boosted to 280 ms compared to 330 ms in the first generation system. Thirdly, the scan FOV (in the x-y plane) of the second detector (Detector B) was widened from 260 to 330 mm to provide better coverage of heart anatomy. Fourthly, a new tin-based selective photon shield was used to filter unnecessary low energy photons from the high energy X-ray tube spectrum. This helps to reduce patient dose and enables the separation of high energy and low energy X-ray spectra during dual-energy imaging. Finally, a new “Flash” scanning mode was introduced in the system, which uses fast gantry rotation time in conjunction with a high helical pitch of up to 3.4. With such high pitch, the system can acquire cardiac images in a quarter of gantry rotation time or 75 ms in a single diastolic phase, compared to scanners that may require several cardiac cycles for image

acquisition, hence eliminating additional radiation dose from overlapping slices (Achenbach et al., 2010; Alkadhi et al., 2010). In this study, it was observed that, although the H_E obtained from the 2 × 64-detector-row DSCT scanner was higher than the 320-detector-row SSCT scanner, the doses delivered to the breasts were actually lower. This was a promising result as breast is one of the most radiosensitive organs in CCTA examination.

The estimated risks for radiation-induced cancer after a prospectively ECG-triggered CCTA examination are generally low for all the scanners and protocols. Both breast and lung are the highest radiosensitive organs and received the highest radiation dose during the CCTA examination, hence the LAR for breast and lung cancers are of the most concern in this study. For young women who are less than 30 year-old, the LAR for breast cancer is higher than lung cancer. However, after 30 year-old, the LAR for lung cancer is higher. This is due to the fact that the radiosensitivity of breast is very much age-dependent compared to other organs. Generally, LAR of cancer decreases with the increase of age as older patients are both less radiosensitive and less likely to survive to the development of radiation attributable cancer (HPA, 2013). Between sex, male patients have significant lower LAR for lung cancer than female patients. Since there is no description on the LAR of breast for male patients in BEIR VII report, no comparison were performed among sex for the LAR of breast cancer. The LAR_{joint}, RR_{joint} and ERR_{joint} for breast or lung cancer incidence is higher compared to the LAR for the individual cancer in young women. Compared to the study conducted by Hurwitz et al. (2007), in this study, ERR_{joint} for breast or lung cancer incidence was reduced by more than 50 % by applying prospectively ECG-triggered CCTA with later generation CT scanners (higher than 64-detector-row).

Using the latest CT scanner models and imaging protocols, i.e. 320-detector-row SSCT and 2 × 64-detector-row DSCT, the LAR for lung and breast cancers can be reduced markedly by up to 80 to 97 %. A relative reduction of LAR of 30 % for lung and more than 50 % for breast cancers in CCTA using 320-detector-row CT compared to 64-detector-row CT has also been reported in a previous study (Khan et al., 2014). These improvements are important when weighing risks versus benefit of CCTA as screening program for female patients since CAD mortality is higher in women than in men (Najafi & Sheikhvatan, 2013).

The radiation doses reported in this study provide medical practitioners with data that can be used to assess risk versus benefit of CCTA examination in patients. However, this study has some limitations. Firstly, since this was a phantom study, only one body type was used. The actual doses will vary from patient to patient, depending on patient body habitus, tube current setting, heart rate and z-axis coverage. Secondly, only five most commonly used CT scanner models for CCTA examination were used in this study, while the most recent CT scanners such as 128-detector-row SSCT scanner, 256-detector-row SSCT scanner, third generation of DSCT scanner and second generation of 320-detetor-row SSCT scanner were not included in data acquisition of this study because the latest CT scanners are not available yet in many clinical centres (Mettler et al., 2009).

Hou et al. (2013) reported H_E of 1.21 ± 0.41 mSv in prospectively ECG-triggered CCTA using 128-detector-row CT scanner. For 256-detector-row CT scanner, H_E ranged from 0.18 to 1.22 mSv was reported in prospectively ECG-triggered CCTA at a cut-off heart rate of 67 bpm (Benz et al., 2016). Gordic et al. (2014) reported that third generation DSCT scanner in high-pitch mode allows diagnostic image quality and H_E of 0.4 mSv at heart rate up to 70 bpm in prospectively ECG-triggered CCTA. The authors further concluded that heart rate viability is not significantly related to image quality of CCTA.

Using second generation DSCT scanner, Scharf et al. (2011) reported that an average heart rate less than 64 bpm is required to obtain the diagnostic depiction of coronary arteries for patients. The better image quality at lower radiation dose in patients with elevated heart rate (70 bpm versus 64 bpm) in third generation DSCT scanner is due to the increase of detector row (2 × 96) with z-coverage of 57.6 mm, gantry rotation speed of 250 ms, scan FOV of 50 cm and high pitch scanning. For second generation 320-detector-row SSCT scanner, estimated H_E of 2.1 and 2.8 mSv were reported for patient with heart rate less than 65 and equal and more than 65 bpm, respectively (Wong et al., 2014). Finally, the assessment of image quality was not included as the focus of this study was to compare the radiation dose among these different CT scanners. Recent developments in CCTA (both prospectively and retrospectively ECG-triggered techniques) with use of iterative reconstruction algorithms have been shown to significantly improve image quality while reducing radiation dose to a greater extent (Oda et al., 2014; Yuki et al., 2014). Thus, further studies with testing of these iterative reconstruction techniques on different CT scanners are needed.

3.7 Conclusion

This study provides the most recent data on specific organ dose measurement and H_E estimation from prospectively ECG-triggered CCTA examination using five commonly used generations of CT scanners and imaging protocols. Underestimation of H_E by 38.3 to 53.2 % was observed in the P_{KL}-to-H_E conversion method. The radiation doses and LAR for cancer incidence from a prospectively ECG-triggered CCTA are generally low and depend on the scanner model and imaging protocol. Although the heart is the organ of interest in CCTA imaging, breasts and lungs received the highest radiation dose due to their high radiosensitivity towards ionizing radiation. The use of CCTA especially in young women should be considered carefully in conjunction with clinical indications, benefits versus risks and alternative imaging modalities.

Among the five commonly used CT scanners, 2 × 32-detector-row DSCT scanner available in University Malaya Medical Centre gave the highest radiation dose in prospectively ECG-triggered CCTA protocol. As mentioned earlier, it is due to limited z-axis coverage (19.2 mm) of the scanner. Thus, this CT scanner is less effective for prospectively ECG triggered CCTA compared to the second generation DSCT scanner. In the next chapter, the development of a low tube voltage retrospectively ECG-triggered CCTA protocol is presented together with the assessment of radiation dose and image quality.

CHAPTER 4: DEVELOPMENT OF LOW TUBE VOLTAGE RETROSPECTIVELY ECG-TRIGGERED CCTA PROTOCOL AND ASSESSMENT OF RADIATION DOSE AND IMAGE QUALITY

4.1 Introduction

CCTA is a well-established imaging technique that has high per-patient sensitivity (99 %), positive predictive value (92 %) and negative predictive value (95 %) for obstructive CAD (Chow et al., 2009). However, the radiation exposure in CCTA with 64-detector-row CT scanners is high and ranged from 12 to 15 mSv for the coronary artery and from 14 to 26 mSv for coronary bypass graft studies with an extended z-axis length. The widespread use of CCTA has raised concern with respect to radiation exposures (Sun & Ng, 2010; Hermann et al., 2008; Peebles, 2006).

To minimize motion artefacts and radiation exposure to patient, ECG-triggered tube current modulation was introduced in retrospectively ECG-triggered CCTA. This technique has successfully reduced the patient dose by 37 to 40 % compared to conventional CCTA protocol (Hausleiter et al., 2006). Another low-dose technique, prospectively ECG-triggered CCTA was introduced later. Using this technique, dose reduction of 44 to 83 %, compared to retrospectively ECG-triggered CCTA has been reported (Lehmkuhl et al., 2010; Gopal et al., 2009; Klass et al., 2009; Shuman et al., 2008).

Prospectively ECG-triggered protocol is currently recommended as the first line default technique for CCTA examination, which should be used whenever possible and practical (Raff et al., 2014). However, there are several challenges when applying this technique. Firstly, it requires a regular and low heart rate (less than 70 bpm). One of the major problems in clinical practice is many patients do not meet this regular and low heart rate requirement as coronary artery pathologies often are associated with higher heart rate

or arrhythmias (Luecke et al., 2012). Unlike retrospectively ECG-triggered CCTA that acquires data throughout the cardiac cycle, only data in a certain phases of cardiac cycle are acquired during prospectively ECG-triggered CCTA. High heart rate or increase of heart rate variation can causes severe motion artefacts in the data acquired and leads to potential failure or unpredictable image quality (Yang et al., 2009).

Secondly, prospectively ECG-triggered CCTA is restricted to non-overlapping scanning or slice increments with a small overlap. As the scan time to cover the heart volume is directly proportional to the slice increment, a longer scan time is required. To solve this problem, other than a high temporal resolution, a wider z-axis coverage of CT scanner is required. For instance, the first generation (2 × 32-detector-row) DSCT scanner has been reported to be able to provide 83 ms temporal resolution. This temporal resolution allows scanning of patients with heart rate ranges from 66 to 104 bpm (Flohr et al., 2006). However, with prospectively ECG-triggered CCTA protocol, this CT scanner has been reported to give higher radiation dose (6.06 mSv) compared to the other SSCT scanners with 64-detector-row. This is due to the limited z-axis coverage of 19.2 mm in this scanner. For coverage of the whole cardiac anatomy, the image acquisition involves a series of slabs over several cardiac cycles. Since there is slight overlap in each acquisition slice, this results in higher dose (Tan et al., 2016). The prolonged scan time also increases the risk of motion and stair-step artefacts due to misregistration between acquired slabs (Lewis et al., 2016).

Thirdly, the functional information about cardiac valve or ventricular wall is not available in prospectively ECG-triggered CCTA as the cardiac images are acquired during a small portion of the R-R interval (Sun, 2012b; Husmann et al., 2008; Stolzmann et al., 2008). CCTA has been reported to be able to provide accurate and reproducible ventricular volume parameters compared to CMR. It has been considered as a reliable

alternative for the assessment of left and right ventricular functions in patients who are not suitable to undergo CMR (Maffei, Messalli, et al., 2012). However, this functional information can only be obtained with retrospectively ECG-triggered CCTA protocol.

As an alternative to prospectively ECG-triggered CCTA, retrospectively ECG-triggered CCTA with low tube voltage has been reported to produce similar image quality at lower radiation dose and TID, compared to the standard 120 kVp protocol. According to an international and multicentre survey (93% of which consisted of retrospectively ECG-triggered CCTA), a 31 % reduction in radiation dose with maintained image quality was reported in patients with BMI less than 30 kgm^{-2} using 100 kVp protocol (Hausleiter et al., 2010). TID reduction of 50 % and 31 to 37 % were also reported with 80 kVp and 100 kVp protocols (Van Cauteren et al., 2017; Cao et al., 2014).

The decline of image quality due to the increase of image noise is the main disadvantage of low tube voltage protocol. A compensatory increase in mAs can be applied to balance the increase of image noise. However, this may increase the radiation dose, especially for larger-sized patients (Aschoff et al., 2017). Numerous tube current adaptation methods have been suggested to reduce image noise in CCTA, based on SPR attenuation, chest wall tissue composition and chest dimensions (Gao et al., 2011; Paul et al., 2011; Rogalla et al., 2010). In another study, adaptation of both tube voltage and tube current based on the noise level measured in the CACS images was suggested. This method has successfully maintained the image noise at 100 kVp, but significantly higher image noise was reported at 80 kVp compared to 120 kVp (Paul, 2011). Generally, it is challenging to apply the abovementioned methods in the clinical setting as it involves measurements which are complex, time consuming and prone to errors (Durmus et al., 2016).

Currently, different automatic tube current modulation software have been developed by CT scanner manufacturers (Smart mA and Auto mA, GE Healthcare, Milwaukee, WI; DoseRight, Philips Healthcare, Cleveland, OH, USA; CareDose 4D, Siemens Healthcare, Forchheim, Germany; SureExposure 3D, Toshiba Medical Systems Corporation, Otawara, Japan). These software allow optimisation of radiation dose by adjusting the tube current in real-time to accommodate differences in X-ray attenuation due to patient anatomy, shape, and size (Lee et al., 2008). Several studies have applied a combination of manual selection of nonobese patients based on BMI and automatic tube current modulation for low tube voltage CCTA protocol. By using this method, similar image quality compared to 120 kVp protocol was reported with substantial radiation dose reduction at 80 (69 to 83%) and 100 kVp (48 to 53%) (Zhang, C. et al., 2015; Zheng et al., 2014; Alkadhi et al., 2008)

This study intends to develop a low tube voltage (100 kVp) retrospectively ECG-triggered CCTA protocol for the current available first generation DSCT scanner at the University of Malaya Medical Centre, using the combination of patient selection and automatic tube current modulation. It is then followed by the assessment of achievable radiation dose reduction and image quality of the developed protocol, compared to the routine 120 kVp protocol.

4.2 Literature review

In the last decade, various studies have tried to reduce radiation exposures in CCTA by lowering the tube voltage from 120 kVp to 80 and 100 kVp (Andreini et al., 2016; Di Cesare et al., 2016; Iyama et al., 2016; Wu et al., 2016; Cao et al., 2014; Blankstein et al., 2011; Gagarina et al., 2011). Less X-ray photons will be generated in the CT tube when lower tube voltage is applied with the same tube current. This is due to lower tube effectiveness at low tube voltage and the heavy filtering of low-kV photons (Aschoff et

al., 2017; Edyvean et al., 2012). As the mean photon energy of lower tube voltage approaches the iodine K-edge energy of 33.2 keV, more x-ray photons are being absorbed by the iodine atoms. This increases the photoelectric effects and produces higher image contrast. At lower tube voltage an equivalent VCE can be achieved at a lower amount of administered iodine (Nakaura et al., 2011; Bae, 2010).

Despite its advantages, increased image noise remains a drawback in the low tube voltage protocol. Since tube output is proportional to the square of tube voltage, a reduction from 120 to 100 kVp will result in 31 % less X-ray photons being produced, and this figure will increase to 56 % with further reduction to 80 kVp. Since image noise is proportional to the square root of X-ray photons, more noise will be generated when using lower tube voltage at the same tube current (Aschoff et al., 2017).

Although it is always feasible to improve image quality by increasing the tube current to balance the image noise. This method should be used with caution as it is associated with substantial increase of radiation dose, especially in larger-sized patients (Aschoff et al., 2017). The tube current modulation software, CareDose4D developed by Siemens Healthcare automatically modulates the tube current based on a reference mAs for a standard-sized patient to achieve constant image quality. It aims to provide adequate image noise, which varies depending on the size of the patient. It operates based on the principle that different-sized patients require different levels of noise to maintain adequate image quality (Lee et al., 2008). As the reference mAs in this software was set based on the standard 120 kVp CCTA protocol, elevation of image noise occurs when a lower tube voltage is applied, especially in larger-sized patients. To overcome this problem, selecting nonobese patients for low tube voltage protocol based on the measurement of BMI (Zhang, C. et al., 2015; Khan et al., 2014; Zheng et al., 2014; Zhang et al., 2011; Alkadhi et al., 2008) and chest circumsference (Lu et al., 2015) could be the

alternative to reduce image noise. Since BMI is a standard parameter measured on every patient undergoing CT and an increase in BMI is related to higher image noise at CT, majority of the studies have used BMI as the parameter for selecting nonobese patients for 80 and 100 kVp protocol. From these studies, radiation dose reduction ranges from 69 to 83 % and 30 to 53 % with preserved image quality were reported at 80 and 100 kVp, compared to 120 kVp (Zhang, C. et al., 2015; Khan et al., 2014; Zheng et al., 2014; Zhang et al., 2011; Alkadhi et al., 2008).

In the earlier studies, patients with BMI less than 25 kgm^{-2} were enrolled for the 100 kVp CCTA protocol (Zhang et al., 2011; Alkadhi et al., 2008). This BMI cut-off point was then extended to 27 and 28 kgm^{-2} (Zhang, C. et al., 2015; Khan et al., 2014). In a guideline established by the SCCT in 2014, BMI cut-off points for patient selection were suggested: 80 kVp was recommended for performing CCTA in patients with BMI less than 18 kgm^{-2}; 100 kVp for patients with BMI less than 30 kgm^{-2}; and between 120 and 140 kVp for those classified as obese (Raff et al., 2014).

4.3 Materials and methods

4.3.1 Development of low tube voltage retrospectively ECG-triggered CCTA protocol

Due to the clinical condition of CCTA patients and the limited z-axis coverage (19.2 mm) of first generation DSCT (Somatom Definition Dual Source, Siemens Healthcare, Forchheim, Germany), the majority of CCTA examinations referred to the University of Malaya Medical Centre were performed using the routine 120 kVp retrospectively ECG-triggered protocol. In an attempt to reduce radiation dose to patients, a low tube voltage (100 kVp) retrospectively ECG-triggered protocol was proposed.

A CCTA group consists of radiographers, medical physicists and cardiac radiologists was established to develop the 100 kVp retrospectively ECG-triggered protocol with a

combination of patient selection and automatic tube current modulation. Reviews on the findings in literature, guidelines published by SCCT (Raff et al., 2014), as well as the manufacturer's recommendation were conducted. Evidence from these reviews was used to support the discussion at the consensus meeting. A meeting session was held to develop the first draft of protocol on 01 May 2017. This version of protocol was further refined and received ethical committee approval by end of May 2017.

4.3.2 Radiation dose and image quality assessment

4.3.2.1 Patients

Between June and August 2017, a group of 30 consecutive, scheduled patients who successfully met the patient selection criteria were scanned with 100 kVp retrospectively ECG-triggered CCTA protocol (thereafter referred as "100 kVp group"). This study was approved by the local ethics committee (reference no: 989.35, approval date: 23 May 2017, Appendix G).

In an attempt to compare the radiation dose and image quality, retrospective data for another 30 patients with comparable BMI with 100 kVp group, who were scanned with routine 120 kVp retrospectively ECG-triggered CCTA protocol were retrieved from University of Malaya Medical Centre database (thereafter referred as "120 kVp group"). The sex, age, body weight, height and BMI (weight / height^2) of all patients were recorded.

The main indication for the included patients was to exclude CAD. In the University of Malaya Medical Centre, the clinical exclusion criteria for CCTA are atrial fibrillation, history of allergy to contrast medium, renal insufficiency (glomerular filtration rate less than 60 mLmin^{-1}1.73 mm^{-2}), pregnancy, congenital heart disease and low left ventricular function (ejection fraction less than 50 %).

Each patient was given oral Lorazepam (1 mg, Lorans 1, Medochemie Ltd, Cyprus) and beta blocker, Metoprolol Tartrate (100 to 150 mg, Betaloc, AstraZeneca Pty Ltd, Australia), 60 minutes before the CCTA examination to achieve a low and regular heart rate (less than 90 bpm). For asthmatic patients, an oral dose of Verapamil Hydrochloride (80 to 120 mg, Akilen 40, Medochemie Ltd, Malta) was given as an alternative to Metoprolol Tartrate. An 18 G intravenous cannula was inserted at the median cubital vein for contrast medium administration. Sublingual nitroglycerin (0.5 mg, Myonit Insta, Troikaa Phamaceuticals Ltd, India) was given, 5 minutes before data acquisition, to dilate the coronary arteries and facilitate comparison of the findings to invasive coronary angiography (ICA).

4.3.2.2 Data acquisition and contrast medium administration protocol

In both groups, CCTA scans were performed using DSCT in helical mode with ECG-controlled dose modulation (CareDose 4D, Siemens Healthcare), covering from the carina of trachea to the apex of the heart. Figure 4.1 shows the positioning of patient and SPR for CCTA examination. Full tube current was applied from 20 to 75 % of R-R interval. Images were reconstructed with a medium smooth reconstruction kernel (B26f), during mid-diastole (at 70 % of the R-R interval) for patients with heart rate less than 70 bpm and during end-systole (at 40 % of the R-R interval) for patients with heart rate equal or more than 70 bpm, at slice thickness of 0.75 mm and pixel matrix of 512 × 512.

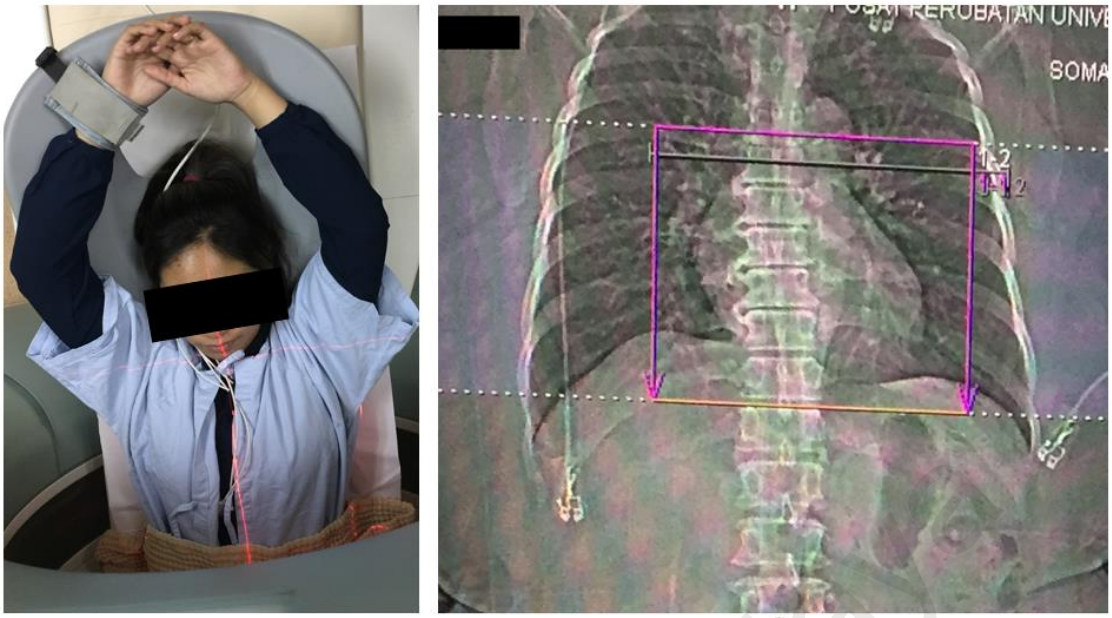

Figure 4.1: Positioning of patient during CCTA examination; (b) SPR image with the scan range planned for CCTA (pink box).

A triphasic protocol recommended by SCCT guidelines was applied for contrast medium (iopromide, Ultravist 370, Bayer HealthCare Pharmaceuticals, Berlin, Germany) administration: an initial undiluted contrast bolus (first bolus), followed by a contrast medium (10 mL, 20 %) and saline (40 mL, 80 %) mixture, administrated at the same injection rate (6 mLs^{-1}) as the first bolus, and completed by a 50 mL saline flush (Abbara et al., 2016). The contrast volume of the first bolus (50, 55 or 60 mL) was adjusted to a product of the estimated scan time and injection rate. Contrast medium injection was performed using dual-syringe power injector with dedicated injection software (Medrad Stellant CT injection system with Certegra workstation, Bayer HealthCare Pharmaceuticals).

A test bolus method was used to determine the circulation time of contrast medium, by an injection of 10 mL contrast medium, followed by 50 mL chaser bolus of saline at 6 mLs^{-1}, prior to the CCTA scan. The scan delay was calculated as TTP during test bolus with additional 2 s.

4.3.2.3 Estimation of radiation dose

The H_E of each CCTA examination was estimated using the approach suggested by European Working Group for Guidelines on Quality Criteria in Computed Tomography. As described in Eq. 2.9, the H_E can be calculated by multiplying the P_{KL} to an E_{KL} (IAEA, 2007; ICRP, 2007). The E_{KL} for chest, 0.014 $mSv.mGy^{-1}cm^{-1}$ as recommended by the EC and PHE (formerly NRPB) was used in this study (Shrimpton et al., 2005; Shrimpton, 2004).

4.3.2.4 Quantitative image quality analysis

The quantitative image quality analysis, including VCE, image noise, SNR and CNR was performed on axial images of both groups, using DICOM viewer (RadiAnt DICOM Viewer, Medixant, Poznan, Poland), by placing a circular ROI in the AA, RCA, LM coronary artery, LAD artery and LCx artery.

For the measurements in AA, three ROIs were placed in AA at the level of LM ostium and one slice above and below this level. For RCA, LM and LAD, three ROIs were placed at the proximal, middle and distal segments of the arteries and for LCx, only two ROIs were placed at the proximal and distal segments of the artery. All ROIs were made as large as possible according to vessel sizes, but vessel walls, calcifications or metallic artefacts were excluded to prevent partial volume effects.

VCE was defined as the mean CT attenuation value (measured in HU) measured in each artery. The image noise was defined as the mean standard deviation of CT attenuation value for the ROIs placed in the AA. The SNR was calculated as the VCE divided by the mean image noise measured in AA (Eq. 4.1). The CNR was calculated by subtracting the mean CT attenuation value (HU) measured in the chest wall muscle (HUcw) from the VCE, and dividing this difference by the mean image noise measured

in AA (Eq. 4.2). The FOM was defined as a ratio of squared CNR to H_E (Eq. 4.3). FOM was calculated to relate the image contrast, noise, and the amount of radiation.

$$\text{SNR} = \frac{\text{VCE}}{\text{Image noise}} \quad \text{Eq. 4.1}$$

$$\text{CNR} = \frac{\text{VCE-HU}_{cw}}{\text{Image noise}} \quad \text{Eq. 4.2}$$

$$\text{FOM} = \frac{\text{CNR}^2}{H_E} \quad \text{Eq. 4.3}$$

4.3.2.5 Qualitative image quality analysis

Dedicated post-processing and evaluation software (Centricity RIS-i, version 5.0, GE Healthcare) was used for qualitative image quality analysis. The analysis was performed by two cardiac radiologists (R. R. Azman and F.M Sani) with 4 years of cardiovascular imaging experience. Reviewers were blinded to the clinical indication for imaging, patient characteristics, assigned protocol and clinical imaging report. Using axial, MPR, and thin-slab MIP images, the studies were interpreted individually and in random order. Window settings were freely adjustable. The VCE in the major coronary arteries (RCA, LM, LAD and LCx) were graded using 5-point scale as follows: VCE was defined as: 1 = poor opacification, insufficient for diagnosis; 2 = suboptimal opacification, low diagnostic confidence; 3 = acceptable opacification, sufficient for diagnosis; 4 = good opacification of proximal and distal segments; and 5 = excellent opacification of proximal and distal segments (Figure 4.2, Appendix H).

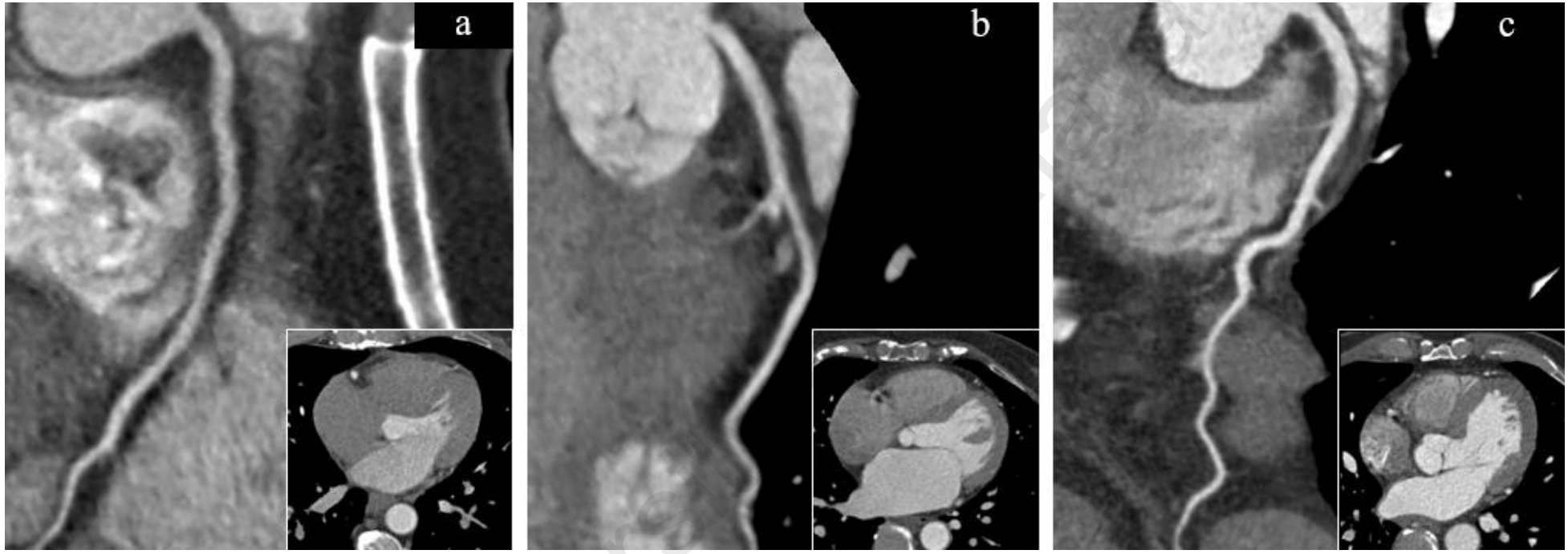

Figure 4.2: Representative curved multiplanar reformations (MPR) images of the left main (LM) coronary artery to left anterior descending (LAD) artery and corresponding axial images (inset), illustrate three vessel contrast enhancement (VCE) scores: (a) acceptable opacification, sufficient for diagnosis (grade 3); (b) good opacification of proximal and distal segments (grade 4); and (c) excellent opacification of proximal and distal segments (grade 5). All displayed at same window width of 800 and window level of 300.

4.3.3 Statistical analysis

Statistical analysis was performed using SPSS software version 23.0 (IBM Corporation, Armonk, New York, USA). Continuous variables were presented as mean ± standard deviation. All data such as age, body weight, height, BMI, heart rate, radiation dose, quantitative and qualitative image quality scores for 100 and 120 kVp groups were compared using Man-Whitney U test. For qualitative image quality scores, Wilcoxon signed-rank test was used to assess interobserver variabilities for 100 and 120 kVp groups. 95 % confidence interval was used in all the statistical tests.

4.4 Results

4.4.1 Development of low tube voltage retrospectively ECG-triggered CCTA protocol

The development of low tube voltage (100 kVp) retrospectively ECG-triggered CCTA protocol involved 2 main steps: setting of patient selection criteria and reference mAs for automatic tube current modulation.

The BMI was chosen to be used as a reference parameter for tube voltage selection (100 or 120 kVp). Patients with BMI less than 30 kgm^{-2} was considered eligible for 100 kVp protocol. Based on manufacturer's recommendation, reference mAs of 320 mAs was used for both 100 and 120 kVp protocols. However, a higher reference mAs, 370 mAs was set for 100 kVp when contrast medium reduction method is applied (Figure 4.3).

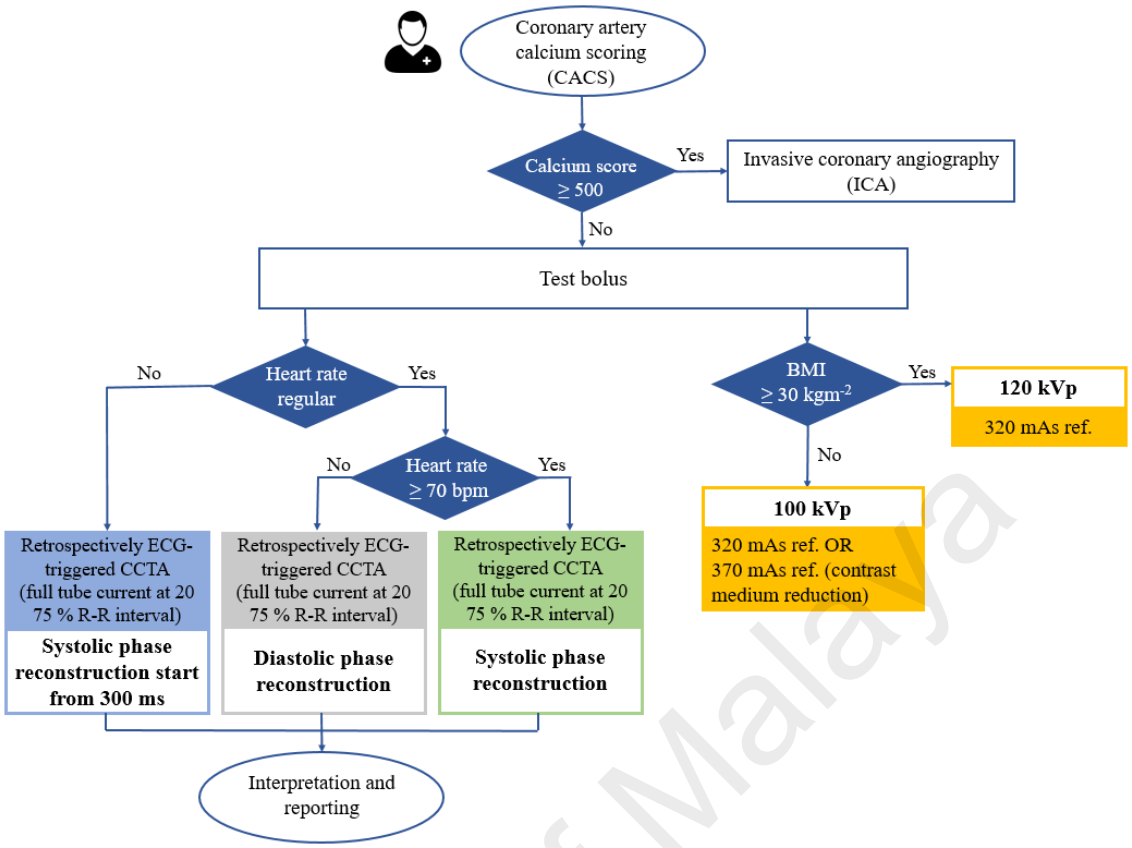

Figure 4.3: Flowchart showing 120 kVp and low tube voltage (100 kVp) retrospectively ECG-triggered CCTA protocols practised in University of Malaya Medical Centre.

4.4.2 Radiation dose

The patient demographics and radiation doses for 100 and 120 kVp groups are summarized in Table 4.1. There were no significant differences ($p > 0.05$) in age, body weight, height, BMI and heart rate between the 100 and 120 kVp groups. $CTDI_{vol}$, P_{KL} and H_E values were all lower in 100 kVp compared to 120 kVp, and the differences between the two protocols were statistically significant ($p < 0.05$). At the new low-dose protocol with 100 kVp, the radiation dose was reduced by 37.8 %.

Table 4.1: Comparison of the patient demographics and radiation dose between 120 kVp and low tube voltage (100 kVp) retrospectively ECG-triggered CCTA protocols.

Parameters	120 kVp	100 kVp	*p*-value
Patients (n)	30	30	
Male / female ratio	13 : 17	12 : 18	
Age (years)	57.6 ± 12.5	58.9 ± 14.9	0.615
Body weight (kg)	64.3 ± 8.6	61.5 ± 11.4	0.203
Height (cm)	162.2 ± 10.8	159.7 ± 8.9	0.407
BMI (kgm^{-2})	24.5 ± 2.8	24.0 ± 3.3	0.387
Heart rate (bpm)	68.7 ± 6.6	65.3 ± 7.6	0.131
$CTDI_{vol}$ (mGy)	37.2 ± 8.1	21.7 ± 5.7	0.0001*
P_{KL} (mGy.cm)	531.2 ± 123.2	329.1 ± 80.0	0.0001*
H_E (mSv)	7.4 ± 1.73	4.6 ± 1.1	0.0001*

* $p < 0.05$ is considered statistically significant different.
BMI, body mass index; $CTDI_{vol}$, CTDI volume; H_E, effective dose; P_{KL}, air-kerma length product.

4.4.3 Image quality

Figure 4.4 shows the location of ROIs selected for image noise, chest wall muscle attenuation and VCE measurements in axial CCTA images. Results of quantitative image quality analysis are summarized in Table 4.2. Image noise of AA was significantly higher ($p < 0.05$) in 100 kVp group (33.8 ± 5.6 HU) compared to 120 kVp group (24.4 ± 3.6 HU). Significantly higher VCE (35.3 to 41.8 %, $p < 0.05$) was observed in 100 kVp group at all ROI locations. There were no significant differences ($p > 0.05$) in SNR and CNR between the two groups. However, the FOM of 100 kVp group was significantly higher (70.5 to 81.7 %, $p < 0.05$) at all ROI locations (Figure 4.5).

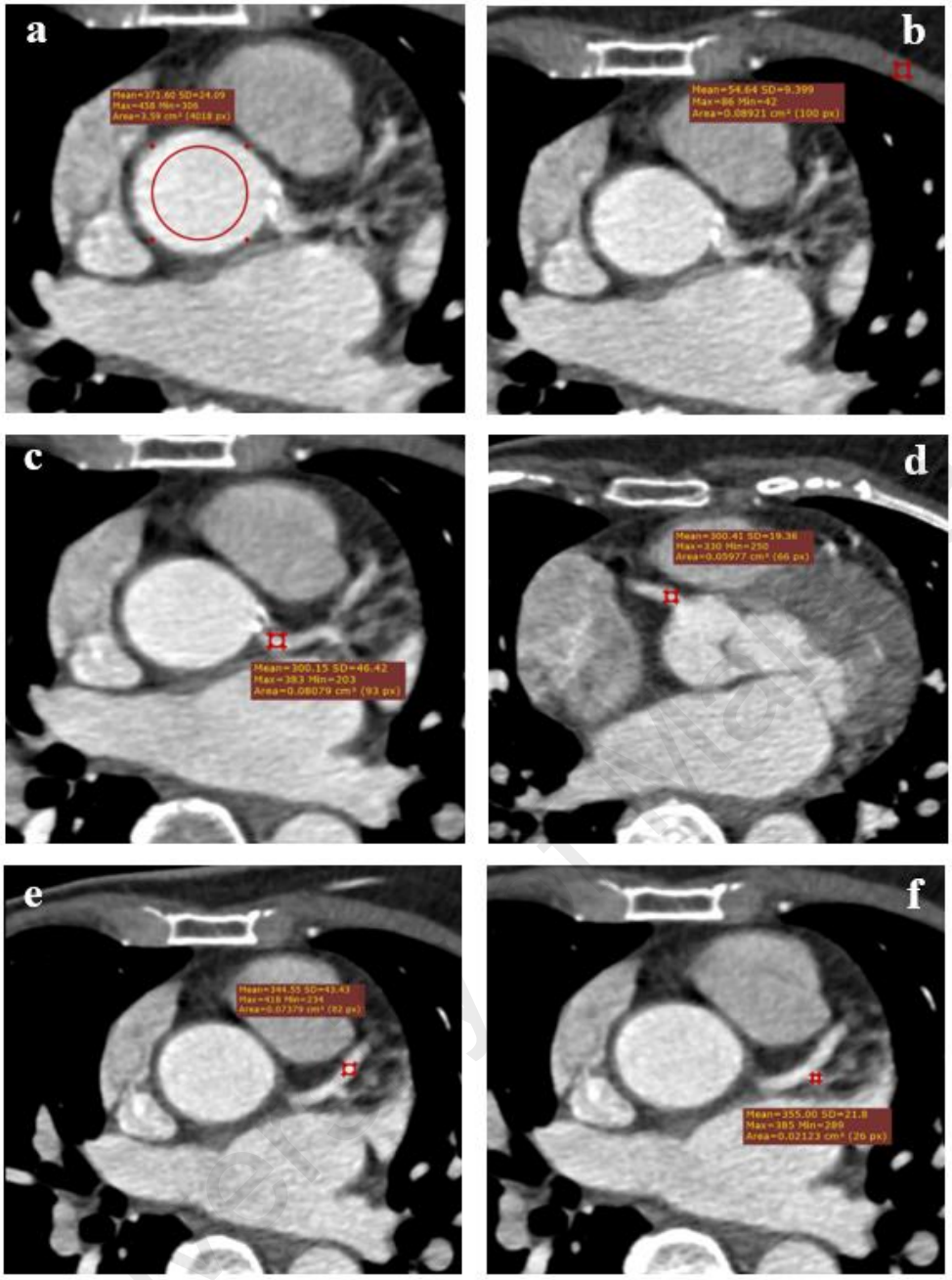

Figure 4.4: Axial CCTA images. (a) Region of interest (ROI) at ascending aorta (AA) for image noise measurement; (b) ROI for chest wall muscle attenuation measurement; ROI for vessel contrast enhancement (VCE) measurement at (c) left main (LM) coronary artery, (d) proximal right coronary artery (RCA), (e) proximal left anterior descending (LAD) artery and (f) proximal left circumflex (LCx) artery.

Table 4.2: Comparison of quantitative image quality parameters between 120 kVp and low tube voltage (100 kVp) retrospectively ECG-triggered CCTA protocols.

Parameters	120 kVp	100 kVp	*p*-value
Quantitative image quality analysis			
Image noise (HU)	24.4 ± 3.6	33.8 ± 5.6	0.0001*
VCE (HU)			
AA	424.0 ± 42.0	593.7 ± 87.8	0.0001*
RCA	461.3 ± 58.7	654.2 ± 107.9	0.0001*
LM	456.4 ± 45.5	617.4 ± 96.2	0.0001*
LAD	439.4 ± 53.4	602.5 ± 80.2	0.0001*
LCx	438.8 ± 44.5	602.2 ± 92.0	0.0001*
SNR			
AA	17.8 ± 3.5	18.0 ± 4.0	0.751
RCA	19.3 ± 4.0	19.9 ± 4.5	0.549
LM	19.1 ± 3.5	18.8 ± 4.4	0.796
LAD	18.4 ± 3.6	18.4 ± 4.2	0.906
LCx	18.4 ± 3.7	18.3 ± 4.2	0.971
CNR			
AA	15.0 ± 3.2	15.6 ± 3.7	0.506
RCA	16.6 ± 3.7	17.4 ± 4.2	0.391
LM	16.3 ± 3.1	16.3 ± 4.1	0.767
LAD	15.6 ± 3.3	16.0 ± 3.8	0.813
LCx	15.6 ± 3.4	15.9 ± 3.9	0.756
FOM (mSv^{-1})			
AA	32.7 ± 14.2	59.4 ± 35.1	0.0001*
RCA	40.8 ± 19.7	73.1 ± 37.8	0.0001*
LM	38.3 ± 15.2	65.3 ± 41.6	0.0001*
LAD	35.3 ± 14.9	61.7 ± 35.5	0.0001*
LCx	35.3 ± 15.1	61.0 ± 36.8	0.0001*
Qualitative image quality analysis			
VCE	4.9 (4.5 – 5.0)	4.9 (4.3 – 5.0)	0.211

* $p < 0.05$ is considered statistically significant different.
AA, ascending aorta; CNR, contrast-to-noise ratio; FOM, figure of merit; LAD, left anterior descending artery; LCx, left circumflex artery; LM, left main coronary artery; RCA, right coronary artery; SNR, signal-to-noise ratio; VCE, vessel contrast enhancement.

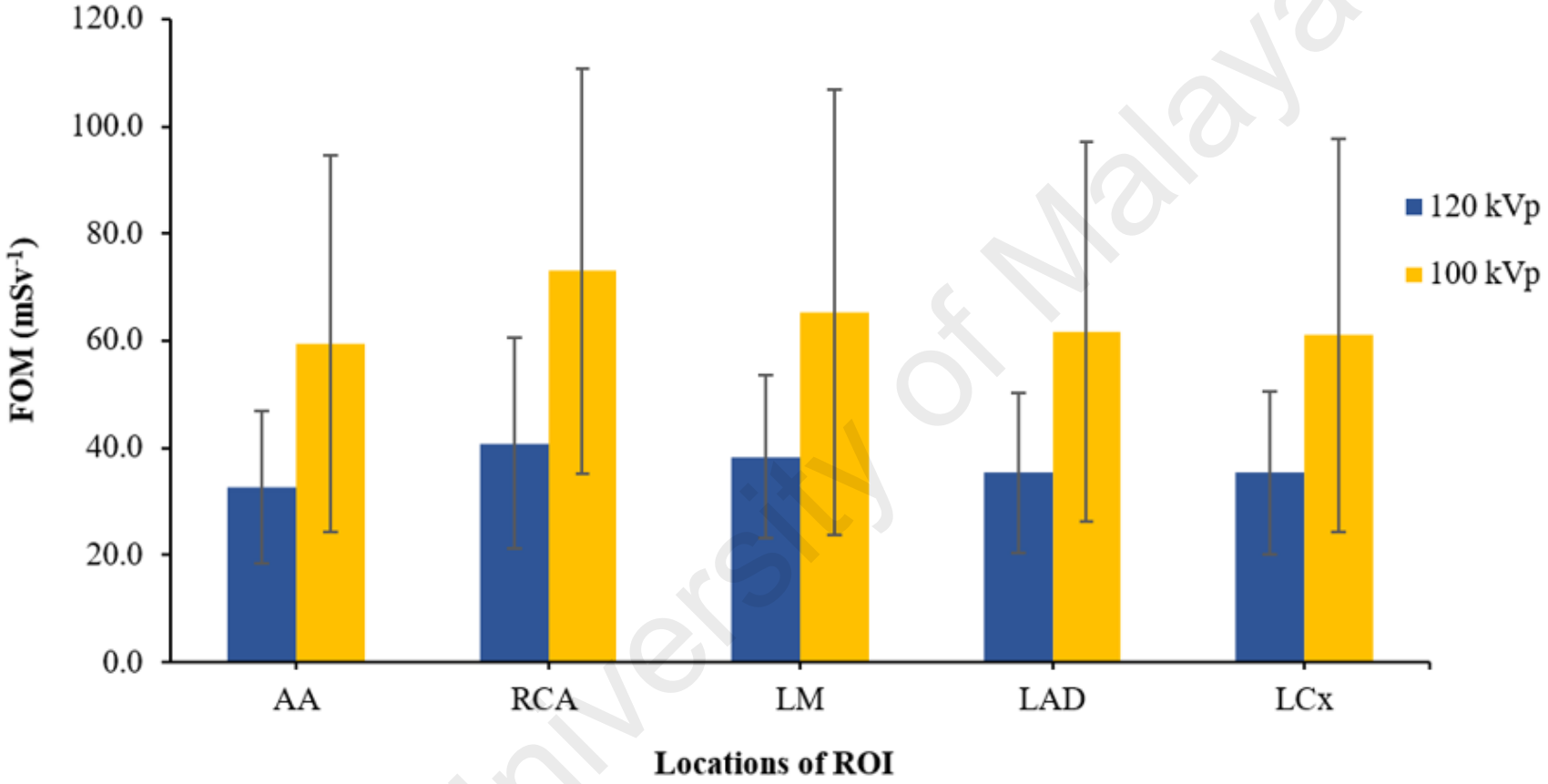

AA, ascending aorta; LAD, left anterior descending; LCx, left circumflex; LM, left main; RCA, right coronary artery; CNR, contrast-to-noise ratio; FOM, figure of merit; SNR, signal-to-noise ratio.

Figure 4.5: Comparison of figure of merit (FOM) between 120 kVp and low tube voltage (100 kVp) retrospectively ECG-triggered CCTA protocol at different locations of ROI.

Image quality was considered sufficient for diagnosis by observers in both groups. The VCE was graded as good to excellent for both 100 kVp (4.9, ranged from 4.3 to 5.0) and 120 kVp (4.9, ranged from 4.5 to 5.0) groups, with no significant difference between the two groups. The Wilcoxon signed-rank test demonstrated no significant interobserver variabilities ($p > 0.05$) in VCE scores made by the two observers for both groups.

4.5 Discussion

In an attempt to reduce patient dose within the limit of performing prospectively ECG-triggered CCTA with first generation DSCT, a low tube voltage (100 kVp) retrospectively ECG-triggered CCTA protocol was developed in this study using a combination of patient selection according to BMI and automatic tube current modulation. During low tube voltage retrospectively ECG-triggered CCTA, the data is acquired throughout the cardiac cycle. Optimal images can be reconstructed by selecting the data with less motion during the cardiac cycle. This technique allows scanning of patients with higher heart rate (more than 85 bpm) and reduction of motion artefacts compared to prospectively ECG-triggered CCTA. It also retains the advantages of the helical CT scan algorithm and associated advantages, such as functional imaging (Meyer et al., 2017; Oda et al., 2011).

BMI was chosen as a parameter for patient selection due to several reasons. Firstly, BMI is directly proportional to image noise and inversely related to VCE. Selection of patients with BMI less than 30 kgm^{-2} for 100 kVp protocol helps in reducing the image noise. Together with the increase of VCE, this method produces a higher SNR and CNR (Bae et al., 2008; Bae et al., 2007). Secondly, BMI has been widely used as a parameter for patient selection in the studies that involved low tube voltage CCTA protocols. By selecting nonobese patients based on BMI, radiation dose reduction of 30 to 53 % with preserved image quality has been reported at 100 kVp compared to 120 kVp (Zhang, C. et al., 2015; Khan et al., 2014; Zhang et al., 2011; Alkadhi et al., 2008). Thirdly, BMI can

be conveniently determined from patient body weight and height measurements. It is also a standard parameter measured on every patient undergoing CT. In this study, BMI less than 30 kgm^{-2} was used to select the patients for low tube voltage (100 kVp) retrospectively ECG-triggered CCTA protocol. This criteria was set by comparing the highest BMI cut-off point used in the literature and the SCCT guideline (Zhang, C. et al., 2015; Khan et al., 2014; Raff et al., 2014; Zhang et al., 2011; Alkadhi et al., 2008).

Ghoshhajra et al. (2011) reported a significant correlation between BMI and chest circumference. The author suggested that chest circumference is a better parameter as BMI might not provide an exact estimation of body mass at heart level. Although only one study applied chest circumference as the reference parameter for patient selection and tube current adaptation at 100 kVp CCTA protocol, the reported result was promising with a 38 % reduction in H_E, improvement in quantitative image quality and similar qualitative image quality compared to 120 kVp protocol (Lu et al., 2015).

Recently, a dedicated software (Care kV, Siemens Healthcare, Forchheim, Germany) was introduced with automatic tube voltage selection (ATVS) technology. ATVS is a fully-automated algorithm that utilises CNR as the image quality index to adjust the CT tube voltage based on patients' size and attenuation characteristics estimated from the scan projection radiograph (SPR). Patient-specific tube current curves are generated for all tube voltage levels to achieve the desired CNR for a selected scan range on the SPR. These patient-specific tube current curves are then used to calculate the estimated radiation dose for all tube voltage levels to determine the optimal dose efficiency. Subsequently, the software suggests the best tube voltage setting by taking into account the optimal dose efficiency and limitation of the scanner, such as the maximum tube current and heat capacity (Lee et al., 2012). These algorithms provide a fast and easy way

for selecting appropriate tube voltage in CCTA examination. Nevertheless, this dedicated software is costly and not available yet in many clinical centres.

In this study, the radiation dose was found to be lowered by 37.8 % in the low tube voltage protocol compared to the routine 120 kVp protocol. This finding was consistent with the findings from the other studies, where the H_E was lower in 100 kVp compared to 120 kVp with a range of 30 to 53 % (Zhang, C. et al., 2015; Khan et al., 2014; Zhang et al., 2011; Alkadhi et al., 2008). The H_E (4.6 mSv) achieved using the low tube voltage retrospectively ECG-triggered CCTA protocol developed in this study was comparable to the H_E (4.5 mSv) reported in another study which applied 120 kVp prospectively ECG-triggered CCTA protocol with the same model of DSCT scanner (Gu et al., 2016). Low tube voltage retrospectively ECG-triggered CCTA protocol may provide an alternative with equivalent radiation dose to the 120 kVp prospectively ECG-triggered CCTA protocol in patients with difficulty to control the heart rate. In a study conducted by Meyer et al. (2017), patients with heart rate of more than 85 bpm or known arrhythmias were scanned with 100 kVp retrospectively ECG-triggered CCTA protocol using second generation DSCT scanner. The authors concluded that the images reconstructed from all phases of cardiac cycle allowed the diagnostic evaluation of all coronary segments for stenosis, in contrast to best diagnostic or best systolic phase alone.

Significant increase of image noise (38.5 %) was observed in the low tube voltage protocol compared to the routine 120 kVp protocol. Although the image noise of 33.8 HU at 100 kVp was higher than the value of image noise suggested by some authors for improved image quality, that is less or equal to 30 HU (Tatsugami et al., 2015; Tatsugami et al., 2012; Leschka et al., 2008). However, as of to date, there is no standard cut-off value for image noise reported. In the previous studies, image noise with a range of between 31.9 to 50.5 HU was reported in 100 kVp protocol. Despite image noise of more

than 30 HU, the image quality was graded as sufficient for diagnosis by the observers in these studies (Mangold et al., 2016; Khan et al., 2014; Nakaura, Kidoh, Sakaino, Nakamura, et al., 2013; Gagarina et al., 2011).

Nevertheless, the increase of VCE at lower tube voltage, due to the increase of photoelectric effect compensated the SNR and CNR (Nakaura, Kidoh, Sakaino, Nakamura, et al., 2013). Therefore, there were no significant differences observed in SNR and CNR between the low tube voltage and routine protocols. The FOM was improved in the low tube voltage protocol as there was a significant reduction of radiation dose with constant CNR. The concept of FOM was proposed to standardize the effects of different doses of radiation on image quality, by considering the image contrast, noise, and the amount of radiation. The higher the value of FOM, the higher is the quality of the images (Schindera et al., 2008). Results from this study demonstrated that low tube voltage retrospectively ECG-triggered CCTA protocol in selected patients allows substantial radiation dose reduction without degrading the image quality.

There are some limitations in this study. Firstly, no optimisation of contrast medium was performed as the focus of this study was to develop a low tube voltage retrospectively ECG-triggered CCTA protocol and assess the radiation dose and image quality. The contrast volume of first bolus for both 100 and 120 kVp groups were determined based on the routine contrast protocol. Due to the increase of X-ray photon absorption of iodine at 100 kVp, high VCE was observed, ranging from 593.7 to 654.2 HU. Based on the guidelines established by SCCT in 2009, an optimal CCTA image requires VCE of more than 250 HU (Abbara et al., 2016; Abbara et al., 2009). However, studies have shown that a decrease in plaque detectability and underestimation of coronary stenosis with high VCE of more than 450 HU (Fei et al., 2008; Horiguchi et al., 2007). Taking into consideration of the detection of coronary stenosis, quantitative analysis of

atherosclerotic plaque and diagnostic performance of CCTA, the optimal range of VCE could fall between more than 250 and less than 450 HU (Abbara et al., 2016; Abbara et al., 2009; Cademartiri et al., 2008; Fei et al., 2008; Horiguchi et al., 2007). Thus, further studies to optimise the contrast medium administration at low tube voltage settings are needed. Secondly, 80 kVp protocol was not included in this study as it is recommended for patient with BMI less than 18 kgm^{-2}. The majority of CCTA patients are not in this category and the application of 80 kVp protocol in patients with BMI more than 18 kgm^{-2} may introduce too much of image noise causing deterioration of the overall image quality (Raff et al., 2014).

4.6 Conclusion

This study developed a low tube voltage (100 kVp) retrospectively ECG-triggered CCTA protocol based on the current clinical situation and technical specification of CT scanner available in University of Malaya Medical Centre. Using a patient selection criteria based on BMI less than 30 kgm^{-2} and automatic tube current modulation, a significant reduction of radiation dose by 37.8 % was achieved without degrading the image quality.

However, in considering the VCE for 100 and 120 kVp in this study, there is a need to further refine the current contrast protocol for achieving VCE within the optimal range. In the next chapter, the process of developing and validating a personalised contrast volume calculation model for 120 kVp retrospectively ECG-triggered CCTA protocol are presented.

CHAPTER 5: OPTIMISATION OF CONTRAST MEDIUM ADMINISTRATION IN 120 KVP RETROSPECTIVELY ECG-TRIGGERED CCTA PROTOCOL: A PERSONALISED CONTRAST VOLUME CALCULATION MODEL

5.1 Introduction

The rapid improvement of MDCT scanner allows CCTA to be performed at a shorter scan time. This may potentially allow the performance of CCTA with a lower TID, which could benefit patients with renal impairment and decrease the risk of contrast-induced nephropathy. The prevalence of contrast-induced nephropathy ranges from 5 to 13% of contrast-enhanced CT examinations (Traub et al., 2013; Mitchell et al., 2010; Hipp et al., 2008; Mitchell & Kline, 2007; Barrett et al., 2006).

Optimal VCE is crucial in CCTA for the detection of coronary stenosis and quantitative analysis of atherosclerotic plaque. Based on the guidelines established by SCCT in 2009, an optimal CCTA image requires VCE of more than 250 HU, however, no upper limit of VCE was recommended (Abbara et al., 2016; Abbara et al., 2009). In a phantom study conducted by Fei et al. (2008), high VCE of 500 HU was reported to be associated with the underestimation of coronary stenosis. The authors further suggested an optimal VCE target of 350 HU for CCTA. Furthermore, VCE was reported to have significant impact on the density of non-calcified plaque (Dalager et al., 2011; Horiguchi et al., 2007). In a phantom study conducted by Horiguchi et al. (2007), VCE of 350 and 450 HU were reported to cause overestimation of non-calcified plaque with a density of 40 HU. VCE of 250 HU with a low heart rate was found to give the most precise measurements. Nevertheless, there were studies that reported the association of higher number of false-positives and negatives with low VCE. In a study conducted by Cademartiri et al. (2008), higher VCE of 326 to 540 HU was found to give a significantly higher sensitivity (96 %) and positive predictive value (92 %) compared to low VCE of 182 to 325 HU. Taking into consideration of the detection of coronary stenosis,

quantitative analysis of atherosclerotic plaque and diagnostic performance of CCTA, the optimal range of VCE could fall between more than 250 and less than 450 HU. In a study conducted by Komatsu et al. (2013), VCE with a range between 250 and 430 HU was used as the targeted VCE for CCTA.

Many studies have been conducted to optimise the contrast medium administration in CCTA, mainly focusing on achieving TID reduction and VCE of more than 250 HU, limited studies have considered the upper limit of VCE. Generally, the optimised contrast protocols presented in these studies are based on the adaptation of iodine dose to patient characteristics and scanning parameters, for instance, the adaptation to body weight, BMI, BSA, scan time and injection rate (Yin et al., 2015; Bae et al., 2008; Heiken et al., 1995). Nonetheless, to achieve VCE within the optimal range in every patient, it is important to also take into account the patient's cardiovascular and contrast pharmacokinetic response, information which can be obtained from the time-attenuation curve of test bolus. Test bolus parameters such as TTP and PCE are closely associated with the patient's circulation during CCTA scanning. PCE and TTP at test bolus scan have been reported as predictable parameters for VCE in previous studies (Zhu et al., 2015; Yang et al., 2013; Mahnken et al., 2007; van Hoe et al., 1995). However, as of to date only one study has been conducted by Komatsu et al. (2013) to develop a CT number-controlling system with the combination of BSA, PCE and TTP at test bolus at iodine delivery rate (IDR) of 1.40 gI/s. This system allowed a target VCE between 250 to 430 HU to be achieved with TID of 4.2 to 16.8 g at 120 kVp. High IDR has been reported to be associated with high PCE, thus helps in lowering TID in CCTA (Faggioni & Gabelloni, 2016; Fleischmann, 2010; Bae et al., 2008). The aim of this study is to develop a personalised contrast volume calculation model using a high IDR of 2.22 gI/s and include other potential parameters to achieve optimal VCE and greater TID reduction in 120 kVp retrospectively ECG-triggered CCTA protocol.

5.2 Literature review

The influence of VCE level on the detection of coronary stenosis and quantitative analysis of atherosclerotic plaque is mainly due to the partial volume effect. Severe partial volume effect occurs in small vessels and area with low degree of stenosis. In these areas, more pixels are affected by the partial volume effect compared to the plaque cross sectional area. Thus, high VCE leads to a large scale increase in the CT attenuation of plaque, causing underestimation of plaque cross-sectional area and percentage of stenosis. Oppositely, overestimation of stenosis always occurred with low VCE (Saremi & Achenbach, 2015; Fei et al., 2008). These have created the interest to determine the most appropriate VCE level for CCTA in several studies. The findings from these studies showed that the optimal range of VCE could fall between more than 250 and less than 450 HU (Abbara et al., 2016; Abbara et al., 2009; Cademartiri et al., 2008; Fei et al., 2008; Horiguchi et al., 2007).

The two main bolus parameters that describe the VCE are PCE and TTP. The VCE is affected by several interacting factors, as described in Figure 2.16. The main patient-related factors that affect the VCE are body weight and cardiac output. The inverse relationship between body weight and PCE is mainly due to the association of body weight and blood volume. Since large patients have larger blood volume compared to small patients, contrast medium administrated into a large patient will be diluted more, results in a lower iodine concentration in blood and lower PCE (Bae, 2010). The 1:1 linear scale is the most commonly used scheme for adjusting the iodine dose to body weight, for instance, doubling the iodine dose when the patient's body weight doubles (Heiken et al., 1995).

Another commonly used parameter for adjustment of iodine dose is BMI, as it is easy to calculate and allow the effect of height to be taken into consideration. BMI was

reported to have inverse correlation with PCE but it is strongly correlated with total body fat content in adults and its accuracy in relation to actual levels of body fat is easily distorted by factors such as fitness level, muscle mass, bone structure, sex, and ethnicity (Husmann et al., 2009). Hence, BMI cannot be used alone to estimate the iodine dose or IDR for a patient, unless it is incorporated with a body size parameter such as body weight and BSA (Bae et al., 2008).

In a later study, BSA was reported to provide a better adjustment of iodine dose across a wide range of body sizes compared to body weight (Bae et al., 2008). Precise measurement of BSA requires body casting with subsequent planometric measurements. In practice, these measurements are difficult to be performed in every patient. Du Bois & Du Bois (1989) derived a mathematical equation relating height and weight to BSA to facilitate BSA prediction from easily obtainable body weight and height measurements. However, this equation was reported to underestimate the BSA in obese patients by as much as 20 %. It is due to the fact that weight increases without a proportional increase in height in obese patients. By considering the obese population, an equation was proposed later by Livingston & Lee (2001), which relates BSA to body weight in a power function.

As another important factor that affect the VCE, the influence of cardiac output is mainly on the TTP and cardiovascular circulation. When cardiac output decreases, the circulation of contrast medium becomes slower and causes a longer TTP or delay in contrast medium arrival, subsequently a delayed PCE. Furthermore, a slower clearance of contrast medium also contributes to a higher and prolonged PCE (Bae, 2010). Other patient-related factors include age, sex, height, venous access, renal function as well as various other pathological conditions. The effect of these factors on PCE and TTP can be best described by their relationship with blood volume and cardiac output (Bae, 2010).

Scan time is the major CT-related factor which affect both PCE and TTP. In common practice, the injection duration of contrast medium is tailored per scan time to achieve optimal VCE (Fleischmann & Kamaya, 2009). The scan time directly affects the injection duration and injection rate or the contrast volume used in CCTA. A shorter scan time can be acquired with a shortened duration of contrast medium injection. However, it is important to keep in mind that the injection duration can only be reduced to an extent without compromising the overall enhancement profile. There is a risk of suboptimal VCE when contrast medium injected with short injection duration is matched to a prolonged scan time or scan delay (Weininger et al., 2011).

Since PCE increases proportionally with the IDR and TID, any contrast-related factors that affect IDR and TID will also influence the PCE. These factors include contrast concentration, contrast volume, injection rate and injection duration. From the literature, contrast concentration of 320 to 400 $mgmL^{-1}$, contrast volume of 30 to 130 mL, injection rate of 3.3 to 6 mLs^{-1} and injection duration of 6 to 25 s have been reported in 120 kVp CCTA studies which were performed using MDCT scanner with a minimum 64 detector-row (Mihl et al., 2017).

In an attempt to optimise contrast medium administration in 120 kVp CCTA protocol, many studies have tried to reduce the TID via adjustment on contrast concentration and contrast volume. Among these two approaches, adjustment on contrast volume is more preferable and two common methods were used to achieve it: (1) a fixed volume ranged from 40 to 80 mL, and (2) adaptation based on body weight with 0.5 to 1.0 $mLkg^{-1}$ (Mihl et al., 2017). It has been reported that a body weight–adapted iodine dose protocol with fixed injection duration gives significantly better image quality than the fixed-volume or fixed-dose protocol in 64-detector-row CCTA. Contrast volume of 1.0 $mLkg^{-1}$ body weight, with contrast concentration of 370 $mgmL^{-1}$ and injection duration of 15 seconds

is recommended in 64-detector-row CCTA for achieving sufficient VCE (Nakaura et al., 2008). With the development of high-pitch prospectively ECG-triggered CCTA protocol, further optimisation of contrast medium was performed with contrast volume of 0.5 to 0.7 $mLkg^{-1}$ body weight (Liu et al., 2013; Tatsugami et al., 2010). Other proposed methods include adaptation of contrast volume to body weight and BMI (Zhu et al., 2013; Zhu et al., 2012), body weight and TTP (Lu et al., 2010), BSA (Pazhenkottil et al., 2010), PCE (Yang et al., 2013) and scan time and injection rate (Yin et al., 2015).

5.3 Materials and methods

5.3.1 Patient and data sources for model derivation and validation

A retrospective analysis of 141 CCTA patients between January 2014 and December 2016 from University Malaya Medical Centre database was performed. These patients were divided into two groups: The first group consisted of 75 patients (53.2 %) that received 60 mL of contrast medium. This group was used for the derivation of a personalised contrast volume calculation model (thereafter referred as "group 1"). The second group consisted of 66 patients (46.8 %) that received 50 and 55 mL of contrast medium was used for validation of the model (thereafter referred as "group 2"). Subsequently, a total of 33 consecutive patients who were scheduled for CCTA from January to October 2017 were prospectively enrolled for application of the personalised contrast protocol (thereafter referred as "group 3"). Data from another group, consisted of 30 patients with comparable BMI with group 3 was chosen from group 1 and 2 (thereafter referred as "group reference"). This group was used as the reference for comparison of TID and qualitative image quality for group 3 (Figure 5.1). Patient characteristics, including sex, age, body weight and heart rate were recorded. This study was approved by the local ethics committee (reference no: 989.35, Appendix G), and all patients in group 3 provided written informed consent.

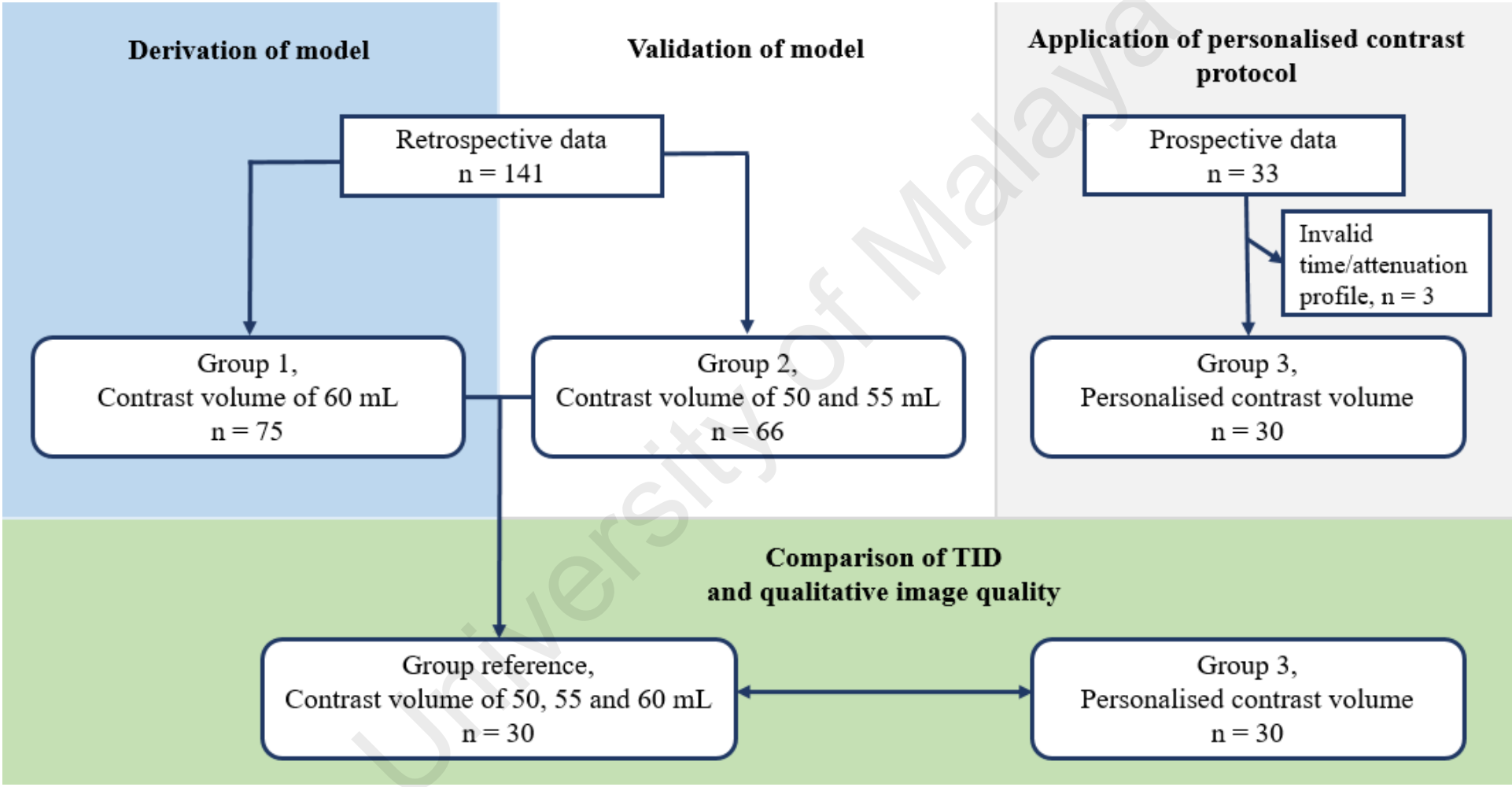

Figure 5.1: Flow diagram of patient assignment for derivation and validation of personalised contrast volume calculation model, the application of personalised contrast protocol and comparison of total iodine dose (TID) and qualitative image quality.

5.3.2 Scanning protocol

CACS was performed with sequential scans and the following scanning parameters: slice acquisition, 6 × 3.0 mm; tube potential, 120 kVp; reference mAs, 74 mAs; reconstructed slice thickness 3.0 mm.

CCTA scan was performed with retrospectively ECG-triggered CCTA protocol, with dose modulation (CareDose 4D, Siemens Healthcare), using DSCT (Somatom definition DS, Siemens Healthcare), tube potential of 120 kVp and reference mAs of 320 mAs. Other scanning parameters were as follows: slice acquisition, 2 × 32 × 0.6 mm (19.2 mm z-axis coverage); full tube current for 20 to 75 % of R-R interval; rotation time, 330 ms; temporal resolution, approximately 82.5 ms; reconstructed slice thickness, 0.6 mm. The scan length was set to cover from the carina of trachea to the apex of the heart.

Contrast medium (iopromide, Ultravist 370, Bayer HealthCare Pharmaceuticals, Berlin, Germany) was injected to median cubital vein using a dual-syringe power injector with dedicated injection software (Medrad Stellant CT injection system with Certegra workstation, Bayer HealthCare Pharmaceuticals). Injection rate of 6 mLs^{-1} was used for both test bolus and full bolus in CCTA scan.

To determine the circulation time of the enhanced scan, contrast medium of 10 mL, followed by 50 mL chaser bolus of saline was used in the test bolus. Sequential scans were obtained every 2 s, from 10 to 30 s after the test bolus injection. The ROI was located in the AA, and a time-attenuation curve was constructed using dedicated software tool (DynEva, Siemens healthcare). The TTP was identified, and the absolute value of PCE of AA at the peak time was measured at the ROI (Figure 5.2). The validity of time-attenuation curve was defined as follows: valid, if the time-attenuation curve showing a unimodal curve and in which the PCE and TTP were measurable; invalid, if time-attenuation curve showing a flat or multimodal curve and/or in which the TTP and PCE

were not determined. Scan delay was defined as 2 s after peak enhancement. The additional 2 s delay is necessary to achieve optimal VCE in the AA and the coronary arteries and low contrast enhancement in the right atrium and ventricle. Thus, this method helps in avoiding the inflow artefacts, which may affect the evaluation of the RCA.

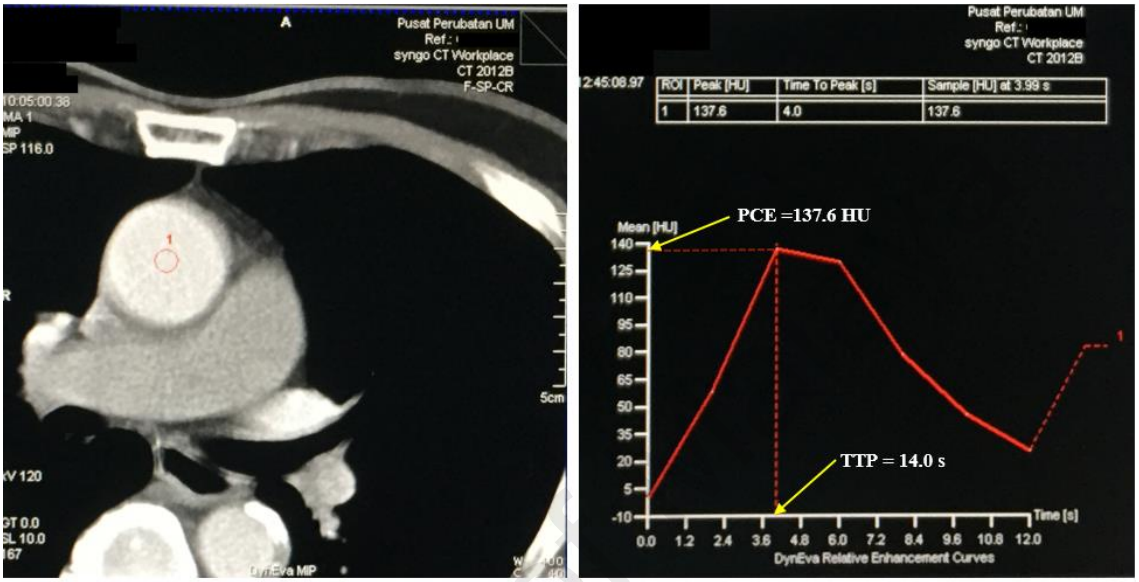

a b

Figure 5.2: (a) ROI placed in the ascending aorta (AA); (b) time-attenuation curve showing the derived TTP and PCE.

A triphasic protocol recommended by SCCT guidelines was applied for the full bolus during CCTA scan, it consists of an initial undiluted contrast bolus (first bolus), followed by a contrast medium (10 mL, 20 %) and saline (40 mL, 80 %) mixture, injected at the same injection rate as the first bolus, and completed by a 50 mL saline flush (Abbara et al., 2016).

For group 1 and 2, the contrast volume of first bolus (50, 55 or 60 mL) was adjusted to a product of the estimated scan time and injection rate (based on the routine contrast protocol). For group 3, the contrast volume of first bolus was calculated using the personalised contrast volume calculation model.

5.3.3 Development of personalised contrast volume calculation model

The development of personalised contrast volume calculation model involved two main steps: (1) establishing the relationship between VCE and contrast volume and (2) establishing the relationship between VCE, patient characteristics and test bolus parameters.

5.3.3.1 Establishing the relationship between vessel contrast enhancement (VCE) and contrast volume

Data from group 1 and group 2 were used in this part of the study. VCE was calculated as the mean CT attenuation value (measured in HU) measured by placing a circular ROI in the LM coronary artery and proximal RCA, using DICOM viewer (RadiAnt DICOM Viewer, Medixant, Poznan, Poland). All ROIs were made as large as possible according to vessel sizes, but vessel walls, calcifications or metallic were avoided to prevent partial volume effects.

Four contrast volumes were included, namely 0, 50, 55 and 60 mL. The VCE corresponding to 0 mL of contrast volume was measured at LM and proximal RCA in CACS images, acquired prior to CCTA scan in every patient.

5.3.3.2 Establishing the relationship between VCE, patient characteristics and test bolus parameters.

The relationship between VCE, patient characteristics and test bolus parameters was assessed using data from the group 1. Mean VCE was compared with age, sex, BSA, heart rate, and PCE and TTP of test bolus. The BSA was calculated from body weight, based on the equation derived by Livingston & Lee (2001), as in Eq. 5.1.

$$BSA = 0.1173 \times \text{body weight}^{0.6466}$$

Eq. 5.1

5.3.4 Validation of personalised contrast volume calculation model

By entering the inputs, including patient characteristics, test bolus parameters and contrast volume (50 and 55 mL), the model developed was used to predict the VCE in group 2 (thereafter referred as "predicted VCE").

VCE was then measured on the acquired axial images, by placing a circular ROI in the LM and proximal RCA. The mean CT attenuation value (HU) for measurements of the arteries was determined (thereafter referred as "measured VCE"). The predicted VCE was then compared to the measured VCE.

5.3.5 Application of personalised contrast protocol

A personalised contrast protocol that utilised the model developed was used in group 3. A targeted VCE of 350 HU at 120 kVp ($VCE_{(t120)}$) was used in this study and the model developed was used to calculate the contrast volume of first bolus based on this targeted VCE (Appendix I). Patients with invalid time-attenuation curve were excluded from the study. Subsequently, the measured VCE obtained from the acquired images was compared to 350 HU.

Qualitative image quality analysis was performed in group 3 and group reference, using the methods described in Chapter 4. The TID and qualitative image quality scores for group 3 was compared to group reference.

Based on the injection duration of first bolus, scan delay and estimated scan time in group 3, a ratio of the injection duration for first bolus to the total scan time (scan delay plus estimated scan time) was calculated. To prevent suboptimal VCE in patient with prolonged scan time or scan delay, the minimum calculated value was proposed as a threshold for the personalised contrast protocol.

5.3.6 Statistical analysis

Statistical analyses were performed (SPSS software version 23.0, IBM Corporation, Armonk, New York, USA). Continuous variables were presented as mean ± standard deviation. Age, body weight, BMI, BSA, heart rate, PCE and TTP at test bolus and measured VCE for group 3 were compared to group reference using Man-Whitney U test. During the derivation of model, VCE was compared to contrast volume using linear regression analysis. Subsequently, VCE was compared to patient characteristics and test bolus parameters using multiple linear regression analysis. During validation of model in group 2, the predicted VCE was compared to the measured VCE using Pearson correlation test. Finally, the TID and VCE scores from qualitative image quality analysis for group 3 was compared to group reference using Man-Whitney U test. For qualitative image quality analysis, Wilcoxon signed-rank test was used to assess interobserver variabilities in VCE scores for group 3 and group reference. 95 % confidence interval was used in all the statistical tests.

5.4 Results

Patient characteristics and test bolus parameters for group 1, 2, 3 and reference are shown in Table 5.1. Three patients were excluded from group 3 due to invalid time-attenuation curve. There were no significant differences ($p > 0.05$) between group 3 and group reference in age, body weight, BMI, BSA, heart rate, PCE and TTP at test bolus.

Table 5.1: Patient characteristics and test bolus parameters for group 1, 2, 3 and reference.

Parameters	Group 1	Group 2	Group 3	Group reference	*p* –value (Group 3 vs. Group reference)
Patient (n)	75	66	30	30	
Male / female ratio	34 : 41	28 : 38	14 : 16	14 : 16	
Age (years)	56.5 ± 10.6	58.2 ± 12.2	56.3 ± 11.7	55.4 ± 12.1	0.830
Body weight (kg)	67.2 ± 9.5	71.0 ± 12.0	80.3 ± 13.7	77.3 ± 8.3	0.158
BMI (kgm^{-2})	25.9 ± 4.1	26.7 ± 4.5	30.2 ± 5.1	30.1 ± 2.9	0.941
BSA (m^2)	1.8 ± 0.2	1.9 ± 0.2	2.0 ± 0.2	2.0 ± 0.1	0.203
Heart rate (bpm)	63.9 ± 7.2	65.2 ± 4.2	64.1 ± 3.1	63.5 ± 5.8	0.911
PCE at test bolus (HU)	100.4 ± 28.5	97.4 ± 28.2	86.5 ± 28.3	95.6 ± 26.6	0.268
TTP at test bolus (s)	16.2 ± 2.5	15.0 ± 1.9	16.4 ± 3.1	15.6 ± 2.3	0.306

BMI, body mass index; BSA, body surface area; PCE, peak contrast enhancement; TTP, time-to-peak;
Group 1, derivation of personalised contrast calculation model;
Group 2, validation of personalised contrast calculation model;
Group 3, personalised contrast protocol;
Group reference, reference for comparison with group 3.

5.4.1 Relationship between VCE and contrast volume

The mean VCE for 0, 50, 55 and 60 mL were 58.5, 450.1, 471.4 and 494.4 HU respectively. These four points were linearly correlated (VCE = 7.42 × contrast volume + 59.57, $r^2 = 0.94$, $p < 0.05$, Figure 5.3).

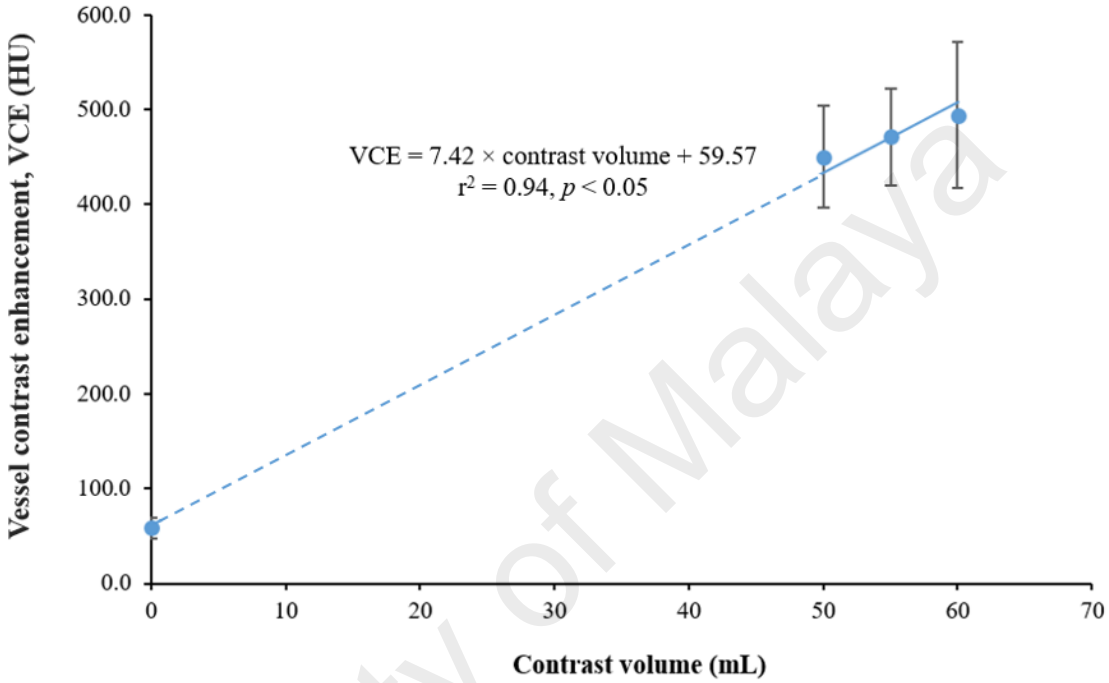

Figure 5.3: The relationship between VCE and contrast volume.

5.4.2 Relationship between VCE, patient characteristics and test bolus parameters

The relationship between VCE, patient characteristics and test bolus parameters is shown in Table 5.2 and Table 5.3. In Table 5.2, BSA showed the strongest inverse correlation with VCE (r = -0.61, $p < 0.05$). Whereas, age (r = 0.52, $p < 0.05$) and PCE at test bolus (r = 0.60, $p < 0.05$) showed significant positive correlation with VCE. No significant correlation ($p > 0.05$) was found between VCE and heart rate, as well as between VCE and TTP at test bolus.

Based on the result of multiple linear regression in Table 5.3, the strongest predictor for VCE is BSA (correlation coefficient -157.36, $p < 0.05$), followed by sex (correlation

coefficient 37.60, $p < 0.05$), age (correlation coefficient 2.15, $p < 0.05$) and PCE at test bolus (correlation coefficient 1.22, $p < 0.05$).

Table 5.2: Relationship between VCE, patient characteristics and test bolus parameters.

Parameters	r	*p*-value
Age (years)	0.52	0.0001*
BSA (m^2)	-0.61	0.0001*
Heart rate (bpm)	0.60	0.616
PCE at test bolus (HU)	0.60	0.0001*
TTP at test bolus (s)	0.17	0.148

* $p < 0.05$ is considered statistically significant different.
BSA, body surface area; PCE, peak contrast enhancement; TTP, time-to-peak; VCE, vessel contrast enhancement.

Table 5.3: Multiple linear regression analysis of patient characteristics and test bolus parameters associated with VCE.

Variables	Correlation	Coefficient standard error	*p*-value	95 % confidence interval
Age (years)	2.15	0.49	0.0001*	1.33 to 2.97
Sex	37.60	10.29	0.0001*	20.45 to 54.75
BSA (m^2)	-157.36	33.86	0.0001*	-213.80 to -100.95
PCE at test bolus (HU)	1.22	0.18	0.0001*	0.92 to 1.53

* $p < 0.05$ is considered statistically significant different.
BSA, body surface area; PCE, peak contrast enhancement; VCE, vessel contrast enhancement.

5.4.3 Development of personalised contrast volume calculation model by multiple linear regression equation

As the VCE is linearly correlated with contrast volume, the relationship between VCE and contrast volume can be described in Eq. 5.2:

$$VCE_{(t120)} = m \times \text{contrast volume} + VCE_0 \quad \text{Eq. 5.2}$$

Where $VCE_{(t120)}$ is the targeted VCE at 120 kVp (350 HU), m is the slope and VCE_0 is the intercept, that is the VCE when no contrast medium is administrated, thus, it

corresponds to mean CT attenuation value (HU) measured at LM and proximal RCA in CACS images.

From the result of multiple linear regression analysis, the relationship of patient characteristics and test bolus parameters associated with VCE can be described in Eq. 5.3. $VCE_{(60/120)}$ is the VCE achieved with 60 mL contrast medium at 120 kVp and $PCE_{(120)}$ is PCE of test bolus at 120 kVp. For the sex, male patient is labelled as 0 and female patient is labelled as 1.

$$VCE_{(60/120)} = 2.15 \times Age + 37.60 \times Sex - 157.36 \times BSA + 1.22 \times PCE_{(120)} + 512.19 \quad \text{Eq. 5.3}$$

These two equations were used to form the personalised contrast volume calculation model. After the test bolus scan, $VCE_{(60/120)}$ can be estimated using Eq. 5.3. Then, m in Eq. 5.2 can be calculated by filling in the VCE_0 measured from CACS, the contrast volume as 60 mL and the estimated $VCE_{(60/120)}$ from Eq. 5.3. Once m is determined, the model can be used to predict the VCE for a given contrast volume (group 2) or to calculate the contrast volume for $VCE_{(t120)}$ of 350 HU (group 3).

5.4.4 Validation of personalised contrast volume calculation model

In group 2, the mean absolute difference between predicted and measured VCE was 38.8 HU (-80.8 to 40.8 HU). There was excellent correlation ($r = 0.82$, $p < 0.05$) between predicted and measured VCE (Figure 5.4). Bland-Altman plot was constructed to evaluate the degree of agreement between predicted and measured VCE (Figure 5.5). The 95 % confidence interval limits of agreement ranged from -96.5 to 42.8 HU, with a negative mean difference or bias of 27.2 HU.

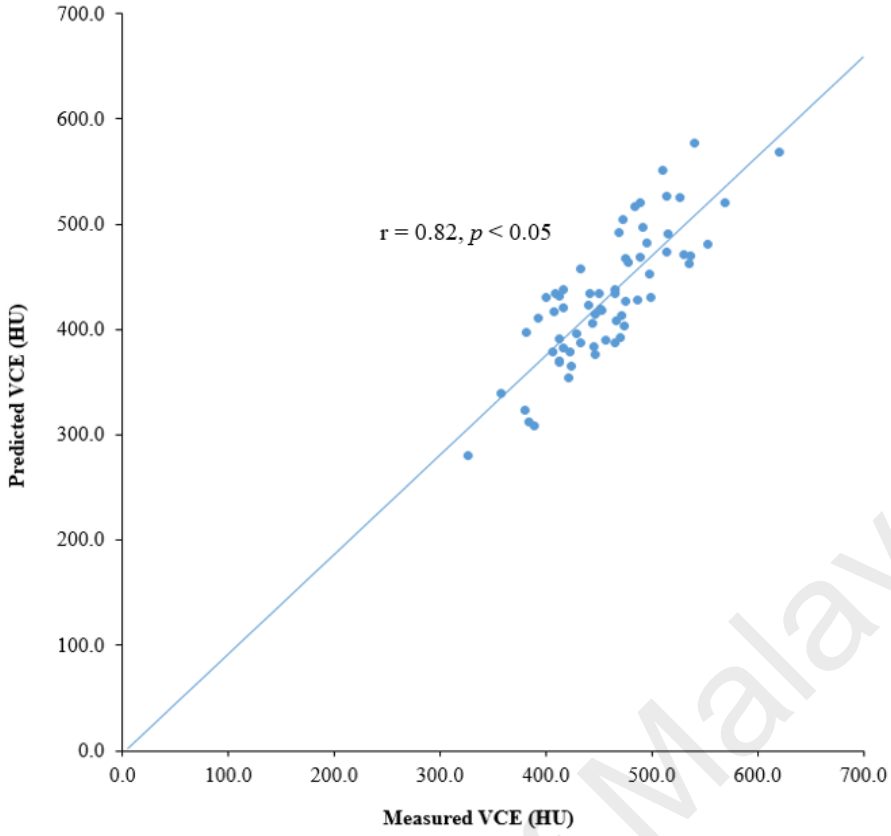

VCE, vessel contrast enhancement

Figure 5.4: Correlation between predicted and measured VCE.

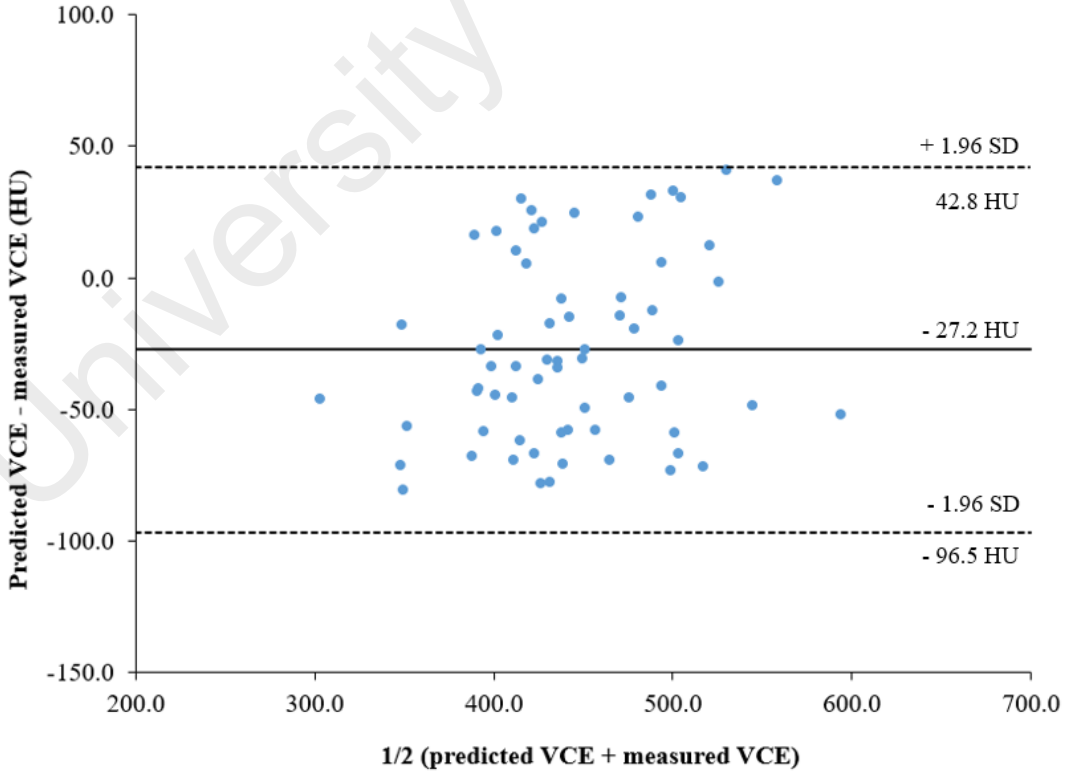

VCE, vessel contrast enhancement

Figure 5.5: Bland-Altman plot comparing the difference between predicted and measured VCE.

5.4.5 Patients imaging with personalised contrast protocol

Table 5.4 shows comparison of measured VCE, contrast volume for first bolus, total contrast volume (test bolus and full bolus), TID and VCE scores for group 3 and group reference. The measured VCE was significantly lower ($p < 0.05$) in group 3 (387.8 ± 42.7 HU) compared to group reference (448.9 ± 57.6 HU). In group 3, all scans for 30 patients were done successfully with measured VCE ranging from 298.3 to 435.4 HU. The mean absolute difference between the measured VCE from 350 HU was 49.9 HU (-51.7 to 85.4 HU). A representative case is shown in Figure 5.6.

Table 5.4: Comparison of measured VCE, contrast volume of first bolus, total contrast volume, TID and VCE scores between group 3 and reference.

Parameters	Group 3	Group reference	*p* –value
Measured VCE (HU)	387.8 ± 42.7	448.9 ± 57.6	0.0001*
Contrast volume of first bolus (mL)	47.8 ± 8.3	55.2 ± 4.8	0.0001*
Total contrast volume (mL)	67.8 ± 8.3	75.2 ± 4.8	0.0001*
TID (g)	25.1 ± 3.1	27.8 ± 1.8	0.0001*
VCE scores (based on qualitative image quality analysis)	4.7 (3.5 to 5.0)	4.7 (4.0 – 5.0)	0.564

* $p < 0.05$ is considered statistically significant different.
TID, total iodine dose; VCE, vessel contrast enhancement;
Group 3, personalised contrast protocol;
Group reference, reference for comparison with group 3.

The TID used in group 3 (25.1 ± 3.1 g) was significantly lower ($p < 0.05$) compared to the TID in group reference (27.8 ± 1.8 g). VCE scores were graded as acceptable to excellent for group 3 and good to excellent for group reference. No significant differences ($p > 0.05$) was found in the VCE scores between both groups. The Wilcoxon signed-rank test demonstrated no significant interobserver variabilities ($p > 0.05$) in VCE scores made by the two observers for both groups.

The mean injection duration of first bolus, scan delay and estimated scan time in group 3 were 8.0 ± 1.4 s (5.2 to 11.3 s), 18.4 ± 3.1 s (14.0 to 24.2 s), 9.9 ± 1.5 s (6.5 to 13.6 s).

The calculated ratio for injection duration of first bolus to the total scan time ranged from 0.21 to 0.41. Thus, to prevent any suboptimal VCE in patient with prolonged scan time or scan delay, a ratio of ≥ 0.21 was proposed as a threshold value for the personalised contrast protocol developed in this study. Scan with a ratio of < 0.21 would not be expected to conform to the model developed.

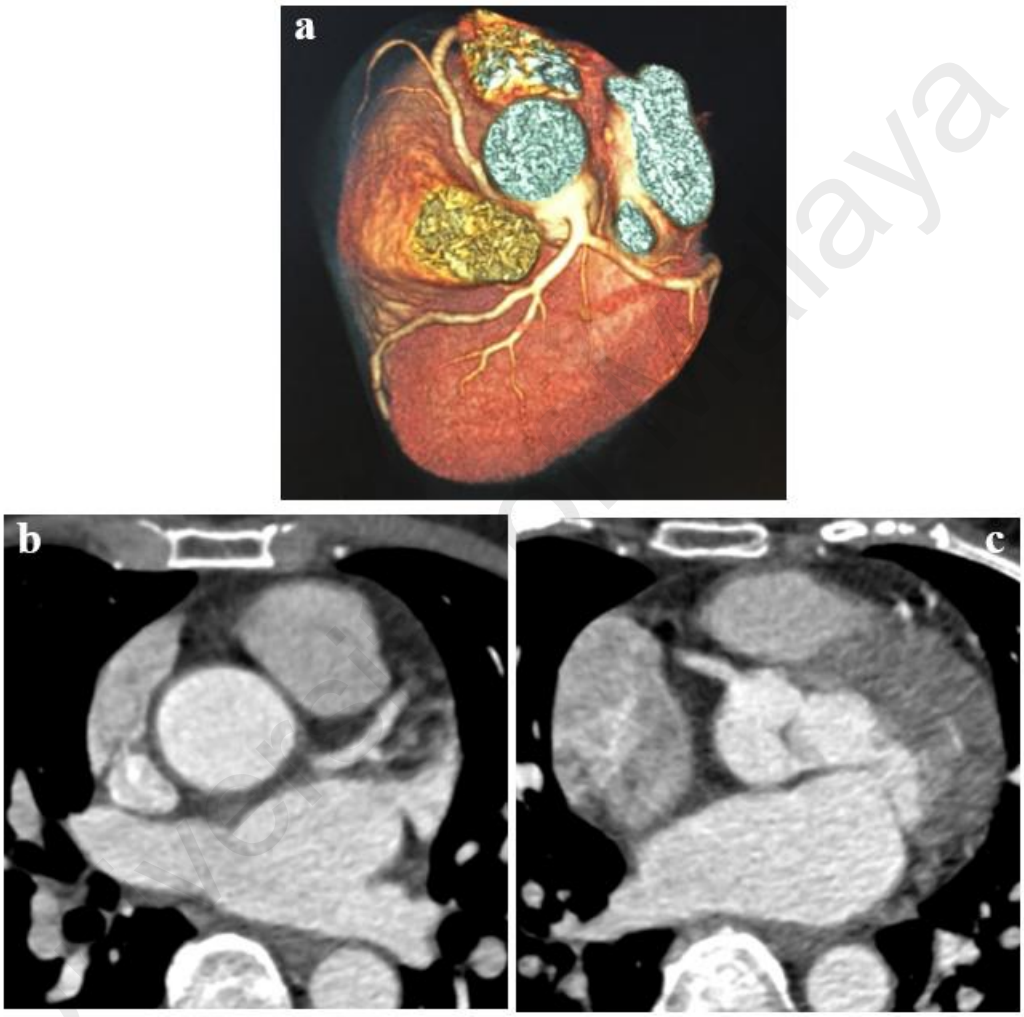

Figure 5.6: A representative case using the personalised contrast protocol; (a) volume rendering image of the heart; axial images at the level of (b) left main (LM) coronary artery and proximal left anterior descending (LAD), (c) proximal right coronary artery (RCA).

5.5 Discussion

There are advantages for applying a personalised contrast protocol in CCTA. Firstly, it reduces the TID used in CCTA, reducing the risk of contrast-induced nephropathy. Secondly, it helps in achieving the VCE within the optimal range for quantitative analysis

of coronary artery and plaque. A third and more controversial advantage is the possible reduction in radiation exposure to the enhanced organ. Studies have reported the association of increase in organ dose by 19 to 71 % with contrast medium application in CT (Amato et al., 2013; Amato et al., 2010). Furthermore, the increase of X-ray photons absorption in the contrast-enhanced organ might lead to biological damage (Sahbaee et al., 2017). In an in vitro study conducted by Grudzenski et al. (2009), the presence to iodinated contrast medium during CT examination has been reported to cause 30 % increase in DNA double-strand breaks in peripheral blood lymphocytes, compared to the unenhanced CT examination. This finding was supported by another recent in vivo study conducted by Wang et al. (2017). In this study, 38 % increase in DNA double-strand breaks in peripheral blood lymphocytes was reported in the contrast-enhanced CT. Furthermore, the injection of iodinated contrast medium prior to a CT examination showed higher DNA damage (90 %) compared to injection after the examination. This proved the potential of biological damage in irradiating the contrast-enhanced organ.

In the analysis of relationship between VCE and contrast volume, although there were no data available for VCE with contrast volume of 10 to 40 mL, a linear fit was chosen to correlate the VCE at 0, 50, 55 and 60 mL. The linear relationship between VCE and contrast volume has been reported by Burbank et al. (1984). By doubling the contrast volume, the peak iodine concentration in the blood and VCE are doubled.

From the result of multiple linear regression analysis between VCE, patient characteristics and test bolus parameters, the best predictor for VCE was BSA, with negative correlation with VCE. Similar result was reported in a study conducted by Komatsu et al. (2013). The inverse relationship between BSA and VCE has also been reported in previous studies (Pazhenkottil et al., 2010; Herzog et al., 2009; Bae et al., 2008). In a study conducted by Pazhenkottil et al. (2010), a BSA-adapted contrast

medium protocol was used to reduce the TID by 11 % compared to the fixed-contrast medium protocol.

Another two patient characteristics, age and sex were found to be significant predictors. The association of age and VCE can be explained by the fact that increasing in age is related with a higher PCE as cardiac output reduces with age (Bae et al., 1998; Nakajima et al., 1998; Katori, 1979). The inverse relationship between PCE and the cardiac output ($Lmin^{-1}$) and cardiac index ($Lmin^{-1}m^{-2}$) was demonstrated in a study conducted by Sakai et al. (2010). In this study, every reduction in cardiac index led to a 38 % increase in PCE. For sex, there is a difference in blood volume between men and women, it is expected to see a slightly difference in PCE and TTP among sex. For a given BMI, male has 5 to 10 % higher blood volume compared to female. Thus, a higher VCE will be observed in female when the same TID per body weight is given (Suzuki et al., 2004).

For test bolus parameters, PCE at test bolus was found to be a significant predictor for VCE in this study. Similar finding was reported in the previous studies that investigated the relationship between PCE at test bolus and VCE (Yang et al., 2013; Mahnken et al., 2007; van Hoe et al., 1995). Every increment of 1.0 HU in PCE at test bolus was found to lead to increment of 1.2 HU in VCE in this study. This is comparable to the result presented in the study conducted Komatsu et al. (2013) that reported an increment of 1.3 HU in VCE with every increment of 1.0 HU in PCE at test bolus.

As TTP increases with the decrease in cardiac output, TTP was reported to be directly correlated to PCE in several studies (Komatsu et al., 2013; Sakai et al., 2010). However, there was no significant relationship found between TTP at test bolus and VCE in this study. This could be due to the less variation of cardiac output in group 1, that can be

indicated by the narrow range of TTP at test bolus (12 to 22 s), compared to the wider range of TTP between 15 to 36 s in the other study (Sakai et al., 2010).

During the validation of the model developed (in group 2), the excellent correlation (r = 0.82) between predicted and measured VCE indicates that the model developed can reliably be used to predict VCE for a given contrast volume. By using the measured VCE as reference, the personalised contrast volume calculation model tends to under-predict the VCE by 27.2 HU. When applying the personalised contrast protocol in group 3, the measured VCE (298.3 to 435.4 HU) for all patients were within the optimal range of VCE (more than 250 HU and less than 450 HU) (Abbara et al., 2016; Abbara et al., 2009; Cademartiri et al., 2008; Fei et al., 2008; Horiguchi et al., 2007).

From the literature, IDR of 1.10 to 2.22 gs^{-1} and TID of 11.1 to 48.1 g were used in 120 kVp CCTA studies (Mihl et al., 2017). TID is a relevant parameter that determines PCE in venous phase while the IDR greatly influences the PCE in arterial phase imaging (Faggioni & Gabelloni, 2016; Fleischmann, 2010; Bae et al., 2008). Thus, when optimising contrast medium administration in CCTA, a high IDR is relevant to achieve PCE at a lower TID. In this study, high injection rate of 6 mLs^{-1} and high contrast concentration of 370 $mgmL^{-1}$ were used to achieve IDR of 2.22 gs^{-1} and TID of 18.9 to 32.6 g. Significant reduction of TID by 9.8 % was achieved in the personalised contrast protocol compared to the routine contrast protocol. Furthermore, the VCE in group 3 was graded as acceptable to excellent with no statistical significant differences with group reference. Thus, it can be concluded that the personalised contrast protocol developed in this study allows optimal VCE and image quality with reduced TID.

This study has several limitations. Firstly, the maximum absolute difference between the predicted and measured VCE (80.8 HU) in group 2 and the maximum absolute difference between measured VCE and target VCE in group 3 (85.4 HU) was considered

large. In a study conducted by Mahnken et al. (2007) that used PCE as the predictor for VCE, a maximum absolute difference of 101.4 HU was reported. Furthermore, maximum absolute difference of more than 90.0 HU was also observed in another study conducted by Komatsu et al. (2013) that developed a prediction model based on BSA, PCE and TTP. This difference is due the limitation of the model developed, which is unable to include all the other possible confounding parameters. Most of these parameters were not accessible, before or during CCTA examination. For instance, measurement of factors which affect the resistance to blood flow within blood vessel, such as the vessel diameter and length, viscosity of blood, as well as the level of stenosis are not possible before the CCTA scan (Klabunde, 2012). Secondly, since the model developed in this study does not take into account the CT-related factors, such as the scan time and scan delay, there is a risk of suboptimal VCE in patients with prolonged scan time or scan delay. By referring to the calculated injection duration of first bolus to total scan time ratio in every patient, a value of ≥ 0.21 was proposed to be used as a threshold. For any scan with a ratio of < 0.21, this personalised contrast protocol is not recommended as the model developed is not expected to be conformable. Thirdly, only one IDR ($2.22\ gs^{-1}$) was investigated in this study as the same contrast concentration and injection rate was applied for every patient in University of Malaya Medical Centre. Further studies with testing of different IDR are needed to make the personalised contrast protocol more robust. Finally, the application of test bolus method in this study causes additional scan time, radiation and iodine dose (3.7 g) when compared to the bolus tracking method.

5.6 Conclusion

A personalised contrast volume calculation model based on patient characteristics and test bolus parameters was developed and validated for 120 kVp retrospectively ECG-triggered CCTA protocol. The personalised contrast protocol based on the model

developed allows optimal VCE and image quality at 120 kVp retrospectively ECG-triggered CCTA and TID reduction of 9.8 % compared to the routine contrast protocol.

As an extension of this chapter, the process of developing and validating a personalised contrast volume calculation model for 100 kVp retrospectively ECG-triggered CCTA protocol are presented in the next chapter.

CHAPTER 6: OPTIMISATION OF RADIATION DOSE, IMAGE QUALITY AND CONTRAST MEDIUM ADMINISTRATION IN CCTA: AN IMPROVED RETROSPECTIVELY ECG-TRIGGERED CCTA PROTOCOL

6.1 Introduction

The use of lower tube voltage in CCTA has been increased over the past 10 years (Hausleiter et al., 2010; Bischoff et al., 2009). It is mainly due to the potential of radiation dose and TID reduction at lower tube voltage compared to the standard 120 kVp. This double low dose technique is based on the concept that the number of X-ray photons and mean energy of the X-ray beam are reduced when a lower tube voltage is applied. The reduction in the number of X-ray photons is the main factor that contributes to the lower radiation dose. As a lower tube voltage is applied, it causes reduction in the tube effectiveness, thus, less X-ray photons are produced. In addition, the heavy filtration of low energy photons further reduce the number of X-ray photons. The number of X-ray photons is generally accepted to be proportional to the square of the X-ray tube voltage. A reduction from 120 to 100 kVp will result in 31 % less X-ray photons being produced, and this figure will increase to 56 % with further reduction to 80 kVp (Aschoff et al., 2017).

The mean photon energy (approximately half of the peak tube voltage) of X-ray beam is reduced and closer to the K-edge of iodine (33.2 keV) when a lower tube voltage is applied. More X-ray photons are being absorbed by the iodine atoms, resulting in an increase in photoelectric effects. This allows a comparable VCE at a lower TID in CCTA, as the CT number of iodine is higher in a CT image produced at lower kVp (Aschoff et al., 2017).

Several studies have tried to reduce the TID in low tube voltage CCTA protocol by reducing the iodine dose in the existing contrast protocol for 120 kVp, via adjustment of

contrast concentration and contrast volume. Among these two approaches, reducing the contrast volume is preferable to achieve TID reduction. When the contrast concentration is reduced, it causes reduction in IDR that leads to lower PCE. Hence, lowering the contrast concentration will produces less TID reduction compared to reducing the contrast volume (Aschoff et al., 2017). Akadhi et al. (2008) reported similar qualitative image quality at 100 kVp protocol compared to 120 kVp protocol by using a body weight-adapted iodine dose protocol. The authors reduced the contrast volume and IDR from 1.0 $mLkg^{-1}$ and 1.8 gs^{-1} at 120 kVp to 0.8 $mLkg^{-1}$ and 1.4 gs^{-1} at 100 kVp. Wang et al. (2014) reported satisfactory VCE at 100 kVp protocol by applying the same IDR of 1.3 gs^{-1} with a 44 % reduction in contrast volume compared to 120 kVp protocol (50 vs. 90 mL). In another study conducted by Kok et al. (2016), contrast volume of 40 mL and injection rate of 5.3 mLs^{-1} was recommended for 100 kVp protocol to achieve a 12 % reduction of TID compared to 120 kVp protocol. This recommendation was developed by applying 12 % reduction in contrast volume, injection rate, scan delay and IDR that used in the contrast protocol of 120 kVp, with a constant injection duration at 7.5 s.

Generally, many studies have focused on reducing radiation dose and TID at low tube voltage CCTA protocol while maintaining VCE above 250 HU. Limited studies have considered the upper limit of VCE. Optimal VCE is crucial in CCTA for the detection of coronary stenosis and quantitative analysis of atherosclerotic plaque. As mentioned in Chapter 5, the optimal range of VCE for the detection of coronary stenosis, quantitative analysis of atherosclerotic plaque and diagnostic performance of CCTA could fall between more than 250 and less than 450 HU (Abbara et al., 2016; Abbara et al., 2009; Cademartiri et al., 2008; Fei et al., 2008; Horiguchi et al., 2007). A personalised contrast volume calculation model which incorporates patient characteristics and test bolus parameters is superior compared to body weight-adapted iodine dose or a fixed contrast volume protocol, as it allows better contrast volume estimation for achieving VCE within

the optimal range and further reduce the TID at lower tube voltage (Komatsu et al., 2013; Yang et al., 2013). The purpose of this study was to develop and clinically validate an improved retrospectively ECG-triggered CCTA protocol, formed by the combination of low tube voltage (100 kVp) and a personalised contrast protocol.

6.2 Literature review

Various studies have reported substantial radiation dose reduction in low tube voltage (80 and 100 kVp) protocol compared to standard 120 kVp protocol in CCTA. In a prospective multicentre survey under Prospective Multicenter Study on Radiation Dose Estimates of Cardiac CT Angiography I (PROTECTION I) study, median H_E of 6.0 mSv was reported in the low tube voltage (100 kVp) retrospectively ECG-triggered CCTA protocol in nonobese patients. When compared to median H_E of 120 kVp (14.0 mSv), there was a reduction of 53 % in radiation dose (Bischoff et al., 2009). Subsequently, in PROTECTION II study, a survey that mainly focused on radiation dose and image quality in retrospectively ECG-triggered protocols was conducted. A 31 % reduction in radiation exposure with maintained image quality was reported in 100 kVp protocol (8.4 mSv) compared to 120 kVp protocol (12.2 mSv) (2010) (Hausleiter et al., 2010). In another study conducted by Oda et al. (2015), H_E of 6.3 mSv was reported in the retrospectively ECG-triggered CCTA protocol with 80 kVp. This low tube voltage protocol has successfully achieved 55 % radiation dose reduction compared to 120 kVp protocol (13.9 mSv), without compromising the image quality and accuracy of cardiac functional analysis. From the findings of these studies, it can be concluded that substantial radiation dose reduction with similar image quality to 120 kVp protocol can be achieved in low tube voltage retrospectively ECG-triggered CCTA protocols.

For studies that involved prospectively ECG-triggered CCTA protocol, the mean H_E reported ranged from 0.31 to 2.75 mSv for 80 kVp, 0.69 to 6.29 mSv for 100 kVp and

1.53 to 10.7 mSv for 120 kVp. Generally, the radiation doses were reduced by 38 to 83 % at 80 kVp protocol and 3 to 80 % at 100 kVp protocol, compared to 120 kVp protocol (Di Cesare et al., 2016; Durmus et al., 2016; Iyama et al., 2016; Mangold et al., 2016; Pan et al., 2016; Wu et al., 2016; Oda et al., 2015; Shen et al., 2015; Sun et al., 2015; Yin et al., 2015; Zhang, C. et al., 2015; Zhang, J. et al., 2015; Khan et al., 2014; Zheng et al., 2014; Nakaura, Kidoh, Sakaino, Nakamura, et al., 2013; Nakaura, Kidoh, Sakaino, Utsunomiya, et al., 2013).

The potential of TID reduction in lower tube voltage is derived from the considerably higher X-ray photon absorption of iodine at low tube voltage (Aschoff et al., 2017). TID reduction can be achieved at lower tube voltage by manipulating the four main contrast-related factors that affect TID: contrast concentration, contrast volume, injection rate and injection duration. One of the drawbacks of reducing contrast concentration or injection rate is the reduction of IDR. Reducing the contrast concentration would result in a lower TID, but it also reduces the PCE as the IDR is reduced. Hence, it is better to maintain a high contrast concentration and reduce only the contrast volume at the same injection rate as the IDR remained high, resulting in greater PCE. This technique potentially improves the image quality and further reduces the TID (Aschoff et al., 2017).

6.3 Materials and methods

6.3.1 Study design

This study was divided into three parts. The first part involved derivation of a personalised contrast volume calculation model for 100 kVp. By using the relationship established between contrast enhancement and iodine concentration at 100 and 120 kVp, the model developed in Chapter 5 was adapted to form a personalised contrast volume calculation model for 100 kVp. Secondly, the personalised contrast volume calculation model developed for 100 kVp was clinically validated with 30 consecutive patients who

were scheduled for CCTA (thereafter referred as “group 1”). Thirdly, an improved retrospectively ECG-triggered CCTA protocol, formed by the combination of low tube voltage (100 kVp) and personalised contrast protocol was then applied in 30 consecutive patients who were scheduled for CCTA (thereafter referred as “group 2”). Retrospective data for another 30 patients with comparable BMI with group 2, scanned with the combination of 120 kVp retrospectively ECG-triggered CCTA and routine contrast protocol were retrieved from the University of Malaya Medical Centre database to form a reference group (thereafter referred as “group reference”). This group reference was used for comparison of radiation dose and image quality with group 2 (Figure 6.1). This study was approved by the local ethics committee (reference no: 989.35, Appendix G), and all patients in group 2 were provided written informed consent.

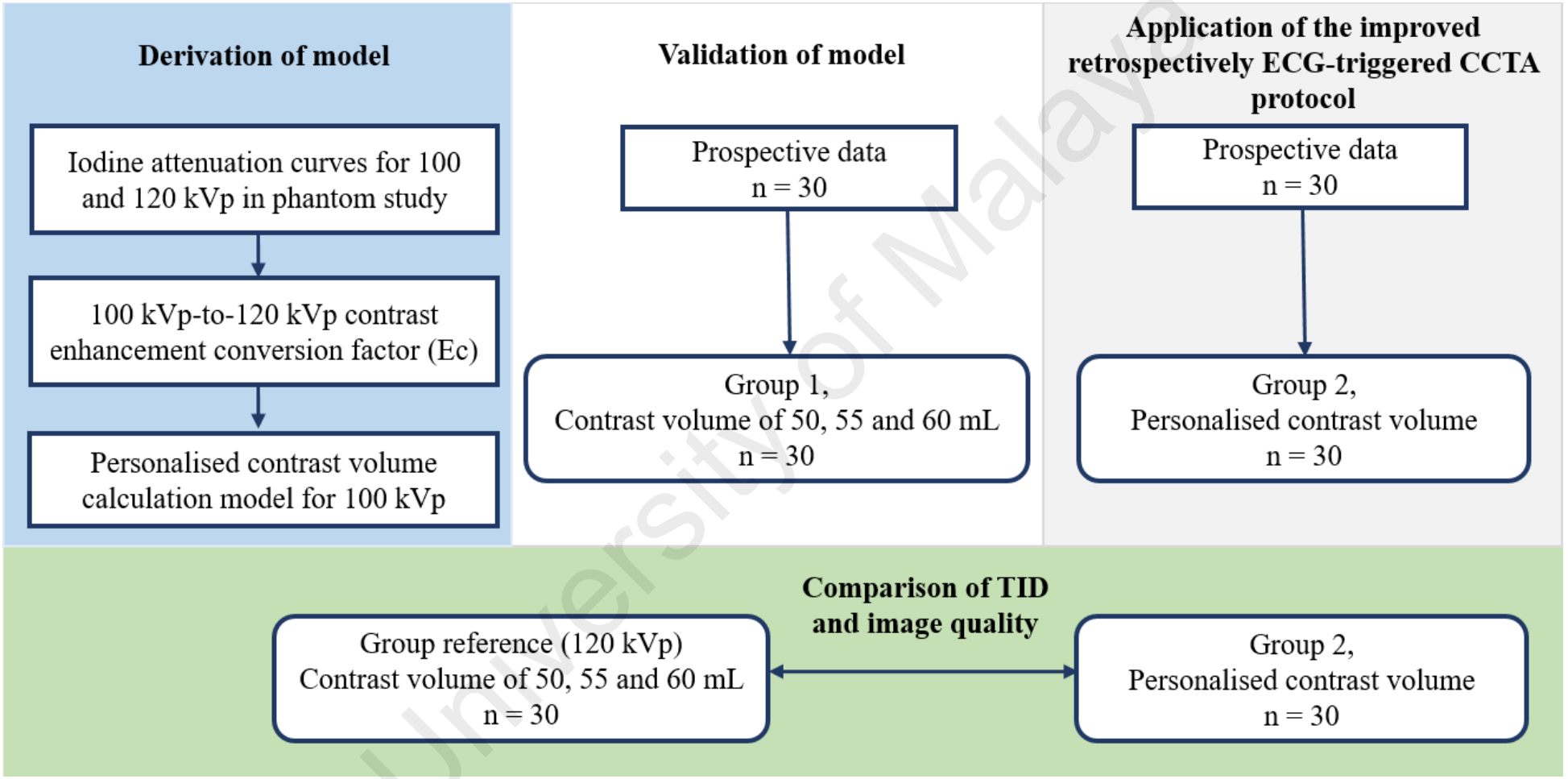

Figure 6.1: Flow diagram showing model derivation, patient assignment for validation of personalised contrast volume calculation model, the application of the improved retrospectively ECG-triggered CCTA protocol and comparison of total iodine dose (TID) and image quality.

6.3.2 Development of personalised contrast volume calculation model for 100 kVp

Since the X-ray attenuation of iodine is relatively higher in 100 kVp compared to 120 kVp, the differences in contrast enhancement between these two different tube voltages was used to establish a personalised contrast volume calculation model for 100 kVp, based on the model developed in Chapter 5.

A phantom study was conducted to construct the iodine attenuation curves for 100 and 120 kVp. Five polyethylene vials were filled with 2 mL of iodinated contrast medium (iopromide, Ultravist 370, Bayer HealthCare Pharmaceuticals, Berlin, Germany) at different concentrations: 5, 10, 15, 20 and 25 $mgmL^{-1}$, respectively. One control vial was filled with 2 mL of saline. The vials were then placed in a plug location for heart, in a female adult anthropomorphic phantom (702-G, CIRS Inc., Norfolk, Virginia, USA) (Figure 6.2). CCTA scan was performed with sequential mode for 100 and 120 kVp, using a DSCT scanner (Somatom Definition Dual Source, Siemens Healthcare, Forchheim, Germany). To avoid the influence of different noise level on the contrast enhancement, 250 and 138 mAs were used for 100 and 120 kVp, respectively, to achieve the same $CTDI_{vol}$ of 28.0 mGy.

Images were reconstructed with a medium smooth reconstruction kernel (B26f), at slice thickness of 0.75 mm and pixel matrix of 512 × 512. The mean CT attenuation value (HU) for saline and each concentration of iodine was measured in axial images by placing a circular ROI in the control and contrast-containing vials (Figure 6.2 (c)) and determined as contrast enhancement.

Figure 6.2: (a) Six polyethylene vials of 2 mL in volume that has been filled with saline and different concentrations of iodinated contrast medium: 5, 10, 15, 20 and 25 mgmL^{-1}; (b) placement of polyethylene vial in female adult anthropomorphic phantom; (c) ROI for contrast enhancement measurement.

The iodine attenuation curves for both 100 and 120 kVp were constructed and relative difference in the contrast enhancement between the two different tube voltages was used to develop a 100 kVp-to-120 kVp contrast enhancement conversion factor (E_c). This conversion factor served for two purposes. Firstly, it was used to convert the PCE of test bolus at 100 kVp ($PCE_{(100)}$) to 120 kVp ($PCE_{(120)}$) (Eq. 6.1), as the test bolus was performed in 100 kVp. Then, the converted value was used for calculation in Eq. 5.3. Secondly, it was used to calculate the modified targeted VCE for 100 kVp ($VCE_{(t100)}$)

from the targeted VCE for 120 kVp ($VCE_{(t120)}$) (Eq. 6.2). The $VCE_{(t100)}$ was used for calculation in Eq. 5.2 to achieve 350 HU at 100 kVp.

$$PCE_{(120)} = PCE_{(100)} \times E_C \quad \text{Eq. 6.1}$$

$$VCE_{(t100)} = VCE_{(t120)} \times E_C \quad \text{Eq. 6.2}$$

6.3.3 Validation of personalised contrast volume calculation model

Between June and August 2017, 30 consecutive scheduled patients with BMI less than 30 kgm^{-2} were enrolled for model validation in group 1 (Figure 6.1). Patients were scanned with low tube voltage (100 kVp) retrospectively ECG-triggered CCTA protocol with the routine contrast protocol.

CACS was performed with sequential scans and the following scanning parameters: slice acquisition, 6 × 3.0 mm; tube potential, 120 kVp; reference mAs, 74 mAs; reconstructed slice thickness 3.0 mm. All CCTA scan were performed with low tube voltage (100 kVp) retrospectively ECG-triggered CCTA protocol, using DSCT (Somatom definition DS, Siemens Healthcare), with dose modulation (CareDose 4D, Siemens Healthcare), with the following scanning parameters: slice acquisition, 2 × 32 × 0.6 mm (19.2 mm z-axis coverage); full tube current for 20 to 75 % of R-R interval; rotation time, 330 ms; temporal resolution, approximately 82.5 ms; and reference mAs, 320 mAs. The scan length was set to cover from the carina of trachea to the apex of the heart. The methods for test bolus and routine contrast protocol for the full bolus were the same as described in Chapter 5.

Subsequently, the VCE was predicted for every patient using the model developed (thereafter referred as “predicted VCE”). VCE was also measured on the axial images

with the methods described in Chapter 5 (thereafter referred as "measured VCE"). The predicted VCE was then compared to the measured VCE.

6.3.4 Application of the improved retrospectively ECG-triggered CCTA protocol

An improved retrospectively ECG-triggered CCTA protocol was developed with the combination of low tube voltage (100 kVp) and personalised contrast protocol (based on the model developed). A total of 30 consecutive patients who were scheduled for CCTA from August to November 2017, with BMI less than 30kgm^{-2} were prospectively enrolled for examining the feasibility of this improved protocol (group 2) (Figure 6.1). Patients were scanned with scanning parameters as in group 1, but with a higher reference mAs of 370 mAs. Patients with invalid time-attenuation curve were excluded from the study. The $VCE_{(t100)}$ calculated from Eq. 6.2 was used for contrast volume calculation of the first bolus (Appendix I). The measured VCE obtained from the acquired images was then compared to 350 HU.

For group reference, patients were scanned with 120 kVp. The rest of the scanning parameters were similar to group 1. Routine contrast protocol was used in this group. The assessment of radiation dose, quantitative and qualitative image quality analysis was performed in group 2 and group reference, with the methods described in Chapter 4. The TID, radiation dose, quantitative and qualitative image quality in group 2 was compared to group reference.

Based on the injection duration of first bolus, scan delay and estimated scan time in group 2, a ratio of the injection duration for first bolus to the total scan time (scan delay plus estimated scan time) was calculated. To prevent suboptimal VCE in patient with prolonged scan time or scan delay, the minimum calculated value was proposed as a threshold for the improved protocol.

6.3.5 Statistical analysis

Statistical analyses were performed (SPSS software version 23.0, IBM Corporation, Armonk, New York, USA). Continuous variables were presented as mean ± standard deviation. Age, body weight, height, BMI, BSA, heart rate, PCE and TTP at test bolus and measured VCE for group 2 was compared to group reference using Man-Whitney U test. During the construction of iodine attenuation curves, the contrast enhancement was compared to iodine concentration using linear regression analysis. During the validation of model in group 1, the predicted VCE was compared to the measured VCE using Pearson correlation test. Finally, the TID, radiation dose, quantitative and qualitative image quality scores obtained using the improved protocol in group 2 were compared to group reference using Man-Whitney U test. For qualitative image quality analysis, Wilcoxon signed-rank test was used to assess interobserver variabilities in VCE scores for group 2 and group reference. 95 % confidence interval was used in all the statistical tests.

6.4 Results

6.4.1 Development of personalised contrast volume calculation model for 100 kVp

A linear relationship between iodine concentration and contrast enhancement was observed for 100 and 120 kVp (Figure 6.3). The contrast enhancement at 100 kVp was higher by 19.6 % compared to 120 kVp. The calculated E_C was (29.089/35.862) = 0.81. By using this conversion factor, a $VCE_{(t100)}$ of 280 HU was calculated (Eq. 6.2) to achieve 350 HU at 100 kVp. By converting the $PCE_{(100)}$ to $PCE_{(120)}$ for every patient (Eq. 6.1), a personalised contrast volume calculation model for 100 kVp was established based on Eq. 5.2 and Eq. 5.3.

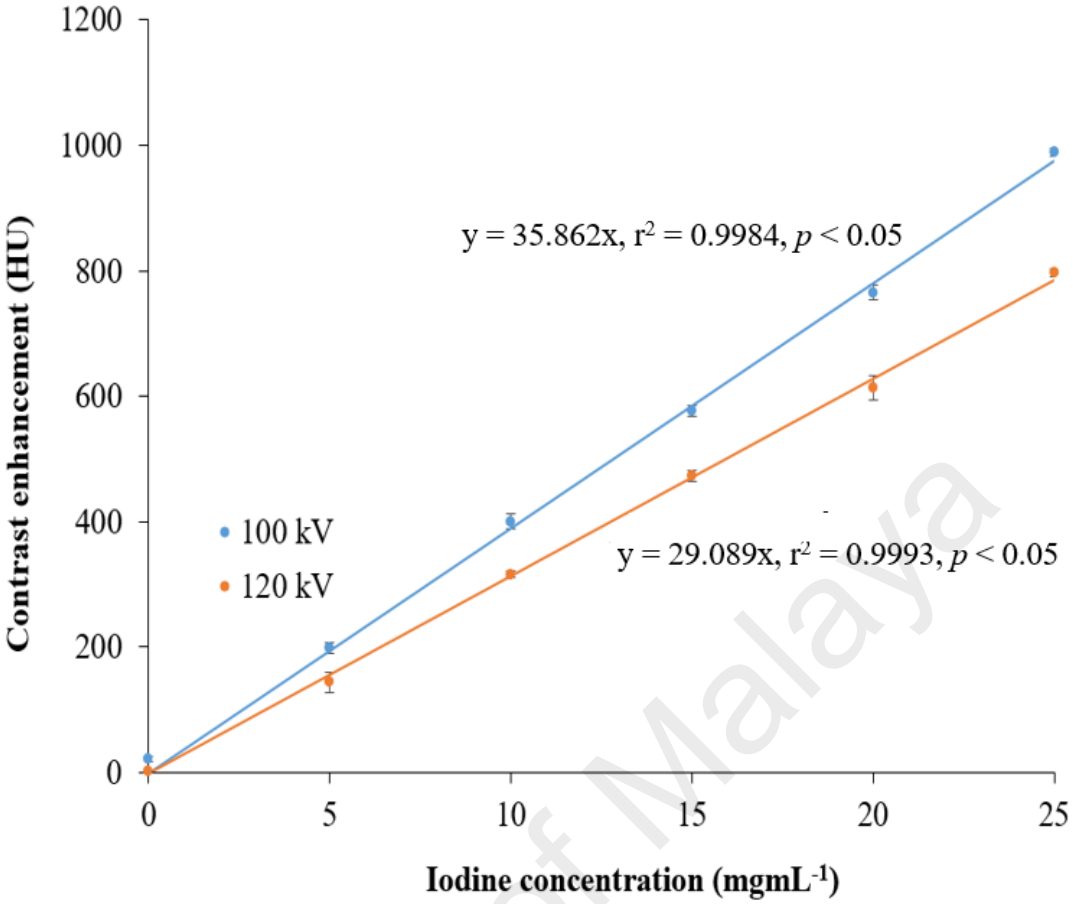

Figure 6.3: Iodine attenuation curves for 100 and 120 kVp.

6.4.2 Validation of personalised contrast volume calculation model

Patient characteristics, test bolus parameters and measured VCE for group 1, 2 and reference are shown in Table 6.1. There were no significant differences ($p > 0.05$) between group 2 and group reference in age, body weight, height, BMI, BSA, heart rate, and TTP at test bolus.

The mean absolute difference between predicted and measured VCE in group 1 was 42.3 HU (-80.7 to 67.8 HU). There was excellent correlation ($r = 0.93$, $p < 0.05$) between predicted and measured VCE (Figure 6.4). Bland-Altman plot was constructed to evaluate the degree of agreement between predicted and measured VCE (Figure 6.5). The 95 % confidence interval limits of agreement ranged from -106.2 to 39.5 HU, with a negative mean difference or bias of 33.3 HU.

Table 6.1: Patient characteristics, scanning and test bolus parameters and measured VCE for group 1, 2 and reference.

Parameters	Group 1	Group 2	Group reference	*p* –value (Group 2 vs. Group reference)
Patient (n)	30	30	30	
Male / female ratio	12 : 18	13 : 17	13 : 17	
Age (years)	58.9 ± 14.9	58.7 ± 15.3	57.6 ± 12.5	0.695
Body weight (kg)	61.5 ± 11.4	64.7 ± 10.6	64.3 ± 8.6	0.745
Height (cm)	159.7 ± 8.9	159.8 ± 8.0	162.2 ± 10.8	0.321
BMI (kgm^{-2})	24.0 ± 3.3	25.3 ± 3.4	24.5 ± 2.8	0.478
BSA (m^2)	1.7 ± 0.2	1.7 ± 0.2	1.7 ± 0.1	0.970
Heart rate (bpm)	65.3 ± 7.6	65.9 ± 7.4	68.7 ± 6.6	0.286
Tube voltage (kVp)	100	100	120	
Reference mAs (mAs)	320	370	320	
PCE at test bolus (HU)	139.5 ± 35.4	113.9 ± 50.6	94.9 ± 31.7	0.044*
TTP at test bolus (s)	16.2 ± 2.4	16.0 ± 3.5	15.0 ± 2.0	0.304
Measured VCE (HU)	633.6 ± 95.9	390.6 ± 36.3	446.4 ± 46.4	0.0001*

* $p < 0.05$ is considered statistically significant different.
BMI, body mass index; BSA, body surface area; mAs, tube current-time product; PCE, peak contrast enhancement; TTP, time-to-peak; VCE, vessel contrast enhancement;
Group 1, validation of personalised contrast volume calculation model;
Group 2, improved retrospectively ECG-triggered CCTA protocol;
Group reference, 120 kVp, reference for comparison with group 2.

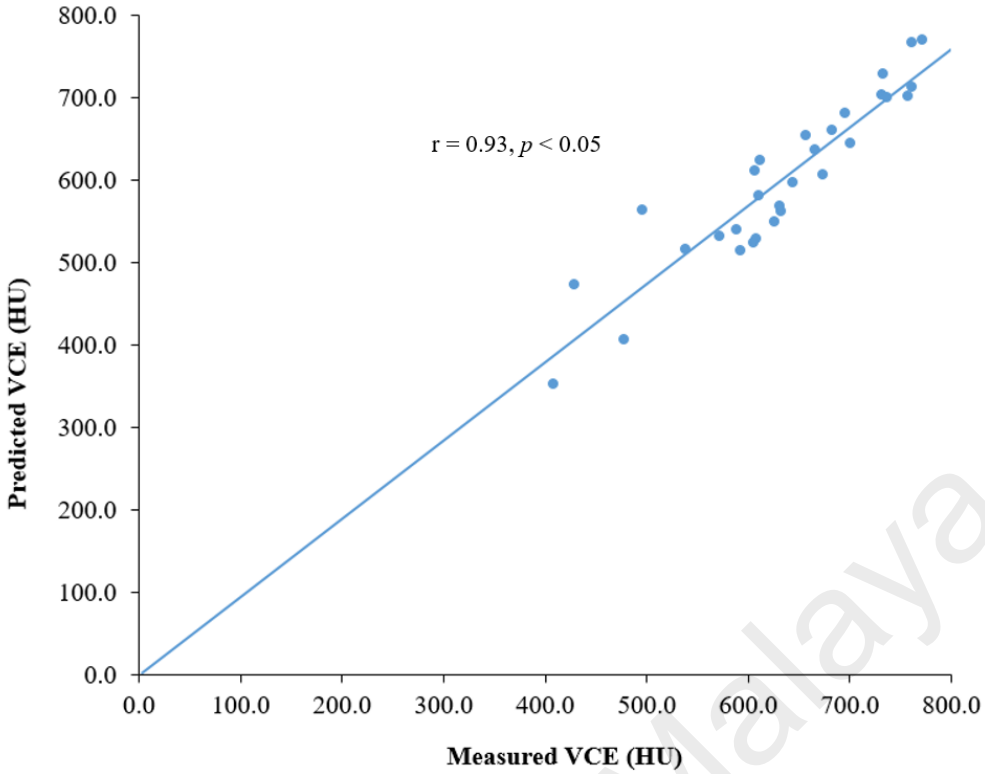

VCE, vessel contrast enhancement

Figure 6.4: Correlation between predicted VCE and measured VCE.

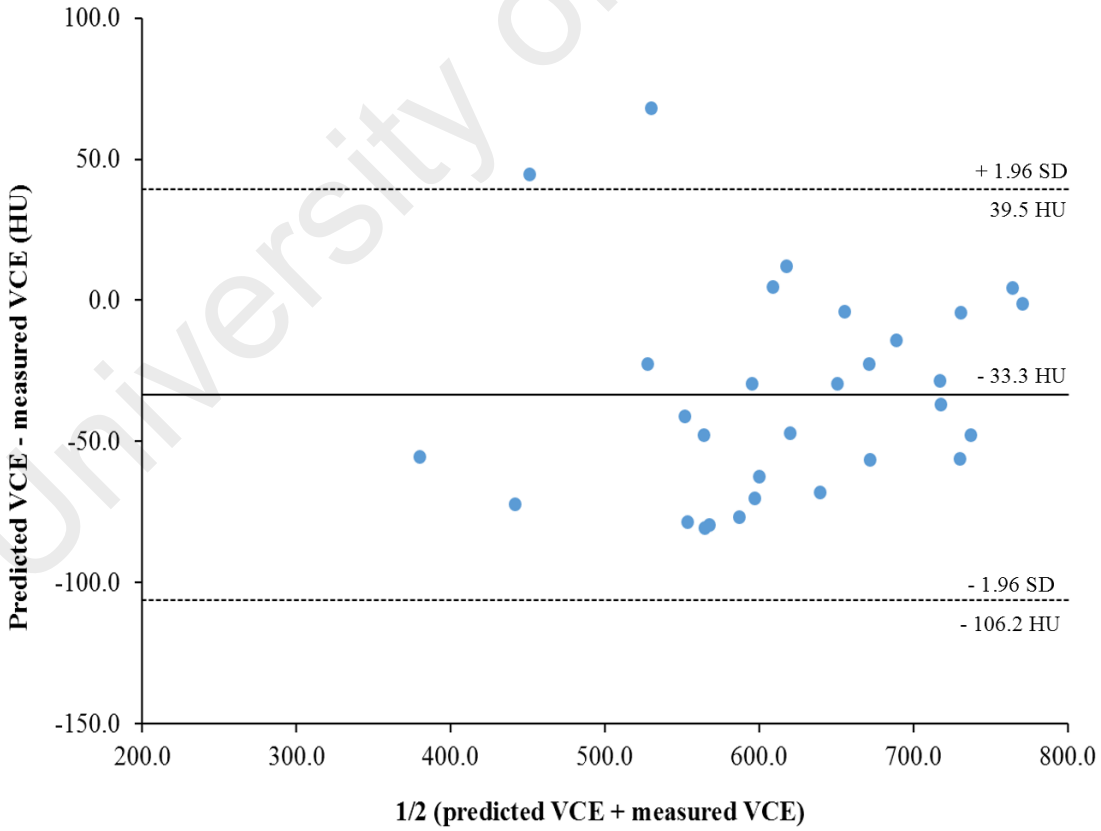

VCE, vessel contrast enhancement

Figure 6.5: Bland-Altman plot comparing the difference between predicted and measured VCE.

6.4.3 Patients imaging with the improved retrospectively ECG-triggered CCTA protocol

All scans for 30 patients were done successfully with mean measured VCE of 390.6 ± 36.3 HU (314.5 to 438.0 HU) (Table 6.1). The measured VCE was significantly lower ($p < 0.05$) in group 2 (390.6 ± 36.3 HU) compared to group reference (446.4 ± 46.4 HU). The mean absolute difference of the measured VCE from 350 HU was 48.2 HU (-35.5 to 88.0 HU). A representative case is shown in Figure 6.6.

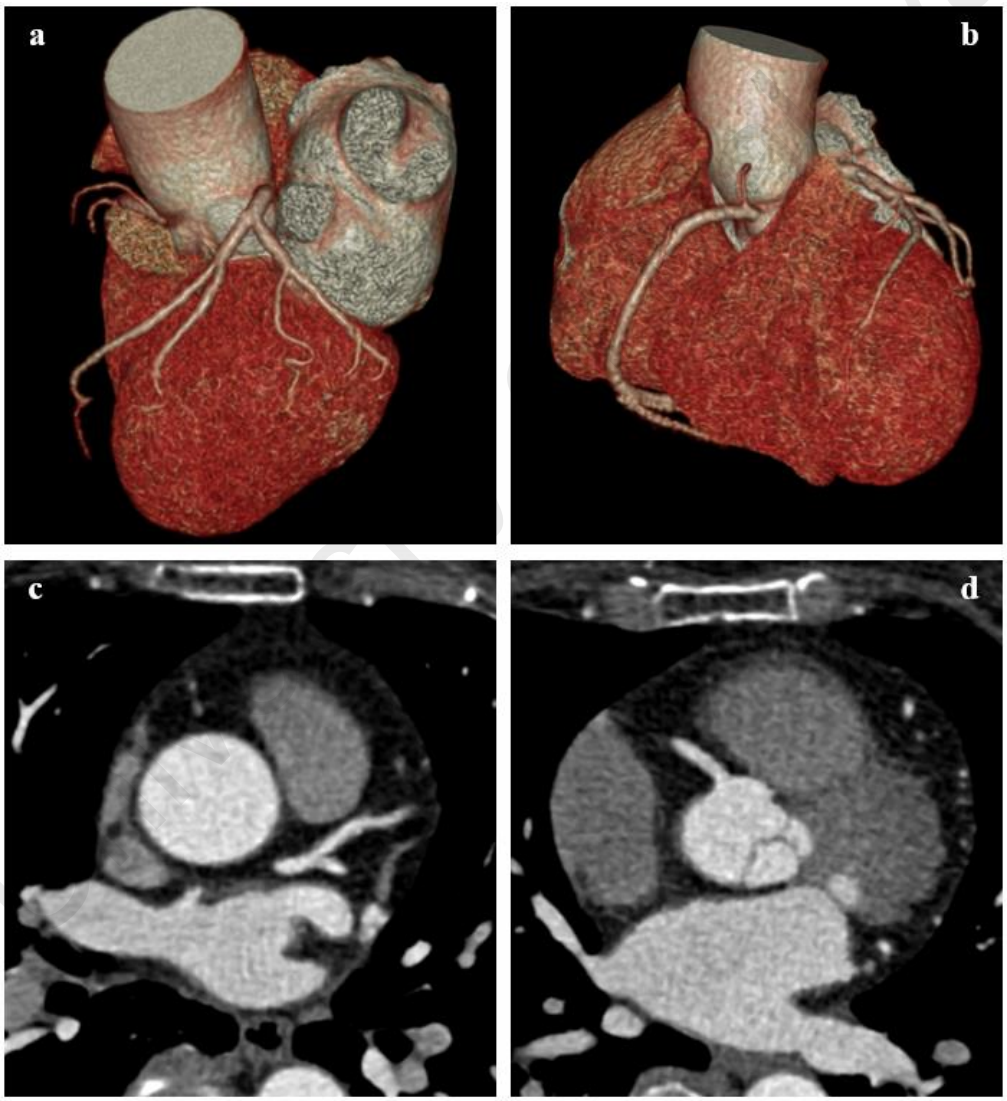

Figure 6.6: A representative case using the improved retrosepectively ECG-triggered CCTA protocol. Volume rendering images showing branches of (a) left coronary artery (LCA), (b) right coronary artery (RCA); axial images showing (c) left main (LM) coronary artery, proximal left anterior desceding (LAD) artery and left circumflex (LCx) artery, (d) proximal RCA.

Table 6.2 shows comparison of radiation dose, contrast volume of first bolus, total contrast volume, TID, quantitative and qualitative image quality analysis for group 2 and group reference. $CTDI_{vol}$, air-kerma length product (P_{KL}) and H_E values were significantly lower ($p < 0.05$) in group 2 compared to group reference. By using the improved retrospectively ECG-triggered CCTA protocol, the radiation dose was reduced by 33.8 %.

Table 6.2: Comparison of radiation dose, contrast volume of first bolus, total contrast volume, TID, quantitative and qualitative image quality analysis between group 2 and reference.

Parameters	**Group 2**	**Group reference**	***p* –value**
$CTDI_{vol}$ (mGy)	22.6 ± 3.3	37.2 ± 8.1	0.0001*
P_{KL} (mGy.cm)	349.2 ± 46.7	531.2 ± 123.2	0.0001*
H_E (mSv)	4.9 ± 0.6	7.4 ± 1.7	0.0001*
Contrast volume of first bolus (mL)	32.7 ± 7.4	51.3 ± 2.2	0.0001*
Total contrast volume (mL)	52.7 ± 7.4	71.3 ± 2.2	0.0001*
TID (g)	19.5 ± 2.7	26.4 ± 0.9	0.0001*
Quantitative image quality analysis			
Image noise (HU)	25.9 ± 5.0	24.4 ± 3.6	0.151
VCE (HU)			
AA	408.4 ± 58.4	424.0 ± 42.0	0.455
RCA	382.5 ± 46.5	461.3 ± 58.7	0.0001*
LM	395.0 ± 35.6	456.4 ± 45.5	0.0001*
LAD	396.4 ± 40.5	439.4 ± 53.4	0.003*
LCx	387.5 ± 36.2	438.8 ± 44.5	0.0001*
SNR			
AA	16.3 ± 3.7	17.8 ± 3.5	0.169
RCA	15.3 ± 11.2	19.3 ± 4.0	0.0001*
LM	15.9 ± 3.4	19.1 ± 3.5	0.001*
LAD	15.8 ± 3.1	18.4 ± 3.6	0.008*
LCx	15.5 ± 3.4	18.4 ± 3.7	0.002*
CNR			
AA	13.2 ± 3.4	15.0 ± 3.2	0.044*
RCA	12.2 ± 3.1	16.6 ± 3.7	0.0001*
LM	12.7 ± 3.0	16.3 ± 3.1	0.0001*

'Table 6.2, continued'

Parameters	Group 2	Group reference	*p* –value
LAD	12.7 ± 2.8	15.6 ± 3.3	0.001*
LCx	12.4 ± 3.0	15.6 ± 3.4	0.0001*
FOM (mSv-1)			
AA	38.9 ± 21.0	32.7 ± 14.2	0.258
RCA	33.1 ± 19.8	40.8 ± 19.7	0.081
LM	35.7 ± 17.1	38.3 ± 15.2	0.460
LAD	35.2 ± 16.8	35.3 ± 14.9	0.679
LCx	34.0 ± 16.6	35.3 ± 15.1	0.647
Qualitative image quality analysis			
VCE	4.7 (3.8 – 5.0)	4.9 (4.5 – 5.0)	0.0001*

* $p < 0.05$ is considered statistically significant different.
$CTDI_{vol}$, CTDI volume; H_E, effective dose; P_{KL}, air-kerma length product;
AA, ascending aorta; LAD, left anterior descending artery; LCx, left circumflex artery;
LM, left main coronary artery; RCA, right coronary artery;
CNR, contrast-to-noise ratio; FOM, figure of merit; SNR, signal-to-noise ratio;
TID, total iodine dose; VCE, vessel contrast enhancement;
Group 2, improved retrospectively ECG-triggered CCTA protocol;
Group reference, reference group (120 kVp) for comparison with group 2.

For group 2, the contrast volume of first bolus, total contrast volume and TID were 32.7 ± 7.4 mL (20.0 to 48.0 mL), 52.7± 7.4 mL (40 to 68 mL) and 19.5 ± 2.7 g (14.8 to 25.2 g). Compared to the TID for group reference (26.4 ± 0.9 g) which applied 120 kVp and the routine contrast protocol, a significant reduction of TID ($p < 0.05$) was achieved in the improved retrospectively ECG-triggered CCTA protocol.

For quantitative image quality analysis, comparable image noise and FOM were observed in group 2 and group reference. The VCE (RCA, LM, LAD and LCx), SNR (RCA, LM, LAD and LCx) and CNR in group 2 were significantly lower ($p < 0.05$) compared to group reference. Image quality was considered sufficient for diagnosis by the observers in all examination in group 2 and reference. The VCE was graded as acceptable to excellent in group 2 (4.7, ranged from 3.8 to 5.0) and good to excellent in group reference (4.9, ranged from 4.5 to 5.0) with significantly lower VCE ($p < 0.05$) in

group 2 compared to group reference. The Wilcoxon signed-rank test demonstrated no significant interobserver variabilities ($p > 0.05$) in VCE scores made by the two observers for both groups.

The mean injection duration of first bolus, scan delay and estimated scan time were 5.5 ± 1.2 s (3.3 to 8.0 s), 17.8 ± 2.8 s (14.0 to 24.0 s), 9.8 ± 1.9 s (7.1 to 16.0 s). The calculated ratio for injection duration of first bolus to the total scan time ranged from 0.10 to 0.33. To prevent any suboptimal VCE in patient with prolonged scan time or scan delay, a ratio of ≥ 0.10 was proposed as a threshold value for the improved retrospectively ECG-triggered CCTA protocol developed in this study. Scan with a ratio of < 0.10 would not be expected to conform to the model developed.

6.5 Discussion

It has been reported that CCTA with lower tube voltage reduces radiation dose; however, it also drastically increases the VCE. High VCE of 500 HU has been reported to be associated with the underestimation of coronary stenosis in a phantom study conducted by Fei et al. (2008). The authors further suggested an optimal VCE target of 350 HU for CCTA. VCE was also reported to have significant impact on the density of non-calcified plaque (Dalager et al., 2011; Horiguchi et al., 2007). In a phantom study conducted by Horiguchi et al. (2007), VCE of 350 and 450 HU were reported to cause overestimation in non-calcified plaque (40 HU). The most precise measurements were reported with VCE of 250 HU. Based on the guidelines established by SCCT in 2009, VCE of more than 250 HU was recommended as optimal VCE for CCTA image , however, no upper limit of VCE was mentioned (Abbara et al., 2016; Abbara et al., 2009). Previous studies have shown that higher VCE facilitates reliable visualization of the coronary arteries (Cademartiri, Mollet, et al., 2006; Roos et al., 2004). VCE ranging from 326 to 540 HU was reported to give a significant higher sensitivity (96 %) and positive

prediction value (92 %) compared to VCE ranging from 182 to 325 HU (Cademartiri et al., 2008). Although there is no consensus on the upper limit of VCE to date, by considering the detection of coronary stenosis, quantitative analysis of atherosclerotic plaque and diagnostic performance of CCTA, an optimal range of VCE of more than 250 and less than 450 HU was used in this study.

From the iodine attenuation curves, an increase of contrast enhancement by 19.6 % at 100 kVp compared to 120 kVp was observed. This finding is comparable to the findings in a study conducted by Higashigaito et al. (2016). By applying the E_C of 0.81, (350 HU × 0.81) ~ 280 HU was used as the targeted VCE in the personalised contrast volume calculation model, to produce VCE of 350 HU at 100 kVp.

During the validation of the model developed, good correlation (r = 0.93) between predicted and measured VCE was observed in group 1, indicating that the personalised contrast volume calculation model can reliably be used to predict VCE with a given contrast volume. By using the measured VCE as reference, the personalised contrast volume calculation model tends to under-predict the VCE by 33.3 HU. The combination of low tube voltage (100 kVp) and the routine contrast protocol in group 1 has resulted in a mean VCE of 633.6 ± 95.9 HU (ranged from 407.9 to 771.5 HU). This VCE has exceeded the optimal range of more than 250 and less than 450 HU. Similarly, the VCE was considered high in group reference, which also applied the combination of 120 kVp and routine contrast protocol (mean VCE of 446.4 ± 46.4 HU, ranged from 357.9 to 553.0 HU). When applying the improved protocol with a combination of low tube voltage (100 kVp) and personalised contrast protocol in group 3, the VCE was reduced to 390.6 ± 36.3 HU (ranged from 314.5 to 438.0 HU). This VCE was within the optimal range, although it was significantly lower compared to group reference.

The radiation dose was found to be lowered by 33.8 % in the improved protocol. This finding was consistent with the findings from the other studies, where the H_E was lower in 100 kVp compared to 120 kVp at a range of between 30 to 53 % (Zhang, C. et al., 2015; Khan et al., 2014; Zhang et al., 2011; Alkadhi et al., 2008).

When compared to the previous studies, a higher TID reduction (43.9 %) was achieved using the improved protocol developed in this study. TID reduction of 14.9 to 27.3 % was reported in several studies that focused on reducing TID at 100 kVp and maintain similar VCE as 120 kVp. IDR of 1.08 to 1.70 gs^{-1} was used in these studies that resulted in TID of 18.9 to 20.9 g at 100 kVp (Pan et al., 2016; Shen et al., 2015; Yin et al., 2015; Zhang et al., 2011). Unlike the previous studies, a higher IDR of 2.22 gs^{-1} was applied in this study, achieved with an injection rate of 6 mLs^{-1} and contrast concentration of 370 $mgmL^{-1}$. As the PCE is proportionally increased with the IDR, a higher IDR results in a greater TID reduction (Weininger et al., 2011; Bae, 2010).

As the image noise increases at lower tube voltage, a higher reference mAs (370 mAs) was used in the improved protocol. Although less reduction in radiation dose was achieved (33.8 %) compared to the protocol utilising a reference mAs of 320 mAs (37.8 %) in Chapter 4, it has successfully produced similar image noise compared to routine protocol. The comparable FOM in group 2 and group reference indicates that the dose efficiency of the improved protocol was similar to the routine protocol. Despite lower VCE, SNR and CNR, the image quality for all examinations performed with the improved protocol were rated as sufficient for diagnosis by the observers.

This study has several limitations. Firstly, the maximum absolute difference between the predicted and measured VCE (80.7 HU) in group 1 and the maximum absolute difference between measured and target VCE in group 2 (88.0 HU) was considered large. This is due to the limitation of the model developed, which has been explained in Chapter

5. Secondly, since the model developed in this study does not consider the CT-related factors, such as the scan time and scan delay, there is a risk of suboptimal VCE in patients with prolonged scan time or scan delay. By referring to the calculated injection duration to total scan time ratio in every patient, a value of ≥ 0.10 was proposed to be used as a threshold. For any scan that has a ratio of < 0.10, the personalised contrast protocol is not recommended, as the model developed is not expected to be conformable. Thirdly, this study did not evaluate the diagnostic accuracy of the improved protocol in the detection of coronary stenosis as not all patients underwent ICA for comparison of stenosis. Since there were changes in tube voltage and contrast protocol, the diagnostic accuracy may be affected. Finally, the comparison of radiation dose, TID and image quality was performed in two different groups of patients, rather than scanning the same patients with two different protocols. The effect of having two different groups for comparison was minimised by matching features (BMI) that could affect the evaluated parameters. The repeat irradiation of a single group of patients with no added clinical benefit was decided to be unethical during methodology development.

6.6 Conclusion

An improved retrospectively ECG-triggered CCTA protocol with combination of low tube voltage (100 kVp) and personalised contrast protocol was developed and validated. This protocol has achieved optimal VCE and image quality with reduction of 33.8 % in radiation dose and 43.9 % in TID, compared to 120 kVp retrospectively ECG-triggered CCTA with routine contrast protocol.

CHAPTER 7: OVERALL CONCLUSION

7.1 Thesis conclusion

In this thesis, a number of studies were conducted to assess the radiation dose and the risk of radiation-induced cancer associated with different prospectively ECG-triggered CCTA protocols, and to optimise the radiation dose, image quality and contrast medium administration in retrospectively ECG-triggered CCTA protocol. This chapter summarises the findings of this thesis and the conclusion drawn. This chapter also discusses possible future works stemming from this work.

7.1.1 Assessment of radiation dose and estimation of lifetime attributable risk (LAR) of cancer incidence associated with prospectively ECG-triggered CCTA protocols

Despite the fact that several clinical studies have reported substantial radiation dose reduction in prospectively ECG-triggered (44 to 83 %) compared to retrospectively ECG-triggered CCTA protocol, however, there has been no study conducted to compare the radiation dose among the different prospectively ECG-triggered CCTA protocols to the best of our knowledge (Lehmkuhl et al., 2010; Gopal et al., 2009; Klass et al., 2009; Shuman et al., 2008). Furthermore, in most of the studies, assessment of radiation dose was mainly relying on the P_{KL} reported at the CT console. The H_E was calculated by multiplying the P_{KL} with an E_{KL} for chest region. This calculated H_E has been reported to underestimate the amount of patient exposure that actually incurred (Hurwitz et al., 2007; Groves et al., 2004). Furthermore, there is limited studies focusing on the assessment of individualised absorbed doses to the major irradiated organs during prospectively ECG-triggered CCTA protocols as well as the risk of radiation-induced cancer associated with CCTA.

The study described in Chapter 3 assessed the radiation dose received from prospectively ECG-triggered CCTA using different generations of CT scanners through direct measurement of organ doses in a standard female adult anthropomorphic phantom and compared the estimated LAR of breast and lung cancer incidence for sex and age.

It was observed that, if excluding skin, breasts received the highest radiation dose, followed by lungs, oesophagus, liver, stomach, sternum and heart. Although the heart is the organ of interest in CCTA imaging, the highest radiation dose was received by breasts (5 to 8 times higher than heart) and lungs (4 to 7 times higher than heart) as they are more radiosensitive to ionising radiation. In the comparison of H_E estimated from the measured organ dose (measured H_E) versus H_E calculated by multiplying the P_{KL} with an E_{KL} for chest region (computed H_E), the mean difference observed from this study was ranged between 38.3 and 53.2 %. Among the prospectively ECG-triggered CCTA protocols in different generations of CT scanners, the highest H_E was received from 2 × 32-detector-row DSCT scanner (6.06 ± 0.72 mSv), followed by 64-detector-row SSCT (5.60 ± 0.68 and 5.02 ± 0.73 mSv), 2 × 64-detector-row DSCT (1.88 ± 0.25 mSv) and 320-detector-row SSCT (1.34 ± 0.48 mSv) scanners. Although the H_E varied from 1.34 ± 0.48 to 6.06 ± 0.72 mSv among different generations of CT scanners and imaging protocols, the radiation doses were relatively low compared to other CT examinations, such as CT for chest (11.0 mSv), abdomen (17.0 mSv) and chest and abdomen (17.0 mSv) (Smith-Bindman et al., 2015).

The estimated risks for radiation-induced cancer after a prospectively ECG-triggered CCTA examination are relatively low for all the scanners and protocols. For female patients, the estimated LAR ranged from less than 0.02 to 66 cases per 100,000 population for breast cancer, 2 to 47 cases per 100,000 population for lung cancer, 2 to 113 cases per 100,000 population for either breast or lung cancer, and less than 0.5 to 28 cases per

100,000 population for other cancers. For male patients, the estimated LAR ranged from 1 to 20 cases per 100,000 population for lung cancer. For young women who are less than 30 years old, the LAR for breast cancer is higher than lung cancer. However, after 30 years old, the LAR for lung cancer is higher. The LAR_{joint}, RR_{joint} and ERR_{joint} for breast or lung cancer incidence are higher compared to the individual cancer in younger women. Between sexes, male patients has significant lower LAR for lung cancer than female patients. Using the latest CT scanner models and imaging protocols, i.e. 320-detector-row SSCT and 2 × 64-detector-row DSCT, the LAR for lung and breast cancers can be reduced markedly by up to 80 to 97 %.

The radiation doses and LAR for cancer incidence from a prospectively ECG-triggered CCTA are generally low and depend on the scanner model and imaging protocol. Although the heart is the organ of interest in CCTA imaging, breasts and lungs received the highest radiation dose as they are more radiosensitive to ionising radiation. The use of CCTA especially in younger women should be considered carefully in conjunction with clinical indications, benefits versus risks and alternative imaging modalities.

7.1.2 Development of low tube voltage retrospectively ECG-triggered CCTA protocol and assessment of radiation dose and image quality

Although prospectively ECG-triggered CCTA has been recommended as the first line default technique for CCTA examination which should be used whenever possible and practical (Raff et al., 2014). There are few limitations when applying this technique. Firstly, it requires a regular and low heart rate (less than 70 bpm), which may not be achievable in all patients; Secondly, it is usually restricted to non-overlapping scanning or slice increments with a small overlap, thus there is a high demand in the z-axis coverage of CT scanner for implementing this protocol; Thirdly, the functional

information about cardiac valve or ventricular wall is not available as the cardiac images are acquired during a small portion of the R-R interval (Sun, 2012b; Husmann et al., 2008; Stolzmann et al., 2008). To overcome these limitations, another dose-reducing strategy that could be considered is the retrospectively ECG-triggered protocol with low tube voltage. Low tube voltage (100 kVp) CCTA protocol has been reported to significantly reduce radiation exposure and contrast medium administration. In Chapter 4, the development of a low tube voltage (100 kVp) retrospectively ECG-triggered CCTA protocol formed by the combination of patient selection and automatic tube current modulation was described, together with the assessment of achievable radiation dose reduction and image quality.

A low tube voltage (100 kVp) retrospectively ECG-triggered CCTA protocol was developed with the combination of patient selection based on BMI of less than 30 kgm^{-2} and automatic tube current modulation with reference mAs of 320 mAs. The radiation dose was found to be lowered by 37.8 % in the low tube voltage protocol compared to the routine 120 kVp protocol. Furthermore, significant increase of image noise (38.5 %) was observed in the low tube voltage protocol. Nevertheless, the increase of VCE at lower tube voltage, due to the increase of photoelectric effect compensated the SNR and CNR (Nakaura, Kidoh, Sakaino, Nakamura, et al., 2013). Therefore, there were no significant differences observed in SNR and CNR between the low tube voltage and routine protocols. The FOM was improved (70.5 to 81.7 %) in the low tube voltage protocol developed in this study, as there was a significant reduction of radiation dose with constant CNR.

Using a patient selection criteria based on BMI less than 30 kgm^{-2} and automatic tube current modulation, a significant reduction of radiation dose by 37. 8 % was achieved without degrading the image quality.

7.1.3 Optimisation of contrast medium administration in 120 kVp retrospectively ECG-triggered CCTA protocol: A personalised contrast volume calculation model

Many studies have been conducted to optimise the contrast medium administration in CCTA, mainly focusing on achieving TID reduction and VCE of more than 250 HU, limited studies have considered the upper limit of VCE. Generally, the optimised contrast protocols presented in these studies are based on the adaptation of iodine dose to patient characteristics and scanning parameters, for instance, the adaptation to body weight, BMI, BSA, scan time and injection rate (Yin et al., 2015; Bae et al., 2008; Heiken et al., 1995). Taking into consideration of the detection of coronary stenosis, quantitative analysis of atherosclerotic plaque and diagnostic performance of CCTA, the optimal range of VCE could fall between more than 250 and less than 450 HU (Abbara et al., 2016; Komatsu et al., 2013; Abbara et al., 2009; Cademartiri et al., 2008; Fei et al., 2008; Horiguchi et al., 2007).

Nonetheless, to achieve VCE within the optimal range in every patient, it is important to also take into account the patient's cardiovascular and contrast pharmacokinetic response, information which can be obtained from the time-attenuation curve of test bolus (Komatsu et al., 2013; Yang et al., 2013). Test bolus parameters such as TTP and PCE are closely associated with the patient's circulation during CCTA scanning. PCE and TTP at test bolus scan have been reported as predictable parameters for VCE in previous studies (Zhu et al., 2015; Yang et al., 2013; Mahnken et al., 2007; van Hoe et al., 1995). A personalised contrast volume calculation model developed based on a combination of patient characteristics and test bolus parameters is expected to allow a better contrast volume estimation for achieving VCE within the optimal range and further reduce the TID (Komatsu et al., 2013; Yang et al., 2013). Limited studies have been conducted to develop personalised contrast volume calculation model based on these parameters. In

Chapter 5, a personalised contrast volume calculation model for 120 kVp retrospectively ECG-triggered CCTA protocol, based on the combination of patient characteristics and test bolus parameters was developed and validated clinically.

A strong linear relationship was found between VCE and contrast volume ($r = 0.97$, $p < 0.05$). From the result of multiple linear regression analysis between VCE, patient characteristics and test bolus parameters, age, sex, BSA and PCE of test bolus were found to be significant predictors for VCE ($p < 0.05$), with BSA as the best predictor. A personalised contrast volume calculation model was then developed by applying these factors. The model was used for prediction of VCE for a given contrast volume and calculation the contrast volume for a targeted VCE. In the validation process, there was excellent correlation ($r = 0.82$) between predicted and measured VCE, indicating that the model developed can reliably be used to predict VCE with a given contrast volume. By using the measured VCE as reference, the personalised contrast volume calculation model tends to under-predict the VCE by 27.2 HU.

When applying the model developed in a personalised contrast protocol for imaging of patients, the VCE measured from the acquired images (298.3 to 435.4 HU) were within the optimal range of VCE (more than 250 HU and less than 450 HU). A significant reduction of TID by 9.8 % was achieved with the personalised contrast protocol compared to the routine contrast protocol. Furthermore, the VCE were graded as acceptable to excellent by the observers. A ratio of injection duration of first bolus to total scan time ratio of ≥ 0.21 was proposed to be used as a threshold in the personalised contrast protocol, to prevent suboptimal VCE in patients with prolonged scan time or delay.

The personalised contrast protocol based on the model developed allows optimal VCE and image quality at 120 kVp retrospectively ECG-triggered CCTA and TID reduction of 9.8 % compared to the routine contrast protocol.

7.1.4 Optimisation of radiation dose, image quality and contrast medium administration in CCTA: An improved retrospectively ECG-triggered CCTA protocol

It has been reported that CCTA with lower tube voltage reduces radiation dose; however, it also drastically increases the VCE. Many studies have focused on reducing radiation dose and TID at low tube voltage CCTA protocol while maintaining VCE above 250 HU. Limited studies have considered the upper limit of VCE. Optimal VCE is crucial in CCTA, especially quantitative analysis of atherosclerotic plaque (Dalager et al., 2011). Based on the literature, the optimal range of VCE could fall between more than 250 and less than 450 HU (Abbara et al., 2016; Komatsu et al., 2013; Abbara et al., 2009; Cademartiri et al., 2008; Fei et al., 2008; Horiguchi et al., 2007). A personalised contrast volume calculation model which incorporates patient characteristics and test bolus parameters is superior compared to body weight-adapted iodine dose or a fixed contrast volume protocol, as it allows better contrast volume estimation for achieving VCE within the optimal range and further reduce the TID at lower tube voltage (Komatsu et al., 2013; Yang et al., 2013). In Chapter 6, an improved retrospectively ECG-triggered CCTA protocol, formed by the combination of low tube voltage (100 kVp) and a personalised contrast protocol was developed and clinically validated.

An increase of contrast enhancement by 19.6 % at 100 kVp compared to 120 kVp was observed, an E_c of 0.81 was used in the model developed in Chapter 5 to establish a personalised contrast volume calculation model for 100 kVp. During the validation of model developed, good correlation ($r = 0.93$) between predicted and measured VCE was observed, indicating that the model developed can reliably be used to predict VCE with a given contrast volume. An improved retrospectively ECG-triggered CCTA protocol, formed by the combination of low tube voltage (100 kVp) and a personalised contrast protocol (based on the model developed) was then applied in the imaging of patients. The

VCE measured in the images acquired using the improved protocol (314.5 to 438.0 HU) was within the optimal range of VCE (more than 250 HU and less than 450 HU). This improved protocol has also resulted in lower radiation dose (33. 8 %) and TID (43.9 %) compared to the routine protocol. Similar image noise was observed in the improved protocol compared to the routine protocol and the comparable FOM indicates that the dose efficiency of the improved protocol was similar to the routine protocol. Despite lower VCE, SNR and CNR, the image quality for all examinations performed with the improved protocol were rated as sufficient for diagnosis by the observers. A ratio of injection duration of first bolus to total scan time of ≥ 0.10 was then proposed to be used as a threshold for the improved protocol, to prevent suboptimal VCE in patients with prolonged scan time or delay.

The improved protocol developed in this study has achieved optimal VCE and image quality with reduction of 33.8 % in radiation dose and 43.9 % in TID, compared to 120 kVp retrospectively ECG-triggered CCTA with routine contrast protocol.

7.2 Research contributions

The research has contributed to the optimisation of the radiation dose, image quality and contrast medium administration in CCTA in the following ways:

i. The radiation doses and LAR for cancer incidence reported from prospectively ECG-triggered CCTA examination using five different generations of CT scanners provide medical practitioners with data that can be used to assess risk versus benefit of CCTA examination in patients.

ii. A personalised contrast volume calculation model focused on achieving VCE within the optimal range and reduction in TID was developed and clinically validated for 120 kVp retrospectively ECG-triggered CCTA protocol.

Currently, this developed model has been routinely used for the calculation of contrast volume for CCTA in University Malaya Medical Centre.

iii. An improved retrospectively ECG-triggered CCTA protocol, formed by a combination of low tube voltage (100 kVp) and a personalised contrast protocol was developed and clinically validated. This protocol allows optimal VCE and image quality to be achieved, together with substantial reduction in radiation dose and TID. Currently, this improved protocol has been applied as routine protocol for CCTA in University Malaya Medical Centre.

7.3 Future work

Currently, iterative reconstruction has been implemented clinically as an effective technique for reducing radiation dose, image noise and artefacts in CCTA (Benz et al., 2018; Halliburton et al., 2017; Padole et al., 2015; Nelson et al., 2011). This research has not evaluated the radiation dose reduction and image quality in the prospectively and low tube voltage (100 kVp) retrospectively ECG-triggered CCTA protocols with iterative reconstruction. By incorporate iterative reconstruction into these protocols, further radiation dose reduction and image quality improvement are expected. With iterative reconstruction, it is also possible to further lower the tube voltage for CCTA to 80 kVp. Therefore, future research on assessing the radiation dose and image quality of these protocols with iterative reconstruction, compared to the existing filtered back projection reconstruction will be carried out.

In this research, the reproducibility of the personalised contrast volume calculation model in achieving the targeted VCE were not evaluated. Furthermore, the model was based on only one IDR (2.22 gs^{-1}) and validated with only one model of CT scanner (Siemens definition DS, Siemens Healthcare). Future work should be carried out to (1)

evaluate the reproducibility of the model, (2) test of different IDR, and (3) validate the model developed with different models of CT scanners, to make it more robust.

REFERENCES

AAPM Task Group 23. (2008). *AAPM report no. 96, the measurement, reporting, and management of radiation dose in CT*. Retrieved from https://www.aapm.org/pubs/reports/RPT_96.pdf

Abada, H. T., Larchez, C., Daoud, B., Sigal-Cinqualbre, A., & Paul, J.-F. (2006). MDCT of the Coronary Arteries: Feasibility of Low-Dose CT with ECG-Pulsed Tube Current Modulation to Reduce Radiation Dose. *AJR Am J Roentgenol, 186*(6_supplement_2), S387-S390.

Abbara, S., Arbab-Zadeh, A., Callister, T. Q., Desai, M. Y., Mamuya, W., Thomson, L., & Weigold, W. G. (2009). SCCT guidelines for performance of coronary computed tomographic angiography: a report of the Society of Cardiovascular Computed Tomography Guidelines Committee. *J Cardiovasc Comput Tomogr, 3*(3), 190-204.

Abbara, S., Blanke, P., Maroules, C. D., Cheezum, M., Choi, A. D., Han, B. K., . . . Leipsic, J. (2016). SCCT guidelines for the performance and acquisition of coronary computed tomographic angiography: A report of the society of Cardiovascular Computed Tomography Guidelines Committee: Endorsed by the North American Society for Cardiovascular Imaging (NASCI). *J Cardiovasc Comput Tomogr, 10*(6), 435-449.

Achenbach, S., Marwan, M., Ropers, D., Schepis, T., Pflederer, T., Anders, K., . . . Lell, M. M. (2010). Coronary computed tomography angiography with a consistent dose below 1 mSv using prospectively electrocardiogram-triggered high-pitch spiral acquisition. *Eur Heart J, 31*(3), 340-346.

Achenbach, S., Ropers, D., Holle, J., Muschiol, G., Daniel, W. G., & Moshage, W. (2000). In-plane coronary arterial motion velocity: measurement with electron-beam CT. *Radiology, 216*(2), 457-463.

Alkadhi, H. (2009). Radiation dose of cardiac CT-what is the evidence? *Eur Radiol, 19*(6), 1311-1315.

Alkadhi, H., Stolzmann, P., Desbiolles, L., Baumueller, S., Goetti, R., Plass, A., . . . Leschka, S. (2010). Low-dose, 128-slice, dual-source CT coronary angiography: accuracy and radiation dose of the high-pitch and the step-and-shoot mode. *Heart, 96*(12), 933-938.

Alkadhi, H., Stolzmann, P., Scheffel, H., Desbiolles, L., Baumuller, S., Plass, A., . . . Leschka, S. (2008). Radiation dose of cardiac dual-source CT: the effect of tailoring the protocol to patient-specific parameters. *Eur J Radiol, 68*(3), 385-391.

Amato, E., Lizio, D., Settineri, N., Di Pasquale, A., Salamone, I., & Pandolfo, I. (2010). A method to evaluate the dose increase in CT with iodinated contrast medium. *Med Phys, 37*(8), 4249-4256.

Amato, E., Salamone, I., Naso, S., Bottari, A., Gaeta, M., & Blandino, A. (2013). Can contrast media increase organ doses in CT examinations? A clinical study. *AJR Am J Roentgenol, 200*(6), 1288-1293.

Andreini, D., Mushtaq, S., Conte, E., Segurini, C., Guglielmo, M., Petulla, M., . . . Pepi, M. (2016). Coronary CT angiography with 80 kV tube voltage and low iodine concentration contrast agent in patients with low body weight. *J Cardiovasc Comput Tomogr, 10*(4), 322-326.

Applegate, E. J. (Ed.) (2010). *The Sectional Anatomy Leaning System : Concepts* (3 ed.). United States: Saunders Elsevier.

Arad, Y., Goodman, K. J., Roth, M., Newstein, D., & Guerci, A. D. (2005). Coronary calcification, coronary disease risk factors, C-reactive protein, and atherosclerotic cardiovascular disease events: the St. Francis Heart Study. *J Am Coll Cardiol, 46*(1), 158-165.

Armstrong, I., Trevor, M., & Widdowfield, M. (2016). Maintaining image quality and reducing dose in prospectively-triggered CT coronary angiography: A systematic review of the use of iterative reconstruction. *Radiography, 22*(1), 84-92.

Aschoff, A. J., Catalano, C., & Kirchin, M. A. (2017). Low radiation dose in computed tomography: the role of iodine. *Br J Radiol, 90*(1076), 20170079.

Awai, K., & Hori, S. (2003). Effect of contrast injection protocol with dose tailored to patient weight and fixed injection duration on aortic and hepatic enhancement at multidetector-row helical CT. *Eur Radiol, 13*(9), 2155-2160.

Bae, K. T. (2003). Peak Contrast Enhancement in CT and MR Angiography: When Does It Occur and Why? Pharmacokinetic Study in a Porcine Model. *Radiology, 227*(3), 809-816.

Bae, K. T. (2005). Test-bolus versus bolus-tracking techniques for CT angiographic timing. *Radiology, 236*(1), 369-370.

Bae, K. T. (2010). Intravenous contrast medium administration and scan timing at CT: considerations and approaches. *Radiology, 256*(1), 32-61.

Bae, K. T., Heiken, J. P., & Brink, J. A. (1998). Aortic and hepatic contrast medium enhancement at CT. Part I. Prediction with a computer model. *Radiology, 207*(3), 647-655.

Bae, K. T., Seeck, B. A., Hildebolt, C. F., Tao, C., Zhu, F., Kanematsu, M., & Woodard, P. K. (2008). Contrast enhancement in cardiovascular MDCT: effect of body weight, height, body surface area, body mass index, and obesity. *AJR Am J Roentgenol, 190*(3), 777-784.

Bae, K. T., Tao, C., Gurel, S., Hong, C., Zhu, F., Gebke, T. A., . . . Hildebolt, C. F. (2007). Effect of patient weight and scanning duration on contrast enhancement during pulmonary multidetector CT angiography. *Radiology, 242*(2), 582-589.

Bae, K. T., Tran, H. Q., & Heiken, J. P. (2004). Uniform vascular contrast enhancement and reduced contrast medium volume achieved by using exponentially decelerated contrast material injection method. *Radiology, 231*(3), 732-736.

Barrett, B. J., Katzberg, R. W., Thomsen, H. S., Chen, N., Sahani, D., Soulez, G., . . . Nelson, R. (2006). Contrast-induced nephropathy in patients with chronic kidney disease undergoing computed tomography: a double-blind comparison of iodixanol and iopamidol. *Invest Radiol, 41*(11), 815-821.

Benz, D. C., Fuchs, T. A., Grani, C., Studer Bruengger, A. A., Clerc, O. F., Mikulicic, F., . . . Buechel, R. R. (2018). Head-to-head comparison of adaptive statistical and model-based iterative reconstruction algorithms for submillisievert coronary CT angiography. *Eur Heart J Cardiovasc Imaging, 19*(2), 193-198.

Benz, D. C., Grani, C., Hirt Moch, B., Mikulicic, F., Vontobel, J., Fuchs, T. A., . . . Kaufmann, P. A. (2016). Minimized Radiation and Contrast Agent Exposure for Coronary Computed Tomography Angiography: First Clinical Experience on a Latest Generation 256-slice Scanner. *Acad Radiol, 23*(8), 1008-1014.

Birnbaum, B. A., Jacobs, J. E., Langlotz, C. P., & Ramchandani, P. (1999). Assessment of a bolus-tracking technique in helical renal CT to optimize nephrographic phase imaging. *Radiology, 211*(1), 87-94.

Bischoff, B., Hein, F., Meyer, T., Hadamitzky, M., Martinoff, S., Schömig, A., & Hausleiter, J. (2009). Impact of a Reduced Tube Voltage on CT Angiography and Radiation Dose: Results of the PROTECTION I Study. *JACC Cardiovasc Imaging, 2*(8), 940-946.

Blankstein, R., Bolen, M. A., Pale, R., Murphy, M. K., Shah, A. B., Bezerra, H. G., . . . Brady, T. J. (2011). Use of 100 kV versus 120 kV in cardiac dual source computed tomography: effect on radiation dose and image quality. *Int J Cardiovasc Imaging, 27*(4), 579-586.

Boas, F. E., & Fleischmann, D. (2012). CT artifacts: causes and reduction techniques. *Imaging Med, 4*(2), 229-240.

Bongartz, G., Golding, S. J., Jurik, A. G., Leonardi, M., van Persijn van Meerten, E., Rodríguez, R., . . . Tosi, G. (2004). *European guidelines for multislice computed tomography*. *FIGM CT2000-20078-CT-TIP*. Retrieved from http://www.drs.dk/guidelines/ct/quality/htmlindex.htm

Brunette, J., Mongrain, R., Rodes-Cabau, J., Larose, E., Leask, R., & Bertrand, O. F. (2008). Comparative rheology of low- and iso-osmolarity contrast agents at different temperatures. *Catheter Cardiovasc Interv, 71*(1), 78-83.

Budoff, M. J. (2009). Maximizing dose reductions with cardiac CT. *Int J Cardiovasc Imaging, 25*(Suppl 2), 279-287.

Burbank, F. H., Brody, W. R., & Bradley, B. R. (1984). Effect of volume and rate of contrast medium injection on intravenous digital subtraction angiographic contrast medium curves. *J Am Coll Cardiol, 4*(2), 308-315.

Cademartiri, F., de Monye, C., Pugliese, F., Mollet, N. R., Runza, G., van der Lugt, A., . . . Krestin, G. P. (2006). High iodine concentration contrast material for noninvasive multislice computed tomography coronary angiography: iopromide 370 versus iomeprol 400. *Invest Radiol, 41*(3), 349-353.

Cademartiri, F., Luccichenti, G., Gualerzi, M., Brambilla, L., Brambilla, V., & Coruzzi, P. (2005). Intravenous contrast material administration in multislice computed tomography coronary angiography. *Acta Biomed, 76*(2), 86-94.

Cademartiri, F., Maffei, E., Arcadi, T., Catalano, O., & Midiri, M. (2013). CT coronary angiography at an ultra-low radiation dose (<0.1 mSv): feasible and viable in times of constraint on healthcare costs. *Eur Radiol, 23*(3), 607-613.

Cademartiri, F., Maffei, E., Palumbo, A. A., Malago, R., La Grutta, L., Meijboom, W. B., . . . Krestin, G. P. (2008). Influence of intra-coronary enhancement on diagnostic accuracy with 64-slice CT coronary angiography. *Eur Radiol, 18*(3), 576-583.

Cademartiri, F., Mollet, N. R., Lemos, P. A., Saia, F., Midiri, M., de Feyter, P. J., & Krestin, G. P. (2006). Higher intracoronary attenuation improves diagnostic accuracy in MDCT coronary angiography. *AJR Am J Roentgenol, 187*(4), W430-433.

Cademartiri, F., Nieman, K. K., van der Lugt, A., Raaijmakers, R. H., Mollet, N., Pattynama, P. M. T., . . . Krestin, G. P. (2004). Intravenous Contrast Material Administration at 16–Detector Row Helical CT Coronary Angiography: Test Bolus versus Bolus-tracking Technique. *Radiology, 233*(3), 817-823.

Cademartiri, F., Runza, G., Mollet, N. R., Luccichenti, G., Belgrano, M., Bartolotta, T. V., . . . Krestin, G. P. (2005). Impact of intravascular enhancement, heart rate, and calcium score on diagnostic accuracy in multislice computed tomography coronary angiography. *Radiol Med, 110*(1-2), 42-51.

Cademartiri, F., van der Lugt, A., Luccichenti, G., Pavone, P., & Krestin, G. P. (2002). Parameters affecting bolus geometry in CTA: a review. *J Comput Assist Tomogr, 26*(4), 598-607.

Cao, J. X., Wang, Y. M., Lu, J. G., Zhang, Y., Wang, P., & Yang, C. (2014). Radiation and contrast agent doses reductions by using 80-kV tube voltage in coronary computed tomographic angiography: a comparative study. *Eur J Radiol, 83*(2), 309-314.

Cassar, A., Holmes, D. R. J., Rihal, C. S., & Gersh, B. J. (2009). Chronic coronary artery disease: diagnosis and management. *Mayo Clin Proc, 84*(12), 1130-1146.

Chen, M. Y., Shanbhag, S. M., & Arai, A. E. (2013). Submillisievert median radiation dose for coronary angiography with a second-generation 320-detector row CT scanner in 107 consecutive patients. *Radiology, 267*(1), 76-85.

Choi, H. S., Choi, B. W., Choe, K. O., Choi, D., Yoo, K. J., Kim, M. I., & Kim, J. (2004). Pitfalls, artifacts, and remedies in multi- detector row CT coronary angiography. *Radiographics, 24*(3), 787-800.

Chow, B. J., Abraham, A., Wells, G. A., Chen, L., Ruddy, T. D., Yam, Y., . . . Beanlands, R. S. (2009). Diagnostic accuracy and impact of computed tomographic coronary angiography on utilization of invasive coronary angiography. *Circ Cardiovasc Imaging, 2*(1), 16-23.

Christner, J. A., Kofler, J. M., & McCollough, C. H. (2010). Estimating effective dose for CT using dose-length product compared with using organ doses: consequences of adopting International Commission on Radiological Protection publication 103 or dual-energy scanning. *AJR Am J Roentgenol, 194*(4), 881-889.

Committee to assess health risks from exposure to low levels of ionizing radiation, N. R. C. (2006). *Health risks from exposure to low levels of ionizing radiation: BEIR VII phase 2.* Vol. 311.

Cui, Y., Zeng, W., Yu, J., Lu, J., Hu, Y., Diao, N., . . . Shi, H. (2017). Quantification of left coronary bifurcation angles and plaques by coronary computed tomography angiography for prediction of significant coronary stenosis: A preliminary study with dual-source CT. *PLoS One, 12*(3), e0174352.

Dalager, M. G., Bottcher, M., Andersen, G., Thygesen, J., Pedersen, E. M., Dejbjerg, L., . . . Botker, H. E. (2011). Impact of luminal density on plaque classification by CT coronary angiography. *Int J Cardiovasc Imaging, 27*(4), 593-600.

Delhaye, D., Remy-Jardin, M., Rozel, C., Dusson, C., Wurtz, A., Delannoy-Deken, V., . . . Remy, J. (2007). Coronary artery imaging during preoperative CT staging: preliminary experience with 64-slice multidetector CT in 99 consecutive patients. *Eur Radiol, 17*(3), 591-602.

Den Harder, A. M., Willemink, M. J., De Ruiter, Q. M., De Jong, P. A., Schilham, A. M., Krestin, G. P., . . . Budde, R. P. (2016). Dose reduction with iterative reconstruction for coronary CT angiography: a systematic review and meta-analysis. *Br J Radiol, 89*(1058), 20150068.

Den Harder, A. M., Willemink, M. J., de Ruiter, Q. M., Schilham, A. M., Krestin, G. P., Leiner, T., . . . Budde, R. P. (2015). Achievable dose reduction using iterative reconstruction for chest computed tomography: A systematic review. *Eur J Radiol, 84*(11), 2307-2313.

Dewey, M. (2011a). Clinical indications. In M. Dewey (Ed.), *Cardiac CT* (pp. 43-52). Berlin Heidelberg: Springer-Verlag.

Dewey, M. (2011b). Examination and reconstruction. In M. Dewey (Ed.), *Cardiac CT* (pp. 72-92). Berlin Heidelberg: Springer-Verlag.

Dewey, M. (2011c). Patient preparation. In M. Dewey (Ed.), *Cardiac CT* (pp. 53-57). Berlin Heidelberg: Springer-Verlag.

Dewey, M., Hoffmann, H., & Hamm, B. (2007). CT coronary angiography using 16 and 64 simultaneous detector rows: intraindividual comparison. *RoFo, 179*(6), 581-586.

Di Cesare, E., Gennarelli, A., Di Sibio, A., Felli, V., Perri, M., Splendiani, A., . . . Masciocchi, C. (2016). 320-row coronary computed tomography angiography (CCTA) with automatic exposure control (AEC): effect of 100 kV versus 120 kV on image quality and dose exposure. *Radiol Med, 121*(8), 618-625.

Diagnostic and Interventional Cardiology. (2013). Toshiba Releases 640-Slice CT Scanner, CT system accurately images patients faster and with less dose . Retrieved from http://www.dicardiology.com/product/toshiba-releases-640-slice-ct-scanner

Dodge, J. T., Brown, B. G., Bolson, E. L., & Dodge, H. T. (1992). Lumen diameter of normal human coronary arteries. Influence of age, sex, anatomic variation, and left ventricular hypertrophy or dilation. *Circulation, 86*(1), 232.

Du Bois, D., & Du Bois, E. F. (1989). A formula to estimate the approximate surface area if height and weight be known. 1916. *Nutrition, 5*(5), 303-311.

Durmus, T., Luhur, R., Daqqaq, T., Schwenke, C., Knobloch, G., Huppertz, A., . . . Lembcke, A. (2016). Individual selection of X-ray tube settings in computed tomography coronary angiography: Reliability of an automated software algorithm to maintain constant image quality. *Eur J Radiol, 85*(5), 963-971.

Earls, J. P., Woodard, P. K., Abbara, S., Akers, S. R., Araoz, P. A., Cummings, K., . . . Min, J. K. (2014). ACR appropriateness criteria asymptomatic patient at risk for coronary artery disease. *J Am Coll Radiol, 11*(1), 12-19.

Edyvean, S., Lewis, M., & Britten, A. (2012). Radiation Dose Metrics and the Effect of CT Scan Protocol Parameters. In D. Tack, M. Kalra, & P. Gevenois (Eds.), *Radiation Dose from Multidetector CT Medical Radiology* (pp. 101-118). Berlin, Heidelberg: Springer.

Einstein, A. J., Henzlova, M. J., & Rajagopalan, S. (2007). Estimating risk of cancer associated with radiation exposure from 64-slice computed tomography coronary angiography. *JAMA, 298*(3), 317-323.

EPA. (1994). Estimating Radiogenic Cancer Risks, EPA Report 402-R-93-076. Washington DC: U.S. Environmental Protection Agency.

EPA. (1999). Estimating Radiogenic Cancer Risks. Addendum: Uncertainty Analysis. Washington DC: U.S. Environmental Protection Agency.

Faggioni, L., & Gabelloni, M. (2016). Iodine Concentration and Optimization in Computed Tomography Angiography: Current Issues. *Invest Radiol, 51*(12), 816-822.

Fei, X., Du, X., Yang, Q., Shen, Y., Li, P., Liao, J., & Li, K. (2008). 64-MDCT coronary angiography: phantom study of effects of vascular attenuation on detection of coronary stenosis. *AJR Am J Roentgenol, 191*(1), 43-49.

Ferket, B. S., Genders, T. S., Colkesen, E. B., Visser, J. J., Spronk, S., Steyerberg, E. W., & Hunink, M. G. (2011). Systematic review of guidelines on imaging of asymptomatic coronary artery disease. *J Am Coll Cardiol, 57*(15), 1591-1600.

Fisher, D. R., & Fahey, F. H. (2017). Appropriate Use of Effective Dose in Radiation Protection and Risk Assessment. *Health Physics, 113*(2), 102-109.

Fleischmann, D. (2010). CT angiography: injection and acquisition technique. *Radiol Clin North Am, 48*(2), 237-247, vii.

Fleischmann, D., & Kamaya, A. (2009). Optimal vascular and parenchymal contrast enhancement: the current state of the art. *Radiol Clin North Am, 47*(1), 13-26.

Flohr, T. G., McCollough, C. H., Bruder, H., Petersilka, M., Gruber, K., Suss, C., . . . Ohnesorge, B. M. (2006). First performance evaluation of a dual-source CT (DSCT) system. *Eur Radiol, 16*(2), 256-268.

Flohr, T. G., Stierstorfer, K., Ulzheimer, S., Bruder, H., Primak, A. N., & McCollough, C. H. (2005). Image reconstruction and image quality evaluation for a 64-slice CT scanner with z-flying focal spot. *Med Phys, 32*(8), 2536-2547.

Foley, S. J., McEntee, M. F., Achenbach, S., Brennan, P. C., Rainford, L. S., & Dodd, J. D. (2011). Breast Surface Radiation Dose During Coronary CT Angiography: Reduction by Breast Displacement and Lead Shielding. *AJR Am J Roentgenol, 197*(2), 367-373.

Frydrychowicz, A., Pache, G., Saueressig, U., Foll, D., Kotter, E., Langer, M., & Bley, T. A. (2007). Comparison of reconstruction intervals in routine ECG-pulsed 64-row-MSCT coronary angiography in frequency controlled patients. *Cardiovasc Intervent Radiol, 30*(1), 79-84.

Fuchs, T. A., Stehli, J., Dougoud, S., Fiechter, M., Sah, B. R., Buechel, R. R., . . . Kaufmann, P. A. (2014). Impact of a new motion-correction algorithm on image quality of low-dose coronary CT angiography in patients with insufficient heart rate control. *Acad Radiol, 21*(3), 312-317.

Funabashi, N., Suzuki, K., Terao, M., Maeda, F., Nakamura, K., Mita, Y., . . . Komuro, I. (2007). New acquisition method to exclusively enhance the left side of the heart by a small amount of contrast material achieved by multislice computed tomography with 64 data acquisition system. *Int J Cardiol, 114*(2), 265-269.

Gagarina, N. V., Irwan, R., Gordina, G., Fominykh, E., & Sijens, P. E. (2011). Image Quality in Reduced-Dose Coronary CT Angiography. *Acad Radiol, 18*(8), 984-990.

Galobardes, B., Costanza, M. C., Bernstein, M. S., Delhumeau, C., & Morabia, A. (2003). Trends in risk factors for lifestyle-related diseases by socioeconomic position in Geneva, Switzerland, 1993-2000: health inequalities persist. *Am J Public Health, 93*(8), 1302-1309.

Gao, J., Li, J., Earls, J., Li, T., Wang, Q., & Dai, R. (2011). Individualized tube current selection for 64-row cardiac CTA based on analysis of the scout view. *Eur J Radiol, 79*(2), 266-271.

Geleijns, J., Jessen, K. A., Panzer, W., Shrimpton, P. C., & Tosi, G. (2000). *European Guidelines on quality criteria for computed tomography. EUR 16262.* Retrieved from Brussels, Belgium: http://www.drs.dk/guidelines/ct/quality/htmlindex.htm

Geleijns, J., Van Unnik, J. G., Zoetelief, J., Zweers, D., & Broerse, J. J. (1994). Comparison of two methods for assessing patient dose from computed tomography. *Br J Radiol, 67*(796), 360-365.

Geyer, L. L., Korner, M., Harrieder, A., Mueck, F. G., Deak, Z., Wirth, S., & Linsenmaier, U. (2016). Dose reduction in 64-row whole-body CT in multiple trauma: an optimized CT protocol with iterative image reconstruction on a gemstone-based scintillator. *Br J Radiol, 89*(1061), 20160003.

Ghekiere, O., Salgado, R., Buls, N., Leiner, T., Mancini, I., Vanhoenacker, P., . . . Nchimi, A. (2017). Image quality in coronary CT angiography: challenges and technical solutions. *Br J Radiol, 90*(1072), 20160567.

Ghoshhajra, B. B., Engel, L.-C., Major, G. P., Verdini, D., Sidhu, M., Károlyi, M., . . . Brady, T. J. (2011). Direct chest area measurement: A potential anthropometric replacement for BMI to inform cardiac CT dose parameters? *J Cardiovasc Comput Tomogr, 5*(4), 240-246.

Givenchi, S., Safari, M. J., Tan, S. K., Md Shah, M. N. B., Sani, F. B. M., Azman, R. R., . . . Wong, J. H. D. (2018). Measurement of coronary bifurcation angle with coronary CT angiography: A phantom study. *Physica Medica: European Journal of Medical Physics, 45*, 198-204.

Gopal, A., & Budoff, M. J. (2009). A new method to reduce radiation exposure during multi-row detector cardiac computed tomographic angiography. *Int J Cardiol, 132*(3), 435-436.

Gopal, A., Mao, S. S., Karlsberg, D., Young, E., Waggoner, J., Ahmadi, N., . . . Budoff, M. J. (2009). Radiation reduction with prospective ECG-triggering acquisition using 64-multidetector Computed Tomographic angiography. *Int J Cardiovasc Imaging, 25*(4), 405-416.

Gordic, S., Husarik, D. B., Desbiolles, L., Leschka, S., Frauenfelder, T., & Alkadhi, H. (2014). High-pitch coronary CT angiography with third generation dual-source CT: limits of heart rate. *Int J Cardiovasc Imaging, 30*(6), 1173-1179.

Gosling, O., Loader, R., Venables, P., Rowles, N., Morgan-Hughes, G., & Roobottom, C. (2010). Cardiac CT: are we underestimating the dose? A radiation dose study utilizing the 2007 ICRP tissue weighting factors and a cardiac specific scan volume. *Clin Radiol, 65*(12), 1013-1017.

Groves, A. M., Owen, K. E., Courtney, H. M., Yates, S. J., Goldstone, K. E., Blake, G. M., & Dixon, A. K. (2004). 16-detector multislice CT: dosimetry estimation by TLD measurement compared with Monte Carlo simulation. *Br J Radiol, 77*(920), 662-665.

Grudzenski, S., Kuefner, M. A., Heckmann, M. B., Uder, M., & Lobrich, M. (2009). Contrast medium-enhanced radiation damage caused by CT examinations. *Radiology, 253*(3), 706-714.

Gu, J., Shi, H. S., Han, P., Yu, J., Ma, G. N., & Wu, S. (2016). Image Quality and Radiation Dose for Prospectively Triggered Coronary CT Angiography: 128-Slice Single-Source CT versus First-Generation 64-Slice Dual-Source CT. *Sci Rep, 6*, 34795.

Guimaraes, L. S., Fletcher, J. G., Harmsen, W. S., Yu, L., Siddiki, H., Melton, Z., . . . McCollough, C. H. (2010). Appropriate patient selection at abdominal dual-energy CT using 80 kV: relationship between patient size, image noise, and image quality. *Radiology, 257*(3), 732-742.

Haage, P., Schmitz-Rode, T., Hubner, D., Piroth, W., & Gunther, R. W. (2000). Reduction of contrast material dose and artifacts by a saline flush using a double power injector in helical CT of the thorax. *AJR Am J Roentgenol, 174*(4), 1049-1053.

Habets, J., van den Brink, R. B., Uijlings, R., Spijkerboer, A. M., Mali, W. P., Chamuleau, S. A., & Budde, R. P. (2012). Coronary artery assessment by multidetector computed tomography in patients with prosthetic heart valves. *Eur Radiol, 22*(6), 1278-1286.

Halliburton, S. S., Abbara, S., Chen, M. Y., Gentry, R., Mahesh, M., Raff, G. L., . . . Hausleiter, J. (2011). SCCT guidelines on radiation dose and dose-optimization strategies in cardiovascular CT. *J Cardiovasc Comput Tomogr, 5*(4), 198-224.

Halliburton, S. S., Tanabe, Y., Partovi, S., & Rajiah, P. (2017). The role of advanced reconstruction algorithms in cardiac CT. *Cardiovasc Diagn Ther, 7*(5), 527-538.

Halsell, R. D. (1987). Heating contrast media: role in contemporary angiography. *Radiology, 164*(1), 276-278.

Hamdan, A., Asbach, P., Wellnhofer, E., Klein, C., Gebker, R., Kelle, S., . . . Fleck, E. (2011). A prospective study for comparison of MR and CT imaging for detection of coronary artery stenosis. *JACC Cardiovasc Imaging, 4*(1), 50-61.

Hansson, G. K. (2005). Inflammation, atherosclerosis, and coronary artery disease. *N Engl J Med, 352*(16), 1685-1695.

Harden, S. P., Bull, R. K., Bury, R. W., Castellano, E. A., Clayton, B., Hamilton, M. C., . . . Nicol, E. D. (2016). The safe practice of CT coronary angiography in adult patients in UK imaging departments. *Clin Radiol, 71*(8), 722-728.

Hausleiter, J., Martinoff, S., Hadamitzky, M., Martuscelli, E., Pschierer, I., Feuchtner, G. M., . . . Achenbach, S. (2010). Image quality and radiation exposure with a low tube voltage protocol for coronary CT angiography results of the PROTECTION II Trial. *JACC Cardiovasc Imaging, 3*(11), 1113-1123.

Hausleiter, J., Meyer, T., Hadamitzky, M., Huber, E., Zankl, M., Martinoff, S., . . . Schömig, A. (2006). Radiation Dose Estimates From Cardiac Multislice Computed Tomography in Daily Practice. *Circulation, 113*(10), 1305.

Hausleiter, J., Meyer, T. S., Martuscelli, E., Spagnolo, P., Yamamoto, H., Carrascosa, P., . . . Achenbach, S. (2012). Image quality and radiation exposure with prospectively ECG-triggered axial scanning for coronary CT angiography: the multicenter, multivendor, randomized PROTECTION-III study. *JACC Cardiovasc Imaging, 5*(5), 484-493.

Hazirolan, T., Turkbey, B., Akpinar, E., Canyigit, M., Karcaaltincaba, M., Peynircioglu, B., . . . Balkanci, F. (2009). The impact of warmed intravenous contrast material on the bolus geometry of coronary CT angiography applications. *Korean J Radiol, 10*(2), 150-155.

Heiken, J. P., Brink, J. A., McClennan, B. L., Sagel, S. S., Crowe, T. M., & Gaines, M. V. (1995). Dynamic incremental CT: effect of volume and concentration of contrast material and patient weight on hepatic enhancement. *Radiology, 195*(2), 353-357.

Hermann, F., Martinoff, S., Meyer, T., Hadamitzky, M., Jiang, C., Hendrich, E., & Hausleiter, J. (2008). Reduction of radiation dose estimates in cardiac 64-slice CT angiography in patients after coronary artery bypass graft surgery. *Invest Radiol, 43*(4), 253-260.

Herzog, B. A., Husmann, L., Valenta, I., Tay, F. M., Burkhard, N., Gaemperli, O., . . . Kaufmann, P. A. (2009). Determinants of vessel contrast in BMI-adapted low dose CT coronary angiography with prospective ECG-triggering. *Int J Cardiovasc Imaging, 25*(6), 625-630.

Higashigaito, K., Schmid, T., Puippe, G., Morsbach, F., Lachat, M., Seifert, B., . . . Husarik, D. B. (2016). CT Angiography of the Aorta: Prospective Evaluation of Individualized Low-Volume Contrast Media Protocols. *Radiology, 280*(3), 960-968.

Hipp, A., Desai, S., Lopez, C., & Sinert, R. (2008). The incidence of contrast-induced nephropathy in trauma patients. *Eur J Emerg Med, 15*(3), 134-139.

Hoffmann, U., Ferencik, M., Cury, R. C., & Pena, A. J. (2006). Coronary CT angiography. *J Nucl Med, 47*(5), 797-806.

Hopper, K. D., Mosher, T. J., Kasales, C. J., TenHave, T. R., Tully, D. A., & Weaver, J. S. (1997). Thoracic spiral CT: delivery of contrast material pushed with injectable saline solution in a power injector. *Radiology, 205*(1), 269-271.

Horiguchi, J., Fujioka, C., Kiguchi, M., Shen, Y., Althoff, C. E., Yamamoto, H., & Ito, K. (2007). Soft and Intermediate Plaques in Coronary Arteries: How Accurately Can We Measure CT Attenuation Using 64-MDCT? *AJR Am J Roentgenol, 189*(4), 981-988.

Hou, Y., Zheng, J., Wang, Y., Yu, M., Vembar, M., & Guo, Q. (2013). Optimizing radiation dose levels in prospectively electrocardiogram-triggered coronary computed tomography angiography using iterative reconstruction techniques: a phantom and patient study. *PLoS One, 8*(2), e56295.

HPA. (2013). Subgroup on human radiosensitivity of the advisory group on ionising radiation. Human radiosensitivity, Report of the independent advisory group on ionising radiation Health Protection Agency.

Hsiao, E. M., Rybicki, F. J., & Steigner, M. (2010). CT coronary angiography: 256-slice and 320-detector row scanners. *Curr Cardiol Rep, 12*(1), 68-75.

Huda, W. (2002). Dose and image quality in CT. *Pediatr Radiol, 32*(10), 709-713; discussion 751-704.

Huda, W., Rowlett, W. T., & Schoepf, U. J. (2010). Radiation dose at cardiac computed tomography: facts and fiction. *J Thorac Imaging, 25*(3), 204-212.

Huda, W., Scalzetti, E. M., & Levin, G. (2000). Technique factors and image quality as functions of patient weight at abdominal CT. *Radiology, 217*(2), 430-435.

Hurwitz, L. M., Reiman, R. E., Yoshizumi, T. T., Goodman, P. C., Toncheva, G., Nguyen, G., & Lowry, C. (2007). Radiation dose from contemporary cardiothoracic multidetector CT protocols with an anthropomorphic female phantom: implications for cancer induction. *Radiology, 245*(3), 742-750.

Husmann, L., Herzog, B. A., Burkhard, N., Valenta, I., Burger, I. A., Gaemperli, O., & Kaufmann, P. A. (2009). Low-dose coronary CT angiography with prospective ECG triggering: validation of a contrast material protocol adapted to body mass index. *AJR Am J Roentgenol, 193*(3), 802-806.

Husmann, L., Herzog, B. A., Pazhenkottil, A. P., Buechel, R. R., Nkoulou, R., Ghadri, J. R., . . . Kaufmann, P. A. (2011). Lowering heart rate with an optimised breathing protocol for prospectively ECG-triggered CT coronary angiography. *Br J Radiol, 84*(1005), 790-795.

Husmann, L., Valenta, I., Gaemperli, O., Adda, O., Treyer, V., Wyss, C. A., . . . Kaufmann, P. A. (2008). Feasibility of low-dose coronary CT angiography: first experience with prospective ECG-gating. *Eur Heart J, 29*(2), 191-197.

IAEA. (2007). Dosimetry in Diagnostic Radiology : An International Code of Practice. Technical Report Series No. 457. Vienna: International Atomic Energy Agency.

ICRP. (1991). 1990 Recommendations of the International Commission on Radiological Protection *Ann ICRP* (1991/01/01 ed., Vol. 21, pp. 1-201). Oxford, UK: International Commission on Radiological Protection.

ICRP. (2007). The 2007 Recommendations of the International Commission on Radiological Protection. ICRP publication 103. *Ann ICRP, 37*(2-4), 1-332.

IHME. (2015, May 2017). Global Burden of Disease 2015 Factsheet. Retrieved from http://www.healthdata.org/briefs/global-burden-disease-2015-factsheet

Iyama, Y., Nakaura, T., Yokoyama, K., Kidoh, M., Harada, K., Oda, S., . . . Yamashita, Y. (2016). Low-Contrast and Low-Radiation Dose Protocol in Cardiac Computed Tomography: Usefulness of Low Tube Voltage and Knowledge-Based Iterative Model Reconstruction Algorithm. *J Comput Assist Tomogr, 40*(6), 941-947.

Jakobs, T. F., Becker, C. R., Ohnesorge, B., Flohr, T., Suess, C., Schoepf, U. J., & Reiser, M. F. (2002). Multislice helical CT of the heart with retrospective ECG gating: reduction of radiation exposure by ECG-controlled tube current modulation. *Eur Radiol, 12*(5), 1081-1086.

Jessen, K. A., Shrimpton, P. C., Geleijns, J., Panzer, W., & Tosi, G. (1999). Dosimetry for optimisation of patient protection in computed tomography. *Appl Radiat Isot, 50*(1), 165-172.

Johnson, P. T., Pannu, H. K., & Fishman, E. K. (2009). IV contrast infusion for coronary artery CT angiography: literature review and results of a nationwide survey. *AJR Am J Roentgenol, 192*(5), W214-221.

Johnson, T. R., Nikolaou, K., Wintersperger, B. J., Fink, C., Rist, C., Leber, A. W., . . . Becker, C. R. (2007). Optimization of contrast material administration for electrocardiogram-gated computed tomographic angiography of the chest. *J Comput Assist Tomogr, 31*(2), 265-271.

Johnson, T. R., Nikolaou, K., Wintersperger, B. J., Leber, A. W., von Ziegler, F., Rist, C., . . . Becker, C. R. (2006). Dual-source CT cardiac imaging: initial experience. *Eur Radiol, 16*(7), 1409-1415.

Jolly, S. S., Amlani, S., Hamon, M., Yusuf, S., & Mehta, S. R. (2009). Radial versus femoral access for coronary angiography or intervention and the impact on major bleeding and ischemic events: a systematic review and meta-analysis of randomized trials. *Am Heart J, 157*(1), 132-140.

Jones, D. G., & Shrimpton, P. C. (1991). *Survey of CT Practice in the UK. Part 3: Normalised Organ Doses Calculated Using Monte Carlo techniques.* Oxon: National Radiological Protection Board.

Judy, P. F. (1976). The line spread function and modulation transfer function of a computed tomographic scanner. *Med Phys, 3*(4), 233-236.

Kalisz, K., Buethe, J., Saboo, S. S., Abbara, S., Halliburton, S. S., & Rajiah, P. (2016). Artifacts at Cardiac CT: Physics and Solutions. *Radiographics, 36*(7), 2064-2083.

Kang, D. K. (2015). CT technical overviews. In T. H. Lim (Ed.), *Practical Textbook of Cardiac CT and MRI*: Springer-Verlag Berlin Heidelberg.

Kannel, W. B., & Feinleib, M. (1972). Natural history of angina pectoris in the Framingham study. Prognosis and survival. *Am J Cardiol, 29*(2), 154-163.

Kannel, W. B., & McGee, D. L. (1979). Diabetes and cardiovascular risk factors: the Framingham study. *Circulation, 59*(1), 8-13.

Katori, R. (1979). Normal cardiac output in relation to age and body size. *Tohoku J Exp Med, 128*(4), 377-387.

Kerl, J. M., Ravenel, J. G., Nguyen, S. A., Suranyi, P., Thilo, C., Costello, P., . . . Schoepf, U. J. (2008). Right heart: split-bolus injection of diluted contrast medium for visualization at coronary CT angiography. *Radiology, 247*(2), 356-364.

Khan, A. N., Khosa, F., Nikolic, B., Shuaib, W., Lin, P. J., & Khan, M. K. (2014). Cancerogenesis Risks between 64 and 320 Row Detector CT for Coronary CTA Screening. *J Clin Imaging Sci, 4*, 18.

Kim, D. J., Kim, T. H., Kim, S. J., Kim, D. P., Oh, C. S., Ryu, Y. H., . . . Choi, B. W. (2008). Saline flush effect for enhancement of aorta and coronary arteries at multidetector CT coronary angiography. *Radiology, 246*(1), 110-115.

Kim, S. Y., Seo, J. B., Do, K. H., Heo, J. N., Lee, J. S., Song, J. W., . . . Lim, T. H. (2006). Coronary artery anomalies: classification and ECG-gated multi-detector row CT findings with angiographic correlation. *Radiographics, 26*(2), 317-333; discussion 333-314.

Kinlay, S., Libby, P., & Ganz, P. (2001). Endothelial function and coronary artery disease. *Curr Opin Lipidol, 12*(4), 383-389.

Klabunde, R. E. (2012). *Cardiovascular physiology concepts.* (Second ed.): Lippincott Willians and Wilkins.

Klass, O., Jeltsch, M., Feuerlein, S., Brunner, H., Nagel, H. D., Walker, M. J., . . . Hoffmann, M. H. (2009). Prospectively gated axial CT coronary angiography: preliminary experiences with a novel low-dose technique. *Eur Radiol, 19*(4), 829-836.

Kok, M., Mihl, C., Hendriks, B. M., Altintas, S., Kietselaer, B. L., Wildberger, J. E., & Das, M. (2016). Optimizing contrast media application in coronary CT angiography at lower tube voltage: Evaluation in a circulation phantom and sixty patients. *Eur J Radiol, 85*(6), 1068-1074.

Kolodgie, F. D., Burke, A. P., Farb, A., Gold, H. K., Yuan, J., Narula, J., . . . Virmani, R. (2001). The thin-cap fibroatheroma: a type of vulnerable plaque: the major precursor lesion to acute coronary syndromes. *Curr Opin Cardiol, 16*(5), 285-292.

Komatsu, S., Kamata, T., Imai, A., Ohara, T., Takewa, M., Miyaji, K., . . . Kodama, K. (2013). Controlling intracoronary CT number for coronary CT angiography. *J Cardiol, 61*(2), 155-161.

Kroft, L. J. M., & Dewey, M. (2011). Reading and reporting. In M. Dewey (Ed.), *Cardiac CT*. Berlin Heidelberg: Springer-Verlag.

Kumar, A., & Cannon, C. P. (2009). Acute coronary syndromes: diagnosis and management, part I. *Mayo Clin Proc, 84*(10), 917-938.

Labounty, T. M., Leipsic, J., Min, J. K., Heilbron, B., Mancini, G. B., Lin, F. Y., & Earls, J. P. (2010). Effect of padding duration on radiation dose and image interpretation in prospectively ECG-triggered coronary CT angiography. *AJR Am J Roentgenol, 194*(4), 933-937.

Latif, M. A., Sanchez, F. W., Sayegh, K., Veledar, E., Aziz, M., Malik, R., . . . Cury, R. C. (2016). Volumetric Single-Beat Coronary Computed Tomography Angiography: Relationship of Image Quality, Heart Rate, and Body Mass Index. Initial Patient Experience With a New Computed Tomography Scanner. *J Comput Assist Tomogr*.

Lee, C. H., Goo, J. M., Ye, H. J., Ye, S. J., Park, C. M., Chun, E. J., & Im, J. G. (2008). Radiation dose modulation techniques in the multidetector CT era: from basics to practice. *Radiographics, 28*(5), 1451-1459.

Lee, J., Heng, D., Chia, K. S., Chew, S. K., Tan, B. Y., & Hughes, K. (2001). Risk factors and incident coronary heart disease in Chinese, Malay and Asian Indian males: the Singapore Cardiovascular Cohort Study. *Int J Epidemiol, 30*(5), 983-988.

Lee, K. H., Lee, J. M., Moon, S. K., Baek, J. H., Park, J. H., Flohr, T. G., . . . Choi, B. I. (2012). Attenuation-based automatic tube voltage selection and tube current modulation for dose reduction at contrast-enhanced liver CT. *Radiology, 265*(2), 437-447.

Lee, W., & Park, E.-A. (2014). Pediatric Cardiac Imaging I: CT and MR Techniques. In I.-O. Kim (Ed.), *Radiology Illustrated: Pediatric Radiology* (pp. 525-551). Berlin, Heidelberg: Springer Berlin Heidelberg.

Lehmkuhl, L., Gosch, D., Nagel, H. D., Stumpp, P., Kahn, T., & Gutberlet, M. (2010). Quantification of radiation dose savings in cardiac computed tomography using prospectively triggered mode and ECG pulsing: a phantom study. *Eur Radiol, 20*(9), 2116-2125.

Leipsic, J., Abbara, S., Achenbach, S., Cury, R., Earls, J. P., Mancini, G. J., . . . Raff, G. L. (2014). SCCT guidelines for the interpretation and reporting of coronary CT angiography: a report of the Society of Cardiovascular Computed Tomography Guidelines Committee. *J Cardiovasc Comput Tomogr, 8*(5), 342-358.

Lell, M., Marwan, M., Schepis, T., Pflederer, T., Anders, K., Flohr, T., . . . Achenbach, S. (2009). Prospectively ECG-triggered high-pitch spiral acquisition for coronary CT angiography using dual source CT: technique and initial experience. *Eur Radiol, 19*(11), 2576.

Leschka, S., Kim, C.-H., Baumueller, S., Stolzmann, P., Scheffel, H., Marincek, B., & Alkadhi, H. (2010). Scan Length Adjustment of CT Coronary Angiography Using the Calcium Scoring Scan: Effect on Radiation Dose. *AJR Am J Roentgenol, 194*(3), W272-W277.

Leschka, S., Stolzmann, P., Desbiolles, L., Baumueller, S., Goetti, R., Schertler, T., . . . Alkadhi, H. (2009). Diagnostic accuracy of high-pitch dual-source CT for the assessment of coronary stenoses: first experience. *Eur Radiol, 19*(12), 2896-2903.

Leschka, S., Stolzmann, P., Schmid, F. T., Scheffel, H., Stinn, B., Marincek, B., . . . Wildermuth, S. (2008). Low kilovoltage cardiac dual-source CT: attenuation, noise, and radiation dose. *Eur Radiol, 18*(9), 1809-1817.

Levine, G. N., Keaney, J. F., Jr., & Vita, J. A. (1995). Cholesterol reduction in cardiovascular disease. Clinical benefits and possible mechanisms. *N Engl J Med, 332*(8), 512-521.

Lewis, M. A., Pascoal, A., Keevil, S. F., & Lewis, C. A. (2016). Selecting a CT scanner for cardiac imaging: the heart of the matter. *Br J Radiol, 89*(1065), 20160376.

Li, J., Udayasankar, U. K., Toth, T. L., Seamans, J., Small, W. C., & Kalra, M. K. (2007). Automatic patient centering for MDCT: effect on radiation dose. *AJR Am J Roentgenol, 188*(2), 547-552.

Liu, J., Gao, J., Wu, R., Zhang, Y., Hu, L., & Hou, P. (2013). Optimizing contrast medium injection protocol individually with body weight for high-pitch prospective ECG-triggering coronary CT angiography. *Int J Cardiovasc Imaging, 29*(5), 1115-1120.

Livingston, E. H., & Lee, S. (2001). Body surface area prediction in normal-weight and obese patients. *Am J Physiol Endocrinol Metab, 281*(3), E586-591.

Lu, C., Wang, Z., Ji, J., Wang, H., Hu, X., & Chen, C. (2015). Evaluation of a chest circumference-adapted protocol for low-dose 128-slice coronary CT angiography with prospective electrocardiogram triggering. *Korean J Radiol, 16*(1), 13-20.

Lu, J. G., Lv, B., Chen, X. B., Tang, X., Jiang, S. L., & Dai, R. P. (2010). What is the best contrast injection protocol for 64-row multi-detector cardiac computed tomography? *Eur J Radiol, 75*(2), 159-165.

Luecke, C., Andres, C., Foldyna, B., Nagel, H. D., Hoffmann, J., Grothoff, M., . . . Lehmkuhl, L. (2012). Impact of heart rate and rhythm on radiation exposure in prospectively ECG triggered computed tomography. *Eur J Radiol, 81*(9), 2221-2230.

Maffei, E., Martini, C., & Cademartiri, F. (2012). Patient Preparation for Cardiac CT. In F. Cademartiri, G. Casolo, & M. Midiri (Eds.), *Clinical Applications of Cardiac CT* (pp. 235-240). Milano: Springer Milan.

Maffei, E., Messalli, G., Martini, C., Nieman, K., Catalano, O., Rossi, A., . . . Cademartiri, F. (2012). Left and right ventricle assessment with Cardiac CT: validation study vs. Cardiac MR. *Eur Radiol, 22*(5), 1041-1049.

Mahesh, M., & Cody, D. D. (2007). Physics of cardiac imaging with multiple-row detector CT. *Radiographics, 27*(5), 1495-1509.

Mahmood, S. (2009). Pathophysiology of Coronary Artery Disease. In A. Movahed, G. Gnanasegaran, J. R. Buscombe, & M. Hall (Eds.), *Integrating Cardiology for Nuclear Medicine Physicians, A Guide to Nuclear Medicine Physicians*. Berlin Heidelberg: Springer-Verlag.

Mahnken, A. H., Rauscher, A., Klotz, E., Muhlenbruch, G., Das, M., Gunther, R. W., & Wildberger, J. E. (2007). Quantitative prediction of contrast enhancement from test bolus data in cardiac MSCT. *Eur Radiol, 17*(5), 1310-1319.

Mangold, S., Wichmann, J. L., Schoepf, U. J., Poole, Z. B., Canstein, C., Varga-Szemes, A., . . . De Cecco, C. N. (2016). Automated tube voltage selection for radiation dose and contrast medium reduction at coronary CT angiography using 3(rd) generation dual-source CT. *Eur Radiol, 26*(10), 3608-3616.

Manolio, T. (2003). Novel risk markers and clinical practice. *N Engl J Med, 349*(17), 1587-1589.

Mayo-Smith, W. W., Hara, A. K., Mahesh, M., Sahani, D. V., & Pavlicek, W. (2014). How I do it: managing radiation dose in CT. *Radiology, 273*(3), 657-672.

McCollough, C. H., Leng, S., Yu, L., Cody, D. D., Boone, J. M., & McNitt-Gray, M. F. (2011). CT dose index and patient dose: they are not the same thing. *Radiology, 259*(2), 311-316.

McNitt-Gray, M. F. (2002). AAPM/RSNA Physics Tutorial for Residents: Topics in CT. *Radiographics, 22*(6), 1541-1553.

Mettler, F. A., Bhargavan, M., Faulkner, K., Gilley, D. B., Gray, J. E., Ibbott, G. S., . . . Yoshizumi, T. T. (2009). Radiologic and Nuclear Medicine Studies in the United States and Worldwide: Frequency, Radiation Dose, and Comparison with Other Radiation Sources-1950-2007. *Radiology, 253*(2), 520-531.

Mettler, F. A., Thorriadsen, B. R., Bhargavan, M., Gilley, D. B., Gray, J. E., Lipoti, J. A., . . . Mahesh, M. (2008). Medical Radiation Exposure in the Us in 2006: Preliminary Results. *Health Physics, 95*(5), 502-507.

Meyer, M., Haubenreisser, H., Schoepf, U. J., Vliegenthart, R., Ong, M. M., Doesch, C., . . . Henzler, T. (2017). Radiation Dose Levels of Retrospectively ECG-Gated Coronary CT Angiography Using 70-kVp Tube Voltage in Patients with High or Irregular Heart Rates. *Acad Radiol, 24*(1), 30-37.

Mihl, C., Maas, M., Turek, J., Seehofnerova, A., Leijenaar, R. T., Kok, M., . . . Das, M. (2017). Contrast Media Administration in Coronary Computed Tomography Angiography - A Systematic Review. *RoFo, 189*(4), 312-325.

Mintz, G. S., Nissen, S. E., Anderson, W. D., Bailey, S. R., Erbel, R., Fitzgerald, P. J., . . . Yock, P. G. (2001). American College of Cardiology Clinical Expert Consensus Document on Standards for Acquisition, Measurement and Reporting of Intravascular Ultrasound Studies (IVUS). A report of the American College of Cardiology Task Force on Clinical Expert Consensus Documents. *J Am Coll Cardiol, 37*(5), 1478-1492.

Mitchell, A. M., Jones, A. E., Tumlin, J. A., & Kline, J. A. (2010). Incidence of contrast-induced nephropathy after contrast-enhanced computed tomography in the outpatient setting. *Clin J Am Soc Nephrol, 5*(1), 4-9.

Mitchell, A. M., & Kline, J. A. (2007). Contrast nephropathy following computed tomography angiography of the chest for pulmonary embolism in the emergency department. *J Thromb Haemost, 5*(1), 50-54.

MOH. (2016). *Number of discharges and deaths in government hospitals*. Retrieved from http://www.moh.gov.my/images/gallery/publications/KKM%20HEALTH%20FACTS%202016.pdf

MOH. (2017). *Clinical Practice Guidelines on Primary & Secondary Prevention of Cardiovascular Disease 2017*. Retrieved from https://www.malaysianheart.org/files/597736485dd17.pdf

Morise, A. P., Haddad, W. J., & Beckner, D. (1997). Development and validation of a clinical score to estimate the probability of coronary artery disease in men and women presenting with suspected coronary disease. *Am J Med, 102*(4), 350-356.

Najafi, M., & Sheikhvatan, M. (2013). Gender Differences in Coronary Artery Disease: Correlational Study on Dietary Pattern and Known Cardiovascular Risk Factors. *Int Cardiovasc Res J, 7*(4), 124-129.

Nakajima, Y., Yoshimine, T., Yoshida, H., Sakashita, K., Okamoto, M., Kishikawa, M., . . . Hayakawa, T. (1998). Computerized tomography angiography of ruptured cerebral aneurysms: factors affecting time to maximum contrast concentration. *J Neurosurg, 88*(4), 663-669.

Nakaura, T., Awai, K., Maruyama, N., Takata, N., Yoshinaka, I., Harada, K., . . . Yamashita, Y. (2011). Abdominal dynamic CT in patients with renal dysfunction: contrast agent dose reduction with low tube voltage and high tube current-time product settings at 256-detector row CT. *Radiology, 261*(2), 467-476.

Nakaura, T., Awai, K., Yauaga, Y., Nakayama, Y., Oda, S., Hatemura, M., . . . Yamashita, Y. (2008). Contrast injection protocols for coronary computed tomography angiography using a 64-detector scanner: comparison between patient weight-adjusted- and fixed iodine-dose protocols. *Invest Radiol, 43*(7), 512-519.

Nakaura, T., Kidoh, M., Sakaino, N., Nakamura, S., Nozaki, T., Izumi, A., . . . Yamashita, Y. (2013). Low radiation dose protocol in cardiac Ct with 100 kVp: usefulness of display preset optimization. *Int J Cardiovasc Imaging, 29*(6), 1381-1389.

Nakaura, T., Kidoh, M., Sakaino, N., Utsunomiya, D., Oda, S., Kawahara, T., . . . Yamashita, Y. (2013). Low contrast-and low radiation dose protocol for cardiac CT of thin adults at 256-row CT: usefulness of low tube voltage scans and the hydrid iterative reconstruction algorithm. *Int J Cardiovasc Imaging, 29*(4), 913-923.

NCRP. (1993). Limitating of Exposure to Ionizing Radiation, NCRP Report No. 116. Bethesda, MD.: National Council on Radiation Protection and Measurements.

Nelson, R. C., Feuerlein, S., & Boll, D. T. (2011). New iterative reconstruction techniques for cardiovascular computed tomography: how do they work, and what are the advantages and disadvantages? *J Cardiovasc Comput Tomogr, 5*(5), 286-292.

NIH. (2003). Report of the NCI-CDC Working Group to Revise the 1985 NIH Radioepidemiological Tables. NIH Publication No. 03-5387. Bethesda, MD.: National Institutes of Health.

NRC. (1990). Health Effects of Exposure to Low Levels of Ionzing Radiation (BEIR V). Washington, DC: National Academy Press.

NRC. (2006). Health risks from exposure to low levels of ionizing radiation: BEIR VII phase 2. Washington, DC: Committee to assess health risks from exposure to low levels of ionizing radiation, National Research Council, National Academies.

Numburi, U. D., Chatzimavroudis, G. P., Stillman, A. E., Lieber, M. L., Uber, A. E., 3rd, Kalafut, J. F., . . . Halliburton, S. S. (2007). Patient-specific contrast injection protocols for cardiovascular multidetector row computed tomography. *J Comput Assist Tomogr, 31*(2), 281-289.

Oda, S., Utsunomiya, D., Funama, Y., Awai, K., Katahira, K., Nakaura, T., . . . Yamashita, Y. (2011). A low tube voltage technique reduces the radiation dose at retrospective ECG-gated cardiac computed tomography for anatomical and functional analyses. *Acad Radiol, 18*(8), 991-999.

Oda, S., Utsunomiya, D., Yuki, H., Kai, N., Hatemura, M., Funama, Y., . . . Yamashita, Y. (2015). Low contrast and radiation dose coronary CT angiography using a 320-row system and a refined contrast injection and timing method. *J Cardiovasc Comput Tomogr, 9*(1), 19-27.

Oda, S., Weissman, G., Vembar, M., & Weigold, W. G. (2014). Iterative model reconstruction: improved image quality of low-tube-voltage prospective ECG-gated coronary CT angiography images at 256-slice CT. *Eur J Radiol, 83*(8), 1408-1415.

Otero, H. J., Steigner, M. L., & Rybicki, F. J. (2009). The "post-64" era of coronary CT angiography: understanding new technology from physical principles. *Radiol Clin North Am, 47*(1), 79-90.

Ozasa, K., Shimizu, Y., Suyama, A., Kasagi, F., Soda, M., Grant, E. J., . . . Kodama, K. (2012). Studies of the mortality of atomic bomb survivors, Report 14, 1950-2003: an overview of cancer and noncancer diseases. *Radiat Res, 177*(3), 229-243.

Padole, A., Ali Khawaja, R. D., Kalra, M. K., & Singh, S. (2015). CT Radiation Dose and Iterative Reconstruction Techniques. *AJR Am J Roentgenol, 204*(4), W384-W392.

Pan, Y. N., Li, A. J., Chen, X. M., Wang, J., Ren, D. W., & Huang, Q. L. (2016). Coronary Computed Tomographic Angiography at Low Concentration of Contrast Agent and Low Tube Voltage in Patients with Obesity:: A Feasibility Study. *Acad Radiol, 23*(4), 438-445.

Pannu, H. K., Alvarez, W., Jr., & Fishman, E. K. (2006). Beta-blockers for cardiac CT: a primer for the radiologist. *AJR Am J Roentgenol, 186*(6 Suppl 2), S341-345.

Paul, J. F. (2011). Individually adapted coronary 64-slice CT angiography based on precontrast attenuation values, using different kVp and tube current settings: evaluation of image quality. *Int J Cardiovasc Imaging, 27*(1), 53-59.

Paul, N. S., Kashani, H., Odedra, D., Ursani, A., Ray, C., & Rogalla, P. (2011). The Influence of Chest Wall Tissue Composition in Determining Image Noise During Cardiac CT. *AJR Am J Roentgenol, 197*(6), 1328-1334.

Pazhenkottil, A. P., Husmann, L., Buechel, R. R., Herzog, B. A., Nkoulou, R., Burger, I. A., . . . Kaufmann, P. A. (2010). Validation of a new contrast material protocol adapted to body surface area for optimized low-dose CT coronary angiography with prospective ECG-triggering. *Int J Cardiovasc Imaging, 26*(5), 591-597.

Peebles, C. (2006). Computed tomographic coronary angiography: how many slices do you need? *Heart, 92*(5), 582-584.

Perisinakis, K., Seimenis, I., Tzedakis, A., Papadakis, A. E., & Damilakis, J. (2010). Individualized assessment of radiation dose in patients undergoing coronary computed tomographic angiography with 256-slice scanning. *Circulation, 122*(23), 2394-2402.

Platt, J. F., Reige, K. A., & Ellis, J. H. (1999). Aortic enhancement during abdominal CT angiography: correlation with test injections, flow rates, and patient demographics. *AJR Am J Roentgenol, 172*(1), 53-56.

Poll, L. W., Cohnen, M., Brachten, S., Ewen, K., & Modder, U. (2002). Dose reduction in multi-slice CT of the heart by use of ECG-controlled tube current modulation ("ECG pulsing"): phantom measurements. *RoFo, 174*(12), 1500-1505.

Polonsky, T. S., McClelland, R. L., Jorgensen, N. W., Bild, D. E., Burke, G. L., Guerci, A. D., & Greenland, P. (2010). Coronary Artery Calcium Score and Risk Classification for Coronary Heart Disease Prediction: The Multi-Ethnic Study of Atherosclerosis. *JAMA, 303*(16), 1610-1616.

Prokop, M., & Van der Mollen, A. J. (2011). Patient Preparation and Contrast Media Application. In M. Prokop & M. Galanski (Eds.), *Spiral and Multislice Computed Tomography of the Body*. New York: Thieme.

Pryor, D. B., Shaw, L., McCants, C. B., Lee, K. L., Mark, D. B., Harrell, F. E., Jr., . . . Califf, R. M. (1993). Value of the history and physical in identifying patients at increased risk for coronary artery disease. *Ann Intern Med, 118*(2), 81-90.

Raff, G. L., Chinnaiyan, K. M., Cury, R. C., Garcia, M. T., Hecht, H. S., Hollander, J. E., . . . Hoffmann, U. (2014). SCCT guidelines on the use of coronary computed tomographic angiography for patients presenting with acute chest pain to the emergency department: a report of the Society of Cardiovascular Computed Tomography Guidelines Committee. *J Cardiovasc Comput Tomogr, 8*(4), 254-271.

Raitakari, O. T., Adams, M. R., & Celermajer, D. S. (1999). Effect of Lp(a) on the early functional and structural changes of atherosclerosis. *Arterioscler Thromb Vasc Biol, 19*(4), 990-995.

Rehani, M. (2011). Radiation units, limits and dose constraints. In Y. Lemoigne & A. Caner (Eds.), *Radiation protection in medical physics*. Netherlands: Springer

Ridker, P. M., Buring, J. E., Shih, J., Matias, M., & Hennekens, C. H. (1998). Prospective study of C-reactive protein and the risk of future cardiovascular events among apparently healthy women. *Circulation, 98*(8), 731-733.

Rogalla, P., Blobel, J., Kandel, S., Meyer, H., Mews, J., Kloeters, C., . . . Paul, N. (2010). Radiation dose optimisation in dynamic volume CT of the heart: tube current adaptation based on anterior–posterior chest diameter. *Int J Cardiovasc Imaging, 26*(8), 933-940.

Roos, J. E., Desbiolles, L. M., Weishaupt, D., Wildermuth, S., Hilfiker, P. R., Marincek, B., & Boehm, T. (2004). Multi-detector row CT: effect of iodine dose reduction on hepatic and vascular enhancement. *RoFo, 176*(4), 556-563.

Rothenberg, L. N., & Pentlow, K. S. (2000). CT dosimetry and radiation safety. In L. W. Goldman & J. B. Fowlkes (Eds.), *2000 Syllabus: Categorical Course in Diagnostic Radiology Physics—CT and US Cross-Sectional Imaging* (pp. 171-188). Oak Brook, IL: Radiological Society of North America.

Saade, C., Bourne, R., Wilkinson, M., & Brennan, P. (2011). Contrast Medium Administration and Parameters Affecting Bolus Geometry in Multidetector Computed Tomography Angiography: An Overview. *J Med Imaging Radiat Sci, 42*(3), 113-117.

Sabarudin, A., & Sun, Z. (2013a). Coronary CT angiography: Diagnostic value and clinical challenges. *World J Cardiol, 5*(12), 473-483.

Sabarudin, A., & Sun, Z. (2013b). Coronary CT angiography: Dose reduction strategies. *World J Cardiol, 5*(12), 465-472.

Sabarudin, A., Sun, Z., & Ng, K. H. (2012). A systematic review of radiation dose associated with different generations of multidetector CT coronary angiography. *J Med Imaging Radiat Oncol, 56*(1), 5-17.

Sabarudin, A., Sun, Z., & Ng, K. H. (2013). Radiation dose in coronary CT angiography associated with prospective ECG-triggering technique: comparisons with different CT generations. *Radiat Prot Dosimetry, 154*(3), 301-307.

Sahbaee, P., Abadi, E., Segars, W. P., Marin, D., Nelson, R. C., & Samei, E. (2017). The Effect of Contrast Material on Radiation Dose at CT: Part II. A Systematic Evaluation across 58 Patient Models. *Radiology, 283*(3), 749-757.

Sakai, S., Yabuuchi, H., Chishaki, A., Okafuji, T., Matsuo, Y., Kamitani, T., . . . Honda, H. (2010). Effect of cardiac function on aortic peak time and peak enhancement during coronary CT angiography. *Eur J Radiol, 75*(2), 173-177.

Sandfort, V., Lima, J. A., & Bluemke, D. A. (2015). Noninvasive Imaging of Atherosclerotic Plaque Progression: Status of Coronary Computed Tomography Angiography. *Circ Cardiovasc Imaging, 8*(7), e003316.

Saremi, F., & Achenbach, S. (2015). Coronary Plaque Characterization Using CT. *AJR Am J Roentgenol, 204*(3), W249-W260.

Scharf, M., Bink, R., May, M. S., Hentschke, C., Achenbach, S., Uder, M., & Lell, M. M. (2011). High-pitch thoracic CT with simultaneous assessment of coronary arteries: effect of heart rate and heart rate variability on image quality and diagnostic accuracy. *JACC Cardiovasc Imaging, 4*(6), 602-609.

Schindera, S. T., Nelson, R. C., Mukundan, S., Jr., Paulson, E. K., Jaffe, T. A., Miller, C. M., . . . Samei, E. (2008). Hypervascular liver tumors: low tube voltage, high tube current multi-detector row CT for enhanced detection--phantom study. *Radiology, 246*(1), 125-132.

Schoellnast, H., Deutschmann, H. A., Berghold, A., Fritz, G. A., Schaffler, G. J., & Tillich, M. (2006). MDCT angiography of the pulmonary arteries: influence of body weight, body mass index, and scan length on arterial enhancement at different iodine flow rates. *AJR Am J Roentgenol, 187*(4), 1074-1078.

Seeram, E. (2015). Multislice computed tomography: physical principles and instrumentation. In E. Seeram (Ed.), *Computed Tomography - E-Book: Physical Principles, Clinical Applications, and Quality Control* (4th ed.): Elsevier Health Sciences.

Seibert, J. A., Boone, J. M., Wootton-Gorges, S. L., & Lamba, R. (2014). Dose is not always what it seems: where very misleading values can result from volume CT dose index and dose length product. *J Am Coll Radiol, 11*(3), 233-237.

Seyal, A. R., Arslanoglu, A., Abboud, S. F., Sahin, A., Horowitz, J. M., & Yaghmai, V. (2015). CT of the Abdomen with Reduced Tube Voltage in Adults: A Practical Approach. *Radiographics, 35*(7), 1922-1939.

Shah, D. J., Sachs, R. K., & Wilson, D. J. (2012). Radiation-induced cancer: a modern view. *Br J Radiol, 85*(1020), e1166-1173.

Shah, S., Gnanasegaran, G., Sundberg-Cohon, J., & Buscombe, J. R. (2009). The heart: anatomy, physiology and exercise physiology. In A. Movahed, G. Gnanasegaran, J. R. Buscombe, & M. Hall (Eds.), *Integrating Cardiology for Nuclear Medicine Physicians, A Guide to Nuclear Medicine Physicians*. Berlin Heidelberg: Springer-Verlag.

Shammakhi, A. A., & Sun, Z. (2015). Coronary CT Angiography with Use of Iterative Reconstruction Algorithm in Coronary Stenting: A Systematic Review of Image Quality,Diagnostic Value and Radiation Dose. *J Med Imaging Health Inform, 5*, 103-109.

Shen, Y., Fan, Z., Sun, Z., Xu, L., Li, Y., Zhang, N., & Yan, Z. (2015). High Pitch Dual-Source Whole Aorta CT Angiography in the Detection of Coronary Arteries: A Feasibility Study of Using Iodixanol 270 and 100 kVp with Iterative Reconstruction. *J Med Imaging Health Inform, 5*(1), 117-125.

Shrimpton, P. C. (2004). *Assessment of patient dose in CT. In: EUR. European guidelines for multislice computed tomography funded by the European Commission 2004: contract number FIGMCT2000-20078-CTTIP, Appendix C.* Retrieved from http://biophysicssite.com/html/msct_quality_criteria_2004.html

Shrimpton, P. C., Hillier, M. C., Lewis, M. A., & Dunn, M. (2005). *Doses from computed tomography (CT) examinations in the UK: 2003 review. Report NRPB-W67*. Retrieved from http://www.biophysicssite.com/Documents/NRPB_W67/NRPB_W67.pdf

Shrimpton, P. C., Jones, D. G., & Hillier, M. C. (1991). *Survey of CT practice in the UK; Part 2: Dosimetric aspects.* London, UK.: National Radiological Protection Board.

Shuman, W. P., Branch, K. R., May, J. M., Mitsumori, L. M., Lockhart, D. W., Dubinsky, T. J., . . . Caldwell, J. H. (2008). Prospective versus Retrospective ECG Gating for 64-Detector CT of the Coronary Arteries: Comparison of Image Quality and Patient Radiation Dose. *Radiology, 248*(2), 431-437.

Siegel, M. J., Schmidt, B., Bradley, D., Suess, C., & Hildebolt, C. (2004). Radiation dose and image quality in pediatric CT: effect of technical factors and phantom size and shape. *Radiology, 233*(2), 515-522.

SIEMENS Healthineers. (2016). SOMATOM Definition Flash, Redefining standards. Retrieved from https://www.healthcare.siemens.com/computed-tomography/dual-source-ct/somatom-definition-flash/technical-specifications

Small, G. R., Chow, B. J., & Ruddy, T. D. (2012). Low-dose cardiac imaging: reducing exposure but not accuracy. *Expert Rev Cardiovasc Ther, 10*(1), 89-104.

Smith-Bindman, R., Moghadassi, M., Wilson, N., Nelson, T. R., Boone, J. M., Cagnon, C. H., . . . Miglioretti, D. L. (2015). Radiation Doses in Consecutive CT Examinations from Five University of California Medical Centers. *Radiology, 277*(1), 134-141.

Sprawls, P. (1992). AAPM tutorial. CT image detail and noise. *Radiographics, 12*(5), 1041-1046.

Stary, H. C., Chandler, A. B., Dinsmore, R. E., Fuster, V., Glagov, S., Insull, W. J., . . . Wissler, R. W. (1995). A definition of advanced types of atherosclerotic lesions and a histological classification of atherosclerosis. A report from the Committee on Vascular Lesions of the Council on Arteriosclerosis, American Heart Association. *Circulation, 92*(5), 1355-1374.

Stolzmann, P., Leschka, S., Scheffel, H., Krauss, T., Desbiolles, L., Plass, A., . . . Alkadhi, H. (2008). Dual-source CT in step-and-shoot mode: noninvasive coronary angiography with low radiation dose. *Radiology, 249*(1), 71-80.

Stone, N. J., Robinson, J., Lichtenstein, A. H., Merz, C. N. B., Blum, C. B., Eckel, R. H., . . . Wilson, P. W. F. (2014). 2013 ACC/AHA Guideline on the Treatment of Blood Cholesterol to Reduce Atherosclerotic Cardiovascular Risk in Adults: A Report of the American College of Cardiology/American Heart Association Task Force on Practice Guidelines. *J Am Coll Cardiol, 63*(25 Pt B), 2889-2934.

Sun, G., Hou, Y. B., Zhang, B., Yu, L., Li, S. X., Tan, L. L., & Chen, D. J. (2015). Application of low tube voltage coronary CT angiography with low-dose iodine contrast agent in patients with a BMI of 26-30 kg/m2. *Clin Radiol, 70*(2), 138-145.

Sun, Z. (2012a). Cardiac CT imaging in coronary artery disease: Current status and future directions. *Quant Imaging Med Surg, 2*(2), 98-105.

Sun, Z. (2012b). Coronary CT angiography with prospective ECG-triggering: an effective alternative to invasive coronary angiography. *Cardiovasc Diagn Ther, 2*(1), 28-37.

Sun, Z. (2013). Coronary CT Angiography in Coronary Artery Disease: Correlation between Virtual Intravascular Endoscopic Appearances and Left Bifurcation Angulation and Coronary Plaques. *BioMed Res Int 2013*, 14.

Sun, Z., & Ng, K. H. (2010). Multislice CT angiography in cardiac imaging. Part III: radiation risk and dose reduction. *Singapore Med J, 51*(5), 374-380.

Sun, Z., & Ng, K. H. (2012a). Diagnostic value of coronary CT angiography with prospective ECG-gating in the diagnosis of coronary artery disease: a systematic review and meta-analysis. *Int J Cardiovasc Imaging, 28*(8), 2109-2119.

Sun, Z., & Ng, K. H. (2012b). Prospective versus retrospective ECG-gated multislice CT coronary angiography: A systematic review of radiation dose and diagnostic accuracy. *Eur J Radiol, 81*(2), e94-e100.

Sun, Z., & Xu, L. (2014). Coronary CT angiography in the quantitative assessment of coronary plaques. *Biomed Res Int, 2014*, 346380.

Suzuki, H., Oshima, H., Shiraki, N., Ikeya, C., & Shibamoto, Y. (2004). Comparison of two contrast materials with different iodine concentrations in enhancing the density of the the aorta, portal vein and liver at multi-detector row CT: a randomized study. *Eur Radiol, 14*(11), 2099-2104.

Tan, S. K., Yeong, C. H., Aman, R. R. A. R., Ng, K. H., Aziz, Y. F. A., Chee, K. H., & Sun, Z. (2018). Low tube voltage prospectively ECG-triggered coronary CT angiography: a systematic review of image quality and radiation dose. *Br J Radiol, 91*(1088), 20170874.

Tan, S. K., Yeong, C. H., Ng, K. H., Abdul Aziz, Y. F., & Sun, Z. (2016). Recent Update on Radiation Dose Assessment for the State-of-the-Art Coronary Computed Tomography Angiography Protocols. *PLoS One, 11*(8), e0161543.

Tatsugami, F., Higaki, T., Nakamura, Y., Yamagami, T., Date, S., Fujioka, C., . . . Awai, K. (2015). A new technique for noise reduction at coronary CT angiography with multi-phase data-averaging and non-rigid image registration. *Eur Radiol, 25*(1), 41-48.

Tatsugami, F., Matsuki, M., Inada, Y., Kanazawa, S., Nakai, G., Takeda, Y., . . . Narumi, Y. (2010). Feasibility of low-volume injections of contrast material with a body weight-adapted iodine-dose protocol in 320-detector row coronary CT angiography. *Acad Radiol, 17*(2), 207-211.

Tatsugami, F., Matsuki, M., Nakai, G., Inada, Y., Kanazawa, S., Takeda, Y., . . . Narumi, Y. (2012). The effect of adaptive iterative dose reduction on image quality in 320-detector row CT coronary angiography. *Br J Radiol, 85*(1016), e378-e382.

Taylor, A. J., Cerqueira, M., Hodgson, J. M., Mark, D. l., Min, J., O'Gara, P., & Rubin, G. D. (2010). ACCF/SCCT/ACR/AHA/ASE/ASNC/NASCI/SCAI/SCMR 2010 Appropriate Use Criteria for Cardiac Computed Tomography: A Report of the American College of Cardiology Foundation Appropriate Use Criteria Task Force, the Society of Cardiovascular Computed Tomography, the American College of Radiology, the American Heart Association, the American Society of Echocardiography, the American Society of Nuclear Cardiology, the North American Society for Cardiovascular Imaging, the Society for Cardiovascular Angiography and Interventions, and the Society for Cardiovascular Magnetic Resonance. *J Am Coll Cardiol, 56*(22), 1864-1894.

Taylor, C. M., Blum, A., & Abbara, S. (2006). Patient Preparation and Scanning Techniques. *Radiol Clin North Am, 48*(4), 675-686.

Torres, F. S., Crean, A. M., Nguyen, E. T., & Paul, N. (2010). Strategies for Radiation-dose Reduction and Image-quality Optimization in Multidetector Computed Tomographic Coronary Angiography. *Can Assoc Radiol J, 61*(5), 271-279.

Tortora, G. J., & Grabowski, S. R. (Eds.). (2003). *Principles of Anatomy and Physiology* (10th ed.). New York: Wiley.

Traub, S. J., Kellum, J. A., Tang, A., Cataldo, L., Kancharla, A., & Shapiro, N. I. (2013). Risk factors for radiocontrast nephropathy after emergency department contrast-enhanced computerized tomography. *Acad Emerg Med, 20*(1), 40-45.

Unal, E., Yildiz, A. E., Guler, E., Karcaaltincaba, M., Akata, D., Kilincer, A., . . . Hazirolan, T. (2015). Comparison of image quality and radiation dose between prospectively ECG-triggered and retrospectively ECG-gated CT angiography: Establishing heart rate cut-off values in first-generation dual-source CT. *Anatol J Cardiol, 15*(9), 759-764.

UNSCEAR. (2000). *Sources and Effects of Ionizing Radiation. UNSCEAR Report to the General Assembly, Volume II: Effects*. Retrieved from http://www.unscear.org/unscear/en/publications/2000_2.html

Utsunomiya, D., Awai, K., Sakamoto, T., Nishiharu, T., Urata, J., Taniguchi, A., . . . Yamashita, Y. (2006). Cardiac 16-MDCT for anatomic and functional analysis: assessment of a biphasic contrast injection protocol. *AJR Am J Roentgenol, 187*(3), 638-644.

Van Cauteren, T., Van Gompel, G., Tanaka, K., Verdries, D. E., Belsack, D., Nieboer, K. H., & Willekens, I. (2017). The Impact of Combining a Low-Tube Voltage Acquisition with Iterative Reconstruction on Total Iodine Dose in Coronary CT Angiography. *Biomed Res Int, 2017*, 2476171.

van Hoe, L., Marchal, G., Baert, A. L., Gryspeerdt, S., & Mertens, L. (1995). Determination of scan delay time in spiral CT-angiography: utility of a test bolus injection. *J Comput Assist Tomogr, 19*(2), 216-220.

Van Mieghem, C. A. G., Thury, A., Meijboom, W. B., Cademartiri, F., Mollet, N. R., Weustink, A. C., . . . de Feyter, P. (2007). Detection and characterization of coronary bifurcation lesions with 64-slice computed tomography coronary angiography. *Eur Heart J, 28*(16), 1968-1976.

Virmani, R., Burke, A. P., Farb, A., & Kolodgie, F. D. (2006). Pathology of the vulnerable plaque. *J Am Coll Cardiol, 47*(8 Suppl), C13-18.

Virmani, R., Burke, A. P., Kolodgie, F. D., & Farb, A. (2002). Vulnerable plaque: the pathology of unstable coronary lesions. *J Interv Cardiol, 15*(6), 439-446.

Virmani, R., Kolodgie, F. D., Burke, A. P., Farb, A., & Schwartz, S. M. (2000). Lessons from sudden coronary death: a comprehensive morphological classification scheme for atherosclerotic lesions. *Arterioscler Thromb Vasc Biol, 20*(5), 1262-1275.

von Ballmoos, M. W., Haring, B., Juillerat, P., & Alkadhi, H. (2011). Meta-analysis: diagnostic performance of low-radiation-dose coronary computed tomography angiography. *Ann Intern Med, 154*(6), 413-420.

Voros, S., Rinehart, S., Qian, Z., Joshi, P., Vazquez, G., Fischer, C., . . . Villines, T. C. (2011). Coronary atherosclerosis imaging by coronary CT angiography: current status, correlation with intravascular interrogation and meta-analysis. *JACC Cardiovasc Imaging, 4*(5), 537-548.

Wang, L., Li, Q., Wang, X. M., Hao, G. Y., Jie, B., Hu, S., & Hu, C. H. (2017). Enhanced radiation damage caused by iodinated contrast agents during CT examination. *Eur J Radiol, 92*, 72-77.

Wang, Y., Bolen, M., Sydow, G., Kottha, A., Soufan, K., Bullen, J., . . . Halliburton, S. S. (2014). Adaptation of Contrast Injection Protocol to Tube Potential for Cardiovascular CT. *AJR Am J Roentgenol, 203*(6), 1181-1191.

Weigold, W. G. (2006). Coronary CT angiography: insights into patient preparation and scanning. *Tech Vasc Interv Radiol, 9*(4), 205-209.

Weinhaus, A. J., & Roberts, K. P. (2005). Anatomy of The Human Heart. In P. A. Iaizzo (Ed.), *Handbook of Cardiac Anatomy, Physiology, and Devices* (3rd ed.). Totowa, New Jersey: Human Press Inc.

Weininger, M., Barraza, J. M., Kemper, C. A., Kalafut, J. F., Costello, P., & Schoepf, U. J. (2011). Cardiothoracic CT angiography: current contrast medium delivery strategies. *AJR Am J Roentgenol, 196*(3), W260-272.

WHO. (2014a). *Malaysia: WHO Statistical profile*. Retrieved from http://www.who.int/gho/countries/mys.pdf

WHO. (2014b). *Noncommunicable diseases country profiles 2014*. Retrieved from Geneva, Switzerland: http://www.who.int/nmh/publications/ncd-profiles-2014/en/

WHO. (2017, May 2017). Cardiovascular diseases (CVDs). Retrieved from http://www.who.int/mediacentre/factsheets/fs317/en/

Wong, D. T., Soh, S. Y., Ko, B. S., Cameron, J. D., Crossett, M., Nasis, A., . . . Seneviratne, S. K. (2014). Superior CT coronary angiography image quality at lower radiation exposure with second generation 320-detector row CT in patients with elevated heart rate: a comparison with first generation 320-detector row CT. *Cardiovasc Diagn Ther, 4*(4), 299-306.

Wu, Q., Wang, Y., Kai, H., Wang, T., Tang, X., Wang, X., & Pan, C. (2016). Application of 80-kVp tube voltage, low-concentration contrast agent and iterative reconstruction in coronary CT angiography: evaluation of image quality and radiation dose. *Int J Clin Pract, 70 Suppl 9B*, B50-55.

Xu, L., & Sun, Z. (2015). Coronary CT angiography evaluation of calcified coronary plaques by measurement of left coronary bifurcation angle. *Int J Cardiovasc Imaging, 182*, 229-231.

Yamamuro, M., Tadamura, E., Kanao, S., Wu, Y. W., Tambara, K., Komeda, M., . . . Togashi, K. (2007). Coronary angiography by 64-detector row computed tomography using low dose of contrast material with saline chaser: influence of total injection volume on vessel attenuation. *J Comput Assist Tomogr, 31*(2), 272-280.

Yamashita, Y., Komohara, Y., Takahashi, M., Uchida, M., Hayabuchi, N., Shimizu, T., & Narabayashi, I. (2000). Abdominal helical CT: evaluation of optimal doses of intravenous contrast material--a prospective randomized study. *Radiology, 216*(3), 718-723.

Yanaga, Y., Awai, K., Nakaura, T., Oda, S., Funama, Y., Bae, K. T., & Yamashita, Y. (2009). Effect of contrast injection protocols with dose adjusted to the estimated lean patient body weight on aortic enhancement at CT angiography. *AJR Am J Roentgenol, 192*(4), 1071-1078.

Yang, C. C., Wu, J., Tsai, C. J., Chen, C. C., Hung, C. F., & Wu, T. H. (2011). Radiation dose in 320-detector-row CT coronary angiography: Prospective ECG triggering combined with multi-segment reconstruction. *Radiat Meas, 46*(12), 2060-2064.

Yang, L., Zhang, Z., Fan, Z., Xu, C., Zhao, L., Yu, W., & Yan, Z. (2009). 64-MDCT coronary angiography of patients with atrial fibrillation: influence of heart rate on image quality and efficacy in evaluation of coronary artery disease. *AJR Am J Roentgenol, 193*(3), 795-801.

Yang, W. J., Chen, K. M., Liu, B., Pang, L. F., Zhang, H., Pan, Z. L., & Yan, F. H. (2013). Contrast media volume optimization in high-pitch dual-source CT coronary angiography: feasibility study. *Int J Cardiovasc Imaging, 29*(1), 245-252.

Yin, W. H., Lu, B., Gao, J. B., Li, P. L., Sun, K., Wu, Z. F., . . . Schoepf, U. J. (2015). Effect of reduced x-ray tube voltage, low iodine concentration contrast medium, and sinogram-affirmed iterative reconstruction on image quality and radiation dose at coronary CT angiography: results of the prospective multicenter REALISE trial. *J Cardiovasc Comput Tomogr, 9*(3), 215-224.

Yuki, H., Utsunomiya, D., Funama, Y., Tokuyasu, S., Namimoto, T., Hirai, T., . . . Yamashita, Y. (2014). Value of knowledge-based iterative model reconstruction in low-kV 256-slice coronary CT angiography. *J Cardiovasc Comput Tomogr, 8*(2), 115-123.

Zeb, I., Abbas, N., Nasir, K., & Budoff, M. J. (2014). Coronary computed tomography as a cost-effective test strategy for coronary artery disease assessment - a systematic review. *Atherosclerosis, 234*(2), 426-435.

Zhang, C., Yu, Y., Zhang, Z., Wang, Q., Zheng, L., Feng, Y., . . . Li, K. (2015). Imaging quality evaluation of low tube voltage coronary CT angiography using low concentration contrast medium. *PLoS One, 10*(3), e0120539.

Zhang, C., Zhang, Z., Yan, Z., Xu, L., Yu, W., & Wang, R. (2011). 320-row CT coronary angiography: effect of 100-kV tube voltages on image quality, contrast volume, and radiation dose. *Int J Cardiovasc Imaging, 27*(7), 1059-1068.

Zhang, D., Li, X., Gao, Y., Xu, X. G., & Liu, B. (2013). A method to acquire CT organ dose map using OSL dosimeters and ATOM anthropomorphic phantoms. *Med Phys, 40*(8), 081918.

Zhang, J., Kang, S., Han, D., Xie, X., & Deng, Y. (2015). Application of intelligent optimal kV scanning technology (CARE kV) in dual-source computed tomography (DSCT) coronary angiography. *Int J Clin Exp Med, 8*(10), 17644-17653.

Zhang, Z., Austen, W. G., Edwards, J. E., Frye, R. L., Gensini, G. G., Gott, V. L., . . . Roe, B. B. (1975). A reporting system on patients evaluated for coronary artery disease. Report of the Ad Hoc Committee for Grading of Coronary Artery Disease, Council on Cardiovascular Surgery, American Heart Association. *Circulation, 51*(4 Suppl), 5-40.

Zheng, M., Liu, Y., Wei, M., Wu, Y., Zhao, H., & Li, J. (2014). Low concentration contrast medium for dual-source computed tomography coronary angiography by a combination of iterative reconstruction and low-tube-voltage technique: feasibility study. *Eur J Radiol, 83*(2), e92-99.

Zhu, X., Chen, W., Li, M., Xu, Y., Xu, H., Zhu, Y., . . . Tang, L. (2012). Contrast material injection protocol with the flow rate adjusted to the heart rate for dual source CT coronary angiography. *Int J Cardiovasc Imaging, 28*(6), 1557-1565.

Zhu, X., Shi, Z., Zhu, Y., Liu, W., Yang, G., Yu, T., . . . Xu, Y. (2015). Individually adapted tube current selection and contrast medium injection protocol of coronary CT angiography based on test bolus parameters: a feasibility study. *Acta Radiol, 56*(6), 666-672.

Zhu, X., Zhu, Y., Xu, H., Yang, G., Tang, L., & Xu, Y. (2013). Dual-source CT coronary angiography involving injection protocol with iodine load tailored to patient body weight and body mass index: estimation of optimal contrast material dose. *Acta Radiol, 54*(2), 149-155.

LIST OF PUBLICATIONS AND PAPERS PRESENTED

Publications in Thomson Reuters (ISI) Web of Science Citation Indexed Journals:

Tan, S. K., Yeong, C. H., Ng, K. H., Abdul Aziz, Y. F., & Sun, Z. (2016). Recent Update on Radiation Dose Assessment for the State-of-the-Art Coronary Computed Tomography Angiography Protocols. PLoS One, 11(8), e0161543.

Tan, S. K., Yeong, C. H., Aman, R. R., Ng, K. H., Abdul Aziz, Y. F., Chee, K. H., & Sun, Z. (2018). Low tube voltage prospectively ECG-triggered coronary CT angiography: A systematic review of image quality and radiation dose. Br J Radiol, 20170874.

Givenchi, S., Safari, M. J., **Tan, S. K.**, Md Shah, M. N. B., Sani, F. B. M., Azman, R. R., Sun, Z., Yeong, C. H., Ng, K. H., & Wong, J. H. D. (2018). Measurement of coronary bifurcation angle with coronary CT angiography: A phantom study. *Physica Medica: European Journal of Medical Physics*, *45*, 198-204.

In Preparation

Tan, S. K., Ng, K. H., Yeong, C. H., Aman, R. R., Sani, F.M, Abdul Aziz, Y. F. & Sun, Z. Optimisation of radiaiton dose, image quality and contrast medium administration in CCTA: An improved retrospectively ECG-triggered CCTA protocol.

Papers presented at Scientific Meeting and Conference:

Oral Presentations

Tan, S. K., Yeong, C. H., Wong, J. H. D., Abdul Aziz, Y. F., Sun, Z., Ng, K. H. An improved method of effective dose estimation using size-specific conversion factor in coronary computed tomography angiography (CCTA). 22th International Conference on Medical Physics (ICMP), Bangkok, Thailand, December 9 – 12, 2016.

Tan, S. K., Yeong, C. H., Azman, R. R., Ng, K. H., Abdul Aziz, Y. F., Sun, Z. Radiation Dose and Lifetime Attributable Risk (LAR) of Cancer Incidence in prospectively ECG-triggered coronary computed tomography angiography (CCTA). 18th Congress of the ASEAN Association of Radiology (AAR), Kuala Lumpur, Malaysia, September 28 – 30, 2017.

Scientific Poster Presentation

Tan, S. K., Yeong, C. H., Ng, K. H., Abdul Aziz, Y. F., Sun, Z. Assessment of Radiation Dose for Selected Contemporary Coronary Computed Tomography Angiography Protocols: Phantom Study. International Conference on Integrated Medical Imaging in Cardiovascular Diseases (IMIC 2016), Vienna, Austria, October 10 - 14, 2016